Applications of O-band semiconductor optical amplifiers in fibre-optic telecommunication networks

Applications of O-band semiconductor optical amplifiers in fibre-optic telecommunication networks

PROEFSCHRIFT

ter verkrijging van de graad van doctor aan de
Technische Universiteit Eindhoven, op gezag van de
Rector Magnificus, prof.dr.ir. C.J. van Duijn, voor een
commissie aangewezen door het College voor
Promoties in het openbaar te verdedigen
op maandag 2 oktober 2006 om 16.00 uur

door

Jarosław Piotr Turkiewicz

geboren te Koszalin, Polen

Dit proefschrift is goedgekeurd door de promotoren:

prof.ir. G.D. Khoe
en
prof.ir. A.M.J. Koonen

Copromotor:
dr.ir. H. de Waardt

The work described in this thesis was performed at the COBRA Research Institute, Eindhoven University of Technology and was supported by the Netherlands Organization for Scientific Research (NWO) under the NRC Photonics Grant and by the European Commission through the IST project FASHION.

CIP-DATA LIBRARY TECHNISCHE UNIVERSITEIT EINDHOVEN

Turkiewicz, Jarosław P.

Applications of O-band semiconductor optical amplifiers in fibre-optic telecommunication networks / by Jarosław Piotr Turkiewicz. - Eindhoven : Technische Universiteit Eindhoven, 2006.
Proefschrift. - ISBN-10: 90-386-1853-0
ISBN-13: 978-90-386-1853-1
NUR 959
Trefw.: optische versterkers / optische signaalverwerking / optische telecommunicatiesystemen / vezeloptica.
Subject headings: semiconductor optical amplifiers / optical information processing / optical fibre networks / optical fibre communication.

Typeset using LaTeX, printed in The Netherlands

to my parents
to my brother

Summary

Optical fibre communication is an essential part of modern telecommunication networks. Research activities are aiming to transport and switch information streams through optical fibre networks most efficiently. This thesis is devoted to applications of 1310 nm semiconductor optical amplifiers (SOAs) in fibre optic telecommunication networks.

The basic application of 1310 nm SOAs is the amplification of optical signals. In this thesis dense wavelength division multiplexed SOA based transmission in the 1310 nm wavelength domain is investigated. The 1310 nm SOAs allow high speed (10-40 Gbit/s) transmission over metro range distances (50-200 km) without any dispersion compensation in standard single-mode fibre based networks. This is important for access and metro systems, where the system cost is shared by the limited number of users.

To alleviate optical-electrical-optical conversion at the interface point between access-metro and core networks a novel wavelength conversion technique is proposed. Nonlinear polarization rotation in the 1310 nm SOA permits the realization of 1310-to-1550 nm wavelength conversion and the aggregation of multiple data streams in the 1310 nm wavelength domain into one time interleaved data stream in the 1550 nm wavelength domain.

By utilizing the 1310 nm SOA in a gain transparent configuration an all-optical optical time domain multiplexed add-drop switch was realized. The proposed add-drop switch was widely tested in the laboratory and field transmission experiments allowing 160 Gbit/s transmission over 550 km of standard single-mode fibre and the realization of a fully functional 160 Gbit/s optical time domain multiplexed network.

Based on this research it is concluded that 1310 nm SOAs are versatile components which support essential transmission and switching functionalities with great opportunities for utilization in advanced telecommunication networks.

Samenvatting

Optische communicatie is een belangrijk onderdeel van de hedendaagse telecommunicatie. Onderzoeksactiviteiten richten zich op het zo efficiënt mogelijk transporteren en schakelen van informatiestromen in een optisch netwerk. Dit proefschrift gaat dieper in op applicaties van 1310 nm optische versterkers (SOAs) in optische telecommunicatie netwerken.

De basistoepassing van de 1310 nm SOA is versterking van optische signalen. In dit proefschrift is signaaltransport met golflengte-gestapelde kanalen, gebaseerd op SOAs in het 1310 nm golflengte domein, onderzocht. Het is mogelijk om met 1310 nm SOAs en met hoge snelheden (10-40 Gbit/s) data te transporteren over een standaard single mode glasvezelnetwerk, over afstanden van 50-200 km en zonder enige vorm van dispersiecompensatie. Dit is belangrijk voor "access" en "metro" systemen, waar de kosten van deze systemen worden gedeeld door een beperkt aantal gebruikers.

Een nieuwe golflengte-conversietechniek is voorgesteld om de optisch-elektrisch-optische omzettingen bij de overgangen van access, metro en core netwerken, te vermijden. Simultane golflengteconversie van 1310 nm naar 1550 nm en het samenvoegen van meerdere datastromen in de 1310 nm golflengtedomein tot één tijdgestapeld datasignaal in het 1550 nm golflengtedomein is gerealiseerd door middel van niet-lineare polarisatie rotatie in de 1310 nm SOA.

Een schakelknooppunt is gerealiseerd met behulp van de 1310 nm SOA in een "gain" transparante configuratie, waarin een specifieke datastroom uit een tijdsdomein gestapeld signaal kan worden toegevoegd, of juist kan worden uitgekoppeld. Deze schakelaar is uitvoerig getest in het laboratorium en in veldexperimenten. 160 Gbit/s transmissie over 550 km standaard single mode glasvezel en een compleet functionerend optisch tijdsdomein gestapeld netwerk is gerealiseerd.

Gebaseerd op dit onderzoek het kan worden geconcludeerd dat 1310 nm SOAs veelzijdige componenten zijn, die essentiële transport- en schakelfunctionaliteiten bevatten met goede mogelijkheden voor toepasbaarheid in geavanceerde telecommunicatie netwerken.

Contents

1 Introduction **1**

2 DWDM transmission in the 1310 nm wavelength domain **5**
2.1 Optical fibre . . . 5
2.1.1 Attenuation . . . 5
2.1.2 Chromatic dispersion . . . 7
2.1.3 Polarization Mode Dispersion . . . 10
2.1.4 Four-Wave Mixing . . . 11
2.2 Semiconductor optical amplifier . . . 19
2.2.1 Amplification technologies . . . 19
2.2.2 Operation of the SOA . . . 20
2.2.3 Static characteristics of the SOA . . . 24
2.2.4 Dynamic operation of the SOA . . . 26
2.3 4×10 Gbit/s transmission experiments . . . 30
2.3.1 Experimental setup . . . 30
2.3.2 Results and discussion . . . 32
2.4 Extended reach 4×10 Gbit/s transmission experiments . . . 35
2.4.1 Experimental setup . . . 36
2.4.2 Results and discussion . . . 37
2.5 4×25 Gbit/s transmission experiments . . . 41
2.5.1 Experimental setup . . . 43
2.5.2 Results and discussion . . . 46
2.6 4×40 Gbit/s transmission experiments . . . 50
2.6.1 Experimental setup . . . 51
2.6.2 Results and discussion . . . 53
2.7 Conclusions . . . 58

3 1310-to-1550 nm transparent optical connectivity **61**
3.1 Introduction . . . 61
3.2 Nonlinear polarization rotation . . . 63

3.2.1 Polarization concept 63
3.2.2 Nonlinear polarization rotation in an SOA 64
3.2.3 Nonlinear polarization rotation in the transparency region of the SOA 66
3.3 1310-to-1550 nm wavelength conversion 69
3.3.1 Wavelength converter setup 69
3.3.2 Non-inverting and inverting operation 70
3.3.3 1310-to-1550 nm wavelength conversion with simultaneous data format conversion 74
3.3.4 1310-to-1550 nm wavelength conversion in between two transmission links 75
3.4 1310-to-1550 nm transmultiplexing 78
3.4.1 Architecture of the transmultiplexing node 80
3.4.2 2×5 Gbit/s 1310 nm to 10 Gbit/s 1550 nm transmultiplexing 81
3.4.3 4×2.5 Gbit/s 1310 nm to 10 Gbit/s 1550 nm transmultiplexing 84
3.5 Synchronization of the 1310-to-1550 nm interconnect 91
3.6 Conclusions 93

4 GT-UNI based add-drop multiplexing 95
4.1 OTDM technology 95
4.2 Gain-transparent ultrafast nonlinear interferometer 99
4.2.1 Gain-transparent switching 99
4.2.2 Principe of ultrafast nonlinear interferometer 100
4.2.3 GT-UNI switch 101
4.3 GT-UNI based add-drop multiplexer 104
4.3.1 Switching window characteristics 104
4.3.2 80 Gbit/s add-drop multiplexing 106
4.4 160 Gbit/s GT-UNI based add-drop node 109
4.4.1 Clock recovery 109
4.4.2 Transmission experiments 114
4.4.3 OTDM add-drop networking experiments 120
4.5 Conclusions 124

5 Conclusions 127

References 129

List of abbreviations 141

List of publications 143

Curriculum vitæ 149

Acknowledgements 151

Chapter 1

Introduction

In this chapter, the historical development and current trends in optical fibre communication are briefly discussed. Furthermore, the motivation and research topics of the thesis are presented.

Optical communication is a form of telecommunications that utilizes the optical signal as the information carrier. In general, any transmission link can be divided in three parts: a transmitter, a transmission channel, and a receiver. The transmitter encodes a message into an optical signal. The transmission channel transports the data to the receiver. The receiver decodes the message from the received optical signal.

Apart from the non-technical forms of optical communication like body language and gesture, many other optical communication techniques were developed through centuries. Fires, smoke signals, mirrors, ship flags, and semaphores were the earliest forms of optical communication. However, the most important and most significant form of optical communication is optical fibre communication.

In [1] K.C. Kao and G.A. Hockham proposed that optical fibre could be used as a transmission medium for long distance communication. The first optical fibre suitable for optical communication (attenuation below 20 dB/km) was developed in 1970 by F.P. Kapron, D.B. Keck, and R.D. Maurer [2]. Further development of optical glass fibre manufacturing technique decreased the fibre attenuation value to below 0.2 dB/km.

Since the invention of optical fibre, optical fibre communication experiences booming growth. Excellent transmission properties, i.e. available bandwidth, low loss, and resilience to electro-magnetic distortions are making the optical fibre almost an ideal transmission medium.

The first generation of the optical fibre communication systems operated at

850 nm and utilized a multimode fibre as a transmission medium. The second generation utilized 1310 nm light sources and a single-mode fibre. Hence, the abbreviation "O-band" stands for "Original-band" since single-mode fibre based optical communication started in the 1310 nm wavelength domain. The third generation of the optical transmission systems utilized the 1550 nm wavelength domain, where standard single-mode fibre has its lowest attenuation but also non-negligible dispersion and distributed feedback lasers as an optical signal source. The forth generation of optical systems utilizes erbium-doped fibre amplifiers and wavelength multiplexing techniques allowing long haul transmission of multiple optical signals in a single optical fibre.

Using optical fibre transmission systems a network of high capacity trans- and inter-continental connections was realized. Recently, in the laboratory experiments a record 2.56 Tbit/s single wavelength channel transmission has been demonstrated [3]. Commercially available multi-wavelength systems offer capacity of 160×10 Gbit/s (1.6 Tbit/s) or 64×40 Gbit/s (2.56 Tbit/s) [4].

Besides fibre based transmission techniques, all-optical signal processing techniques attract considerable attention of researchers. By manipulating optical signals exclusively in the optical domain several functionalities have been realized omitting optical-electrical-optical conversions in routing nodes. As an example error-free 320 Gbit/s wavelength conversion in a single 1550 nm semiconductor optical amplifier [5] or an all-optical 1×2 routing node [6] can be mentioned.

Next important step in the development of optical fibre communication is integration of all-optical signal processing functionalities into photonic integrated circuits. Significant achievements have been already reported like a compact integrated optical crossconnect [7] or an all-optical memory element [8]. New materials, like strained silicon are under development to allow integration of optical components like modulators with the existing silicon-based electronics [9].

Excellent transmission properties of optical fibre allow realization of high capacity and long distance transmission networks. These networks form a back-bone of the world-wide network utilized to deliver voice and data services like Internet. Recently attention moved from the long haul transmission to the short-range transmission to allow end-users unlimited access to interactive services provided by Internet or broadband distributive services like HDTV.

Accelerated roll-out of optical access networks takes place in countries like South Korea, Japan, and United States [10]. Also in Europe several initiatives are undertaken to provide fibre-based infrastructures to the end-users. An example of that is undertaking in Nuenen, The Netherlands, where a broadband optical network "OnsNet" is connecting 7500 premises [11].

Further advancement of optical communication aims at development of in-house optical networks. Such networks based on easy-to-handle optical fibre like a polymer optical fibre will allow efficient delivery of network services in house premises or offices. Already, the delivery technique of radio signals over polymer optical fibre has been developed and successfully tested [12]

It is clear that optical communication research and applications is moving towards

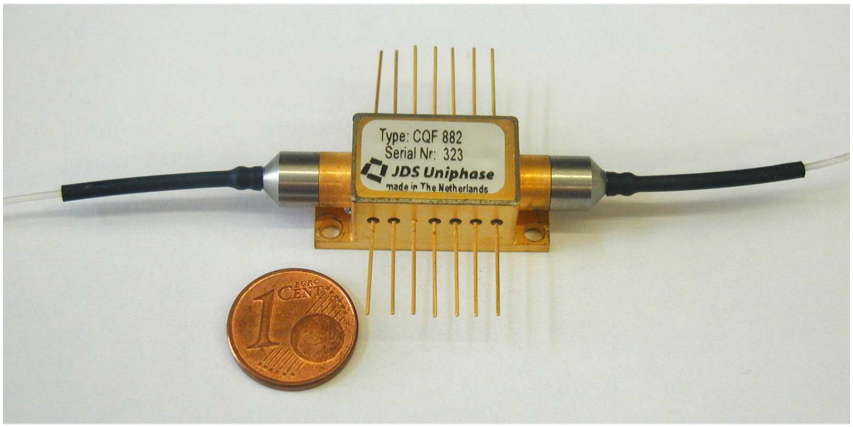

Figure 1.1: Photography of the packaged and pigtailed semiconductor optical amplifier

the end-user, i.e. access and local networks. The main constrain is here the cost of the network infrastructure that is shared by a limited number of users in comparison with the long-haul networks. Therefore the applied solutions have to offer high quality services while remaining at low cost.

Although single-mode fibre based optical communication started in the 1310 nm wavelength domain, contemporary applications of the 1310 nm wavelength domain are limited. This phenomena can be clearly observed in the conferences where the number of papers dealing with the 1310 nm wavelength domain is scarce. In the Proceedings of Optical Fibre Communications Conference 2006 the search inquiry "1310" results in 25 papers out of 700. This can be explained by the fact that in the past research was mainly concentrated on long-haul high-capacity transmission and switching systems. Theses systems are traditionally located in the 1550 nm wavelength domain.

The standard single-mode fibre is characterized by low value of attenuation and dispersion in the 1310 nm wavelength domain. These properties allow realization of cost-effective transmission systems in the 1310 nm wavelength domain that can be successfully applied in the access and metro systems, e.g. in access systems bidirectional communication is commonly established by coarse 1310/1550 nm wavelength multiplexing. Moreover, transmission systems utilizing the 1310 nm wavelength domain can be used in parallel to the already existing 1550 nm wavelength domain based transmission, which allows more efficient exploitation of installed fibre infrastructure. This is particularly important in highly urbanized areas, where the fibre installation cost is extraordinary high.

The motivation behind the research presented in this thesis is to demonstrate that the 1310 nm SOAs, and therefore the 1310 nm wavelength domain, have great potential in modern communication networks. In particular novel applications of 1310 nm semiconductor optical amplifiers are explored in this thesis.

Specific subject areas that have been investigated here include:

- the suitability of the 1310 nm SOAs in cost-effective high-speed multi-wavelength transmission systems
- the capability of the 1310 nm SOAs to support transparent optical signal routing via all-optical signal processing
- the applications of 1310 nm SOAs in switching of the 1550 nm data signals.

The thesis has been structured in three chapters and their content is briefly outlined below:

Chapter 2 DWDM transmission in the 1310 nm wavelength domain

Access and metro networks have to be cost-effective since they are shared by a limited number of users. The potential of the 1310 nm wavelength domain to support multi-wavelength dispersion-compensation-free transmission is extensively analyzed. Properties of semiconductor optical amplifiers and standard single-mode fibre regarding multi-wavelength transmission are evaluated. Based on the analysis results dispersion-compensation-free transmission experiments over distances 50-200 km at bit rates 10-40 Gbit/s are performed.

Chapter 3 1310-to-1550 nm transparent optical connectivity

To realize transparent optical connectivity between access and core networks, all-optical 1310-to-1550 nm wavelength conversion is necessary. A wavelength conversion technique utilizing nonlinear polarization rotation in the transparency region of the SOA is proposed. Several 1310-to-1550 nm wavelength conversion experiments are performed. Moreover, the proposed wavelength conversion technique is applied to realize 1310-to-1550 nm transmultiplexing. That is the aggregation of multiple data streams from the 1310 nm wavelength domain into one time interleaved data stream in the 1550 nm wavelength domain.

Chapter 4 GT-UNI based add-drop multiplexing

To achieve maximum switching flexibility in optical time domain multiplexed networks, an all-optical add-drop switch is necessary. A 1310 nm semiconductor optical amplifier is applied in a gain-transparent ultrafast nonlinear interferometer configuration to realize all-optical add-drop multiplexing of OTDM signals. The proposed add-drop switch is tested in the laboratory as well as in field trial experiments. Transmission of 160 Gbit/s signal over distances up to 550 km and a fully functional 160 Gbit/s add-drop network is realized using the developed switch.

Chapter 2

DWDM transmission in the 1310 nm wavelength domain

In this chapter, feasibility of the DWDM transmission in the 1310 nm wavelength domain using semiconductor optical amplifiers is investigated. First, fundamental properties and limitations of optical fibre, and semiconductor optical amplifiers are described and analyzed. Based on the analysis, potential applications of the multi-wavelength 1310 nm transmission are explored and the transmission experiments are performed. First, repeated and unrepeated 4×10 Gbit/s transmission is evaluated. Moreover, unrepeated 100 Gbit/s Ethernet and unrepeated 4×40 Gbit/s transmission are shown over a 50 km distance using exclusively semiconductor components.[1]

2.1 Optical fibre

The optical fibre characteristics determine the design of fibre-optic transmission systems. Three important fibre characteristics are attenuation, dispersion, and polarization mode dispersion (PMD). Moreover, nonlinear fibre effects may cause signal distortions.

2.1.1 Attenuation

Attenuation of the optical fibre determines the maximum transmission distance between a transmitter and a receiver, or in-line amplifier(s). The basic attenuation mechanisms in a fibre are absorption, scattering, and radiative losses of optical energy. As the optical signal travels along a fibre, its power decreases exponentially with distance. If $P(0)$ is the optical power in a fibre at the origin ($z = 0$), then the

[1] Parts of this chapter are published in [13, 14]

power $P(z)$ further down the fibre attenuates as

$$P(z) = P(0)e^{-\alpha z}, \tag{2.1}$$

where α is the fibre attenuation coefficient given in units of Neper per kilometre (Np/km). The common procedure is to express the attenuation coefficient in units of decibels per kilometre, denoted by dB/km. Designating this parameter by α, we have

$$\alpha(\text{dB/km}) = 4.343\alpha. \tag{2.2}$$

Figure 2.1 shows optical fiber attenuation as a function of wavelength. Modern optical fibre shows minimum attenuation of α=0.2 dB/km at 1550 nm. At the wavelength of 1310 nm fibre attenuation increases to about 0.3-0.4 dB/km. The peak in attenuation at around 1383 nm results from absorption by water molecules. Recently developed manufacturing process eliminates the incorporation of OH^- molecules into fibre opening the whole range 1290-1570 nm [15].

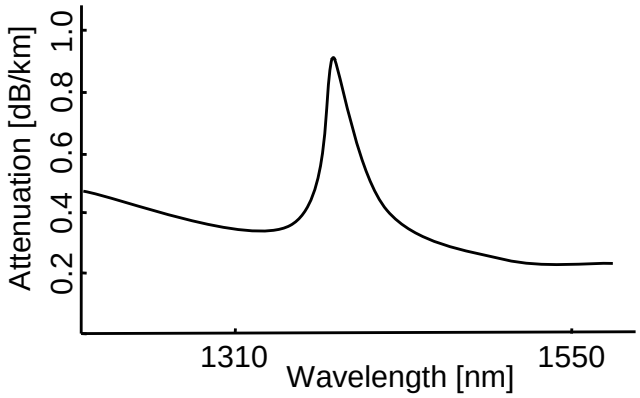

Figure 2.1: Optical fiber attenuation in a function of wavelength

The important observation is that the optical signal experiences roughly two times higher attenuation in the 1310 nm wavelength domain in comparison with the 1550 nm wavelength domain. Therefore for the same transmitter output power and receiver sensitivity, the transmission distance is almost doubled in the 1550 nm wavelength domain with respect to the 1310 nm wavelength domain. This implies that the 1550 nm wavelength domain is preferred for the long-haul transmission, and that the potential applications of the 1310 nm wavelength domain are medium and short range transmission systems.

Taking into account the typical values for a 10 Gbit/s transmission system: the transmitter output power +3 dBm and the receiver sensitivity -18 dBm, the power budget of 21 dB will result in the transmission range of about 50 km in the 1310 nm wavelength domain. To cope with attenuation and to increase the transmission distance optical amplifiers have to be used. Optical amplifier technology will be discussed in Section 2.2.

2.1.2 Chromatic dispersion

The second important property of a single-mode fibre is chromatic dispersion. In a single-mode fibre different spectral components travel at slightly different group velocities. This phenomenon is called group-velocity dispersion (GVD) or simply fibre dispersion. As a result, different spectral components arrive at different times at the receiver causing pulse broadening. After a certain amount of broadening, adjacent pulses can not be individually distinguished and errors will occur at the receiver. The parameter D

$$D = -\frac{2\pi c}{\lambda^2}\beta_2, \tag{2.3}$$

is called the dispersion parameter, where λ is wavelength, c is speed of the light (both in vacuum), and β_2 is the group velocity dispersion (GVD) parameter [16]. The dispersion parameter defines the pulse spread as a function of wavelength and is expressed in the units of ps/nm×km. The GVD parameter $\beta_2 \equiv d^2\beta/d\,\omega^2$ determines how much an optical pulse would broaden propagating inside the fibre, where β is the propagation constant, and ω is angular frequency. Table 2.1 presents the dispersion coefficient values for different types of single-mode fibre (SMF).

The dispersion limit (the 1 dB power penalty caused by dispersion) for the directly modulated laser can be expressed analytically by

$$B^2L = \gamma\left\{\frac{c}{|D|\lambda^2}\right\}, \tag{2.4}$$

where B is the bit rate of a data stream, L is the fibre length, and γ is the system dispersion index which can be maximized by a proper design of the laser linewidth enhancement factor in combination with the fibre dispersion parameter D [18].
The 1 dB power penalty limit for the system with an external modulator is [16]

$$B^2L = \frac{c}{2|D|\lambda^2}. \tag{2.5}$$

Further work will refer to this limit. It is clear, that four times the increase in the transmitted bit rate implies 16 times the reduction of the maximum allowable transmission distance. The calculated maximum allowable transmission distance for the

Table 2.1: Typical attenuation and dispersion values for different types of optical fibres [17]

Fibre type	**Attenuation [dB/km]**		**Dispersion [ps/nm×km]**	
	1310 nm	**1550 nm**	**1310 nm**	**1550 nm**
Standard SMF	0.34	0.19	0	17
Dispersion Shifted SMF	0.35	0.22	-17	0
WDM optimized SMF	0.35	0.20	-12	3

10 Gbit/s standard single-mode fibre (SSMF) based transmission in the 1550 nm wavelength domain is about 50 km. The distance reduces to 10 km in the case of 25 Gbit/s transmission, and finally to about 3 km in the case of 40 Gbit/s transmission.

Obviously, countermeasures can be applied to overcome the dispersion limitation like passive dispersion compensation, spectrum conjugation, forward-error correction, or electronic dispersion compensation [19]. But these countermeasures will increase the system cost and complexity, and reduce flexibility. The compensation cost of 50 km long SSMF using a dispersion compensation fibre varies between 10000 USD and 25000 USD. Moreover, in the case of 40 Gbit/s transmission the compensation accuracy requires precise measurements of dispersion, which complicates and increases cost of the installation.

On the other hand, one may propose usage of a different type of fibre than SSMF, e.g. Dispersion Shifted single-mode Fibre (DSF). However, SSMF is currently the most installed fibre [15] and SSMF is the fibre of choice for metro systems. 99% of the 10 Gbit/s metro systems use SSMF [20]. Therefore a promising candidate to realize metro (<100 km) and access range high speed transmission (<20 km) is the 1310 nm wavelength domain.

The ITU-T Recommendation G.652 describes characteristics of SSMF [21]. The chromatic dispersion limit for any wavelength λ in the 1310 nm region, is calculated using the minimum zero-dispersion wavelength λ_{0min} (the minimum wavelength at which dispersion vanishes), the maximum zero-dispersion wavelength λ_{0max} (the maximum wavelength at which dispersion vanishes), and the maximum zero-dispersion slope coefficient S_{0max} (the maximum value of dispersion slope at the zero-dispersion wavelength) according to [21]:

$$\frac{\lambda S_{0max}}{4}\left[1-\left(\frac{\lambda_{0max}}{\lambda}\right)^4\right] \leq D(\lambda), \leq \frac{\lambda S_{0max}}{4}\left[1-\left(\frac{\lambda_{0min}}{\lambda}\right)^4\right]. \qquad (2.6)$$

The values are specified to be: $\lambda_{0min} = 1300$ nm, $\lambda_{0max} = 1324$ nm, and $S_{0max} = 0.093$ ps/nm^2×km. The above equation, when used with these values, can be used to determine upper limits of the chromatic dispersion coefficient in the 1550 nm region [21].

Figure 2.2 shows maximum and minimum dispersion values in the 1310 nm wavelength domain calculated using Equation 2.6. The absolute dispersion values for the "O-band" boundary wavelengths (1260 and 1360 nm) can be as high as 6 ps/nm×km. Obviously, the lowest values of dispersion can be expected between 1300 and 1324 nm, the zero-dispersion wavelength band.

The wavelength band that guarantees at least 10 times extension of the transmission distance, with respect to the dispersion value 17 ps/nm×km, is located between 1306 and 1319 nm. The lowest maximum dispersion value of 1.1 ps/nm×km is at 1312 nm. This is particularly important for the systems operating with the bit rate 25 Gbit/s or 40 Gbit/s, where instead of the transmission distance of few kilometres, a few dozen kilometres ca be easily reached.

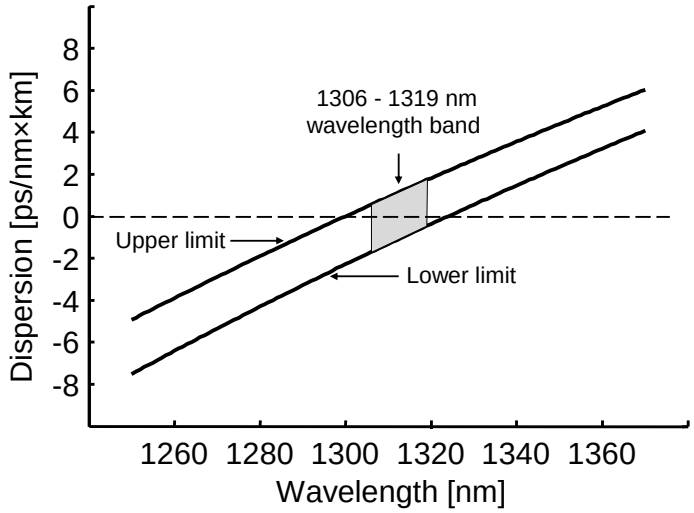

Figure 2.2: Calculated dispersion values in the 1310 nm wavelength domain [21]

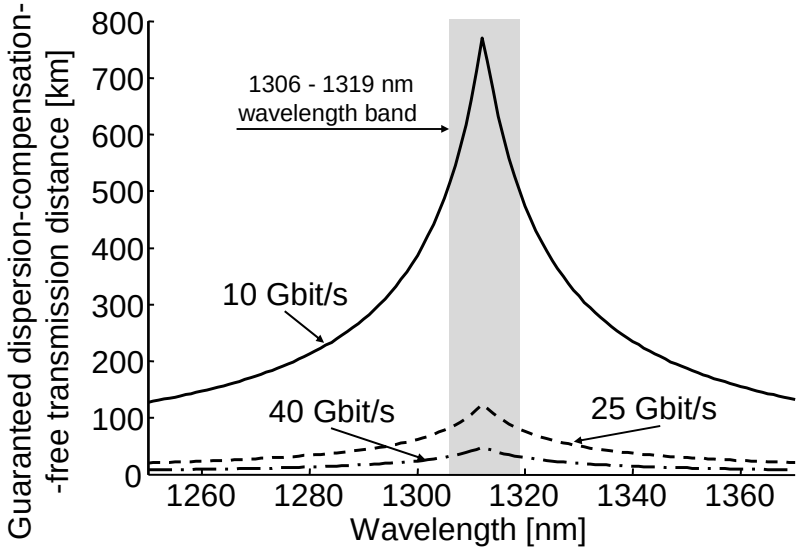

Figure 2.3: Calculated guaranteed dispersion-compensation-free distance in the 1310 nm wavelength domain at 10, 25, and 40 Gbit/s

The calculated guaranteed dispersion-compensation-free distance versus wavelength is presented in Figure 2.3. The distance was calculated using Equation 2.5 and the maximum absolute value of dispersion at the certain wavelength. In such a way, the minimum distance that can be bridged without dispersion compensation was obtained. Obviously, for low values of dispersion, e.g. 0.01 ps/nm×km much longer distances can be bridged without dispersion compensation. However, the presented graph is based on the highest absolute dispersion value at a given wavelength. It can be seen that at 10 Gbit/s, the maximal guaranteed dispersion-compensation-free distance is about 800 km, at 25 Gbit/s 110 km and at 40 Gbit/s 40 km respectively.

From the presented analysis it can be concluded that the systems utilizing the 1310 nm wavelength domain should operate between 1306 and 1319 nm to maximize dispersion-compensation-free transmission distance. In the 1306-1319 nm wavelength band, 22 channels can be placed based on 100 GHz spacing between adjacent channels. When higher dispersion values (shorter transmission distances) are permitted, a wider wavelength band can be utilized to realize dispersion-compensation-free transmission, e.g. 1300-1325 nm. In such a wavelength band more transmission channels can be placed. Therefore the required transmission distance determines the available wavelength band in the case of dispersion-compensation-free transmission.

2.1.3 Polarization Mode Dispersion

The next fibre phenomenon that can limit the range of optical transmission systems is polarization mode dispersion (PMD). In a single-mode optical fibre, the signal energy at any given wavelength is resolved into two orthogonal polarization modes. The difference in propagation time between the polarization modes $\Delta\tau$, is called the differential group delay (DGD). This difference will result in pulse spreading. A conceptual model of PMD is presented in Figure 2.4.

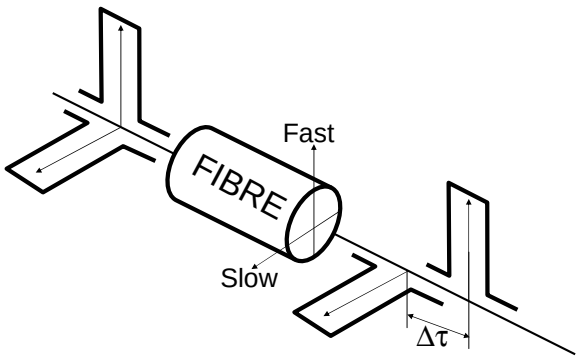

Figure 2.4: A conceptual model of PMD

In a single-mode fibre, birefringence originates from non-circularity of the fibre core, internal stress on it, or externally applied mechanical stress. External stresses are induced by bending, twisting, or pinching of the fibre. An important feature of PMD, (in contrast to chromatic dispersion, which is a deterministic phenomenon),

is that PMD at any given wavelength is not constant. The actual value of the $\Delta\tau$ varies with time and wavelength, and can be much lower or higher than the average value $<\Delta\tau>$. This feature makes passive compensation of PMD very difficult. The average value of DGD can be calculated according to relationship [17]:

$$< \Delta\tau >= \mathrm{PMD_C}\sqrt{L}, \tag{2.7}$$

where $\mathrm{PMD_C}$, which is measured in $\mathrm{ps}/\sqrt{\mathrm{km}}$ is the PMD coefficient. Because fibre imperfections are random $<\Delta\tau>$ is proportional to the square root of the propagation distance and differential group delay follows the Maxwellian distribution [22]. The example of the DGD distribution for $<\Delta\tau>$ = 10 ps is presented in Figure 2.5.

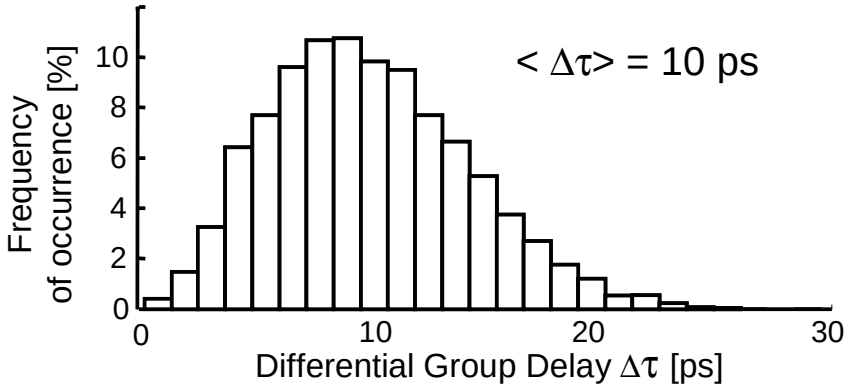

Figure 2.5: Example of the DGD distribution for $<\Delta\tau>$ = 10 ps

For modern fibres, $\mathrm{PMD_C}$ is $\leq 0.1\,\mathrm{ps}/\sqrt{\mathrm{km}}$, for older fibres values of $2\,\mathrm{ps}/\sqrt{\mathrm{km}}$ easily can be reached. To minimize influence of PMD on the signal quality in an intensity modulated NRZ system, the average value of PMD should be kept below one-tenth of a bit period [17], e.g. 10 ps in 10 Gbit/s transmission. According to Equation 2.7 the transmission distance of a 10 Gbit/s transmission system varies between 10000 km for a low $\mathrm{PMD_C}$ value ($0.1\,\mathrm{ps}/\sqrt{\mathrm{km}}$), and 25 km for a high $\mathrm{PMD_C}$ value ($2\,\mathrm{ps}/\sqrt{\mathrm{km}}$), at 40 Gbit/s respectively 625 km and 1.5 km.

It is important to remember that a $\mathrm{PMD_C}$ value measured for a particular fibre in the laboratory or the factory may be different from the one measured when the fibre is field installed, exposed to many additional stresses and changes in environmental conditions. Field measurements must be performed to assure correct values of the PMD coefficient.

2.1.4 Four-Wave Mixing

An increase in the number of transmitted data channels enhances the transmitted optical power. This can cause nonlinear interactions in the fibre like four-wave mixing (FWM), cross-phase modulation (XPM), or self-phase modulation (SPM). Those nonlinear effects can cause significant system penalty.

In the FWM effect, two or more waves co-propagating in the nonlinear medium interact with each other and new waves are generated according to:

$$f_{ijk} = f_i + f_j - f_k, \qquad i, j \neq k. \tag{2.8}$$

An example of three co-propagating waves and 12 newly generated waves is presented in Figure 2.6.

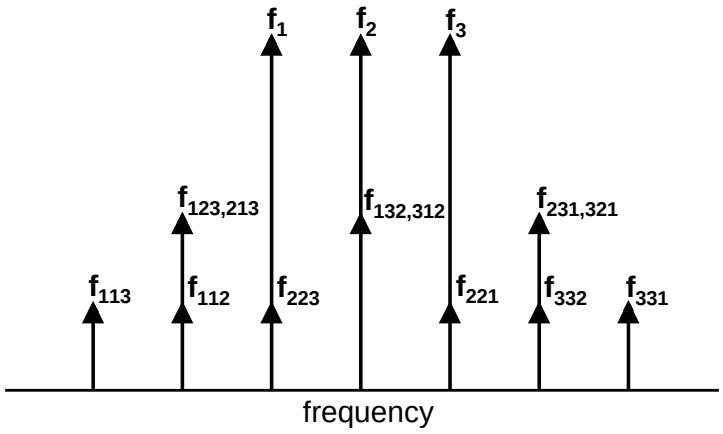

Figure 2.6: The FWM effect for three co-propagating waves

As we can observe some of the FWM products can appear on the frequencies of the initial waves, which can cause cross-talk related penalty. The total number of FWM products N_{PT} generated by the N WDM channels is

$$N_{PT} = \frac{1}{2}(N^3 - N^2). \tag{2.9}$$

Table 2.2 contains the N_{PT} values for 4, 8, 16, and 32 channels. It is clear, that with an increasing number of WDM channels, the number of FWM products grows rapidly.

Table 2.2: Total number of FWM products

N-number of channels	4	8	16	32
N_{PT}-number of FWM products	24	224	1920	15872

The source of FWM in an optical fibre is the Kerr effect. The refractive index n of many optical materials depends on the optical intensity I [23]:

$$n = n_0 + n_2 I, \tag{2.10}$$

where n_0 is the ordinary refractive index of the material and n_2 is the nonlinear coefficient. The optical intensity I can be expressed as P/A_{eff}, where P is the

optical power, and A_{eff} is the mode effective area. In silica fibre, the factor n_2 varies from 2.2 to 3.4 10^{-8} μm^2/W [24]. The typical values of A_{eff} are 80 μm^2 for the standard single-mode fibre, 50 μm^2 for the dispersion shifted fibre, and 20 μm^2 for the dispersion compensating fibre.

The output power of the FWM product, generated at optical frequency f_{ijk} due to the interaction of signals at frequencies f_i, f_j, and f_k is equal to [25,26]

$$P_{ijk}(L) = \eta \frac{1024\pi^6}{n^4\lambda^2c^2}(D_{ijk}\chi)^2 \left(\frac{L_{eff}}{A_{eff}}\right)^2 P_i(0)P_j(0)P_k(0)e^{-\alpha L}, \tag{2.11}$$

where η is the efficiency of FWM, L is the fibre length, n is the refractive index of the fibre, λ is the wavelength, c is the light velocity in free space, D_{ijk} is the degeneracy factor, which has value 3 or 6 for two waves mixing or three waves mixing, χ is the third-order nonlinear susceptibility, $P_i(0)$, $P_j(0)$, and $P_k(0)$ are the powers of the input signals launched into a single-mode fibre, and α is attenuation of the fibre. The effective interaction length L_{eff}, takes into account power absorption along the fibre and assumes the power is constant over a ceratin fibre length, is given by [24]

$$L_{eff} = \frac{1 - e^{-\alpha L}}{\alpha}. \tag{2.12}$$

The efficiency η of FWM is defined as

$$\eta = \frac{\alpha^2}{\alpha^2 + \Delta\beta^2}\left[1 + \frac{4e^{-\alpha L}\sin^2\left(\frac{\Delta\beta L}{2}\right)}{\left(1 - e^{-\alpha L}\right)^2}\right], \tag{2.13}$$

where the phase mismatch $\Delta\beta$ is equal to [27]

$$\Delta\beta = \beta(f_i) + \beta(f_j) - \beta(f_k) - \beta(f_{ijk}). \tag{2.14}$$

Here β indicates the propagation constant. After expanding $\Delta\beta$ in a Taylor series we get

$$\Delta\beta = \frac{2\pi\lambda^2}{c}(f_i - f_k)(f_j - f_k)\left[D(f_0) - \{(f_i - f_0) + (f_j - f_0)\}\frac{\lambda^2}{2c}D'(f_0)\right], \tag{2.15}$$

where $D(f)$ is the chromatic dispersion coefficient, and $D'(f)$ is the chromatic dispersion slope.
For $D(f_0) = 0$, (f_0 is a zero dispersion frequency) we get

$$\Delta\beta = -(f_i - f_k)(f_j - f_k)\{(f_i - f_0) + (f_j - f_0)\}\frac{\pi\lambda^4}{c^2}D'(f_0), \tag{2.16}$$

and for $D'(f_0) = 0$ (constant dispersion value) we get

$$\Delta\beta = (f_i - f_k)(f_j - f_k)D(f_0)\frac{2\pi\lambda^2}{c}. \tag{2.17}$$

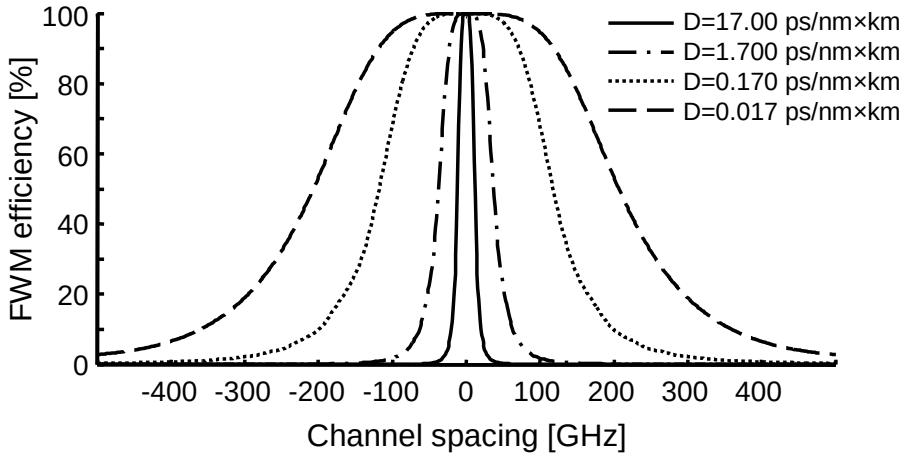

Figure 2.7: Calculated FWM efficiency vs. channel spacing for different values of chromatic dispersion

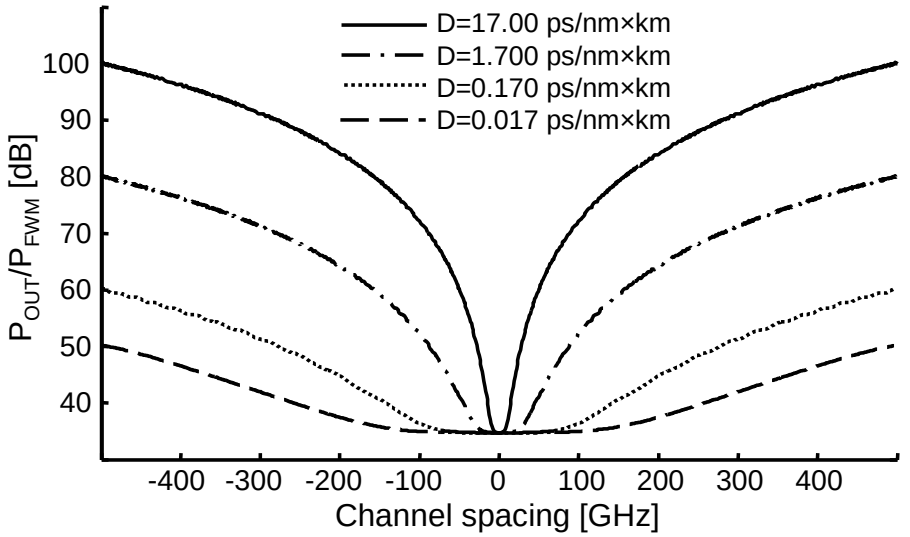

Figure 2.8: Calculated P_{out}/P_{FWM} vs. channel spacing for different values of chromatic dispersion; P_{IN}= +3 dBm

FWM in the optical fibre depends on the fibre parameters like dispersion and effective mode area, as well as also system parameters like wavelength, channel spacing, and the signal input power.

Figures 2.7 and 2.8 illustrate the effect of fibre dispersion and channel spacing on the four-wave mixing effect. Figure 2.7 presents, based on Equations 2.13–2.17, the calculated FWM efficiency at 1310 nm versus the channel spacing for different values of chromatic dispersion of the 50 km long fibre. Fibre parameters are from [24].

Figure 2.8 shows the calculated ratio of the transmitted power to the FWM products ($f_{132,312}$) power as a function of channel spacing for four different values of dispersion for the same fibre link.

Large channel spacing significantly reduces FWM. Moreover, a high value of dispersion can effectively suppress FWM generation. However, in the wavelength band 1306 to 1319 nm the absolute dispersion value varies between 0 and 1.7 ps/nm×km. As it can be seen, quite small absolute values of dispersion ($<$0.17 ps/nm×km) can have a dramatic effect. For such small values of dispersion large channel spacing ($>$200 GHz) has to be adopted.

Equation 2.11 shows that the power of the FWM products depends strongly on the power of the initial wavelengths. Figure 2.9 presents the calculated, using Equation 2.11, ratio between the power of the output signal and the power of the FWM products $f_{132,312}$ versus the power of the input signal for different values of the FWM efficiency. It can be seen that for the input power in the range of a few dBm, FWM can cause severe cross-talk in transmitted data channels. However, for the input power below 0 dBm or the FWM efficiency $\leq$10%, the FWM cross-talk will be significantly reduced.

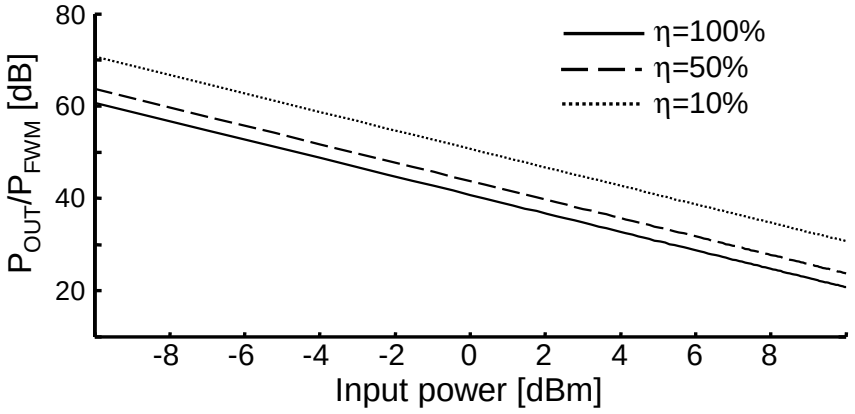

Figure 2.9: Calculated P_{out}/P_{FWM} vs. the input power for different values of FWM efficiency

Figure 2.10 shows another example of a three channel system. In contrast to the three channel system presented in Figure 2.6 the spacing between adjacent channels is not equal. The spacing between channels one and two, is twice the spacing between channels two and four. It can be observed that none of the FWM products appear on the WDM channels. This example shows us that it is possible to find a specific channel allocation scheme, in which none of the FWM products will appear on the WDM channels. Such a channel allocation scheme is called an unequal channel spacing allocation scheme.

To realize an unequal channel spacing allocation scheme, the frequency separation between each pair of WDM channels must be different [28]. This method is a generalization of what had been proposed in the 1950's to reduce the effect of

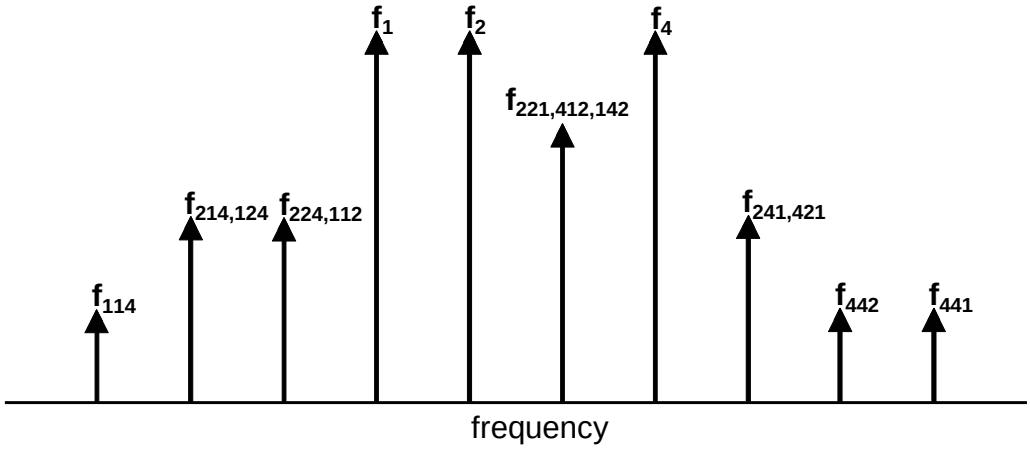

Figure 2.10: The FWM effect for three co-propagating waves with unequal channel spacing

third-order intermodulation interference in radio systems [29] and is also commonly applied in CATV coaxial cable systems. In general, for any number of WDM channels several unequal channel spacing allocation schemes exist. Table 2.3 summarizes optimal solutions for 3, 4, 8, and 16 WDM channels. Unequal channel spacing allocation schemes were optimized taking into account the occupied bandwidth. The spacing between adjacent channels is expressed in auxiliary units [a.u.]. One unit is equal to the minimum channel spacing between two adjacent channels.

Table 2.3: Examples of an unequal channel spacing allocation scheme

N	Spacing between adjacent channels [a.u.]	Bandwidth [a.u.]
3	1, 2	3
4	1, 3, 2	6
8	1, 3, 5, 6, 7, 10, 2	34
16	1, 3, 7, 25, 6, 24,1 2, 8, 39, 2, 17, 16, 13, 5, 9	177

The unequal channel spacing allocation scheme can be bandwidth inefficient in the case of large channel numbers (8, 16, ...). The bandwidth occupied by WDM channels allocated according to the presented schemes can be very large in comparison with equal channel spacing allocation schemes. However, it depends on the system design parameters, namely a channel allocation grid.

The channel allocation grid is based on the *Minimum-Channel-Spacing* determined by the wavelength resolution of the applied wavelength multiplexing technique, e.g. an arrayed waveguide grating or a passive fibre coupler in combination with band-pass filters. To achieve sufficient suppression of the FWM products for the given input power in the equal channel spacing allocation scheme, the *Required-Channel-Spacing* is necessary. When *Required-Channel-Spacing*=*Minimum-Channel-Spacing*,

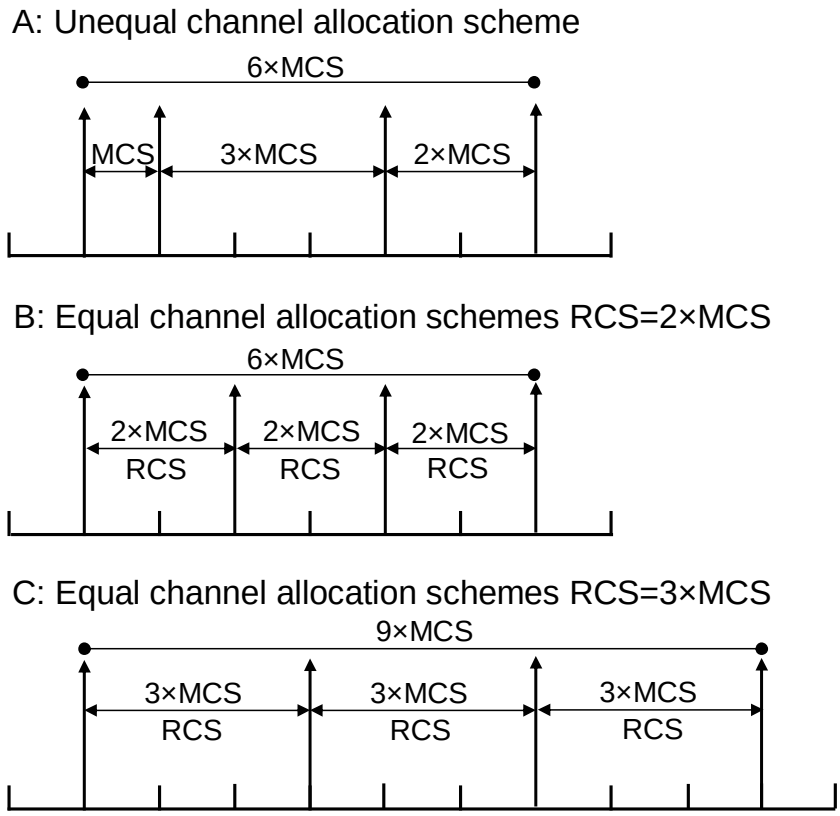

Figure 2.11: Comparison between equal and unequal channel spacing allocation schemes; four data channels, *MCS-Minimum-Channel-Spacing and RCS-Required-Channel-Spacing*

the unequal channel spacing allocation scheme is not necessary.

For the four channel system with *Required-Channel-Spacing=2×Minimum-Channel-Spacing* both allocation schemes will occupy the same bandwidth, Figure 2.11a-b. However, for *Required-Channel-Spacing=3×Minimum-Channel-Spacing*, the unequal channel spacing allocation scheme will be more bandwidth efficient, Figure 2.11a, c. Therefore in four channel systems with *Required-Channel-Spacing >2×Minimum-Channel-Spacing* the unequal channel spacing allocation scheme is more bandwidth efficient. In the case of the eight channel system, the unequal channel spacing allocation scheme will occupy bandwidth of 34×*Minimum-Channel-Spacing*. Hence the unequal channel spacing allocation scheme will require *Required-Channel-Spacing>5×Minimum-Channel-Spacing* to be more bandwidth efficient. The 16 channel system will required bandwidth equal to 177×*Minimum-Channel-Spacing* to eliminate virtually FWM and *Required-Channel-Spacing>11×Minimum-Channel-Spacing* to be more bandwidth efficient.

In the case of systems, with large number of channels (8, 16, ...) another solution can be applied to alleviate the FWM effect. The repeated unequally spaced

channel allocation scheme guaranties sufficient suppression of FWM products while is more bandwidth efficient in comparison with the unequal channel spacing allocation schemes [30, 31]. The proposed solution is based on periodical allocation of the unequally spaced channels. Figure 2.12 shows an example of such an allocation scheme.

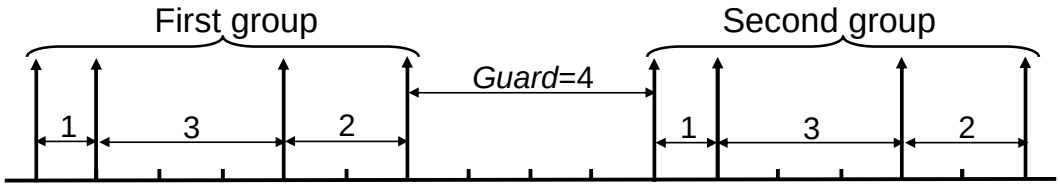

Figure 2.12: Example of the repeated unequally spaced channel allocation scheme

The first group of channels is formed by four unequally spaced channels with the grid sequence 1-3-2. The first channel group is separated from the second group of unequally spaced channels, with the same channel grid 1-3-2, by a guard band *Guard* equal to 4. The FWM products generated within the single channel group do not appear at the data channels (the unequal channel spacing allocation scheme). The FWM products generated due to interactions between channels in different groups may occur at the data channels. However, these products are insignificant due to the low efficiency of the FWM effect caused by a large channel spacing equal to at least *Guard*. Groups of the unequally spaced channels separated by the guard band can be repeated over the available wavelength band.

The resulting channel allocation scheme is more efficient than in the case of the unequal channel spacing allocation scheme. For example, the unequally spaced eight channel system will occupy bandwidth of 34. The eight channel system with the repeated unequally spaced channels based on a grid sequence 1-3-2-(*Guard*=4) will occupy bandwidth of 16. Therefore the bandwidth efficiency will be improved of about 50%. Using the same concept, bandwidth utilization will be improved 75% in the case of the 16 channel system.

It has to be stressed that the mentioned above channel allocation schemes have to be applied only in the systems with the high input power. When a limited transmission distance is required, the optical power can be limited to the levels where the FWM effect is insignificant. Therefore it is a matter of particular application which channel allocation grid will be applied.

2.2 Semiconductor optical amplifier

2.2.1 Amplification technologies

The optical signal propagating through the optical fibre suffers from attenuation, see Section 2.1.1. To increase transmission distance and to prevent optical-electrical-optical conversions all-optical amplification is necessary. In general, three optical amplifier technologies are available: a Raman amplifier, a doped fibre amplifier (DFA), and a semiconductor optical amplifier (SOA).

The Raman amplifier relies on nonlinear interaction in the optical fibre. The doped fibre amplifier and the SOA are based on stimulated emission phenomena. Stimulated emission requires an optical pomp in the case of the fibre amplifier or an electrical pomp in the case of the SOA. The Raman amplifier and the doped fibre amplifier suffer from the complexity and high cost. But, they show excellent transmission properties, i.e. high gain, low noise figure, and high saturation output power as well as due to the large time constant are less pattern depended for the bit rates in range of Gbit/s. The SOA shows less ideal transmission properties, i.e. lower gain, higher noise figure, lower saturation output power, and is pattern depended at bit rates in the range of Gbit/s due to the short time constant. However, this is compensated by advantage such as low cost, small size, coverage of the whole fibre low-loss transmission band, and high potential for photonic integration. The SOA is approximately two times cheaper than the doped fibre amplifier. The Raman pomp costs approximately ten times more than the semiconductor optical amplifier. In addition, the SOA can be used as a functional device to realize on-chip amplification, wavelength conversion, optical memories etc. It has to be mentioned that the amplification applications favour amplifiers with the large time constant (continuous operation) due to the lack of pattern effects. However, in the switching applications the small time constant is preferred (instantaneous operation).

On the whole, all three amplification technologies are available in the 1310 nm wavelength domain. The praseodymium-doped fibre amplifier (PDFA) is the fibre amplifier operating in the 1310 nm wavelength domain. The main drawbacks of the PDFA are low conversion efficiency and coupling losses. Nevertheless, experiments showed transmission using the PDFA in combination with the Raman amplifier [32]. However, due to the high cost the PDFA market penetration and market prospect is low. Another doped fibre amplifier operating in the 1310 nm wavelength domain is a bismuth-doped silica fibre amplifier [33]. The advantages of the Bi-doped silica fibre amplifier are 300 nm wide amplification bandwidth, very common 800 nm lasers can be used for excitation of this medium, and it can be easily spliced to the silica fibre. However, the Bi-doped silica fibre amplifier is in a very early stage of development and shows only very limited gain of less than 6 dB [34]. Therefore the focus will be the SOA as the most promising and interesting candidate for the applications in the 1310 nm wavelength domain.

2.2.2 Operation of the SOA

The SOA can be regarded as a semiconductor laser diode without reflective mirrors at its facets. Laser oscillations are prevented by applying low reflectivity coatings, angled facets, and a buried-facet structure. The structure of an SOA is similar to a laser diode structure. A bulk active layer, multiple quantum well (MQW), or quantum dot (QD) active layers are used in the SOA structure. A bulk SOA has one single active layer. A MQW structure consists of a sandwich of different layers. A QD SOA has an active layer comprising quantum dots. The typical dimensions of the MQW SOA active area are: width 3 μm, height 0.08 μm, and length 500 μm.

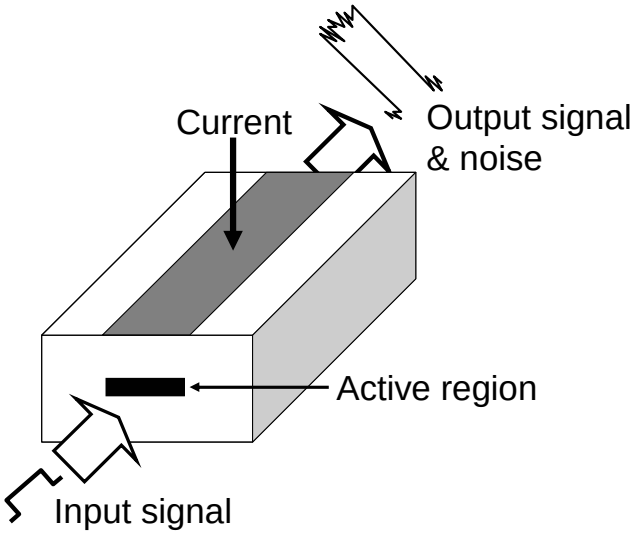

Figure 2.13: The SOA schematic diagram

Operation of the SOA can be modelled by the following equations [35,36]:

$$\frac{dN}{dt} = \frac{I}{q} - \frac{N}{\tau_e} - \frac{F(N)}{E}P_{in}, \tag{2.18}$$

$$F(N) = \beta\frac{e^{(\beta-\alpha_{int})L}-1}{\beta-\alpha_{int}} = (G-1)\left(1+\frac{\alpha_{int}L}{\ln G}\right), \tag{2.19}$$

$$\beta = \frac{\Gamma a}{AL}(N-N_{tr}), \tag{2.20}$$

$$G = e^{(\beta-\alpha_{int})L}, \tag{2.21}$$

$$P_{out} = GP_{in}, \tag{2.22}$$

$$\phi(t) = \frac{2\pi\Gamma n_{eh}}{\lambda A}N, \tag{2.23}$$

where N is the SOA carrier number, I is the SOA injection current, q is the electronic charge, τ_e is the carrier lifetime, P_{in} is the optical input power, E is the energy of a

photon at wavelength λ, G is the SOA gain, α_{int} represents the SOA intrinsic losses, L is the SOA length, N_{tr} is the carrier number at the SOA transparency, where the SOA losses are compensated by gain of the SOA, Γ is the confinement factor, which defines fraction of the optical beam transmitted in the optical waveguide, A is the SOA active region area, a is the gain coefficient, n_{eh} is the refractive index change per carrier pair and λ is the wavelength of the light signal.

When the SOA is pumped electrically with an external injection current, population inversion will take place. The SOA's active medium will provide gain to an externally injected optical signal falling within the gain bandwidth of the amplifier. Under high optical injection the population inversion will be reduced due to the carrier depletion by the stimulated emission and the spontaneous emission. As a consequence the SOA gain depends on the internal optical intensity, and the output signal will eventually saturate. In multi-channel systems, gain saturation caused by one channel modifies response of the other channels, introducing crosstalk between channels. Furthermore, the amplified optical signal has a slowly time-varying phase with respect to the phase of the input optical signal, which is given by $\phi(t)$.

The SOA recovery time expresses the speed with which the SOA carrier number returns to the initial value after removal of the injected optical signal. Figure 2.14 visualizes simulated, based on Equations 2.18–2.22, the output signal and the carrier number in the case of injection of a very short pulse. The input optical pulse is

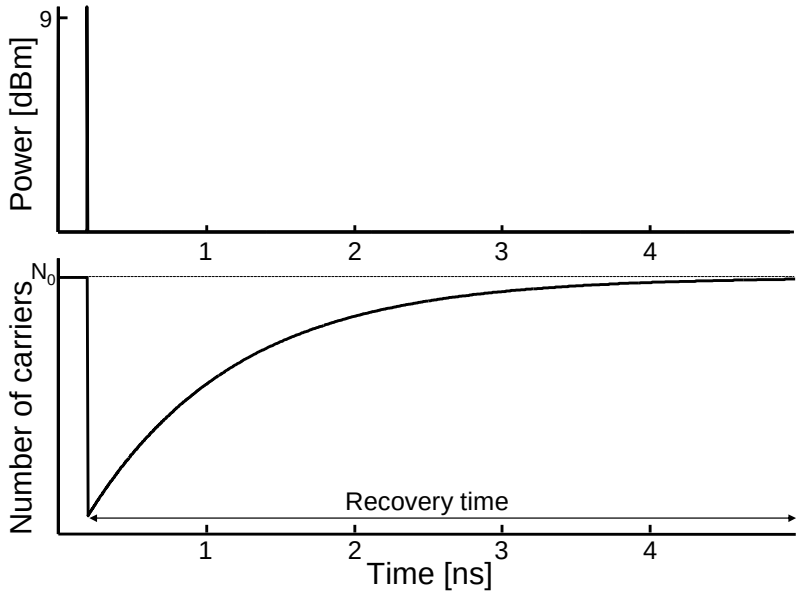

Figure 2.14: Calculated response of the SOA to the very short pulse

amplified. First, the carrier number decreases and then recovers to the initial value N_0. Taking into account that the gain of the SOA depends on the carrier number, following pulses will experience smaller gain, especially in the case of significant depletion of carriers. Therefore the SOA recovery time can limit the repetition rate

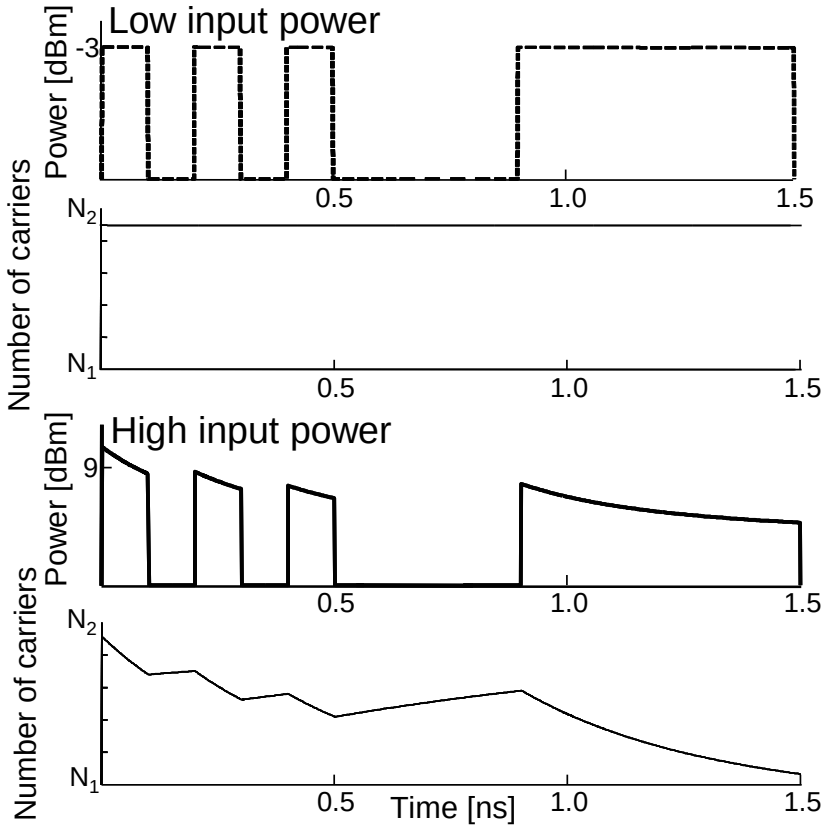

Figure 2.15: Simulated response of the SOA to the random data signal

of the optical signals injected into the SOA. Typical values of the SOA recovery time are in the range of several tens to several hundreds of picoseconds.

Many approaches have been shown to reduce the SOA recovery time. The most straightforward approach is based on increase of the SOA current. But this is limited by the maximum value of the SOA current. It has been shown that the long SOAs have shorter recovery time [37]. The SOA recovery can also be accelerated by injection of an external holding beam [38]. However, it is difficult to achieve the SOA recovery in order of few picoseconds using these techniques [39]. Another approach is utilization of pattern-effect-free quantum dot semiconductor optical amplifiers [40].

Figure 2.15 shows simulated response of the SOA for two different input signals. Please note that the carrier number "Y" axes have the same scale. When power of the input signal is low, the SOA is unsaturated and the signal is amplified without distortions. This is because the carrier number is insignificantly affected by the incoming signal and in principle the same gain is provided to the whole data pattern. Therefore the SOA output signal is an exact replica of the input signal.

However, at high input power the output signal is distorted. The carrier number is significantly affected by the incoming optical signal and therefore gain varies signif-

icantly in time. When an optical signal is injected into the SOA, the carrier number decreases. However, when there is no optical signal injected into the SOA the carrier number recovers, providing more gain to the incoming data signal. These gain variations depending on the data pattern cause the pattern effect. The pattern effect is a source of distortions and crosstalk in the SOA output signal. Therefore to prevent signal degradation due to the pattern effect, operation in the linear amplification regime (low input power) is required.

The spontaneous recombination of electrons and holes in the amplifier medium is a source of an amplified spontaneous emission (ASE) noise. The total power of the ASE noise for both polarizations can be expressed as [41]

$$P_{ASE} = 2n_{sp}(G-1)h\nu B_0, \tag{2.24}$$

where n_{sp} is the spontaneous emission factor, h is Planck's constant, ν is the light frequency, and B_0 is the spontaneous emission bandwidth. The ASE noise is a dominant noise source in the SOA and causes several noise components after detection in the receiver: shot noise, signal-spontaneous beat noise, and spontaneous-spontaneous beat noise [41].

A figure of merit describing degradation of the signal-to-noise ratio (SNR) through passage of an optical amplifier is the noise figure, NF, defined as [17]

$$NF = \frac{SNR_{in}}{SNR_{out}}. \tag{2.25}$$

The SNR is referred to the output of an ideal photodetector and only the following photocurrent noise terms are taken into account: the signal shot noise and the signal-spontaneous beat noise. Hence, the noise figure can be expressed [17]

$$NF = \frac{1 + 2n_{sp}(G-1)}{G}. \tag{2.26}$$

When G is large the noise figure becomes $NF = 2n_{sp}$. The minimum value possible for n_{sp} is 1. Hence, the noise figure of an ideal optical amplifier is 2 (3 dB). The SOA noise figure is usually between 7 and 10 dB.

The optical signal-to-noise ratio (OSNR) at the output of a chain of M amplifiers is [42]

$$OSNR = \frac{P_{out}}{NFGh\nu B_0 M}, \tag{2.27}$$

where P_{out} is the output power per channel, NF is the amplifier noise figure, G is the amplifier gain, h is the Planck's constant, ν is the light frequency, and B_0 is the optical bandwidth [Hz]. The OSNR in [dB] can be written as

$$OSNR[dB] = P_{out} - L_S - NF_{dB} - 10\log M - 10\log[h\nu B_0], \tag{2.28}$$

where all terms are in dB and it is assumed that each amplifier is compensating for the loss of the previous span $G = L_S$. From Equation 2.28 it can be concluded

that the OSNR declines with the number of amplifiers in the transmission line. Furthermore, the OSNR increases with the output power of the signals launched into the transmission line. However, high input power may lead to increased influence of saturation effects as well as nonlinear effects in the fibre. Hence, a trade-off exists between the OSNR after the transmission line and saturation effects in the optical amplifier as well as nonlinear effects in the fibre. In the amplifier chain the ASE noise contributes not only to the OSNR reduction but also to the saturation of the following optical amplifiers.

An important practical remark is that for the proper operation the SOA requires optical isolators at the input and at the output. The isolator at the SOA output prevents saturation of the SOA from the back-coming signals, e.g. the ASE noise from the following SOAs or the reflected signals. The isolator at the input prevents the ASE noise from being sent back along the link. In the system without signal reflections in the transmission path just one isolator at the SOA input or output will prevent unwanted SOA saturation.

2.2.3 Static characteristics of the SOA

The most important parameters characterizing optical amplifiers are: gain, saturation output power, noise figure, amplification bandwidth, and polarization sensitivity. At a high output power, the SOA gain is saturated and compressed. A common parameter for quantifying gain saturation is the 3 dB saturation output power P_{sat}. The P_{sat} is defined as the amplifier output power at which the amplifier small signal gain is reduced two times (has dropped with 3 dB). The amplifier gain can be written implicitly as a function of the output power P_{out} to the P_{sat} [17]

$$G = G_0 \exp\left[-\frac{G-1}{G}\frac{P_{out}}{P_{sat}}\right], \tag{2.29}$$

where G_0 is small signal gain. The typical gain versus the output power characteristics of the SOA is presented in Figure 2.16.

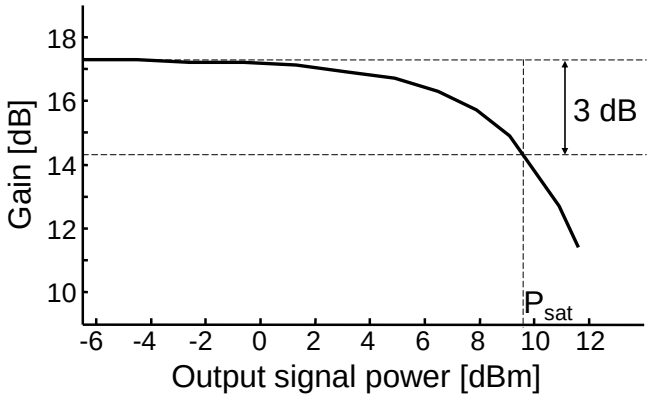

Figure 2.16: SOA gain versus the output power characteristics

The typical optical amplification bandwidth of the 1310 nm SOA is presented in Figure 2.17. The estimated 3 dB optical amplification bandwidth is about 70 nm. The short wavelength tail of the gain profile saturates faster and therefore provides less gain, which is caused by lower density of carriers in the conduction band corresponding to higher energy levels. Hence, the long wavelength tail of the SOA gain profile should be used as the operating regime in the amplification applications. However, in the applications like wavelength conversion based on cross-gain modulation operation with shorter wavelengths is preferred due to the pronounced saturation [43].

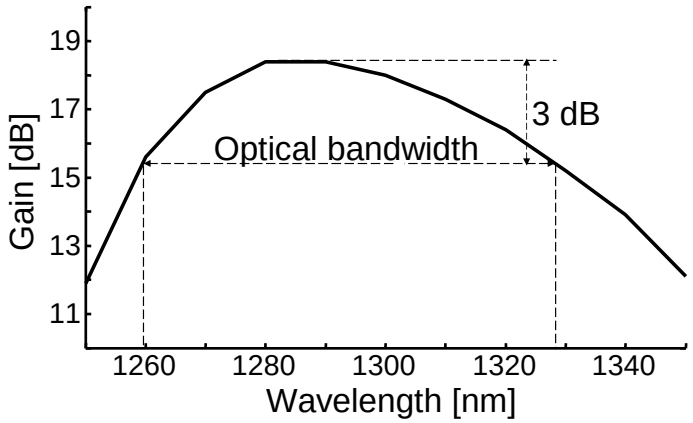

Figure 2.17: SOA gain versus wavelength characteristics

The polarization state of the input signal can vary with time and wavelength. Due to the waveguide structure and the gain material the SOA is polarization dependent. Cascading of the SOA can pronounce the polarization dependence. The polarization sensitivity is defined as the ratio between provided gains for the orthogonal polarization modes. Polarization insensitivity is a desirable feature. Several techniques for realizing the SOA with low polarization sensitivity ($<$1 dB) have been developed, for example, square cross-section waveguide, ridge waveguide, and strained-layer superlattice structure. Polarization sensitivity of the SOA is undesirable in the transmission applications. However, in the Chapter 2 the SOA polarization sensitivity will be explored to realize all-optical signal processing.

Table 2.4 summarizes measured values of the bulk SOA parameters. The parameters were measured with the nominal SOA current of 300 mA. All parameters except the gain peak were measured at 1310 nm. The characterized SOAs showed gain between 13.6 and 19.4 dB, saturation output power between 9.0 and 13.0 dBm and NF between 7 and 9 dB. The SOAs with low gain and high saturation power can be used as booster amplifiers. The SOAs with high gain, moderate saturation output power, and low NF can be used as in-line amplifiers or pre-amplifiers.

Table 2.4: Measured values of bulk SOA parameters

SOA Symbol	Gain [dB]	P_{SAT} [dBm]	Gain Peak [nm]	Pol. Dep. <1	NF
#1	18.5	9.0	1300	<1	7
#2	17.4	9.0	1300	<1	8
#3	13.6	11.0	1280	<1	9
#4	14.6	13.0	1280	<1	8
#5	18.8	10.0	1280	<1	8
#6	14.0	13.0	1280	<1	9
#7	14.0	13.0	1290	<1	9
#8	18.8	10.6	1290	<1	9
#9	22.7	9.0	1300	<1	9
#10	20.7	11.5	1290	<1	8

2.2.4 Dynamic operation of the SOA

In the previous sections the ASE noise, the polarization dependent gain, and the saturation effects were pinpointed as a main source of the signal distortions in the SOA. Here, the dynamic operation of the SOA will be evaluated in detail by means of bit error ratio (BER) measurements.

Single channel dynamic operation of the SOA

A single channel test setup is presented in Figure 2.18.

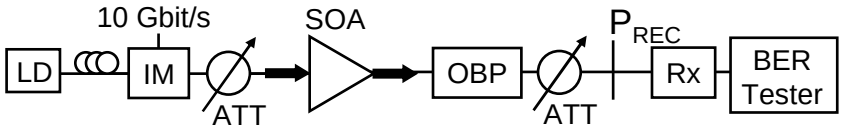

Figure 2.18: Single channel experimental setup

The setup consisted of a continuous wave (CW) laser diode (LD) operating at 1311.5 nm. The CW laser signal was modulated at 10 Gbit/s with the pseudo-random bit sequence (PRBS) of length $2^{31} - 1$. After an intensity modulator (IM), a variable attenuator (ATT) was placed to adjust the SOA input power level. The isolators at the SOA input and output were used to eliminate unwanted signal as well as the ASE noise reflections. After the SOA, operating with current 200 mA at temperature 25°C, an optical bandpass filter (OBP) was placed to reduce the ASE noise. The power of the data signal P_{REC} was measured by a power meter directly before a 10 Gbit/s receiver. By adjusting the first ATT different levels of the SOA input (output) power were obtained. The second ATT was used to measure BER.

The SOA operation point was set to demonstrate both noise and saturation effects. Operation with the low output power refers to pre-amplification applications

where the ASE noise is a source of penalties. Operation with the high output power refers to booster applications. In-line amplification is characterized by the moderate output power. Obviously, in booster and in-line applications distortions due to the pattern effects should be limited.

Figure 2.19 presents the measured gain and the power penalty at BER=10^{-9} versus the output power. Figure 2.20 shows captured eye diagrams. The measured SOA gain was 18.2 dB and the P_{SAT} measured with the nonreturn-to-zero (NRZ) signal was 5.7 dBm. In the case of the low output power, the data signal was affected by the ASE noise and suffered from the OSNR reduction, see Figure 2.20b. The OSNR value for the output power equal to -6.3 dBm was 23.8 dB and 18.8 dB for the output power equal to -11.2 dBm.

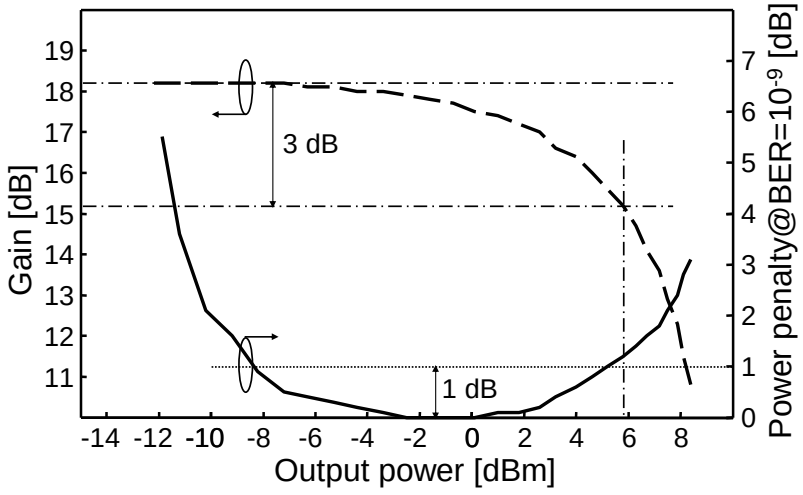

Figure 2.19: Results of single channel measurements: gain and the power penalty vs the output power

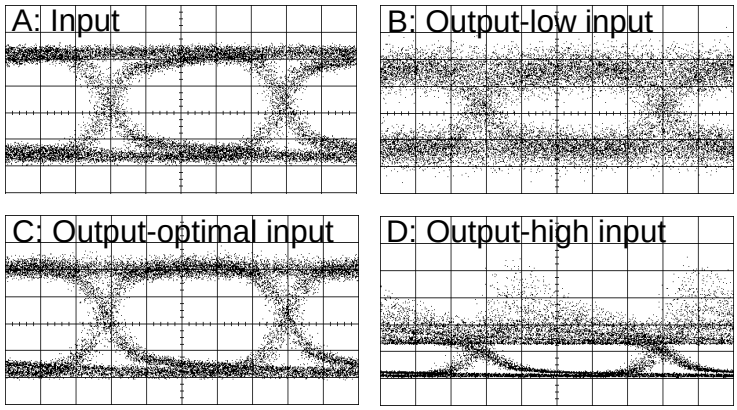

Figure 2.20: Measured eye diagrams: (a) SOA input signal, (b-d) SOA output signals for different values of the input signal power

The signal with the high output power suffered from pattern effect related distortions, see Figure 2.20d. The OSNR for the input power >-18 dBm was higher than 30 dB. As shown in Figure 2.15 and Figure 2.20d, the pattern effect occurs in the "1" rail. The eye centre remained unaffected. Therefore after proper adjustment of the decision threshold in the receiver, operation with the small power penalty can be achieved even for the operation in saturation. The power penalty at 3 dB gain reduction was ≈1 dB. The low power penalty (< 1dB) operation range was stretched over 14 dB range of the output power and was limited in the linear amplification regime by the ASE noise related distortions.

Using another SOA (#10) similar results were achieved in the saturation tail, i.e. the 1 dB power penalty occurred approximately at 3 dB gain reduction. However, the 1 dB power penalty in the ASE tail was shifted into the linear regime of amplification. This can be explained by the fact that a new SOA had better NF, namely 8 dB instead of 9 dB. Therefore the low power penalty (< 1dB) operation range was stretched over 17 dB dynamic range of the output power.

In the presented experiments the low power penalty operation range in the saturation regime was limited by the 3 dB gain reduction point. In the linear amplification regime the low power penalty operation range depended on noise of the SOA. To maximize quality of the output data signal operation in moderate saturation was desirable.

Multi-channel dynamic operation of the SOA

In the experiment presented, single channel operation was investigated. In the next experiment, multi-channel operation was verified where the investigated data signal was influenced by the additional data channels. First, the setup used in the previous experiments was modified, see Figure 2.21.

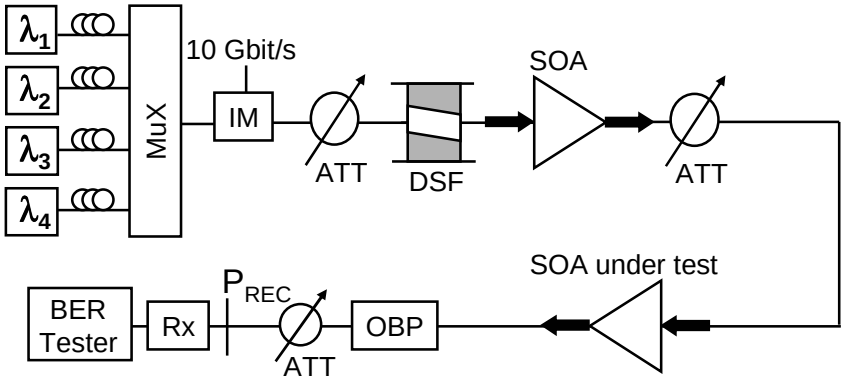

Figure 2.21: Multi-channel experimental setup

Besides the three extra lasers operating at 1312.9 nm, 1314.3 nm, and 1315.6 nm, the 5 km long dispersion shifted fibre (DSF) as well as the SOA were added. The DSF had an absolute dispersion value of 17 ps/nm×km and partially decorrelated

the data channels without causing dispersion related signal distortions. The booster SOA compensated for the losses in a wavelength multiplexer, a modulator, and the DSF. Moreover, the booster SOA allowed to achieve the high input power injected into the SOA under test.

Figure 2.22 visualizes results of the performed measurements. As a reference single channel measurements were used. It is clear from the presented results, that the single channel and the four channels experienced approximately the same gain and the same power penalty in the operation with low input power where the impact of the ASE noise dominates. However, the single channel and the four channel operation differed significantly in the saturation regime.

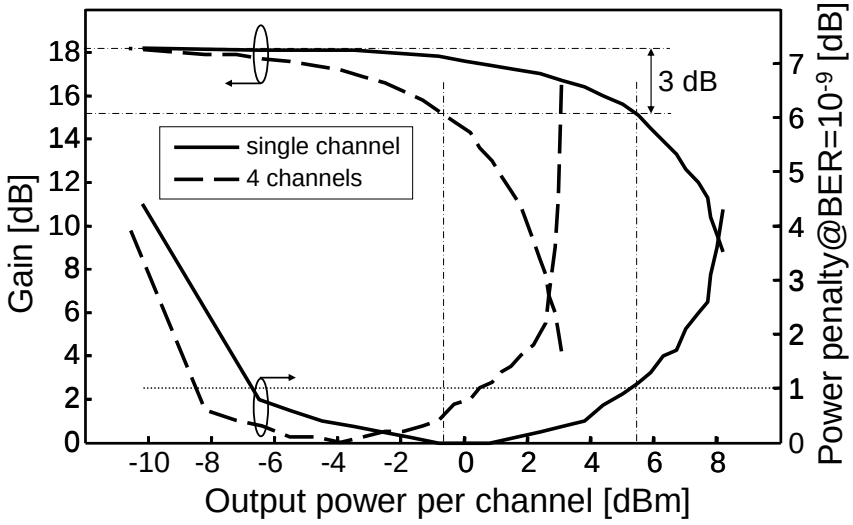

Figure 2.22: Results of multi-channel measurements: gain and the power penalty vs the output power

First, the gain saturation occurs much faster in the case of multi-channel operation. In the presented experiment, the P_{SAT} of the multi-channel operation was 6 dB lower than in the case of the single channel operation. This agrees with the fact that the four channels have 6 dB more power than one channel and gain of the SOA depends on the total optical power in the SOA. Approximately the same happened to the 1 dB power penalty output power in the saturation regime. The total low power penalty ($<$ 1dB) operation range in the case of four channel operation reduced approximately 3 dB in comparison with the single channel operation.

In short, the single and multi-channel operation had similar penalty in low input (output) power (linear amplification) regime. However, they diverge in the saturation regime. The optimum operation occurred approximately at the 1 dB gain reduction point. It is concluded from the presented results that to achieve optimum operation and to minimize signal distortions in the case of multi-channel operation, the total input power has to be taken into account. Moreover, the SOA can be driven into moderate (1-3 dB) saturation without causing significant signal distortions.

2.3 4×10 Gbit/s transmission experiments

Recently, optical communication systems operating at multi-Gbit/s transmission speed have become increasingly important in local area networks (LANs), metropolitan area networks (MANs) and storage area networks (SAN) [44].

Unrepeated transmission employs amplifiers only in a transmitter and a receiver. The advantage of unrepeated transmission is a lack of in-line amplifiers. This reduces the system cost and simplifies system management. Therefore it is particularly interesting for metro and access range networks. The limitation here is the transmitter output power and the sensitivity of the receiver. The difference between those two values forms the available power budget and therefore the transmission reach.

This particular cost-effective, high-speed, and high-capacity transmission is especially interesting for the transmission within big city agglomerations like London, or Paris, or in countries with short distances between major cities like the Netherlands or highly industrialized areas like Ruhr Area in Germany. More applications are connections between SAN's massive data processing centres separated by the metro distances or applications where a huge amount of data has to be collected and transported like a system of radio telescopes [45]. Application of the 1310 nm wavelength domain is interesting here because it allows already existing telecom traffic to be kept in the 1550 nm wavelength domain. Therefore the data traffic at 1310 nm can be carried in parallel to the 1550 nm data traffic without any disturbances and changes in the system architecture using an already existing fibre infrastructure. Obviously, this applies only to unrepeated and uncompensated SSMF links, which are in general access and metro links.

The previously reported unrepeated WDM transmission experiment in the 1310 nm wavelength domain (2×10 Gbit/s, 1314.8 nm, and 1316.3 nm) reached the transmission distance of 63.5 km using semiconductor pre-amplifiers [46]. In [47] unrepeated 8×10 Gbit/s (1305.8 nm, 1306.7 nm, 1307.4 nm, 1308.1 nm, 1309.0 nm, 1309.8 nm, 1310.7 nm, and 1311.6 nm) transmission over 141 km is presented. However, it required two complicated and expensive Raman amplifiers. Moreover, the data channels were not demultiplexed in the receiver but only filtered to perform the BER measurements. Here, an unrepeated 4×10 Gbit/s transmission experiment using semiconductor optical amplifiers over 75 km of SSMF will be described.

2.3.1 Experimental setup

Figure 2.23 presents the experimental setup. The experimental setup had three parts: a 4×10 Gbit/s transmitter, a SSMF link, and a 4×10 Gbit/s receiver. In the transmitter, four laser diodes operated in CW conditions at wavelengths 1311.5 nm, 1312.9 nm, 1314.3 nm, and 1315.6 nm. A following arrayed wave-guide grating (AWG) multiplexed all four CW signals in the wavelength domain. Figure 2.24 shows the transmittance characteristics of the applied AWG. The AWG wavelengths were: 1311.5 nm, 1312.9 nm, 1314.3 nm, 1315.6 nm, 1317.0 nm, 1318.4 nm, 1319.8 nm, and 1321.2 nm. The average AWG insertion loss was 3.2 dB. The 3 dB passband

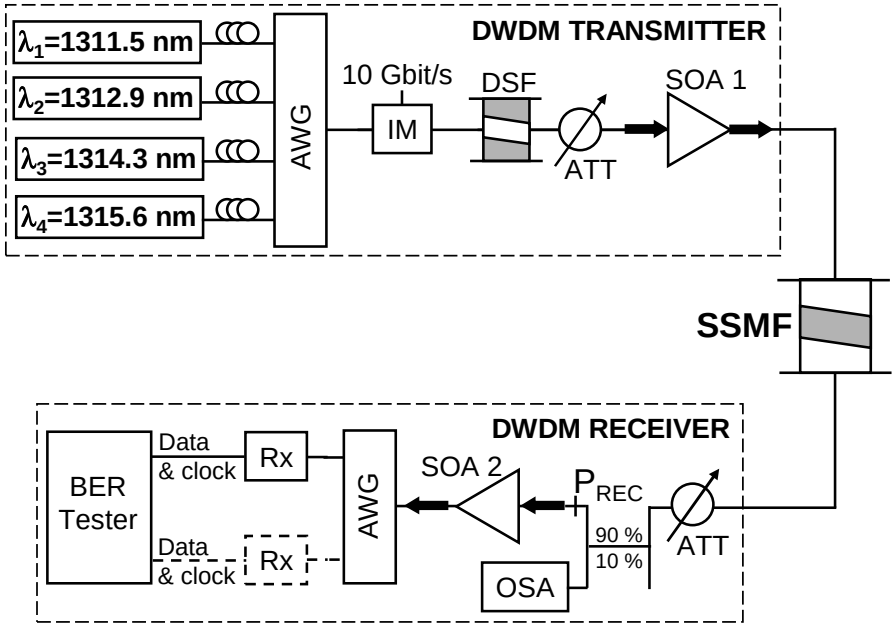

Figure 2.23: Unrepeated 4×10 Gbit/s experimental setup

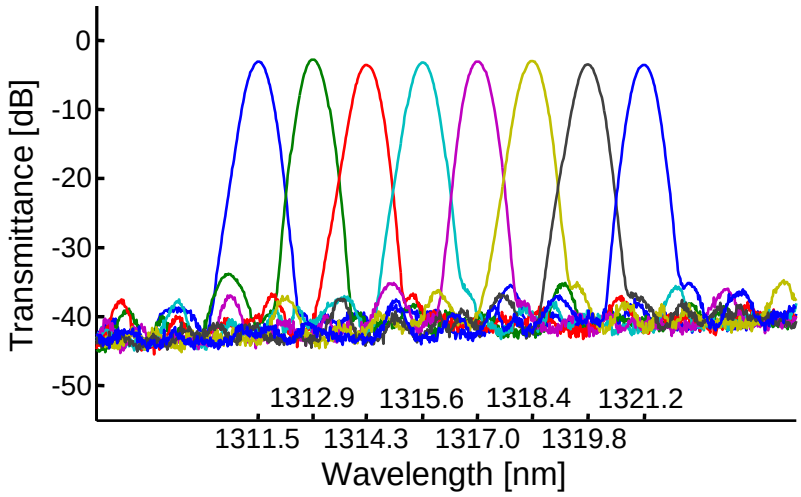

Figure 2.24: Transmittance of the AWG

width was measured to be 0.5 nm. The polarization dependent loss was about 1 dB.

A subsequent Mach-Zehnder intensity modulator (IM) modulated simultaneously all four CW signals at the bit rate 10 Gbit/s with the PRBS of length $2^{31} - 1$. The polarization controllers adjusted the polarization state of the input CW signals to achieve optimal modulation performance. A 5 km long DSF (|D|=17 ps/nm×km)

decorrelated the signals after the modulator. Such a short DSF did not cause any signal distortions related to dispersion. A variable ATT attenuated the modulated signals at the input of an SOA 1 (G = 14.0 dB, P_{sat} = 13.0 dBm, NF = 9) to achieve optimized signals at the SOA 1 output. The SOA 1 operated with the current 400 mA. After the SOA 1 all signals entered a transmission link.

The 12.9 km long SSMF was the basis span of the transmission link. Therefore the total length of the transmission link was a multiple of 12.9 km. The effective length of the transmission link was about 13.5 km. The applied SSMF conformed ITU-T Recommendation G.652. Average fibre attenuation at 1310 nm was 0.32 dB/km, the zero dispersion wavelength 1314 nm, and average dispersion at 1310 nm 0.26 ps/nm×km. However, the measured loss of the 12.9 km long fibre span was a bit higher, ≈4.5 dB due to the connector and splice losses. After the transmission line the data signals entered an optical receiver.

The optical receiver consisted of a variable attenuator, an asymmetrical coupler, a pre-amplifying SOA 2 (G = 20.7 dB, P_{sat} = 11.5 dBm, NF = 8), a demultiplexing AWG, an optical-to-electrical converter with data and clock recovery, and a BER tester. The AWG performed wavelength demultiplexing as well as ASE-cutting. The variable attenuator and the asymmetrical coupler were necessary to perform the BER measurements.

2.3.2 Results and discussion

To establish the power budget two values are necessary, i.e. the transmitter output power and the receiver sensitivity. To minimize SOA saturation effects and maximize the signal quality, the SOA was driven into moderate saturation and the transmitter output power was set to about 0 dBm per channel, see Figure 2.25a. Therefore optimal signals at the transmitter output were achieved, left column in Figure 2.26. In the next step, back-to-back (without a transmission fibre) sensitivity of the receiver was measured. The receiver ATT adjusted power of the optical signals to perform the BER measurements.

Figure 2.27a shows the measured BER in the function of the receiver input power P_{REC} in a back-to-back configuration (without transmission fibre). The average power sensitivity at BER=10^{-9} was -32.4 dBm. The limiting factor was the ASE noise. Taking into account the transmitter output power, the power budget was about 33 dB. Unfortunately, attenuation of the 100 km transmission link was about 38 dB. Therefore the 100 km transmission distance could not be bridged. Driving the SOA into deep saturation will cause penalty related to the saturation effects and FWM in a fibre. Moreover, to perform reliable BER measurements the ATT and the asymmetrical coupler were necessary. As a result, the 75 km long transmission link was utilized in the following experiments.

In the next experiment, the SSMF transmission link was inserted between the transmitter and the receiver. Figure 2.25b presents the optical spectrum measured at the output of the transmission line. The FWM products were not visible. However, after increasing the input power to about +3 dBm per channel the FWM products

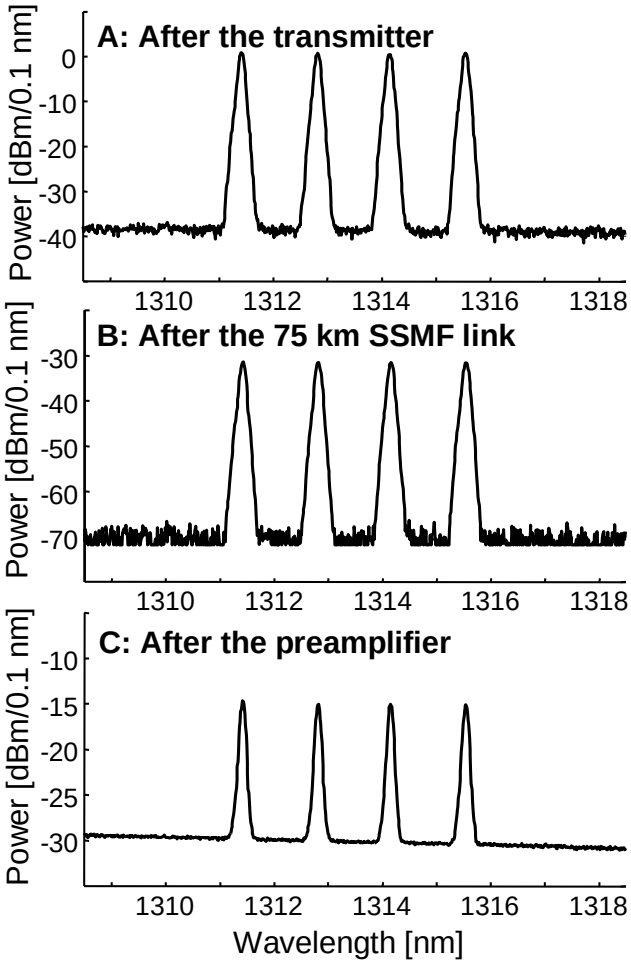

Figure 2.25: Measured optical spectra of unrepeated 4×10 Gbit/s transmission

became visible. Figure 2.25c shows the optical spectrum measured after the preamplifying SOA 2. Due to the low input power, significant OSNR reduction occurred in the SOA 2. As mentioned earlier, the ASE noise and therefore the OSNR reduction limited performance of the receiver. Hence, it is important to apply the amplifiers with low noise figure. The right column in Figure 2.26 shows the eye diagrams measured at the output of demultiplexing AWG. The eye diagrams are clearly open. However, beating of the ASE noise with the data signal is visible in the right column of Figure 2.26.

Finally, the BER performance after the 75 km transmission was measured. The measured average power sensitivity at BER=10^{-9} was -31.8 dBm. Therefore insignificant reduction (0.6 dB) of the receiver sensitivity occurred. No error floor was observed at the measured BER levels. The receiver sensitivity reduction is attributed to the polarization sensitivity of the receiver. The employed SOA 2 polarization sen-

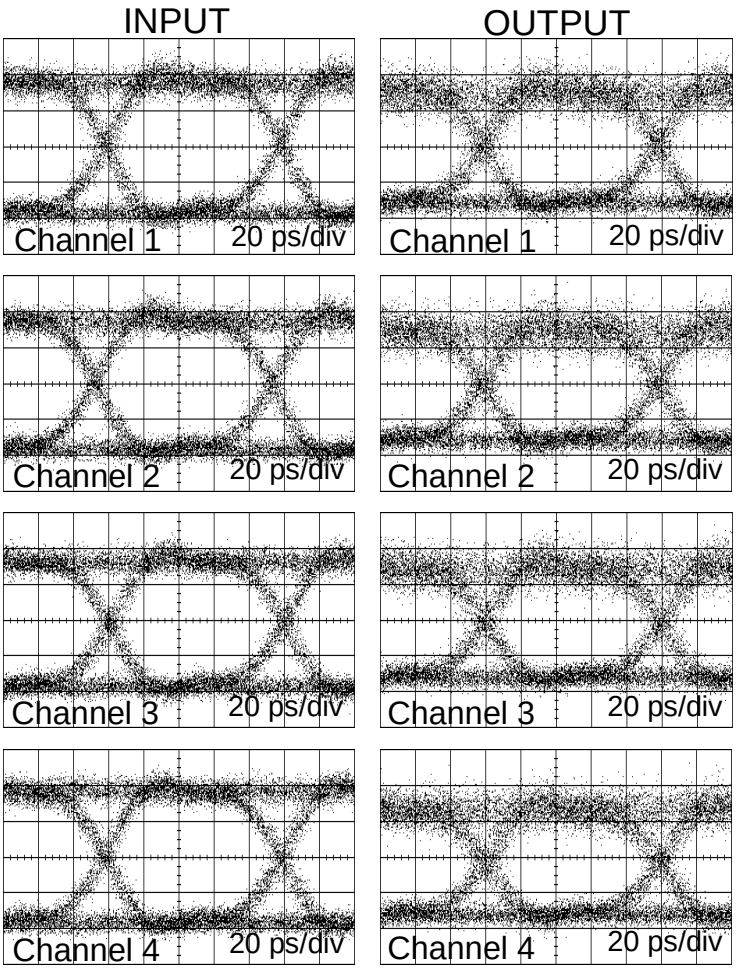

Figure 2.26: Measured eye diagrams of the transmitted 10 Gbit/s data signals

sitivity was about 1 dB. After removing the ATT and the asymmetrical coupler the long term measurements of one channel were performed. No error occurred during 2 days 21 hours 50 minutes long measurement.

To perform BER measurements in the range of 10^{-15} the extremely long measurement time is required. The BER measurement of 10^{-15} in a four channel system will take almost two weeks at 10 Gbit/s. During such long measurements environmental stability play a critical role. Additionally, availability of the laboratory equipment for such a long time period is also a serious limitation. Definitely, such long measurements are performed in the case of commercial systems. In the research work the BER values are usually measured in the range 10^{-12} to 10^{-3}. Moreover, in the research papers the BER value of 10^{-9} is often refereed as an error-free value. Hence, in the next experiments, the BER values were measured exclusively between 10^{-12} and 10^{-3}. Therefore the absence of the error floor will always refer to the measured

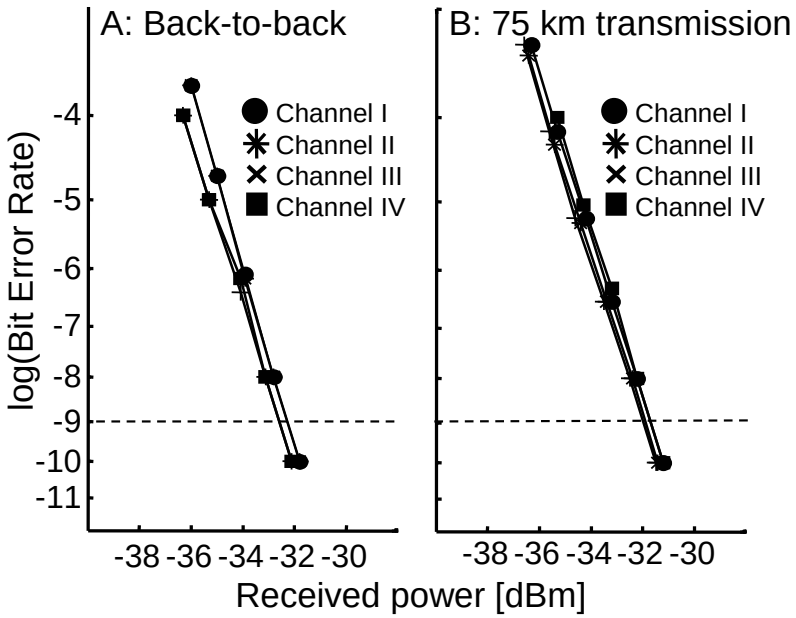

Figure 2.27: Results of 4×10 Gbit/s BER measurements

BER range.

In this section, unrepeated 4×10 Gbit/s transmission was demonstrated in the 1310 nm wavelength domain over the 75 km long SSMF. The presented results show that unrepeated multi-wavelength transmission can be applied to bridge metro distances at 10 Gbit/s. Moreover, using unrepeated transmission the transmission distance previously reported with the repeated transmission [48] was reached. Unfortunately, the 75 km distance is on the edge of what can be reached without dispersion compensation in the 1550 nm wavelength domain. Therefore to fully explore the potential of the 1310 nm wavelength domain, next experiments will concentrate on extended reach repeated 10 Gbit/s transmission and higher bit rate unrepeated transmission in the 1310 nm wavelength domain.

2.4 Extended reach 4×10 Gbit/s transmission experiments

Previously reported 1310 nm semiconductor based WDM systems operated at distances below 100 km [46, 48, 49], therefore not fully exploiting advantages of the transmission in the 1310 nm wavelength domain. The simulation results presented in [50] showed the feasibility of more than 100 km transmission in the 1310 nm wavelength domain using SOAs. However, there was no experimental evidence of that. Here, error-free 4×10 Gbit/s 1310 nm dense WDM (DWDM) transmission using SOAs over 200 km of SSMF will be demonstrated. The whole system has a simplified and cost-effective design.

2.4.1 Experimental setup

Figure 2.28 shows a schematic diagram of the experimental setup.

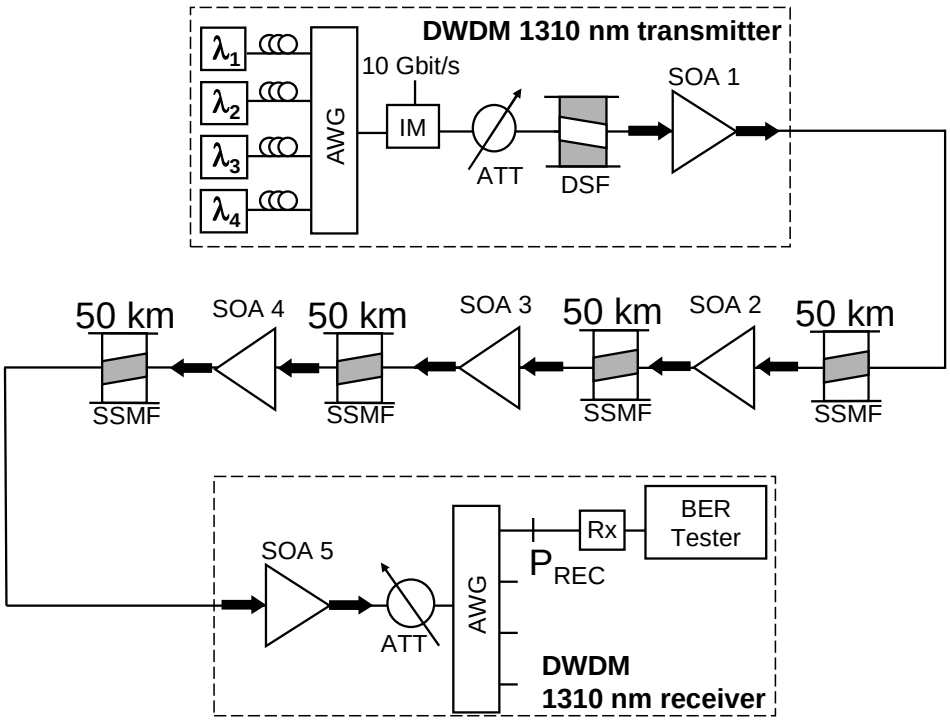

Figure 2.28: Extended reach 4×10 Gbit/s experimental setup

Four low-cost distributed feedback laser diodes (DFB) operating in CW conditions formed the input of a Mach-Zehnder IM. The lasers operated at: 1311.5 nm, 1312.9 nm, 1314.3 nm, and 1315.6 nm following the AWG grid. The external IM modulated all four channels at 10 Gbit/s with the PRBS of length $2^{31} - 1$. After passing through a DSF (total dispersion 42.5 ps/nm), to partially decorrelate the bit-patterns, an SOA booster (SOA 1) amplified simultaneously four 10 Gbit/s DWDM signals. An variable ATT adjusted the SOA 1 input signal level to achieve optimal quality of the signal at the SOA output, i.e. maximized OSNR and reduced saturation effects.

After amplification the DWDM signals entered a 200 km long transmission line. The transmission line consisted of four 50 km long spans of SSMF. The average span loss was 19 dB. The polarization state of the transmitted signals was not controlled in the transmission line. PMD was not influencing the signal quality. The effective length of the transmission line was 13.2×4 [24]. The average power per channel injected into the transmission spans was -3.8 dBm. Therefore the FWM effect was alleviated. Three SOAs (SOA 2–SOA 4) compensated for the transmission losses. Packaged and pigtailed SOAs were used. Table 2.5 summarizes the key parameters of all SOAs used in the experiments.

Table 2.5: Key parameters of the employed bulk SOAs

SOA #	Gain [dB]	Psat [dBm]	Gain Peak [nm]	Noise Figure [dB]
1	14.0	13.0	1290	9
2	19.4	11.1	1290	8
3	20.7	11.5	1290	8
4	19.3	10.2	1290	8
5	18.5	9.0	1300	7

The SOA characterization wavelength was 1310 nm and the nominal SOA driving current was 300 mA. However, during the experiments the following SOA currents: 300 mA (SOA 1), 150 mA (SOA 2), 225 mA (SOA 3), 250 mA (SOA4), and 134 mA (SOA 5) were applied. Those currents provided sufficient gain to compensate for transmission losses and the saturation output power, while minimizing the ASE noise. The SOA polarization dependence of gain was less than 1 dB. After the transmission line the DWDM signals entered a DWDM receiver.

The DWDM receiver consisted of a pre-amplifying SOA 5, a variable ATT, a demultiplexing AWG, a 10 Gbit/s data receiver and a BER tester. In contrast to the previous experiments, the received optical power P_{REC} was measured just before the 10 Gbit/s receiver. By doing so, it was stressed that the receiver card, e.g. 10 Gbit/s Ethernet card does not have to be collocated with the preamplifier. The possible scenario is that all four signals will enter an office building. After pre-amplification and wavelength demultiplexing they will be distributed within the building through the existing fibre network for example, plastic optical fibre based network. However, is such a combined-fibre transmission link, POF can only be used for down-stream communication.

2.4.2 Results and discussion

Figure 2.29 shows the optical spectra taken by an optical spectrum analyzer before and after the 200 km transmission. No FWM in the SOAs and the transmission fiber was observed. Simulations indicate that in such a system configuration, excluding the ASE noise, the FWM effect can be observed after transmission of more than 1500 km. All SOAs in this experiment were in moderate saturation in order to balance the output signals for highest OSNRs. The accumulated ASE noise drove the SOAs into saturation and therefore limited the maximum allowable data signal output power. As a result the OSNR, averaged over all channels, decreased from 36 dB to 21 dB. Figure 2.30 shows degradation of the signal OSNR along the transmission link. The highest degradation 6.8 dB of the OSNR occurred in the SOA 2, the lowest 0.7 dB in the SOA 5.

Accumulation of the ASE noise is visible in Figure 2.31. Comparing the optical spectra after the SOA 1 and the SOA 5 the ASE noise bandwidth compression is evident. Moreover, the ASE noise peak shifted towards the longer wavelengths.

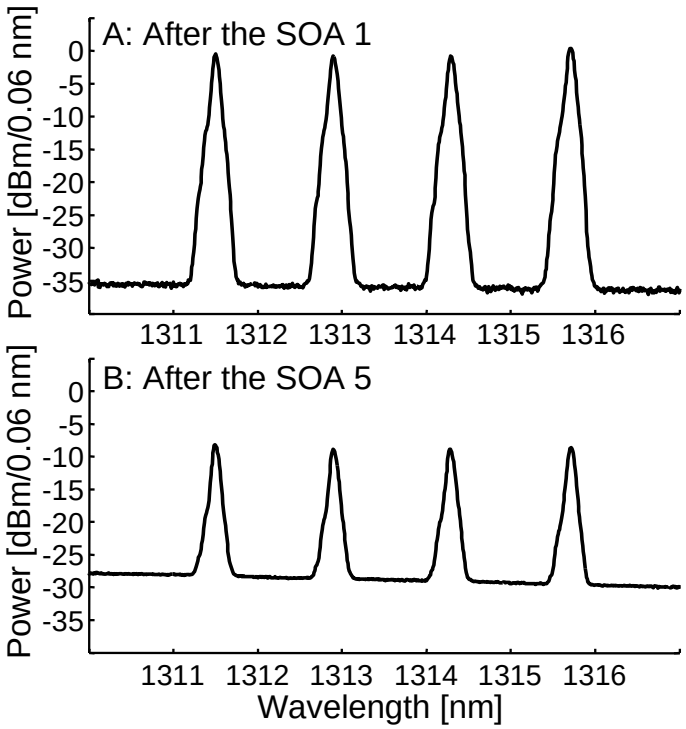

Figure 2.29: Measured optical spectra of repeated 4×10 Gbit/s transmission

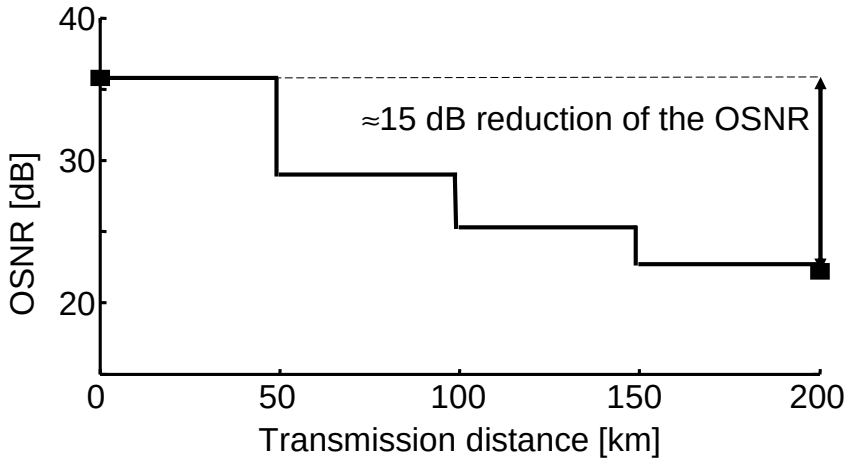

Figure 2.30: Reduction of the OSNR in the 200 km long transmission link

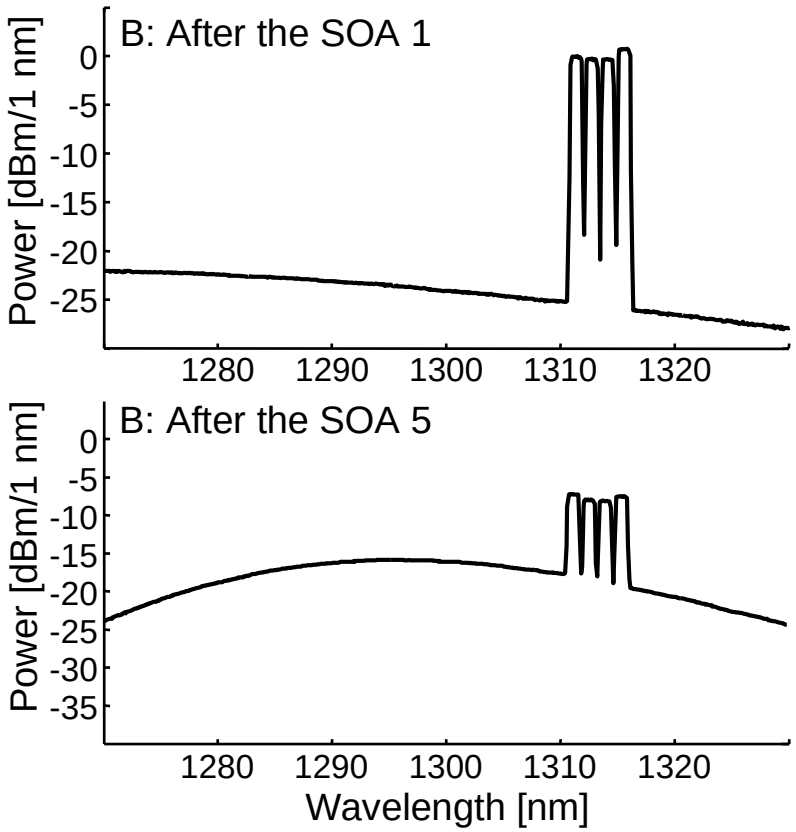

Figure 2.31: Accumulation of the ASE noise in the 200 km long transmission link

A solution to the ASE noise accumulation can be application of intermediate filtering. The intermediate filters placed at the output of each SOA will reduce the ASE noise injected into the transmission link and therefore reducing saturation of the following SOAs. The drawback of the proposed solution is limitation of the available wavelength band.

Figure 2.32 shows the measured eye diagrams. The eye diagrams of all channels show a clear eye opening and indicate excellent operation of the transmission system. However, the beating of the signal with accumulated ASE noise and the residual saturation effects in the SOAs can be observed on the "1" rail of the output eye diagrams.

Figure 2.33 visualizes results of the BER measurements. The SOA settings were preserved during all measurements. The back-to-back (B2B) performance was measured by directly connecting the transmitter to the receiver section. No BER error floor was observed and the average power penalty after 200 km transmission at BER=10^{-9} was 2.5 dB. The power penalty is attributed to the accumulation of the ASE noise, therefore degradation of the OSNR and residual saturation effects in the SOAs.

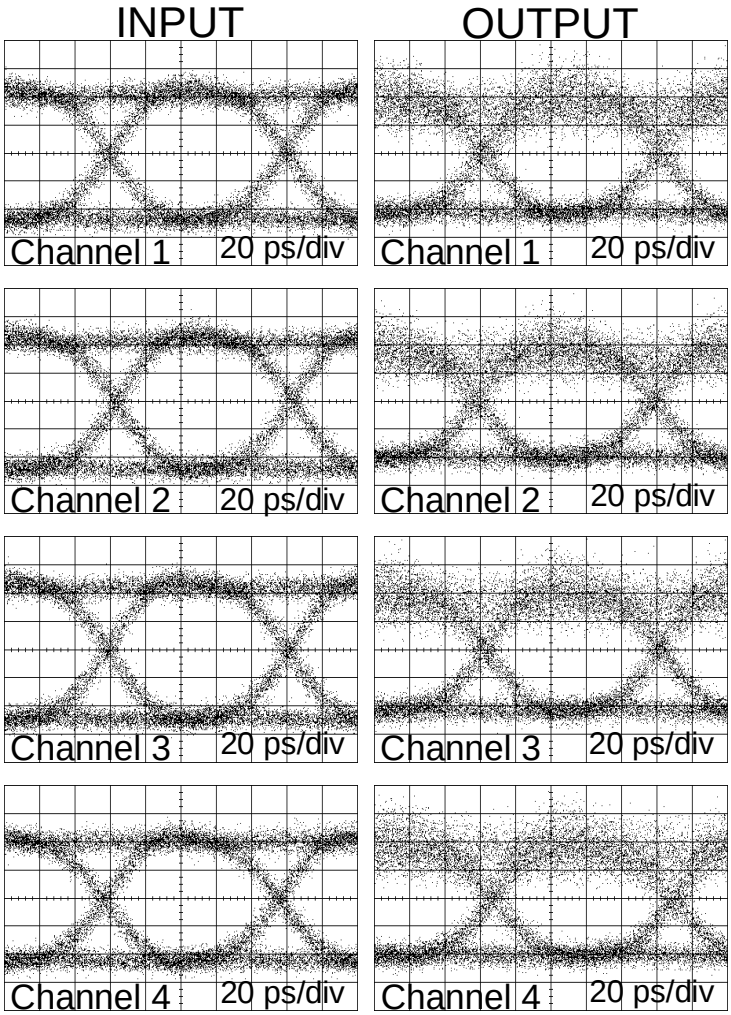

Figure 2.32: Measured eye diagrams of the transmitted 10 Gbit/s signals in the extended transmission reach experiments

Here, DWDM transmission of 4×10 Gbit/s over 200 km SSMF without any dispersion compensation has been demonstrated. The ASE noise and the saturation effects limited the system performance and the transmission distance to 200 km of SSMF. The FWM effect appeared not to be a limiting factor. To the best of author's knowledge [46–49], a transmission record of WDM transmission distance in the 1310 nm wavelength domain was reached, confirming the results of simulations [50].

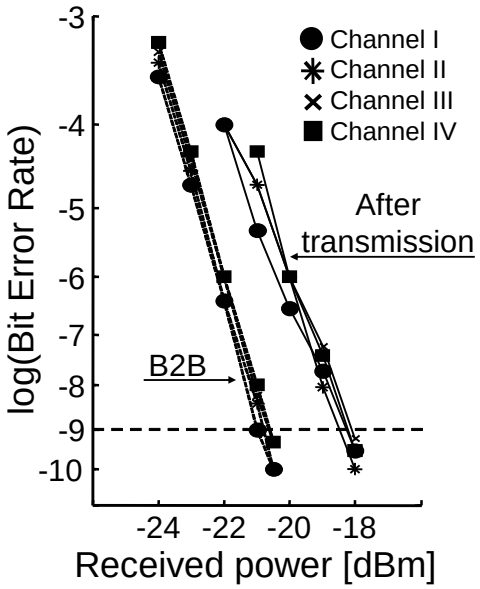

Figure 2.33: Results of 4×10 Gbit/s extended reach BER measurements

2.5 4×25 Gbit/s transmission experiments

One of the solutions to fulfill the ever growing demand for bandwidth in the metro area, with already high market penetration is Ethernet. The existing physical layer (PHY) optical standards for 10 Gbit/s Ethernet [51] are summarized in Table 2.6.

Table 2.6: Existing Optical PHY standards for 10 Gbit/s Ethernet [51]

10 GbE Medium Access Controller (MAC)							
10 Gigabit Media Independent Interface (XGMII) 10 Gigabit Attachment Unit Interface (XAUI)							
WWDM LAN PHY (8B/10B)		Serial LAN PHY (64B/66B)			Serial LAN PHY (64B/66B+WIS)		
WWDM PMD 850 nm	WWDM PMD 1310 nm	Serial PMD 850 nm	Serial PMD 1310 nm	Serial PMD 1550 nm	Serial PMD 850 nm	Serial PMD 1310 nm	Serial PMD 1550 nm
SX4	LX4	SR	LR	ER	SW	LW	EW
10GBase-X		10GBase-R			10GBase-W		

The 10 Gbit/s Ethernet standard defines eight physical medium dependents (PMDs). A serial local area network (LAN) PHY is defined for short reach (SR) over multi-mode fibre (MMF) or long reach (LR) and extended reach (ER) over single-mode fibre. The short reach PMDs utilize 850 nm wavelength domain, long and extended reach PMDs 1310 nm and 1550 nm wavelength domains, respectively. The reach of the existing 10 Gbit/s varies between 300 m for MMF at 850 nm,

through 10 km of SSMF at 1310 nm, and up to 80 km of SSMF at 1550 nm. The wide WDM (WWDM) PHY uses four parallel lanes at 3.125 Gbit/s [51].

The traditional bit rate growing factor for the Ethernet hierarchy is 10. However, it is still not clear if the next Ethernet standard will be 100 Gbit/s, or the tradition will be broken and it will be set to 40 Gbit/s. The most probable 100 Gbit/s PHY standard is discussed in [51]. Due to the limited bandwidth-distance product of MMFs and the targeted market of high capacity switches connections in the metro range, most likely the 100 Gbit/s Ethernet standard will support only SSMF transmission. Table 2.7 shows the proposed 100 Gbit/s Ethernet PHY standard.

Table 2.7: Proposed Optical PHY standard for 100 Gbit/s Ethernet [51]

100 Gigabit Media Independent Interface (CGMII) 100 Gigabit Attachment Unit Interface (CAUI)					
WWDM LAN PHY (nB/mB)		DWDM LAN/MAN PHY (xB/yB)		Serial WAN PHY (FEC)	
WWDM PMD 1310 nm	WWDM PMD 1550 nm	DWDM PMD 1310 nm	DWDM PMD 1550 nm	Serial PMD 1310 nm	Serial PMD 1550 nm
LX4	EX4	LX10	EX10	LW	EW
100GBase-X4		100GBase-X10		100GBase-W	

In general, three possible solutions can be distinguished: 4×25 Gbit/s WWDM, 10×10 Gbit/s dense WDM (DWDM), and single channel 100 Gbit/s transmission. All solutions can operate in the 1310 nm wavelength domain as well as in the 1550 nm wavelength domain. However, the 100 Gbit/s Ethernet has not been yet standardized. Definitely, in the 1550 nm wavelength domain the 100 Gbit/s Ethernet standard has to follow the ITU-T wavelength grid. However, the ITU-T standardization does not cover yet DWDM in the 1310 nm wavelength domain. Therefore all possible solutions can be considered.

Obviously, dispersion is one of the major limitations. Without dispersion compensation the transmission distance at 100 Gbit/s is limited to the 2-5 km in the 1310 nm wavelength domain and to 0.4-0.8 km in the 1550 nm wavelength domain. To bridge longer distances a tuneable dispersion compensation will be required to adapt for changes over time in the dispersion value.

Very recently, several 100 Gbit/s experiments were demonstrated [52–55]. The presented experiments based on the single channel 100 Gbit/s transmission. However, this transmission concept requires very accurate dispersion and PMD compensation, or application of forward-error correction (FEC). FEC is accomplished by adding redundant information to the data signal. The redundancy is used at the receiver to correct bit-errors. In 100 Gbit/s Ethernet applications, FEC can operate at the base rate of multiplexed signals, e.g. 10 Gbit/s using Reed-Solomon codes. However, FEC introduces delays, increases size and power consumption. Moreover, the cost of this state-of-the-art transmission system will probably be very high due to the technological difficulties to make such an advanced product.

The solution based on wavelength multiplexing will be more resistant to dispersion and at the bit rate 25 Gbit/s distances between 25-50 km can be bridged at 1310 nm and between 6-13 km at 1550 nm. Respectively, distances of 150-300 km and 40-80 km can be bridged at the bit rate 10 Gbit/s [51]. Several companies are already working on integrated multi-wavelength transmitters and receivers [56]. But the large number of transmission wavelengths leads to increased number of backplane channels, which complicates design, adds more opto-electronic components, and is definitely less bandwidth efficient.

Therefore it is believed that the most feasible solutions to realize a 100 Gbit/s Ethernet is 4×25 Gbit/s WDM transmission in the 1310 nm wavelength domain. It requires much less sophisticated technology, much longer distances can be bridged without any dispersion compensation, which reduces the system cost and simplifies the installation procedure, and the power consumption can be kept low. The transmitter and the receiver module can be in general integrated providing a very good manufacturing yield. Here, 4×25 Gbit/s WDM transmission experiments in the 1310 nm wavelength domain will be described. It will be demonstrated that already existing technology can support cost-effective 100 Gbit/s Ethernet transmission.

2.5.1 Experimental setup

Figure 2.34 presents the experimental setup. The setup can basically be divided in three parts: an optical 100 Gbit/s transmitter, a fibre link, and an optical 100 Gbit/s receiver. The transmitter consisted of four DFB lasers operating in CW condition.

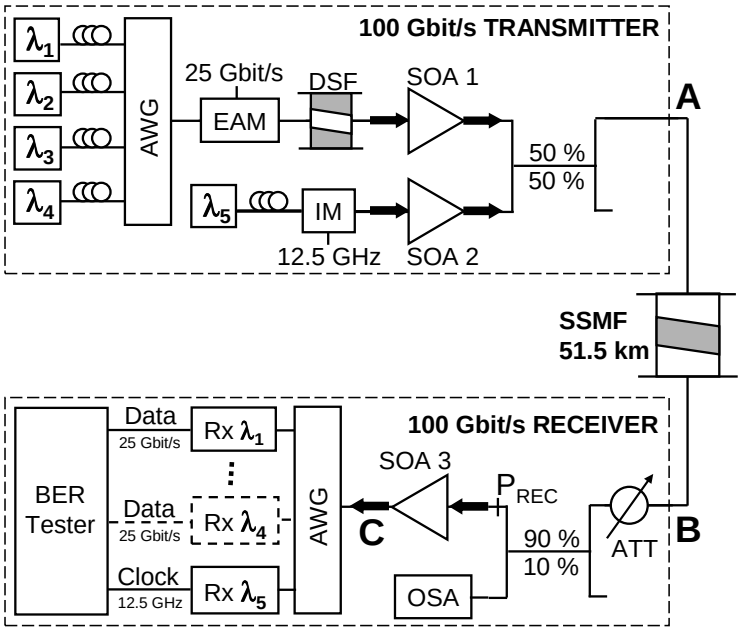

Figure 2.34: 4×25 Gbit/s experimental setup

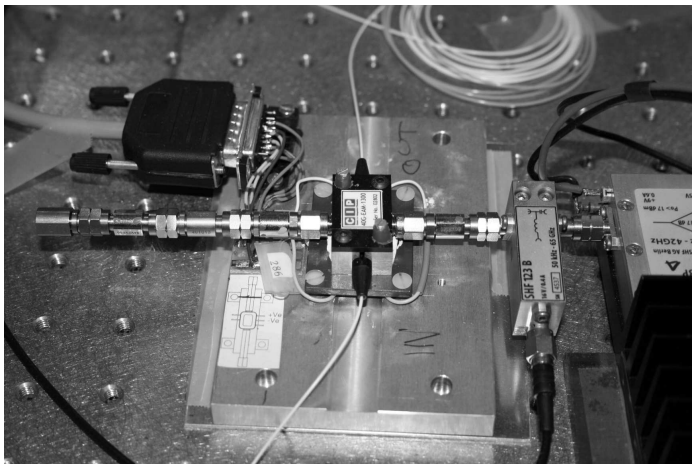

Figure 2.35: Picture of the mounted EAM

The laser's wavelengths were based on a wavelength grid of a following AWG. To assure maximum transmission distance we chose an operation in the band 1306-1319 nm (see Section 2.1.2) at wavelengths 1311.5 nm (channel I), 1312.9 nm (channel II), 1314.3 nm (channel III), and 1315.6 nm (channel IV). The channel spacing was equal to 1.4 nm, which corresponds to ≈250 GHz at the wavelength of 1310 nm.

After passing through the polarization controllers, that were used to achieve optimal signal quality at the output of a modulator, all four signals were combined by an AWG and then simultaneously modulated by an electro-absorption modulator (EAM) at the bit rate 25 Gbit/s. The data format was nonreturn-to-zero (NRZ) with PRBS of a repetitive length $2^{31} - 1$.

The EAM applied in the experiments is a commercially available device, designed for the operation in the 1310 nm wavelength domain with the maximum bit rate 40 Gbit/s. The device was manufactured by CIPhotonics, UK and has typically the modulation depth of 13 dB, the minimum insertion loss of 8.5 dB, the small signal 3 dBe RF bandwidth of 31 GHz, and maximum RF voltage (peak-to-peak) of 4 V. Figure 2.35 shows a picture of the mounted EAM. To achieve proper operation of the EAM additional external components were necessary. To terminate the electrical signal a DC-block and a 50 Ω termination was connected to the electrical output of the EAM. At the electrical input a bias-tee was used to set the desired level of the DC-bias voltage. Under the EAM a Peltier cooler was placed to assure constant temperature of an EAM package. The temperature sensor was mounted in the copper plate between the EAM and the Peltier cooler. Probably, in the next versions of the 1310 nm EAM the supplier will already mount all necessary components inside the package. Following the advice of the producer the EAM temperature was set to 20°C. It was communicated by the producer that at higher temperatures higher extinction ratios were measured as well as higher insertion losses.

First, before employing the 1310 nm EAM in transmission experiments the static

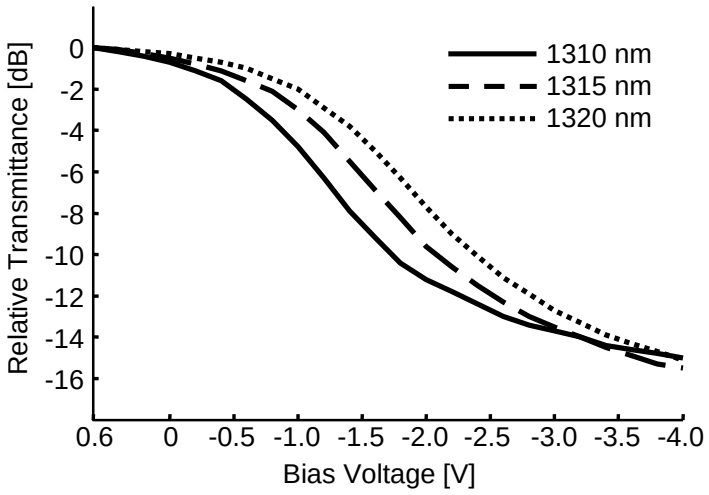

Figure 2.36: Measured characteristics of the 1310 nm EAM

characteristics of the EAM were measured. By applying different levels of the DC voltage, changes in the EAM absorption were measured by the optical power meter at the EAM optical output. Measurements at three different wavelengths: 1310 nm, 1315 nm, and 1320 nm, (the wavelength range of the AWG used in the experiments) were performed. Figure 2.36 presents measured characteristics. It can be seen that for the maximum voltage swing of 4.6 V the extinction ratio of ≈15 dB can be achieved at 1310 nm. For the voltage swing between -0.5 V and -2.2 V the extinction ratio of ≈10 dB can be achieved. The presented characteristics also show the wavelength dependency of the EAM. The wavelength dependency can be compensated by applying different values of the swing voltage and the DC-bias for different wavelengths. The measured dynamic insertion loss was 11.5 dB.

After the 1310 nm EAM, the modulated signals passed through 2.5 km of the DSF, with the absolute dispersion value of 17 ps/nm×km at 1310 nm, in order to partially decorrelate the bit sequences of the data channels. By doing so, the next optical amplifiers did not receive identical data signal levels at once. After being amplified by an SOA booster (SOA 1, $G = 14.0$ dB, $P_{sat} = 13.0$ dBm) the signals were coupled in a 3 dB coupler with a 12.5 GHz clock signal. The SOA 1 was operating with the current 400 mA.

To drive a bit error ratio (BER) tester, a clock signal at a frequency equal to the half bit rate is necessary. Unfortunately, 25 Gbit/s data and clock recovery units are not commercially available yet and their design goes beyond scope of this thesis. Therefore to avoid usage of the back-to-back clock signal an intermediate solution was applied. The 12.5 GHz clock signal was transmitted at the separate wavelength channel. To compensate the delay of each data channel with respect to the clock signal the clock delay in a BER tester was adjusted to achieve the best BER performance.

The clock signal was generated by modulating a CW signal in an external Mach-

Zehnder modulator at frequency 12.5 GHz. After amplification in a second booster SOA 2 (G = 22.7 dB, P_{sat} = 9.0 dBm), operating with current 400 mA, the clock signal was coupled with the data signals and injected into transmission line. At the receiver, after pre-amplification the clock signal was separated from the data channels in a demultiplexing AWG and after the O/E conversion was used to drive the 25 Gbit/s BER tester. The optical power of the clock signal was set 3 dB higher than the optical power of the data channels to assure operation of the BER tester, even for the low values of the input power at the receiver. However, in the field installed systems a clock recovery from each data channel is necessary.

Four spans of SSMF, conforming the ITU-T Recommendation G.652, each 12.9 km long formed the transmission link. The total length of the transmission link was 51.5 km. The average attenuation at 1310 nm was 0.33 dB/km, the average zero-dispersion wavelength 1314.1 nm and the average dispersion slope 0.0871 ps/nm$^2\times$km. The transmission link loss, with connector and splice losses was 18.5 dB.

After 51.5 km transmission, the signals entered a 100 Gbit/s receiver. A variable ATT at the receiver input adjusted the input power levels for the purpose of the BER measurements. To measure the receiver sensitivity, the power level of WDM channels at the ATT output was tapped off by an asymmetrical coupler. An optical spectrum analyzer (OSA) measured the optical power and spectral locations of the WDM signals. The receiver section consisted of a pre-amplifying SOA 3 (G = 20.7 dB, P_{sat} = 11.5 dBm), operated with current 350 mA, a demultipexing AWG, and a photoreceiver module connected to a BER tester.

2.5.2 Results and discussion

Figure 2.37 shows the optical spectra measured at the following points: A-the transmitter output, B-the fibre output, and C-the pre-amplifier (SOA 3) output. All these points are marked in the Figure 2.34. The input signal levels were set to about 0 dBm per channel and the clock signal was set 3 dB higher. These power levels did not cause significant FWM in the fibre. To observe the FWM effect the power levels >3 dBm will be required. The input OSNR of the data signals was about 30 dB and about 36 dB for the clock signal. After the transmission link the the optical power dropped to about -19 dBm for the data channels and to about -16 dBm for a clock channel. Obviously, the OSNR value was preserved.

The pre-amplifying SOA 3 amplified the signal to about -3 dBm per channel. Accumulation of the ASE noise is visible. The accumulated ASE noise in the SOAs decreased the OSNR value. The OSNR value of data channels dropped to about 23 dB. The OSNR value was preserved after the AWG. However, the total amount of the ASE noise injected into the photodiode was reduced by the AWG filtering. The data and clock signals were further demultiplexed in the wavelength domain by an AWG, similar to the one already described in the previous section, and fed into a photodiode in combination with the transimpedance amplifier. The presented power values indicate that none of the used SOAs was operating in a deep saturation regime. Therefore mainly noise contributed to the signal distortions.

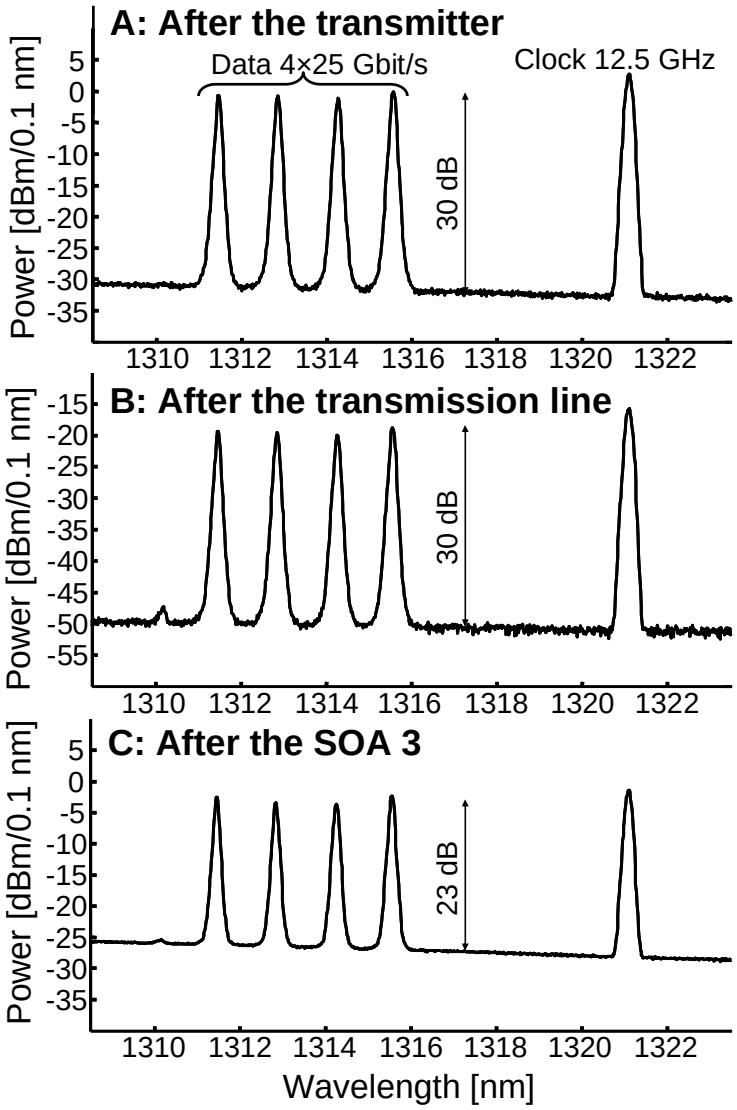

Figure 2.37: Measured optical spectra 4×25 Gbit/s transmission

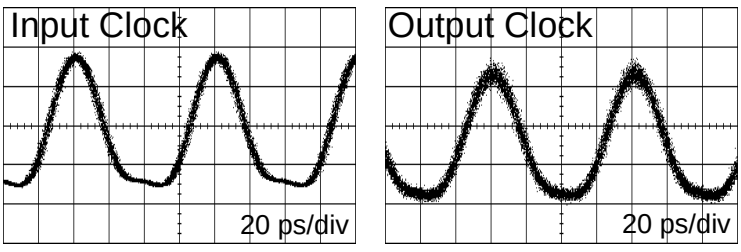

Figure 2.38: Input and output 12.5 GHz clock signal

Figure 2.38 shows signal traces of the transmitted clock signal. The 12.5 GHz transmitted clock had a period of 80 ps. Figure 2.39 presents input and output eye diagrams of the transmitted 25 Gbit/s data signals. All eye diagrams show clear eye openings and indicate excellent operation of the transmission system. The accumulation of the ASE noise and the beating of the signal with the ASE noise in the "1" rail can be observed in the output eye diagrams. Despite the wavelength dependency of the EAM all eye diagrams show a similar shape. It was achieved by adjusting the EAM DC-bias to the following levels: -1.3 V Channel I, -1.3 V Channel II, -1.6 V Channel III, and -1.5 V Channel IV. The same values of the DC-bias were used during the BER measurements.

The performance of all channels was evaluated by measuring BER versus the input optical power, P_{REC} in Figure 2.34. The results of the BER measurements are shown in Figure 2.40. The back-to-back measurements were performed by di-

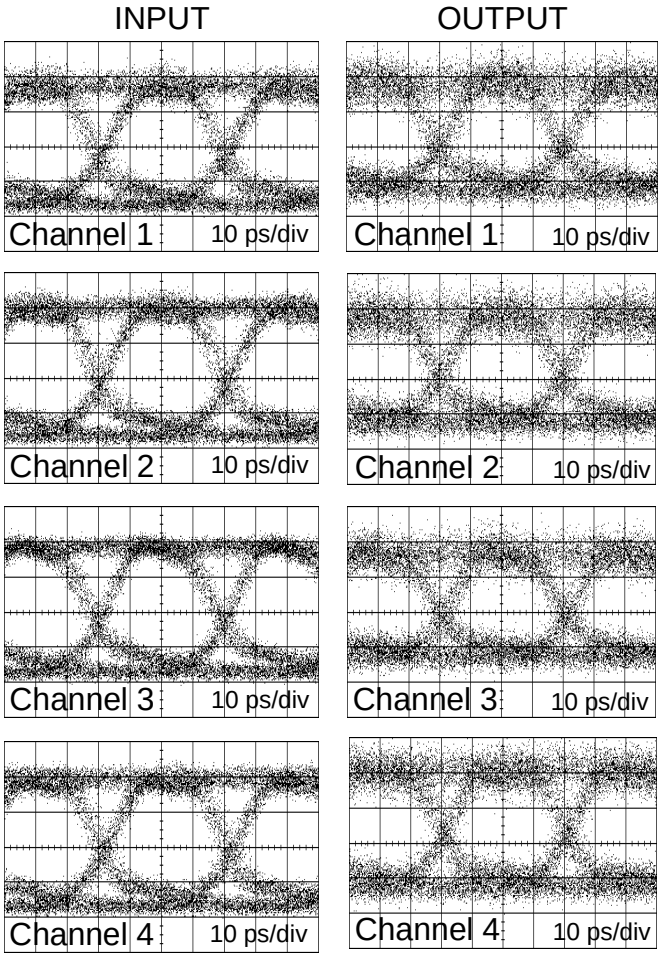

Figure 2.39: Measured eye diagrams of the transmitted 25 Gbit/s data signals

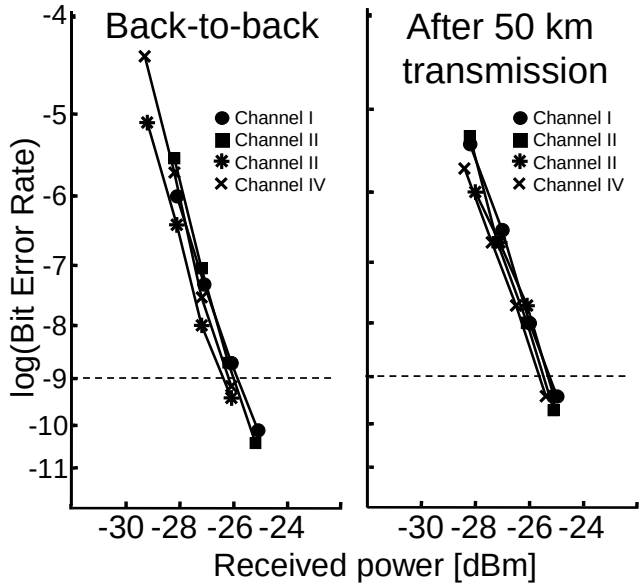

Figure 2.40: Results of 4×25 Gbit/s BER measurements

rectly connecting the transmitter to the receiver. The average power sensitivity at BER=10^{-9} was -26.1 dBm. No error floor was observed. All channels showed similar BER performance. Residual difference in the optical power of the data channels visible in Figure 2.37 will cause spreading in the BER values of different channels. This can be overcome by the power adjustment to assure proper operation of the worst channel. Hence, all other channels will show better performance. The second solution is the perfect alignment of the power levels of the data channels. The average power sensitivity at BER=10^{-9} after transmission was -25.5 dBm. This resulted in a negligible power penalty of 0.6 dB for the 50 km transmission. Again, no error floor was observed and all channels showed similar BER performance. The very small value of the power penalty indicates that the FWM effect is not a significant issue in this experiment. The optical spectra confirm this observation.

The presented system has still some margins that can be further explored to increase the transmission reach. In the transmitter, the 3 dB coupler used to provide clock signal to the BER tester can be removed. Obviously, clock recovery from the data signal has to be provided at the receiver. This directly increases the available transmitter output power. However, the increased input power may lead to generation of FWM effect products. The FWM effect can be omitted by an unequal channel spacing (Section 2.1.4). Therefore the transmitter output power in the range of few dBm per channel can be expected. It is believed that this solution should be included in the future 100 Gbit/s Ethernet standard.

To perform the BER measurements an asymmetrical coupler and a variable attenuator was inserted in the receiver. The combined (internal) losses of those two components are equal to 4 dB. These components are not necessary in real systems

giving additional margin in a power budget. To summarize, the presented system has some margins that can be used to increase the transmission reach. Based on these observations it can be concluded that the transmission distance of about 60-70 km is feasible. Figure 2.41 shows a sketch of a potential implementation of the 4×25 Gbit/s transmission system in the 1310 nm transmission domain.

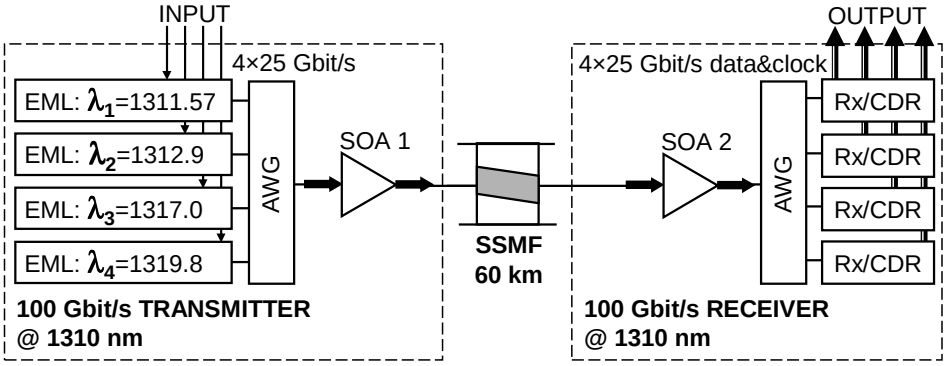

Figure 2.41: A possible realization of the 100 Gbit/s transmission system

In this section, the feasibility of the 100 Gbit/s Ethernet transmission in the 1310 nm wavelength domain was evaluated. The 4×25 Gbit/s transmission was indicated as the most promising candidate to realize the 100 Gbit/s Ethernet transmission. The proposed transmission system has several major advantages over the other solutions: the components and technology already exist, exclusively semiconductor optical components are used, which allows for sub-system integration, no dispersion compensation is required for the considered (≈50 km) distances, the installation cost is reduced, and the limited number of data channels reduces the size and power consumption. Disadvantages here are the maximum dispersion-compensation-free transmission distance in the range of 60-70 km, potential low spectral efficiency due to the FWM effect countermeasures, and the increased number of optical components with respect to the single channel transmission. Taking into account the design rules presented earlier in this chapter the 4×25 Gbit/s transmission system with the data channels between 1311.5 nm, and 1315.6 nm was designed. The results of measurements showed error-free operation with negligible penalty for 50 km transmission. A limiting factor was accumulation of the ASE noise. The FWM effect was not significant in these experiments. Additionally, possible sources of system reach extension were pointed out.

2.6 4×40 Gbit/s transmission experiments

In contrast with the Ethernet standard described in Section 2.5 the bit rate increase factor for the synchronous digital hierarchy (SDH) transmission systems is four. The SDH multi-Gbit/s bit rates are: 2.48832 Gbit/s, 9.95328 Gbit/s, and

39.81312 Gbit/s. As was explained in Section 2.1.2, 40 Gbit/s transmission in the 1550 nm wavelength domain using SSMF will require dispersion compensation accuracy of 3 km. One of the viable markets for 40 Gbit/s transmission systems is in the metro area. This implies additional inconvenience when utilizing the 1550 nm wavelength domain. To achieve such accurate dispersion compensation first the chromatic dispersion measurements are necessary. The necessity of dispersion measurements complicates the system installation. Again, the 1310 nm wavelength domain offers a viable solution to support 40 Gbit/s transmission without any dispersion compensation for the considered distances.

The previously reported 40 Gbit/s transmission experiments in the 1310 nm wavelength domain, e.g. [57] addressed only a single channel transmission. Here, 4×40 Gbit/s transmission experiments will be described. The experimental setup allowed unrepeated 4×40 Gbit/s error-free transmission over the 50 km long SSMF. Again, only semiconductor components were used.

2.6.1 Experimental setup

In a first trial, it was anticipated to reuse the setup from the previous 4×25 Gbit/s experiments by basically increasing the bit rate. Unfortunately, it was not possible to achieve error-free operation of all channels for the desired transmission length, namely 50 km of SSMF. The optical power delivered to the receiver was too low to assure error-free operation. As a next step it was considered to increase the input power to the level of about +5 dB. However, this led to the significant generation of the FWM effect products. After changing the wavelength grid from the equal one to the unequal one and removing the variable attenuator the worst channel BER of $4 \cdot 10^{-9}$ was achieved, which was still below expectations. It must be stressed that for a shorter transmission length, i.e. 37.5 km the system operated error-free in the initial configuration. Finally, an extra semiconductor amplifier was added in the receiver to provide enough optical power to the photodiode. By gain distribution, higher net gain was achieved while keeping the low ASE noise level. This configuration was used in the experiments described below.

Figure 2.42 shows the final experimental setup. The transmitter consisted of four DFB lasers operating in CW condition at wavelengths: 1311.5 nm (Channel I), 1312.9 nm (Channel II), 1317.0 nm (Channel III), and 1319.8 nm (Channel IV). The unequal channel allocation scheme $1.4 - 4.1 - 2.8$ nm was used to eliminate the FWM related penalty. All four CW signals were combined in a following AWG. The polarization controllers were used to adjust input polarization to an EAM. In the EAM all signals were modulated simultaneously at the bit rate 40 Gbit/s with the PRBS of length $2^{31} - 1$. To decorrelate the bit patterns a 2.5 km long DSF was used. The DSF had the absolute dispersion value of 42.5 ps/nm. Application of a 5 km long DSF will lead to signal distortions due to accumulated dispersion. To compensate for the losses in the EAM, the DSF, and to maximize the transmitter output power an SOA booster was used. To drive the SOA 1 ($G = 14.0$ dB, $P_{sat} = 13.0$ dBm) a current of 400 mA was used and the SOA was cooled down to -3.1°C. The 20 GHz

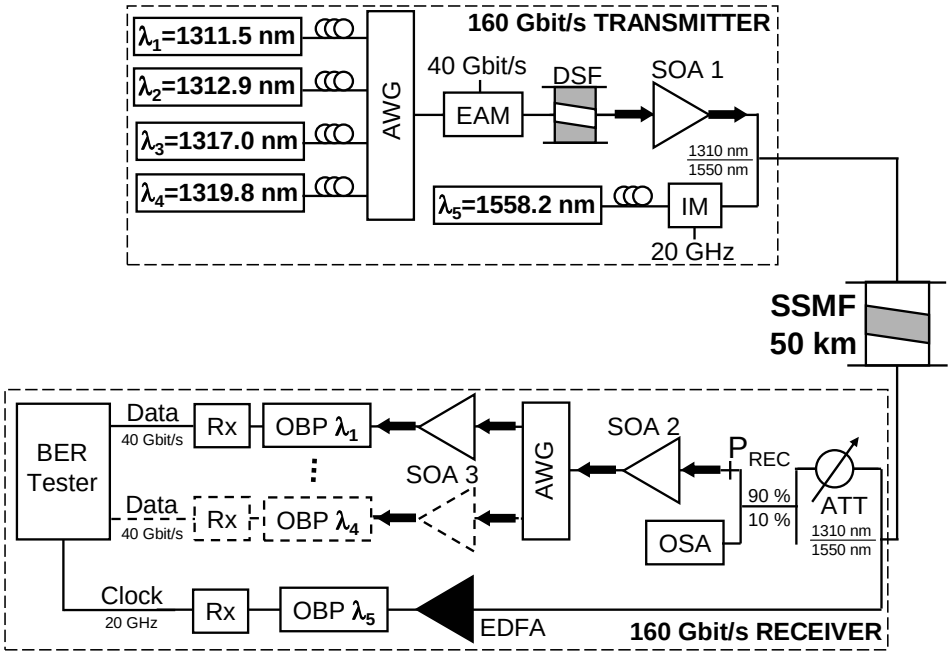

Figure 2.42: 4×40 Gbit/s experimental setup

clock signal needed to drive a BER tester was transmitted at 1558.2 nm. To couple the data and the clock signals a 1310/1550 nm wideband coupler was used.

Next, the data and the clock signals were fed into a transmission line. The transmission line was formed by four spans of SSMF, conforming the ITU-T specification G.652. The parameters of all four spans are summarized in Table 2.8.

Table 2.8: Parameters of the used fibre spans; L-length, α-attenuation, ZDW-zero-dispersion wavelength, D-dispersion @ 1310 nm, and DS-dispersion slope

Span	L [km]	α [dB/km]	ZDW [nm]	|D| [ps/nm×km]	DS [ps/nm×km^2]
I	12.89	0.327	1313.4	0.257	0.0876
II	12.88	0.326	1313.3	0.255	0.0872
III	12.87	0.326	1312.6	0.248	0.0871
IV	12.88	0.325	1313.7	0.258	0.0869

After the transmission link, the transmitted signals entered a 160 Gbit/s WDM receiver. First, the data and the clock signals were separated in a wideband coupler. Then the clock signal was amplified in an erbium-doped fibre amplifier (EDFA). After filtering in a following OBP (0.5 nm bandwidth) the clock signal was injected into a photodiode. Finally, a 20 GHz electrical signal was used to drive the BER

tester. The input power of the data channels was measured by an OSA at the 10% port of an asymmetrical coupler. All data channels coming from the 90% port of the asymmetrical coupler were amplified simultaneously by an SOA 2 ($G = 14.0$ dB, $P_{sat} = 13.0$ dBm) operating with current 200 mA. Next, the data wavelengths were demultiplexed in a subsequent AWG. Finally, a single channel was amplified in an SOA 3 ($G = 18.5$ dB, $P_{sat} = 9.0$ dBm) and filtered in an OBP of the 3 dB passband width equal to 1.2 nm. The optical signal was converted to the electrical signal in a following photodiode connected to a BER tester.

The major difference between the 4×25 Gbit/s setup and the 4×40 Gbit/s setup is utilization of an unequal channel allocation scheme to prevent the FWM effect related penalty. The second difference is transmission of the clock signal at the 1550 nm. This was the only solution, taking into account the available infrastructure, to prevent usage of the back-to-back clock signal in the 50 km transmission experiments. It was verified that due to the signal walk-off the BER measurements with the back-to-back clock signal were not stable enough to give credible data. Again the difference in delay between data channels and clock signal was compensated manually in the BER tester. The third difference is application of the additional SOA in the receiver, which increased the available gain.

2.6.2 Results and discussion

Figure 2.43 and Figure 2.44 show optical spectra captured at the various points of the experimental setup. The optical spectrum after the DSF is shown in Figure 2.43a. The average channel power was -10.6 dBm. The average channel power after the SOA 1 was +5.7 dBm, see Figure 2.43b. Therefore the gain provided by the SOA 1 was 16.3 dB. The average channel power injected into the transmission line was +4.6 dBm, see Figure 2.43c. The calculated insertion loss of the 1310/1550 nm wideband coupler was 1.1 dB. The OSNR value at the beginning of the transmission link was 36 dB.

After the transmission link the average channel power dropped to -13.5 dBm, see Figure 2.43d. The insertion loss of the transmission link was 18.1 dB. The OSNR value was preserved. The strong FWM effect product is clearly visible at the wavelength 1314.3 nm. The ratio between the average channel power and the power of the FWM product was 23.2 dB. It is clear, that such a strong signal will cause crosstalk in the data channel. Therefore an unequal channel spacing allocation scheme was necessary to prevent FWM related penalty. The other peaks in the optical spectrum around 1308 nm were the sidemodes of the applied lasers. These sidemodes are also visible in Figure 2.43b-c.

Figure 2.44e presents the 90% output of the asymmetrical coupler. The average channel power was -18.6 dBm. The 5.1 dB drop in the optical power, with respect to the power value directly after fibre, was caused by the insertion loss of the 1310/1550 nm wideband coupler, the variable attenuator and the losses in the asymmetrical coupler. The power difference between the 90% and the 10% output of the asymmetrical coupler was 10.3 dB. The 10% output of the asymmetrical coupler

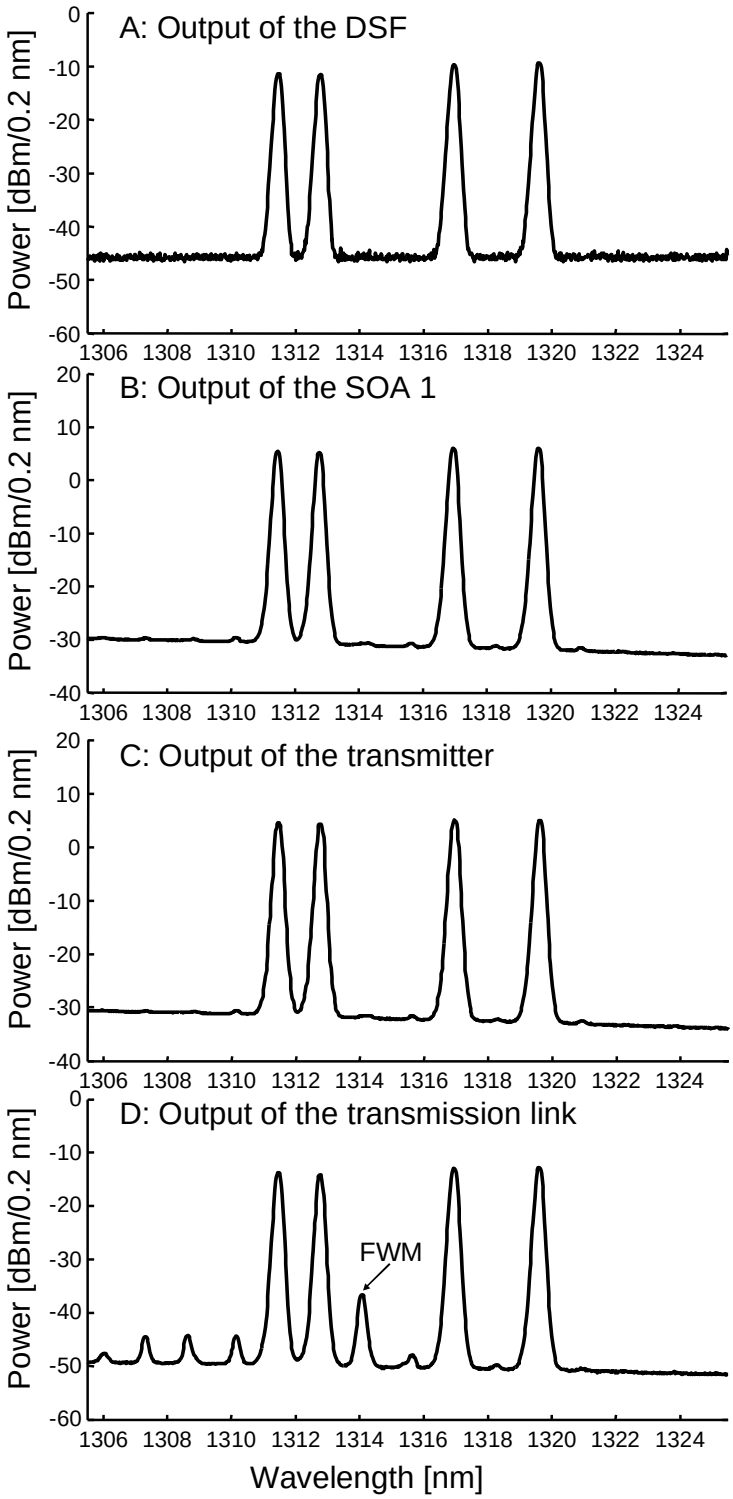

Figure 2.43: Measured optical spectra 4×40 Gbit/s transmission

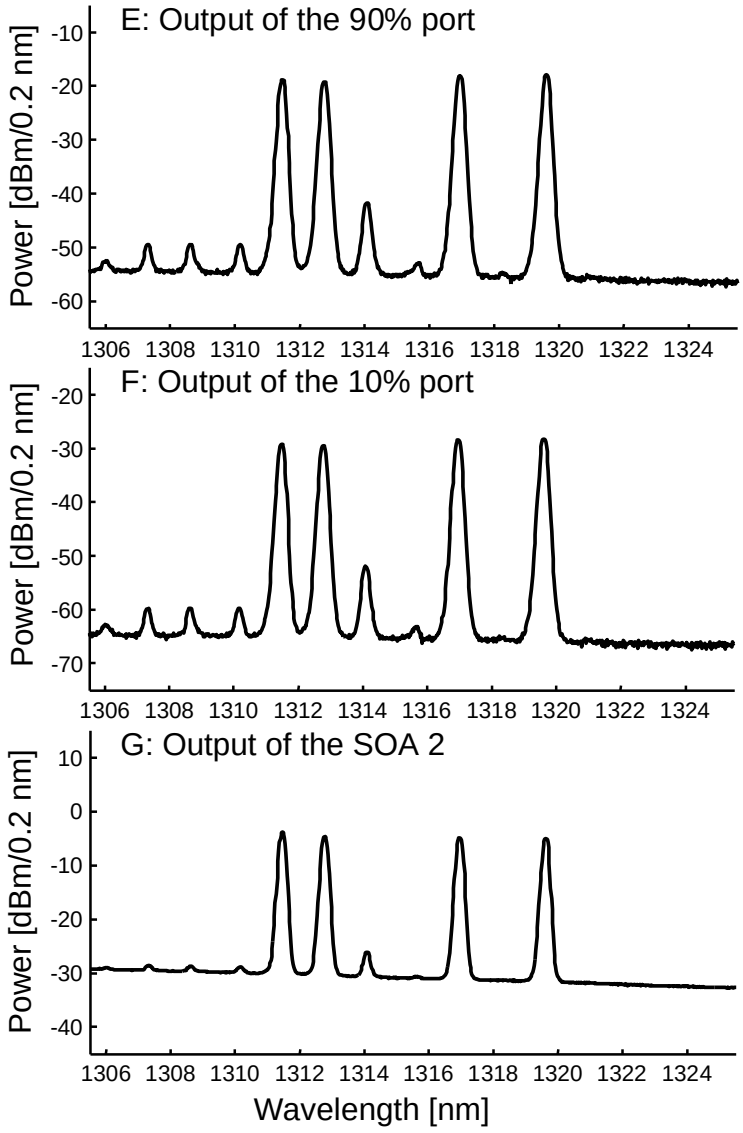

Figure 2.44: Measured optical spectra 4×40 Gbit/s transmission

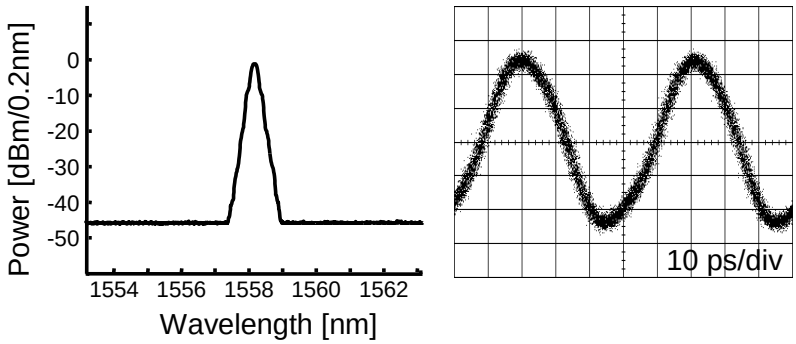

Figure 2.45: Optical spectrum and signal trace of the transmitted clock

was used to monitor the power level during the BER measurements, see Figure 2.44f. Figure 2.44g presents the optical spectrum after the SOA 2. The average channel power was -4.6 dBm and the OSNR value dropped to 24.7 dB. The reduction of the OSNR value was caused by the accumulation of the ASE noise. Figure 2.45 presents the optical spectrum and the eye-diagram of the transmitted 20 GHz clock signal. The transmitted clock had a period of 50 ps.

Figure 2.46 shows input (after the transmitter) and output (after the OBP) eye-diagrams of the transmitted 40 Gbit/s data signals. All eye diagrams show clear eye opening and indicate excellent operation of the transmission system. To compensate the wavelength dependence of the applied EAM the DC-bias voltage of the EAM was set to -1.45 V for Channel I, -1.45 V for Channel II, -2.10 V for Channel III, and -2.25 V for Channel IV. Additionally, the SOA 3 current was adjusted to values: ≈110 mA Channel I, ≈115 mA Channel II, ≈150 mA Channel III, and ≈250 mA Channel IV. The different values of the SOA 3 current and therefore SOA gain, compensated for the differences in transmittance of the demultiplexing AWG and the polarization sensitivity. Signal optimization (the EAM DC bias and the SOA 3 current) was applied on each individual channel. Hence, in general all signals had the same power levels after the SOA 1 and the SOA 2. Application of the additional SOA 3 in the receiver gave more flexibility when optimizing the performance of all channels. This is allowed, as in a real system four separate EAMs and SOAs 3 will be applied. The presented values of the EAM DC-bias voltage and the SOA 3 current were used during all BER measurements. The accumulation of the ASE noise and the beating of the signal with the ASE noise in the "1" rail as well as saturation effects can be observed in the output eye diagrams. The saturation effects were caused by the SOA 1 that was driven into the saturation to obtain the high output power.

The performance of all channels was evaluated by measuring BER versus the input optical power, P_{REC} in Figure 2.42. Results of the BER measurement are shown in Figure 2.47. The back-to-back measurements were performed by directly connecting the transmitter to the receiver. The average power sensitivity at BER=10^{-9} was -20.1 dBm. No error-floor was observed. All channels showed similar BER performance. The average power sensitivity at BER=10^{-9} in the 50 km transmission

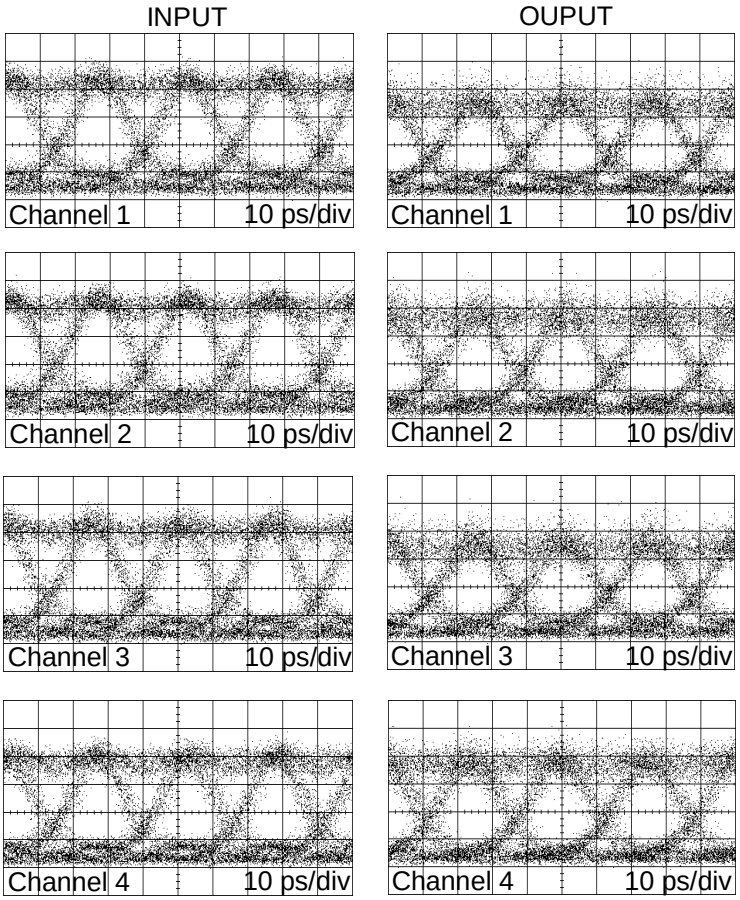

Figure 2.46: Measured eye diagrams of the transmitted 40 Gbit/s data signals

experiment was -19.3 dBm. This resulted in a negligible power penalty of 0.8 dB for the 50 km transmission. Again, no error floor was observed and all channels showed similar BER performance. Additionally, the penalty caused by the multi-channel operation was verified. It was realized by turning off three lasers, while leaving one operating. The improvement in the power sensitivity at BER=10^{-9} was ≈2 dB. From the system design and operating conditions was concluded that the SOA 1 was operating in the saturation regime.

In this experiment, 4×40 Gbit/s transmission in the 1310 nm wavelength domain was successfully demonstrated. Error-free transmission was achieved with negligible penalty over the 50 km of SSMF. A limiting factor was accumulation of the ASE noise. The FWM effect was omitted by an unequal channel spacing allocation scheme. The total power budget of the designed system was 25 dB with the receiver sensitivity ≈ −19.0 dBm.

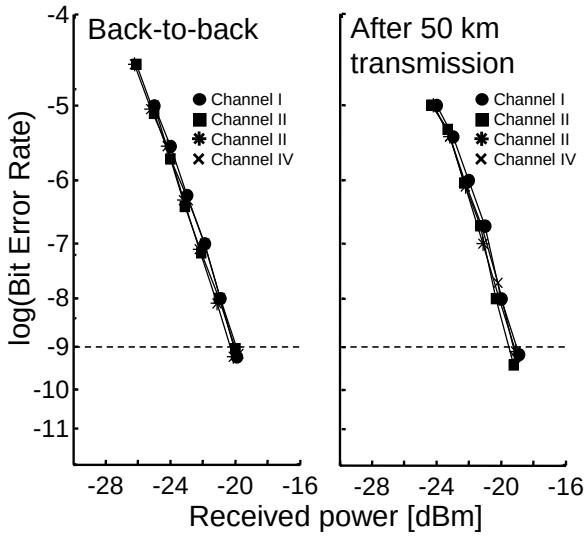

Figure 2.47: Results of 4×40 Gbit/s BER measurements

2.7 Conclusions

In this chapter, feasibility of the DWDM transmission using the SOAs in the 1310 nm wavelength domain was investigated extensively. First, two essential components, namely SSMF and an SOA were analyzed. From the presented analyses it was concluded that due to higher attenuation, with respect to the 1550 nm wavelength domain and less ideal amplification properties of SOAs, with respect to EDFAs, transmission in the 1310 nm wavelength domain can be applied to cover metro range distances. As an optimal wavelength band the wavelength range 1306-1319 nm was pinpointed. Operation in this particular wavelength band guaranties ten times distance extension for SSMF, with respect to the 1550 nm wavelength domain, taking into account the dispersion related penalty. Four-wave mixing in an optical fibre can limit the system performance. To avoid this, the input optical power has to be limited or a channel allocation scheme with unequal channel spacing has to be applied.

By analyzing the SOA operation it was concluded that the amplification performance of the SOA is limited by the ASE noise and the saturation effects. The ASE noise limits performance for the low SOA input power, i.e. pre-amplifier applications. The saturation effects limit the performance for the high SOA input power, i.e. booster applications. It was shown in 10 Gbit/s experiments that operation at P_{SAT} causes the power penalty of 1 dB. In multi-wavelength systems the total input power has to be taken into account when setting the SOA operation point. The optimal amplification performance occurs in the moderate saturation.

Secondly, transmission experiments were performed. An error-free operation was achieved with the negligible power penalty without any dispersion compensation in the following experiments: unrepeated 4×10 Gbit/s transmission over 75 km

of SSMF, repeated 4×10 Gbit/s transmission over 200 km of SSMF, unrepeated 4×25 Gbit/s (100G Ethernet) transmission over 50 km of SSMF, and unrepeated 4×40 Gbit/s transmission over 50 km of SSMF. The proposed transmission systems bridged in general the maximal dispersion-compensation-free distance in the case of 4×25 Gbit/s and 4×40 Gbit/s transmission. In comparison with the previously reported transmission experiments in the 1310 nm wavelength domain [46–48], the transmission distance and the system capacity was increased significantly while remaining cost effective. Taking into account 4×10 Gbit/s transmission [48] the distance was extended 2.5 times. Such an extension was predicted using simulations in [50]. On the other hand the bit rate of the transmitted signals was increased up to four times when comparing to the results published by the others [46–48]. The distance and capacity extension was achieved by applications of the SOAs with appropriate transmission properties, a high speed electro-absorption modulator, and an AWG as a wavelength multiplexer. The presented experiments showed that the 1310 nm wavelength domain can support high speed DWDM transmission.

DWDM transmission in the 1310 nm wavelength domain has important advantages over the other technologies in the distance range considered. The DCF based dispersion compensation costs in the range of 10000-25000 USD per 50 km of SSMF. Moreover, increased bit rates require increased dispersion compensation accuracy. The 2.5 Gbit/s transmission link after upgrade to 10 Gbit/s will require most likely readjustment of dispersion compensation. Therefore by omitting the dispersion compensation the system cost is directly reduced. Additionally, it reduces installation cost and time as well as simplifies future upgrades. For example, in the place of initial 4×10 Gbit/s transmission 2×10 Gbit/s and 2×40 Gbit/s transmission can be realized just by changing the transmitter and the receiver card. Such an upgrade in the 1550 nm wavelength domain may require additional dispersion compensation which increases the upgrade cost. Application of semiconductor components gives the prospect of sub-system integration, efficient manufacturing and therefore significant size, power consumption and cost reduction.

Moreover, the data traffic in 1310 nm wavelength domain can be carried in parallel to the already existing data traffic in the 1550 nm wavelength domain. The 1310 and 1550 nm signals can be multiplex using low-loss wide-band couplers. This will be particularly interesting in the areas where the fibre capacity in the 1550 nm wavelength domain is exhausted. A 100 Gbit/s Ethernet link can be added, over the existing fibre infrastructure without any changes in the existing 1550 nm infrastructure scheme. However, such a direct upgrade can be only realized in the case of unrepeated 1550 nm transmission links. In the case of repeated transmission links the EDFAs have to be bypassed by the 1310 nm signals.

DWDM systems in the 1310 nm wavelength domain may have poor spectral efficiency and therefore the limited capacity. For a required transmission distance, a dispersion-compensation-free wavelength band is limited. Moreover, the FWM effect can enforce usage of less bandwidth efficient channel allocation schemes. Nevertheless, using the repeated unequal channel allocation scheme the WDM systems with capacity 10×40 Gbit/s can be realized to bridge dispersion-compensation-free

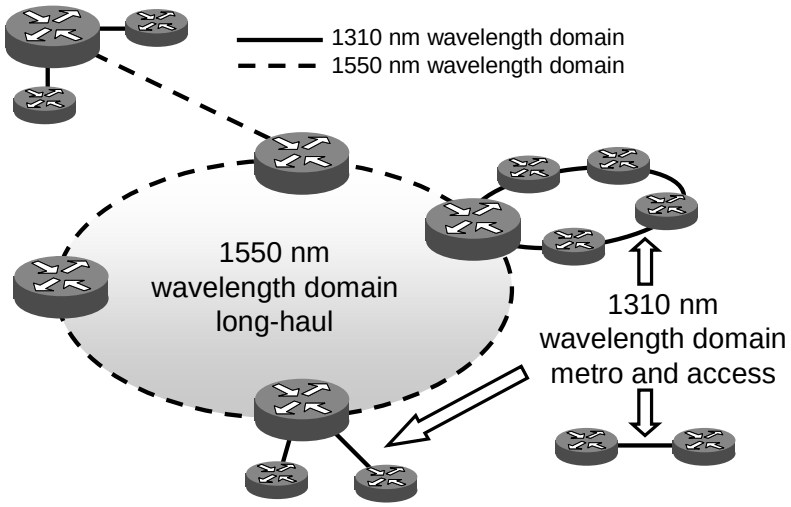

Figure 2.48: An example of the network utilizing the 1310 nm and 1550 nm wavelength domains

distances of 40-50 km. However, shorter transmission distances allow utilization of wider wavelength bands. Furthermore, short transmission distances can be bridged, for a given receiver sensitivity, with the lower optical input power. Therefore the FWM effect can be significantly alleviated without necessity of special channel allocation schemes. This significantly increases the spectral efficiency and the offered system capacity.

Based on the results presented in this chapter, it is believed that there is an attractive potential to utilize the 1310 nm wavelength domain in the metro and access area, especially to realize high speed (>10 Gbit/s) transmission. From the point of Ethernet or IP switching it is not important, which wavelength domain is utilized. However, the applied solutions have to be cost-effective because the system cost is shared by a limited number of users. Figure 2.48 shows an example of a network architecture utilizing the 1550 nm wavelength domain for long-haul transmission and the 1310 nm wavelength domain for access and metro range transmission. In such a network all-optical 1310-to-1550 nm bridging can be required. The next chapter is devoted to that.

Chapter 3

1310-to-1550 nm transparent optical connectivity

This chapter is dedicated to transparent connectivity between the 1310 nm and 1550 nm wavelength domain. First, nonlinear polarization rotation in an SOA is phenomenologically described and analyzed. Then potential system applications are explored. All-optical 1310-to-1550 nm wavelength conversion is evaluated and error-free wavelength conversion is realized at bit rates up to 20 Gbit/s. The final experiments are dedicated to all-optical 1310-to-1550 nm transmultiplexing. Multiple wavelength channels in the 1310 nm wavelength domain are aggregated all-optically into one time domain multiplexed channel in the 1550 nm wavelength domain.[1]

3.1 Introduction

In the previous chapter, it was demonstrated that the 1310 nm wavelength domain can successfully support cost-effective high-speed DWDM transmission. The proposed transmission systems can be applied to bridge short and medium distances. An already established and a widely applied application of the 1310 nm wavelength domain is up-stream transmission in passive access networks.

Passive optical networks (PONs), like broadband PON (BPON) or asynchronous transfer mode PON (APON), Ethernet PON (EPON), and gigabit PON (GPON) utilize the 1310 nm wavelength domain for communication from an optical network terminal (ONT) to an optical line terminal (OLT) [10,64,65]. A reverse down-stream communication is realized in the 1490 nm wavelength domain, see Figure 3.1. The ONT is placed in a user site and the OLT in a central office.

[1] Parts of this chapter are published in [58–63]

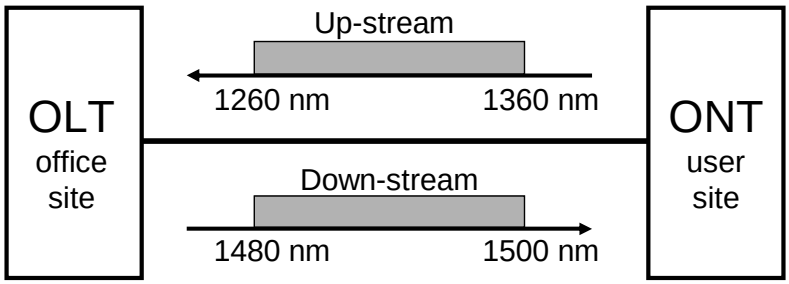

Figure 3.1: PON wavelength allocation scheme

Coarse wavelength domain multiplexing (CWDM) systems utilize the whole low-loss fibre wavelength band (1270–1610 nm) to realize short and medium reach transmission. CWDM is characterized by wide channel spacing, namely 20 nm. Therefore cost-effective transmission through a combination of uncooled lasers, larger tolerance windows for wavelength selection, and wide pass-band filters can be realized [66]. Another application of the 1310 nm wavelength domain is Ethernet transmission, described in Section 2.5. To summarize, systems operating in access and metro range utilize the 1310 nm wavelength domain (PON and Ethernet) or the 1270–1610 nm low-loss fibre wavelength band (CWDM). However, the long-haul network is traditionally centred on the 1550 nm wavelength domain, see Figure 3.2.

Therefore in order to realize end-to-end signal-transparent connectivity between access network users, transparent optical connectivity between metro-access and core network is necessary. A key component in the all-optical metro-access to core network interface is an ultra wideband wavelength converter. Taking into account potential mass applications, research focusses on transparent connectivity between access and core network, i.e. wavelength up-conversion. Utilization of all-optical wavelength up-converters enhances network flexibility, allowing all-optical wavelength conversion between different transmission windows and therefore avoiding the bottleneck of optical-electrical-optical conversions. Ultra wideband wavelength up-converters applied in metro-access systems have to deliver high performance while remaining cost-effective.

Several 1310-to-1550 nm wavelength converters have been reported [67–70]. The wavelength converter based on a $LiNbO_3$ waveguide has an advantage of ultra fast operation and modulation-format independency [67]. However, signal regeneration is not possible and reported device is polarization sensitive. A cost-effective alternative to wavelength converters utilizing an expensive $LiNbO_3$ waveguide are wavelength converters employing semiconductor optical amplifiers.

The demonstrated wavelength converter based on a split contact SOA [68] utilized a polarization insensitive integrated device. However, the device operation was limited due to the limited recovery time to 500 Mbit/s and the output signal had limited on-off ratio equal to 3. A distributed feedback SOA [69] showed similar performance. Error-free 1.25 Gbit/s 1310-to-1550 nm wavelength conversion was achieved by an

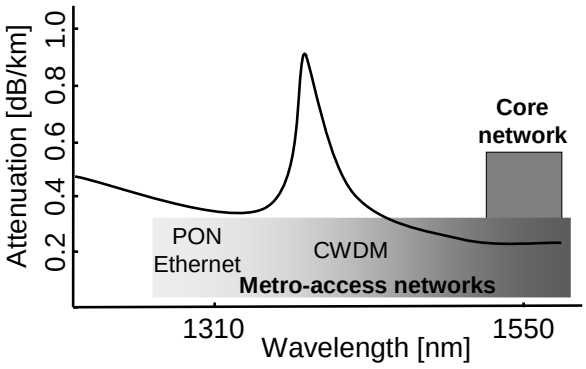

Figure 3.2: Utilization of the fibre low-loss wavelength band

SOA operating in a hybrid Mach-Zehnder Interferometer configuration [70]. The reported wavelength converter required low input power and showed limited (1.5 dB) polarization sensitivity. However, a complicated control mechanism was necessary. The 1310-to-1550 nm wavelength converters presented until now suffered from high cost or in general low performance. Here, a novel all-optical 1310-to-1550 wavelength converter based on nonlinear polarization rotation in a single SOA will be described and evaluated.

3.2 Nonlinear polarization rotation

3.2.1 Polarization concept

Polarization is defined in terms of the pattern traced out in the transverse plane by the electric field vector as a function of time [17]. The propagating optical signal consists of two transverse components: electric (TE) and magnetic (TM). Transverse Electric and Transverse Magnetic components of polarized light can by represented mathematically by [71]

$$E_{TE}(z,t) = E_{0TE}\cos(\tau + \delta_{TE}) \tag{3.1}$$

$$E_{TM}(z,t) = E_{0TM}\cos(\tau + \delta_{TM}) \tag{3.2}$$

where $\tau = \omega t - kz$ is the propagator. The subscripts TE and TM refer to the components in the x and y directions, E_{0TE} and E_{0TM} are the maximum amplitudes, δ_{TE} and δ_{TM} are the corresponding phases, respectively. The resultant pattern traced out in a fixed xy-plane by the electric field is described by

$$\frac{E_{TE}^2}{E_{0TE}^2} + \frac{E_{TM}^2}{E_{0TM}^2} - 2\frac{E_{TE}}{E_{0TE}}\frac{E_{TM}}{E_{0TM}}\cos\delta = \sin^2\delta \tag{3.3}$$

where $\delta = \delta_{TM} - \delta_{TE}$ is the difference in phase between the two transversal components [71]. Figure 3.3 shows the transverse components of the electrical field and the polarization ellipse. It is clear that changes in the signal amplitude and the relative signal phase will introduce changes of the polarization ellipse.

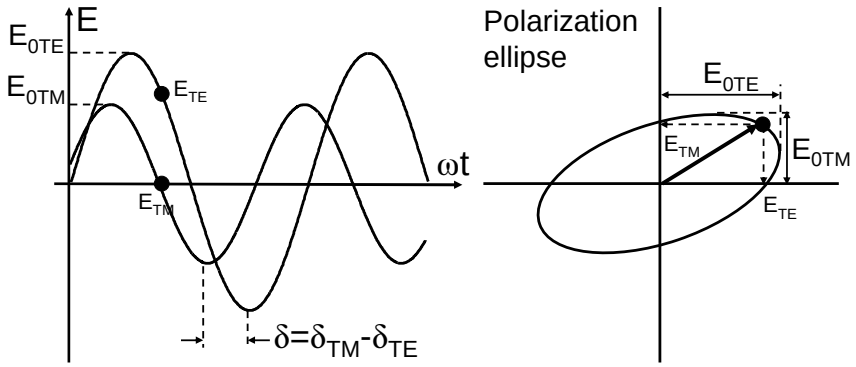

Figure 3.3: E_{TE} and E_{TM} components of the electric field and the polarization ellipse [17]

3.2.2 Nonlinear polarization rotation in an SOA

The waveguiding characteristics of an SOA are described by two orthogonal polarization modes: the transverse electric (TE) and the transverse magnetic (TM) modes. Due to the asymmetric waveguide geometry the SOA is generally a birefringent device [72]. The TE/TM gain asymmetry introduces additional birefringence in the SOA via carrier density changes when external light is injected into the SOA [72–74]. The refractive index changes are different for the TE and TM components, see Figure 3.4.

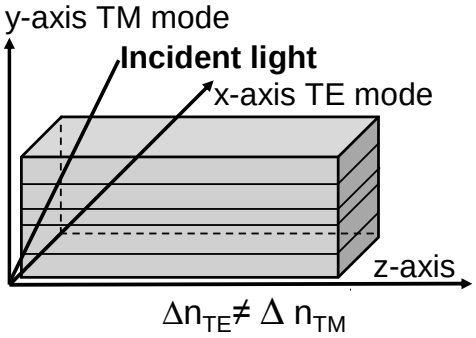

Figure 3.4: SOA waveguide structure

Changes in the refractive index for the propagating modes result in variations of the signal phase. The phase difference θ between the TE and TM modes can be expressed as [73]:

$$\theta = \phi^{TE} - \phi^{TM} = \frac{1}{2}\left(\frac{\alpha^{TE}\Gamma^{TE}g^{TE}}{\upsilon_g^{TE}} - \frac{\alpha^{TM}\Gamma^{TM}g^{TM}}{\upsilon_g^{TM}}\right)L \tag{3.4}$$

where ϕ^{TE} and ϕ^{TM} are the phases for the TE and TM components, $\alpha^{TE/TM}$ is the phase modulation factor that relates the carrier (gain) change and the phase change,

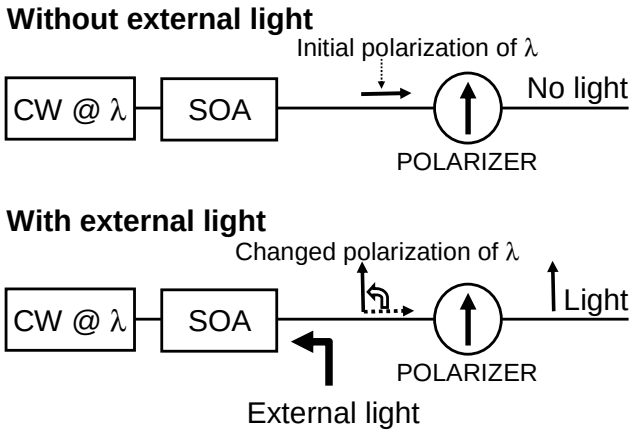

Figure 3.5: Polarization based switching in an SOA

$\Gamma^{TE/TM}$ is the confinement factor, $g^{TE/TM}$ is the gain, $v_g^{TE/TM}$ is the group velocity for the TE and TM components respectively, and L is the length of the SOA.

The variable SOA birefringence leads to changes of the signal polarization state at the SOA output [72–74]. This polarization rotation can be explored in a subsequent polarizer. After proper adjustment, the signal without the rotated polarization can not pass through the polarizer. However, the signal with the rotated polarization can pass through the polarizer.

Graphical representation of switching based on polarization rotation in the SOA is presented in Figure 3.5. First, the signal passes through the SOA unaffected. A subsequent polarizer is adjusted in such a way that the signal can not pass through it. In the second case, an additional signal is injected into the SOA. The SOA birefringence is changing. The polarization state of the initial signal rotates due to the changed SOA birefringence. As a result the signal with the rotated polarization can pass through the polarizer. Therefore on/off switching can be achieved by injecting an external signal into an SOA.

Nonlinear polarization rotation is a nonlinear function of the input light intensity. The advantage of nonlinear polarization rotation is that it allows all-optical signal switching in a single semiconductor component like the SOA or the EAM [75]. Hence, no challenging integration is required to achieve interferometric switching. However, the polarization state of the optical signals has to be carefully tuned. Because the polarization rotation depends on the SOA gain the limitation here is the SOA recovery time, which affects the carrier number and therefore gain of the SOA, see Section 2.2. Therefore to optimize performance of nonlinear polarization rotation, semiconductor optical amplifiers with high polarization dependency, high gain, and the short recovery time have to be applied [76].

Nonlinear polarization rotation in the SOA has been already applied for: demultiplexing [77], wavelength conversion in the gain region of the SOA [78–80], realization of logical functions [81,82], 3R regeneration [83], and a flip-flop memory [84].

3.2.3 Nonlinear polarization rotation in the transparency region of the SOA

The phase change due to the changes in the carrier number occurs in the gain region of the SOA as well as in the transparency region of the SOA, where the data energy is below the bandgap energy [70]. Taking into account the 1310 nm SOA, the full width gain region of the SOA is the 1310 nm wavelength domain and the transparency region is the 1550 nm wavelength domain. The phase change in the transparency region of the 1310 nm SOA was demonstrated and utilized for 1310-to-1550 nm wavelength conversion using the Mach-Zehnder Interferometer [70]. Other applications of this effect will be discussed in the next chapter. Here, nonlinear polarization rotation in the transparency region of the SOA will be investigated and potential applications will be extensively explored.

Figure 3.6 shows the experimental setup used to verify nonlinear polarization rotation in the transparency region of the SOA. A CW signal at 1310 nm with adjustable signal power was injected into a 1310 nm SOA. The SOA current was set to 300 mA. The 1310 nm SOA was employed in a bidirectional configuration.

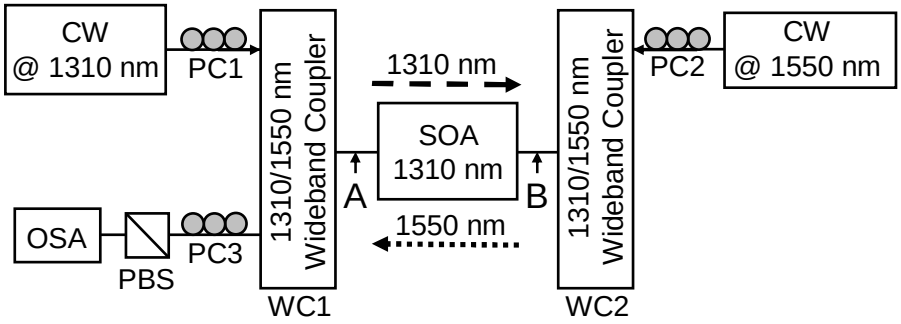

Figure 3.6: Experimental setup used to verify nonlinear polarization rotation in the transparency region of the SOA

In the previous wavelength conversion experiments based on nonlinear polarization rotation in the SOA, a bidirectional configuration [79] or an unidirectional configuration [76, 78] was applied. Both configurations supported excellent operation of the wavelength converter. Therefore in general both modes of operation can be applied to achieve 1310-to-1550 nm wavelength conversion. The advantage of the bidirectional configuration is possibility of wavelength conversion to the same wavelength. However, this advantage does not apply in the case of gain transparent operation. The bidirectional configuration was chosen to prevent two high power incoming signals (1310 nm and 1550 nm) to appear at the same facet of the SOA. This countermeasure was necessary to prevent damage of the switching SOA.

A linearly polarized 1550 nm CW signal coming from the opposite direction was fed into the 1310 nm SOA. The 1310 nm signal introduced changes in the 1310 nm SOA birefringence. As a result, the polarization of the 1550 nm signal at the SOA output was changed. This was explored by a subsequent polarization beam splitter

(PBS) in combination with a polarization controller (PC3). After passing through the PBS, the optical power of the 1550 nm signal was measured by an optical spectrum analyzer (OSA).

Figure 3.7 presents optical spectra emerging from point A in Figure 3.6 and from point B in Figure 3.6 of the 1310 nm SOA; to perform measurements an additional 3 dB coupler was inserted at the given points. It can be seen that no ASE noise was added to the 1550 nm signal. Due to reflections in the SOA, some of the 1310 nm data signal was also present at the A output. It is however subsequently supresses by the WC1. The 1550 nm signal experienced high attenuation in the 1310 nm SOA. The SOA attenuation at 1550 nm was measured to be 20 dB at 400 mA SOA current. This high attenuation values are due to fibre-SOA coupling loss, waveguide scattering and free-carrier absorption [70].

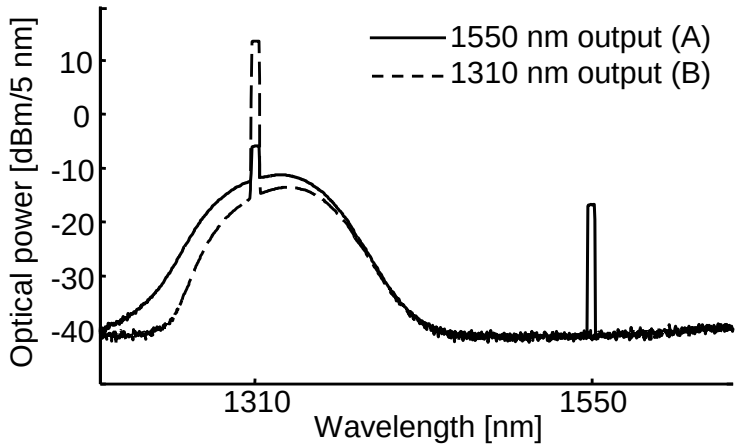

Figure 3.7: Optical spectra captured at either side of the 1310 nm SOA

High losses in the 1310 nm SOA can be compensated in two ways. First, by applying a 1550 nm CW laser with high output power. The commercially available CW lasers can easily deliver +13 dBm optical output power. The limitations here are put by the power handling capabilities of the SOA. Second, by utilizing optical post-amplification. An optical amplifier, an EDFA or a 1550 nm SOA will provide amplification to the 1550 nm signal coming from the SOA and therefore compensate for losses in the switching SOA. Combination of both solutions gives the best system performance. The CW signal with high input power assures a high OSNR value after the 1550 nm optical amplifier. This is particularly important in the case of subsequent transmission of the 1550 nm signal.

Two modes of operation were investigated. These two modes correspond to the non-inverting and the inverting operation respectively and were realized by the proper adjustment of the PC1–PC3. The PC1 and the PC2 adjusted the polarization stste of the incoming 1310 nm and 1550 nm CW signals respectively. The PC3 adjusted the polarization state of the 1550 nm signal before the PBS to maximize the contrast between signal with and without rotated polarization. In the non-inverting

mode of operation, the PCs were adjusted in such a way that increased power of the 1310 nm signal caused increase in power of the 1550 nm signal. In the inverting mode of operation, increased power of the 1310 nm signal caused decrease in power of the 1550 nm signal. Figure 3.8 shows the normalized power of the 1550 nm signal in the function of the 1310 nm signal power for both modes of operation. The 0 dB reference is equal to about -15 dBm of the optical power. It is clear that to obtain nonlinear polarization rotation, high input power is needed.

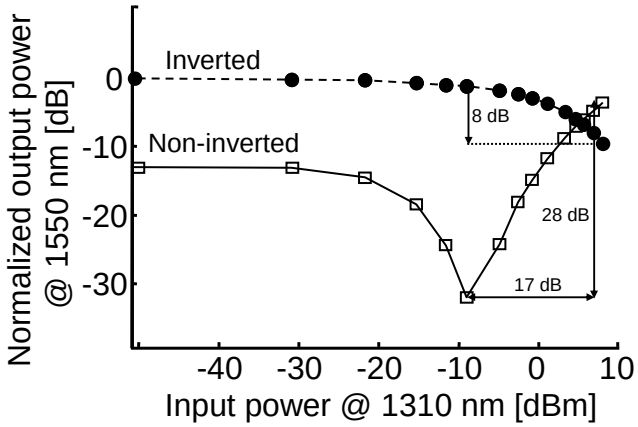

Figure 3.8: Static measurements of the 1550 nm output power vs. the 1310 nm input power

Changes in the 1310 nm input power lead to changes in the 1550 nm output power. The 1550 nm signal was in the transparency region of the 1310 nm SOA and no gain was provided to the 1550 nm signal. Therefore cross-gain modulation (XGM) did not cause these changes. By removing the PBS it was verified that the 20 dB change in the 1310 nm input power caused the 1.2 dB change in the SOA absorption at 1550 nm. Moreover, the non-inverting and the inverting operation was achieved, which basically can not be achieved by XGM or cross-absorption modulation. These results indicated that nonlinear polarization rotation in the transparency region of the SOA was a dominant effect in the presented experiment.

The curves presented in Figure 3.8 are similar to the ones of a Mach-Zehnder Interferometer (MZI). This reflects that the proposed polarization switch operates in a similar way to the MZI, since both are based on intensity driven phase changes and the different polarizations play the role of different light paths in the MZI [73]. Therefore important properties of interferometric switches like non-inverting and inverting mode of operation and the signal regeneration capability apply to the proposed concept. The signal reshaping capability is clearly visible in the non-inverting operation. For the input power dynamic range of 17 dB the output power dynamic range was 28 dB. It was verified that at 2.5 Gbit/s for an input extinction ratio (ER) 3.5 dB at 1310 nm the output ER equal to 7.7 dB could be obtained at 1550 nm, which basically agrees with the static measurements and proves regenerative capabilities.

However, at 10 Gbit/s the signal reshaping capability was not observed. The

similar observation is reported for in-band wavelength conversion based on nonlinear polarization rotation [79]. In the dynamic operation, the SOA carrier number does not reach a steady-state value due to the slow recovery time of the SOA. In the static measurements, the SOA carrier number can reach the steady state value.

The inverting operation showed for the same range of input power, an output power range equal to 8 dB. Therefore to achieve the reshaping capability higher input power is required. Here, the limitations were: the available 1310 nm input power and the maximum allowable input power to the 1310 nm SOA. The state-of-the-art SOAs can handle power up to +15 dBm. However, the device used in the presented experiments is from the early 1310 nm SOA generations. Therefore input powers needed to be limited, as extra precautions were necessary to prevent damage to the device.

3.3 1310-to-1550 nm wavelength conversion

In the previous section, nonlinear polarization rotation in the transparency region of the SOA was described phenomenologically and demonstrated experimentally. A straightforward application of this mechanism is all-optical wavelength conversion from the 1310 nm wavelength domain to the 1550 nm wavelength domain. In this section applications of the investigated mechanism to the various kinds of 1310-to-1550 nm wavelength conversion will be demonstrated. Inverting and non-inverting wavelength conversion, and wavelength conversion with simultaneous nonreturn-to-zero to return-to-zero data format conversion will be investigated. Finally, 1310-to-1550 nm wavelength conversion in between two transmission links will be shown.

3.3.1 Wavelength converter setup

Figure 3.9 shows a schematic of the 1310-to-1550 nm wavelength converter setup. An intensity modulated NRZ signal at 1310 nm entered the wavelength converter through a polarization controller (PC1). Next, the 1310 nm NRZ signal passed through a 1310/1550 nm wideband coupler (WC1) and finally entered a 1310 nm SOA. The PC1 was adjusted to achieve the optimum wavelength conversion performance. The multi-quantum well SOA employed, had an active area with a length of 800 μm. A 1550 nm CW signal passed through a second wideband coupler (WC2) and was fed into the 1310 nm SOA.

The 1310 nm SOA was employed in a bidirectional configuration and the 1550 nm signal travelled through the 1310 nm SOA in the opposite direction to the 1310 nm NRZ signal. The polarization of a 1550 nm CW signal was adjusted by a polarization controller (PC2) to be approximately 45° to the orientation of the SOA polarization axes. This adjustment maximized the effect of nonlinear polarization rotation on the 1550 nm signal. In the system applications, the 1550 nm signal will be generated locally in the converter node. Therefore the polarization state of the 1550 nm CW signal can be easily controlled and ensured to be stable, to guarantee optimal performance of wavelength conversion. The presence of the WC2 was not essential for the

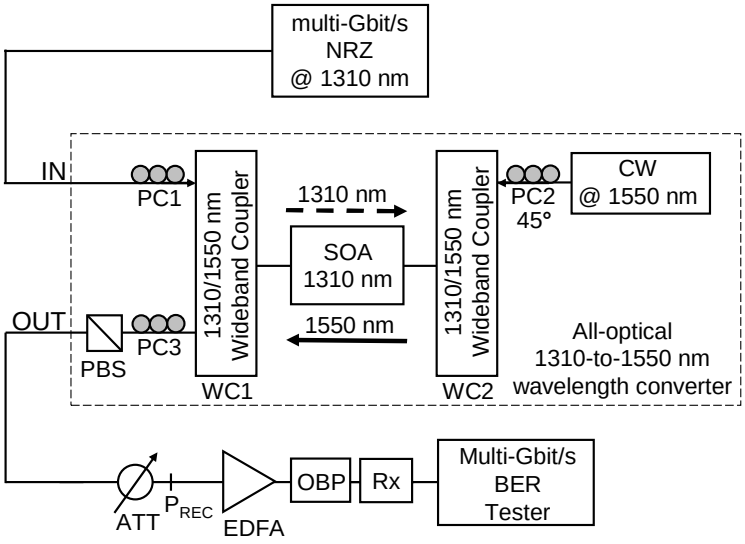

Figure 3.9: 1310-to-1550 nm wavelength converter setup

proper operation of the wavelength converter and the CW signal at 1550 nm coming from the PC2 could be directly fed into the 1310 nm SOA. During experiments the 1310 nm output of the WC2 was used for monitoring purposes.

Due to the changeable SOA birefringence the 1550 nm signal at the SOA output had a changed state of polarization with respect to the 1550 nm signal without any 1310 nm signal present. After passing through the SOA, the 1550 nm signal was separated from the 1310 nm signal in the WC1 and entered a polarization filter formed by a PBS and a polarization controller (PC3). The PBS had an extinction ratio better than 20 dB. After the PBS, the 1550 nm signal entered a pre-amplified receiver. The pre-amplified receiver consisted of a variable attenuator (ATT), an EDFA, an optical band-pass filter (OBP), and a multi-Gbit/s data receiver in combination with a BER tester.

3.3.2 Non-inverting and inverting operation

First, the non-inverting and inverting operation under dynamic conditions were investigated. Figure 3.10 schematically visualizes both modes of operation. As transfer functions, the curves from Figure 3.8 are applied. In the non-inverting mode of operation the low input signal level corresponds to the low output signal level. In the inverting mode of operation the low input signal level corresponds to the high output signal level.

It is clear that the transfer curves determine the signal shape after conversion. In the case of non-inverting conversion, the signal shape is preserved due to the positive slope of the almost linear transfer curve. In the case of inverting conversion, the signal shape will be distorted due to the nonlinear transfer curve. Moreover, a significant reduction of the extinction ratio can be expected if the slope is shallow.

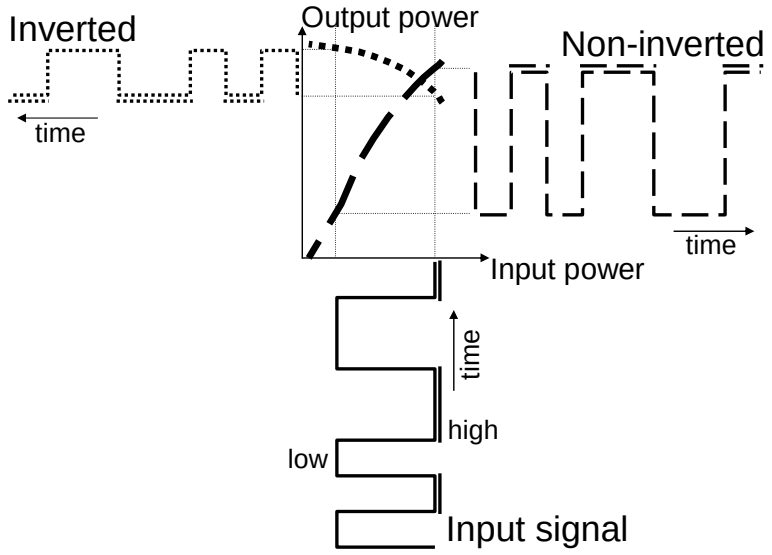

Figure 3.10: Non-inverting and inverting mode of operation

A 10 Gbit/s NRZ signal was generated in an IM with a PRBS of length $2^{31} - 1$. The power of the input 1310 nm signal was set to 4.6 dBm and the power of the 1550 nm CW laser was set to 7.0 dBm. The output 1550 nm signal was evaluated in the pre-amplified 10 Gbit/s receiver. In the experiments an SOA current of 300 mA was maintained. The system was optimized to achieve first non-inverting and then inverting wavelength conversion.

Figure 3.11 shows captured eye diagrams and signal traces. Both inverting and non-inverting conversions are presented. The eye diagram and the signal trace for non-inverting conversion show clear open eye and indicate excellent operation of the wavelength converter. Some asymmetry in the eye diagrams can be observed. It was demonstrated in [85–87], that the injected light reduces the SOA recovery time. Therefore the rise time of the non-inverted signal, when the signal is injected into the SOA, is shorter than the fall time, when there is no signal.

The inverted signal is distorted. The strongly nonlinear transfer function causes signal distortions and reduction of the extinction ratio. Moreover, the inverted signal has the long rise time and the short fall time, which agrees with the principle of the inverting operation. However, pronounced difference between the fall time of the non-inverting operation and the rise time of the inverting operation can be observed.

This apparent difference is caused by the limitations of the digital communication analyzer, used to capture eye diagrams and signal traces. In the non-inverting operation, the falling edge of the signal could not be entirely visualized due to the minimal value of the signal that can be visualized. In the inverting mode of operation, the slow rising edge is entirely visible. High optical power in "0" and "1" levels overcomes limitations of the digital communication analyzer. Nevertheless, in both cases the eye is clearly open giving a prospect for an error-free detection.

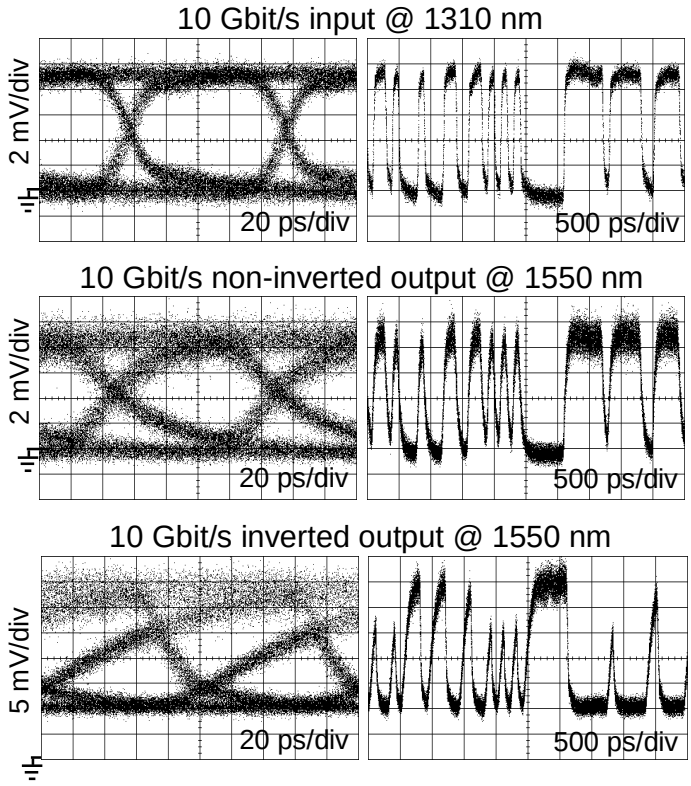

Figure 3.11: 10 Gbit/s eye diagrams and signal traces

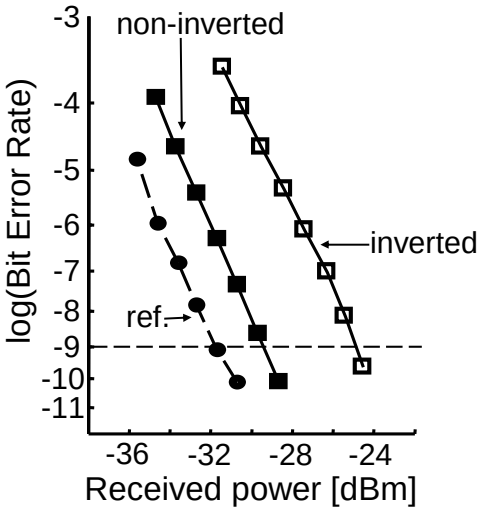

Figure 3.12: Results of the BER measurements at 10 Gbit/s; PRBS $2^{31}-1$

In the next step, the performance of the proposed wavelength converter was investigated by measuring the BER. Results of the BER measurements are visualized in Figure 3.12. The BER of a non-inverted and an inverted 1550 nm signal as well as a 10 Gbit/s reference signal was measured as a function of optical power before a pre-amplifying EDFA. As a reference an optimized 1550 nm NRZ signal generated in the same IM was used. In all cases no error-floor was observed, which indicated again excellent operation of the wavelength converter. The power penalty at BER=10^{-9} for the non-inverting conversion was 2.4 dB and 6.9 dB for the inverting conversion. The power penalty was caused by the slow recovery time of the SOA. By adjusting the PC1 we verified the polarization sensitivity at BER=10^{-9} to be less than 1 dB.

In the next non-inverting wavelength conversion experiment the bit rate was increased to 20 Gbit/s. The SOA current was increased to the maximum value, namely 400 mA. Average power of the input NRZ 1310 nm signal was set to 5.3 dBm, while power of the 1550 nm laser CW was set to 7.0 dBm.

As a reference a 1550 nm NRZ signal generated in the same IM was used. Results of the BER measurements and the captured 20 Gbit/s eye diagrams are shown in Figure 3.13. No error-floor was observed and the power penalty at BER=10^{-9} was 3.8 dB. This higher power penalty, in comparison with the 10 Gbit/s operation, originated from the limited extinction ratio of the converted signal, due to the pronounced influence of the SOA recovery time. The limited extinction ratio between "0" and "1" level is visible in the captured eye diagram. Nevertheless, error-free wavelength conversion at 20 Gbit/s was achieved.

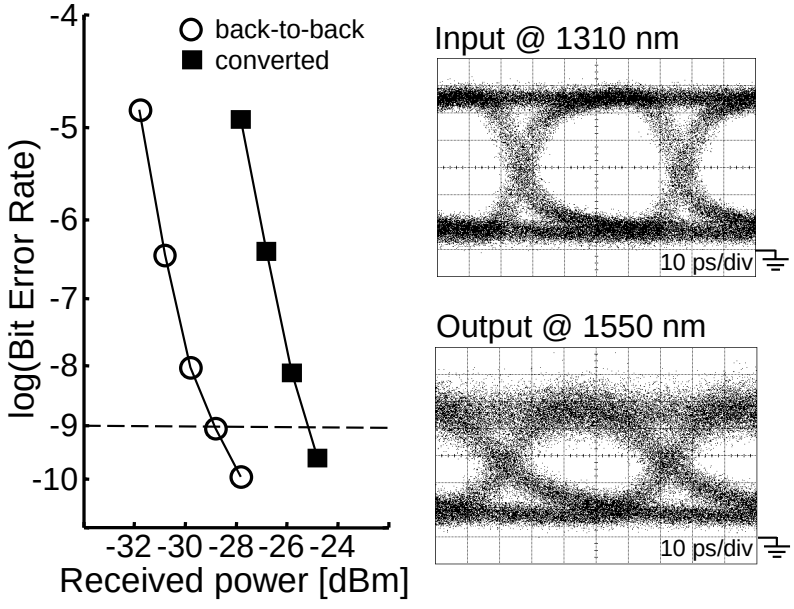

Figure 3.13: Results of the BER measurements and the captured eye diagrams of non-inverting wavelength conversion at 20 Gbit/s ; PRBS $2^{31}-1$

3.3.3 1310-to-1550 nm wavelength conversion with simultaneous data format conversion

Core network transmission systems intended for operation at bit rates higher than 40 Gbit/s usually transmit return-to-zero (RZ) pulses with a pulse duration of a few picoseconds and utilizing optical time domain multiplexing (OTDM) technique [88] to overcome the speed limitations of electronic multiplexing, see Section 4.1. Therefore to realize a transparent optical network a new network subsystem is required to change the NRZ data format, widely used in the access-metro networks, to the RZ data format used in high speed OTDM networks.

Desirably, the data format conversion subsystem should perform simultaneously 1310-to-1550 nm wavelength conversion to reduce system complexity, i.e. instead of separate 1310-to-1550 nm wavelength conversion and afterwards NRZ-to-RZ data format conversion or vice versa, both operations should be performed simultaneously in one subsystem. An ultra wideband wavelength and data format converter should offer all-optical multi Gbit/s wavelength and data format conversion capability to avoid optical-electrical-optical conversions, while remaining cost-effective. Again, nonlinear polarization rotation in the transparency region of the SOA offers a solution to this problem.

To achieve simultaneous 1310-to-1550 nm wavelength conversion and NRZ-to-RZ data format conversion a CW laser source in the wavelength converter setup presented in Figure 3.9 was replaced by an optical clock source. The optical clock source provided at the multi-GHz repetition rate a train of very short optical pulses, with the pulse width in the range of few picoseconds. A mode-locked ring laser was applied for this, which generated a 10 GHz clock signal at 1550 nm with the pulse full-width at half maximum (FWHM) =2 ps, measured using an autocorrelator.

An additional variable time delay line was inserted after the optical clock source to adjust the position of the 10 GHz clock pulses in the time domain. The position of the pulses in the time domain was adjusted to achieve optimum wavelength and data format conversion. The power of the input 1310 nm NRZ signal (PRBS $2^{31}-1$) remained unchanged and the average power of the 1550 nm clock signal was set to 6.0 dBm.

Based on the previous results, further experiments concentrated on 1310-to-1550 nm non-inverted conversion. Using the autocorrelator the 1550 RZ signal pulse FWHM was measured to be 2.2 ps at the converter output. Figure 3.14 shows the input 1310 nm NRZ eye diagram, the output 1550 nm RZ eye diagram, and the reference back-to-back 1550 nm RZ eye diagram. The eye diagram of the converted 1550 nm RZ signal shows a clear open eye and indicates excellent operation of the converter. However, some residual, not completely suppressed clock signal in the "0" level can be observed as well as variations in the "1" level.

Finally, the BER measurements were performed. The results of the BER measurements are visualized in Figure 3.14. As a reference an optimized 1550 nm RZ signal was used. The reference signal was generated in the same clock source and modulated in a following intensity modulator. No error-floor was observed and the

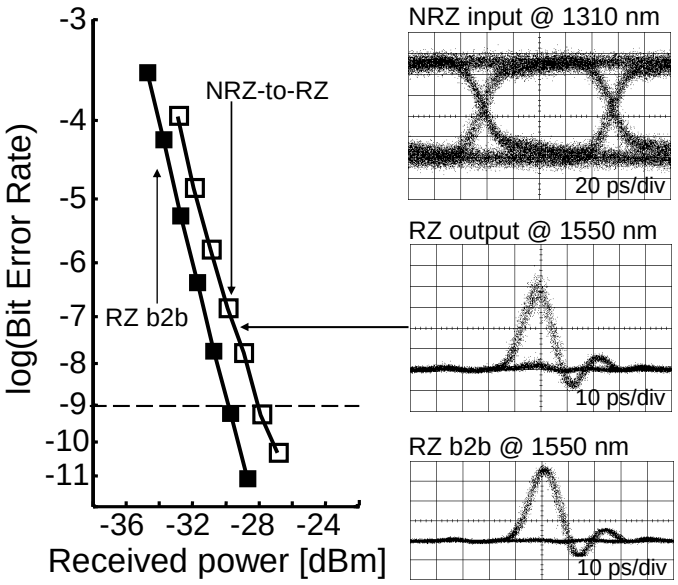

Figure 3.14: BER measurements and captured eye diagrams of the 1310 nm NRZ to 1550 nm RZ non-inverted conversion; PRBS $2^{31}-1$

power penalty at BER=10^{-9} was 2.0 dB. This result is similar to the power penalty for 1310-to-1550 nm conversion without NRZ-to-RZ data conversion.

The experimental results indicated that the converted 1550 nm RZ signal could be used as a tributary channel in an OTDM data stream up to 160 Gbit/s. Again, by adjusting the PC1 (the 1310 nm signal) the polarization sensitivity at BER=10^{-9} was verified to be less than 1 dB.

3.3.4 1310-to-1550 nm wavelength conversion in between two transmission links

Although nonlinear polarization rotation in the SOA was applied previously for in-band wavelength conversion [78–80] the transmission feasibility of the converted signals has not been verified. Moreover, the transmission feasibility was not verified in the case of other ultra wide-band wavelength conversion techniques [67–70]. In this section, all-optical 1310-to-1550 nm wavelength conversion in between two transmission links is reported.

Figure 3.15 shows the experimental setup. In a transmitter the 10 Gbit/s NRZ signal at 1310.7 nm with the PRBS of length $2^{31}-1$ was generated. The power of the 1310 nm NRZ signal was set to 0 dBm. Then the modulated signal was fed into a 25 km long SSMF based transmission line. SSMF is currently the most deployed fibre, particularly in the access and metro systems [15, 20]. The transmission reach of access systems is specified to be less than 20 km [10, 64]. Therefore undoubtedly the maximum transmission distance in the 1310 nm wavelength domain was bridged

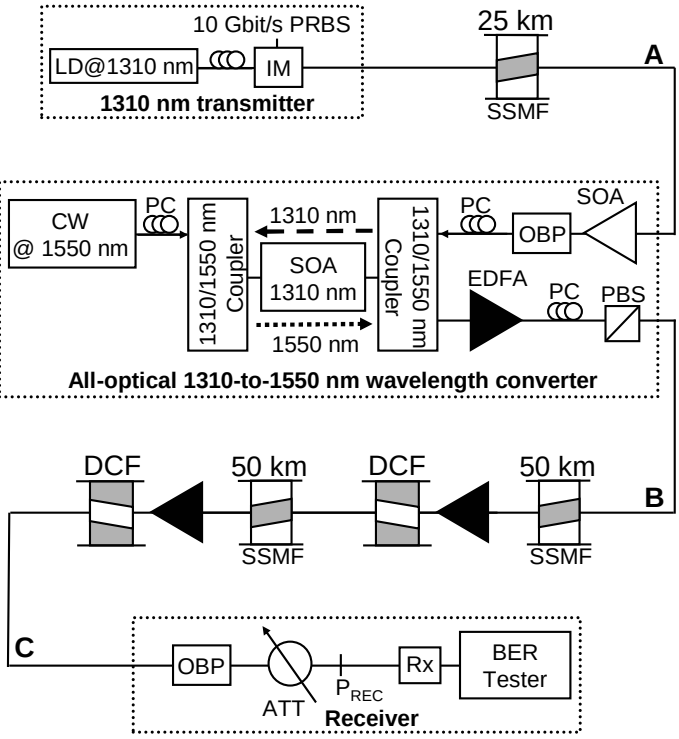

Figure 3.15: Experimental setup of 1310-to-1550 nm wavelength conversion in between two transmission links

in this experiment.

After the first transmission line, the 1310 nm signal entered an all-optical 1310-to-1550 nm wavelength converter. The power of the input signal to the wavelength converter was equal to -8.4 dBm (point A in Figure 3.15). The applied wavelength converter was a modified version of the one used in the previous experiments. At the wavelength converter input a 1310 nm SOA was added to increase power of the 1310 nm signal injected into the switching SOA. To prevent unwanted saturation of the switching SOA the ASE noise originating from the pre-amplifying 1310 nm SOA was reduced in a following OBP with the 3 dB bandwidth of 1.2 nm.

The switching SOA operated with 400 mA driving current. Power of the 1550 nm laser was set to 7.0 dBm. To improve OSNR of the 1550 nm signal, the amplifying EDFA was applied directly after the 1310/1550 nm coupler. After the EDFA, a PBS in combination with a PC was placed. As an additional advantage, 3 dB reduction of the ASE noise was achieved in the PBS. The power of the 1550 nm signal at the wavelength converter output was set to 0 dBm (point B in Figure 3.15).

The second transmission line was formed by two 50 km long SSMF spans, two dispersion compensation fibre (DCF) modules and two EDFAs to compensate for losses in the transmission link. Together, the DCF modules compensated for dispersion of 1619 ps/nm. Therefore full compensation of accumulated dispersion of

a 100 km SSMF link was achieved. After passing through the second transmission line, the 1550 nm signal was evaluated in a 10 Gbit/s receiver, consisting of an OBP, a variable ATT and a 10 Gbit/s data receiver in combination with the BER tester.

Figure 3.16 presents the measured 10 Gbit/s eye diagrams and the optical spectra: a 1310 nm signal after 25 km transmission at the wavelength converter input (A), a 1550 nm signal at the wavelength converter output (B), and a 1550 nm signal after the 100 km transmission line (C); points A, B, and C in Figure 3.15 respectively. All eye diagrams show a clear open eye.

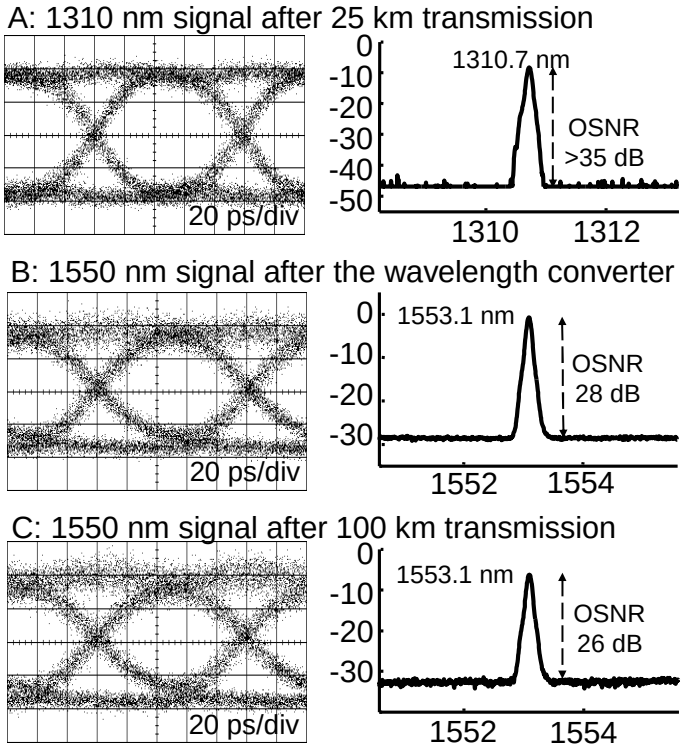

Figure 3.16: Eye diagrams and optical spectra measured at the various points of the experimental setup

The input 1310 nm signal had the best OSNR, namely 38 dB. The converted 1550 nm signal had the OSNR value equal to 28 dB and the 1550 nm signal after transmission had the OSNR value equal to 26 dB, shown in the right column of Figure 3.16. The OSNR degradation was caused by accumulation of the ASE noise in the EDFAs applied in the transmission line. Reduction of the 1550 nm signal OSNR leaded to the BER degradation.

Figure 3.17 shows the measured BER curves. No BER error-floor was observed. By comparing the 1310 nm input signal with the 1550 nm converted signal the wavelength conversion power penalty at BER=10^{-9} was estimated to be 1.2 dB. By comparing the 1550 nm signal before and after transmission the transmission power penalty at BER=10^{-9} was estimated to be 0.5 dB.

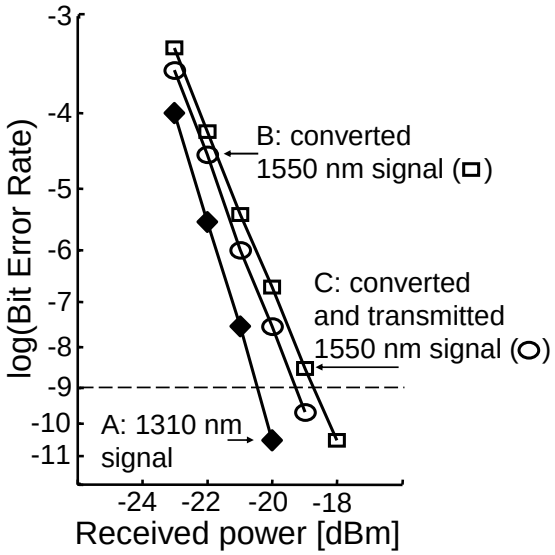

Figure 3.17: BER measurements of 1310-to-1550 nm wavelength conversion in between two transmission links

In conclusion, in this section 1310-to-1550 nm wavelength conversion in between two SSMF based transmission links was demonstrated. Error-free wavelength conversion and transmission at 10 Gbit/s was achieved. Therefore the transmission feasibility of the 1310-to-1550 nm converted signals was verified experimentally.

3.4 1310-to-1550 nm transmultiplexing

In the previous section 1310-to-1550 nm wavelength conversion has been demonstrated utilizing nonlinear polarization rotation in a single SOA. In the experiments presented a single NRZ data channel in the 1310 nm wavelength domain was converted into a single NRZ data channel in the 1550 nm wavelength domain. This approach is bandwidth inefficient in the particular case of a large number of data channels at low bit rate, i.e. at the interface between access and core networks. Obviously, it is desirable and economically advantageous to combine multiple low bit rate data streams from the 1310 nm wavelength domain into one data stream in the 1550 nm wavelength domain. Conversion of WDM data streams into one OTDM data stream is called transmultiplexing.

Figure 3.18 shows a conceptual model of transmultiplexing. The incoming data streams at different wavelengths are processed in such a way that the output data stream at a certain wavelength is formed from the time interleaved input data streams. Therefore from the multiple input data streams a single OTDM data stream is created at the transmultiplexer output. The bit rate of the OTDM data stream is a multiple of the bit rate of the input data streams. Transmultiplexing can be performed on multiplexed data from different wavelengths as well as on the same

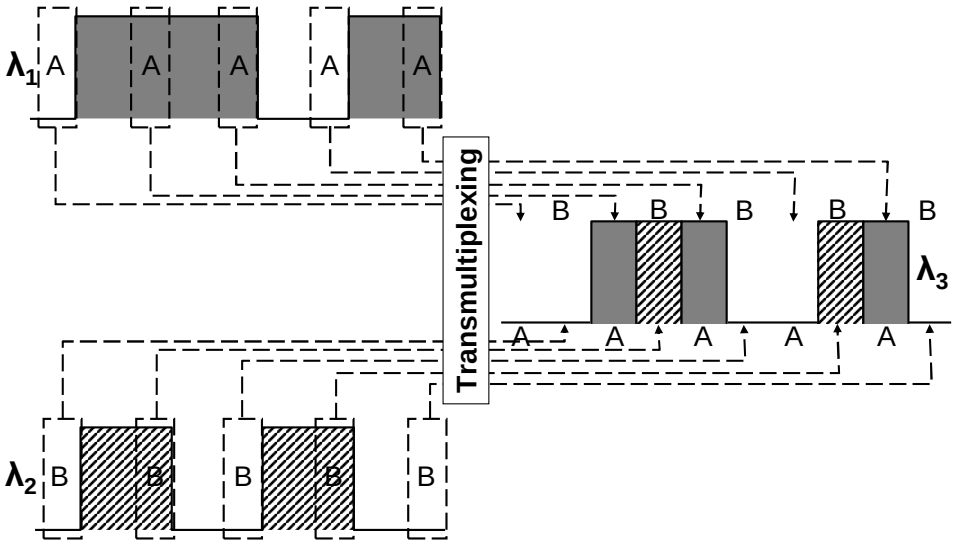

Figure 3.18: Conceptual model of transmultiplexing

wavelength to form one data stream at the chosen wavelength.

Several transmultiplexing techniques have been demonstrated [89–95]. Presented techniques utilized cross-gain modulation in an SOA [89–91], cross-phase modulation in an optical fibre [92–94], or cross-absorption modulation in an electro-absorption modulator [95]. However, the demonstrated transmultiplexing techniques operated exclusively in the 1550 nm wavelength domain. Here, nonlinear polarization rotation in the SOA will be utilized to achieve 1310-to-1550 nm transmultiplexing, i.e. multiple WDM data streams in the 1310 nm wavelength domain will be combined into one OTDM data stream in the 1550 nm wavelength domain, see Figure 3.19.

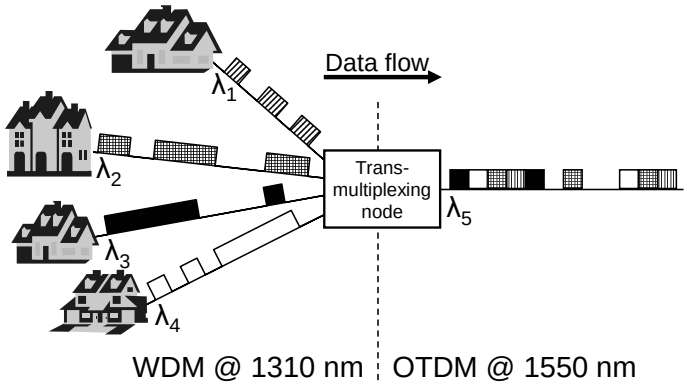

Figure 3.19: 1310-to-1550 nm transmultiplexing

3.4.1 Architecture of the transmultiplexing node

In general, two architectures of the transmultiplexing node can be distinguished, see Figure 3.20. In both architectures the following functional blocks are required: the NRZ-to-RZ data format converter, the optical delay, and the wavelength converter. Certainly, if the appropriate RZ data format is used in the access network NRZ-to-RZ data format conversion is not necessary.

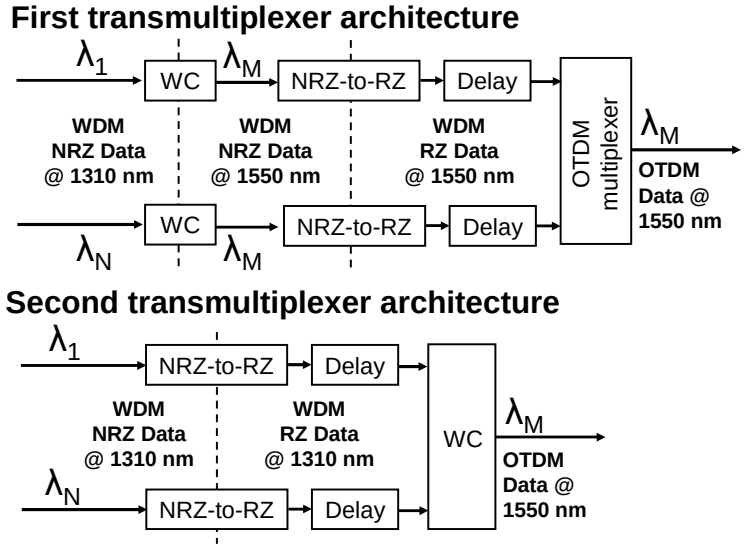

Figure 3.20: Transmultiplexer architectures; WC–wavelength converter

In the first architecture, all 1310 nm WDM channels are converted into the 1550 nm wavelength domain separately. Hence, for N data channels N wavelength converters are required. After NRZ-to-RZ data format conversion, that can be done also in the wavelength converters, the converted data streams are delayed against each other to achieve an uniform ODTM data stream at the OTDM multiplexer output. As an OTDM multiplexer, a passive fibre coupler can be used. The disadvantage of the first scheme is that each wavelength channel requires a separate wavelength converter. This increases system complexity, cost, and reduces scalability.

In the alternative architecture, transmultiplexing is achieved utilizing one 1310-to-1550 nm wavelength converter performing simultaneously wavelength conversion and OTDM multiplexing. To achieve that, the incoming NRZ data streams are first converted to the RZ data streams. Then the signals are delayed appropriately. Finally, all signals are injected into a wavelength converter where transmultiplexing is performed. The advantages of this architecture are simplified design, limited complexity, and lower cost; the disadvantages: requires N separate NRZ-to-RZ converters or all data streams have to be in-phase. Hence, the second architecture will be utilized in the further experiments. In both architectures synchronization of the transmultiplexing node is an important issue and it will be discussed in the separate section.

3.4.2 2×5 Gbit/s 1310 nm to 10 Gbit/s 1550 nm transmultiplexing

First, feasibility of 1310-to-1550 nm transmultiplexing based on nonlinear polarization rotation in a single SOA was verified. Figure 3.21 presents the experimental setup. The experimental setup can be divided in three parts: a 1310 WDM transmitter, a transmultiplexing subsystem, and an OTDM receiver. In the transmitter, two 5 Gbit/s NRZ signals were generated by modulating CW signals at 1310.9 nm and 1313.8 nm in a first intensity modulator (IM) driven with a PRBS of length $2^{31} - 1$.

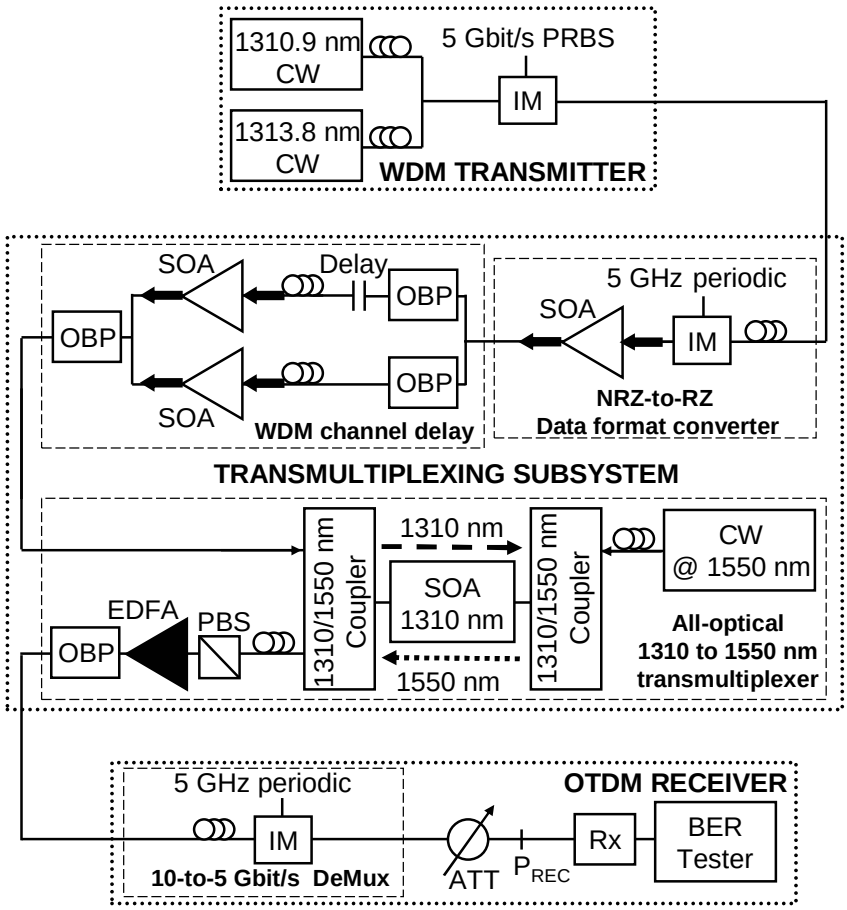

Figure 3.21: Experimental setup of 2×5 Gbit/s to 10 Gbit/s transmultiplexing

Next, the 1310 nm WDM signals entered the transmultiplexing subsystem. In a data format converter, a second IM was driven by a periodic electrical signal. The driving signal had a pulse width of 100 ps and period of 200 ps, see Figure 3.22a. Hence, the data format converter reshaped the incoming NRZ signals into the 50% duty cycle RZ signals with a pulse width set to 100 ps, which equals the pulse width of a 10 Gbit/s NRZ signal, see Figure 3.22b. It has to be mentioned that it can be

only done in the presented way when the two data streams are sufficiently in-phase. The NRZ-to-RZ data format conversion allowed further time domain multiplexing to achieve a 10 Gbit/s signal at the transmultiplexer output. A following SOA compensated for losses in both intensity modulators.

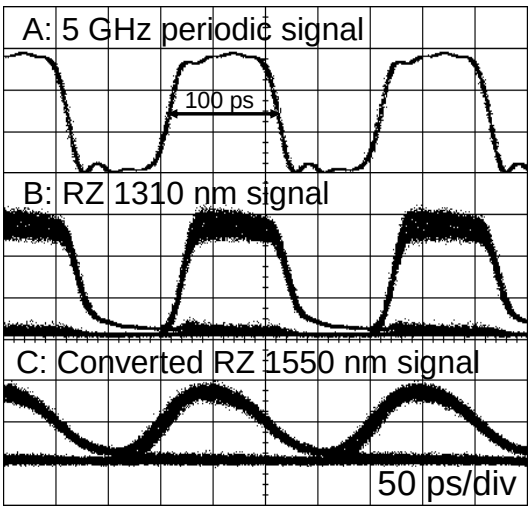

Figure 3.22: The 5 GHz periodic signal (A), the RZ 1310 nm signal (B), and the converted RZ 1550 nm signal (C)

After the data format converter, the WDM signals were split by a fibre coupler into two arms. Each arm consisted of an OBP to select one of the wavelengths, an SOA to amplify the signal to the desired level, and a polarization controller to adjust the signal polarization state. In one of the arms an optical delay line was inserted. The WDM data channels were delayed approximately 350 bits with respect to each other to decorrelate them, and to align them correctly in the time domain. As a result, an aggregate 10 Gbit/s data stream consisting of two time domain interleaved 5 Gbit/s signals, at two different wavelengths was formed at the output of a following fibre coupler. The optical power of the WDM channels was set to be 4 dBm per channel at the coupler output. After passing through the next OBP (3 dB bandwidth 5 nm) the signals were injected into a 1310-to-1550 nm transmultiplexer.

As a transmultiplexer the 1310-to-1550 nm wavelength converter described in Section 3.3.1 was used. The incoming time interleaved RZ signals introduced additional birefringence in the 1310 nm SOA. Therefore the 1550 nm signal at the transmultiplexing SOA output had a changed state of polarisation with respect to a 1550 nm signal without any 1310 nm signal present. This resulted in multiplexing of the 1310 nm WDM signals into one 1550 nm OTDM signal. The power of the 1550 nm CW signal was set to 6 dBm and the transmultiplexing SOA driving current was set to 400 mA.

After passing through the transmultiplexing SOA the 1550 nm signal entered a polarization filter formed by a PC in combination with a PBS. The polarization filter

was adjusted in such a way that the 1550 nm signal with the rotated polarization passed through the PBS. After amplification in an EDFA to compensate for attenuation in the transmultiplexing SOA followed by an OBP, the 1550 nm signal was fed into an OTDM receiver. The OTDM receiver consisted of a 10-to-5 Gbit/s demultiplexer, realized by an intensity modulator driven by a 5 GHz periodic electrical signal, a variable ATT, a data receiver and a BER tester.

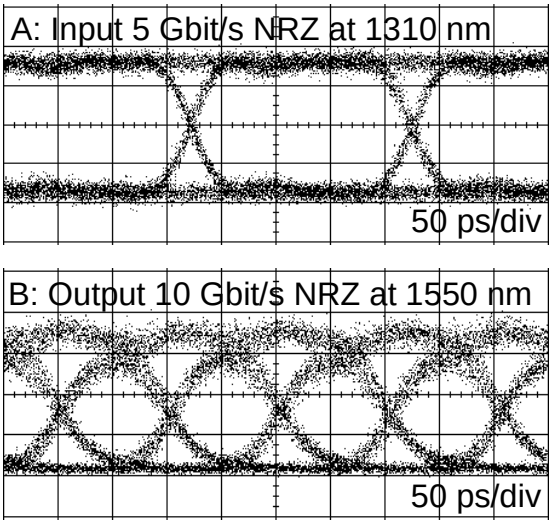

Figure 3.23: Measured eye diagrams of 2×5 Gbit/s to 10 Gbit/s transmultiplexing

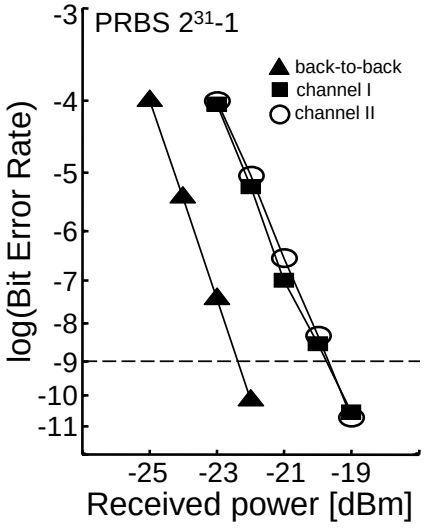

Figure 3.24: BER measurements of 2×5 Gbit/s to 10 Gbit/s transmultiplexing

Figure 3.23a presents an input 5 Gbit/s signal at 1310 nm captured using a communication analyzer. The eye diagram of the converted 10 Gbit/s 1550 nm signal (see Figure 3.23b) shows a clear open eye and indicates excellent operation of the transmultiplexer. Finally, the performance of the proposed transmultiplexer was investigated in the BER measurements.

Figure 3.24 shows the BER curves for the converted two channels and a reference back-to-back signal as a function of measured optical power before a 5 Gbit/s data receiver. As a reference an optimized 5 Gbit/s NRZ signal at 1550 nm was used. To allow reliable comparison with the converted signals the reference 5 Gbit/s signal was reshaped in the 10-to-5 Gbit/s demultiplexer driven by the 5 GHz periodic signal. No BER error-floor was observed, both channels showed almost identical performance and the power penalty for the conversion at BER=10^{-9} was 2.6 dB.

In conclusion, a novel transmultiplexing technique based on nonlinear polarization rotation in a single SOA has been demonstrated. The time interleaved signals at two different wavelengths in the 1310 nm wavelength domain introduced alternate changes in the SOA birefringence. As a result, the polarization state of the 1550 nm output signal rotated, which was explored by the polarization filter.

3.4.3 4×2.5 Gbit/s 1310 nm to 10 Gbit/s 1550 nm transmultiplexing

Figure 3.25 presents the experimental setup used to realize 4×2.5 Gbit/s 1310 nm to 10 Gbit/s 1550 nm transmultiplexing. The 2.5 Gbit/s bit rate is the standardized bit rate for up-stream communications in access networks such as GPON [10,64,65]. Similarly to the previous experiment, the experimental setup can be divided into three parts: a 4×2.5 Gbit/s transmitter, a transmultiplexing subsystem, and a 1550 nm OTDM receiver.

In the transmitter, four CW signals at 1311.5 nm, 1312.9 nm, 1314.3 nm and 1315.6 nm were coupled together in a passive fibre coupler and modulated simultaneously in an IM at bit rate 2.5 Gbit/s with PRBS of length $2^{31}-1$. The polarization state of the CW signals was adjusted to achieve maximum modulation performance. To compensate for losses in the 6 dB fibre coupler and the modulator, all four NRZ 2.5 Gbit/s signals were amplified simultaneously in an SOA. The power level of each signal was set to -7 dBm per channel at the transmitter output, see Figure 3.26a.

After the transmitter the signals entered a transmultiplexing subsystem. The transmultiplexing subsystem comprised a NRZ-to-RZ data format converter, a WDM channel time delay, and an all-optical 1310-to-1550 nm transmultiplexer. In the data format converter the NRZ data format of 2.5 Gbit/s signals was changed to the RZ data format with 25% duty cycle, i.e. FWHM 100 ps.

As a data format converter a second IM driven by an electrical signal sequence "1000" was used. The "1000" sequence was repeated with the period equal to 400 ps (2.5 GHz). The data format converter was synchronized using a back-to-back electrical clock signal. In general, as a data format converter an EAM driven by the 2.5 GHz sinusoidal electrical signal can be used. Unfortunately, a 1310 nm EAM

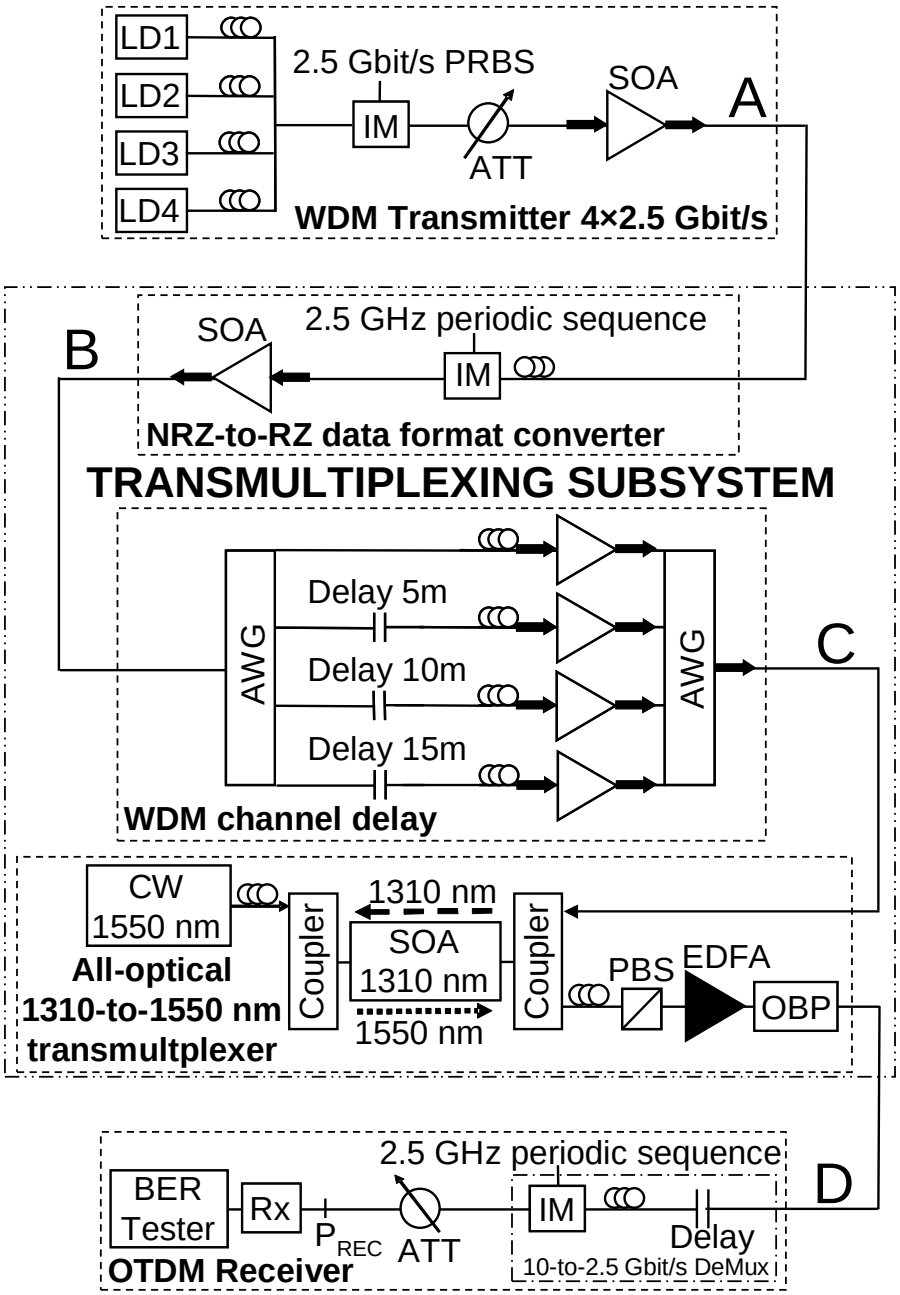

Figure 3.25: Experimental setup of 4×2.5 Gbit/s to 10 Gbit/s transmultiplexing

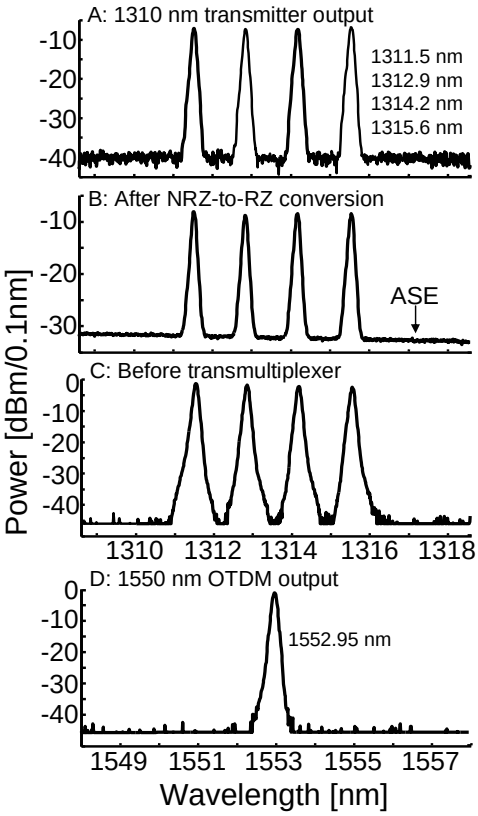

Figure 3.26: Optical spectra of 4×2.5 Gbit/s to 10 Gbit/s transmultiplexing

was not available at the moment of experiments. To compensate for losses in the IM an SOA was applied. Figure 3.27 presents the input 1310 nm 2.5 Gbit/s NRZ signal, the periodic "1000" electrical signal and the converted 1310 nm RZ signal. Optical spectrum after the NRZ-to-RZ data converter is presented in Figure 3.26b.

After the data format converter the RZ WDM signals entered a WDM channel delay. The WDM channel delay had two functions: to decorrelate and to adjust the WDM channels to form the uniform OTDM data stream at the output of the transmultiplexer. In a real system the first function will not be necessary because the incoming data streams will be anyway decorrelated. The second function will be realized by the delay lines placed in the incoming fibre links, see Figure 3.20. However, those two functions were necessary to achieve proper operation of the proposed transmultiplexer in the laboratory experiments.

In the WDM channel delay, first all signals were demultiplexed in the wavelength domain by an AWG described in Section 2.3. The AWG not only performed a demultiplexing operation on the wavelength channels but also the ASE noise filtering. Then the data channels were delayed against each other. The time delay was realized by inserting the fibre spans of length 5 m, 10 m, and 15 m and the

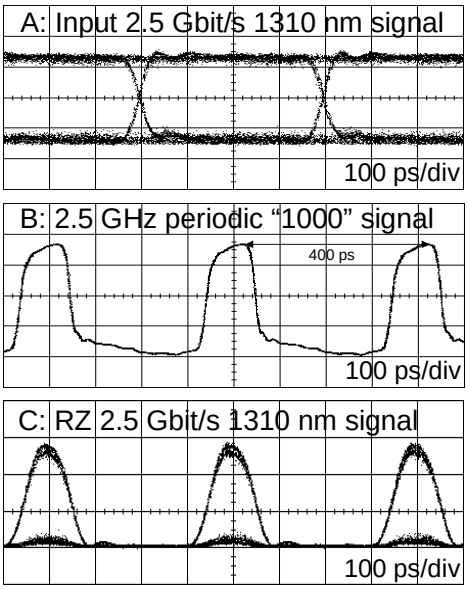

Figure 3.27: 1310 nm signal before (A) and after (C) NRZ-to-RZ data format conversion, and the driving 2.5 GHz "1000" electrical signal (B)

variable delay lines. The variable delay lines synchronized exact positions of the RZ pulses in the time domain to form the uniform output data stream. In practical realizations, the optical delay lines of 400 ps will be required to achieve the necessary delay at a bit rate of 2.5 Gbit/s. Assuming the same aggregate bit rate, where $AggregateBitRate = NumberOfChannels \times BaseBitRate$, for the higher transmultiplexing factor, e.g. 8-to-1 longer delay lines will be required according to the relationship: $RequiredDelay = 1/BaseBitRate$. Such long delay lines allow maximum flexibility when adjusting position in the time domain of the RZ pulses before the transmultiplexing sub-system.

To compensate for losses and to set output power to the desired value the 1310 nm SOAs were used. After the SOAs all signals were combined in the following AWG. The application of the AWG has advantages of low insertion loss and simultaneous ASE filtering. The drawback of the proposed solution is the necessity of a fixed wavelength allocation grid in the access network.

Finally, an aggregate 10 Gbit/s data stream consisting of four time domain interleaved 2.5 Gbit/s signals at four different wavelengths was formed at the output of the second re-combining AWG. Further, the composite 10 Gbit/s signal entered a 1310-to-1550 nm transmultiplexer described in the previous section. Optical power of the WDM channels was adjusted to be -2 dBm per channel at the wide-band coupler output, see Figure 3.26c. In the all-optical transmultiplexer, all four 1310 nm signals were simultaneously multiplexed in the time domain and converted into the 1550 nm wavelength domain. The optical spectrum of the 1550 nm output signal is presented in Figure 3.26d.

Figure 3.28 shows eye diagrams for the converted 1550 nm signals. All eye diagrams demonstrate a clear open eye and indicate excellent operation of the transmultiplexer. Transmultiplexing of single or three channels was achieved by blocking the optical signal paths of the other channels. Asymmetry in the rise and the fall time is visible. This asymmetry is a main cause of the transmultiplexing penalty.

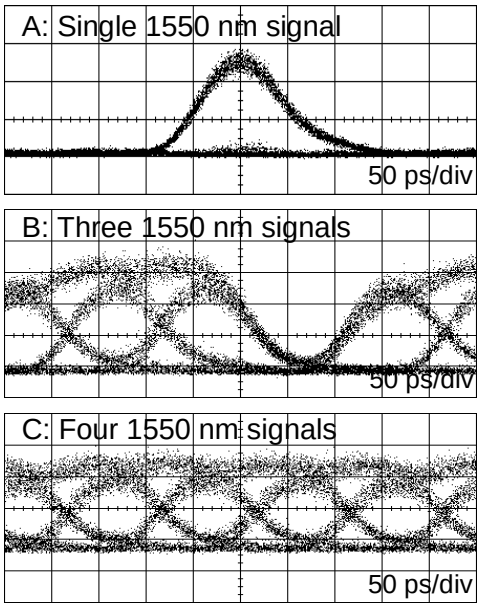

Figure 3.28: Transmultiplexed 1550 nm signals

In the presented experiments, the final OTDM signal has an NRZ data format, i.e. N incoming neighbouring in the time domain "1" signals with the pulse width T lead to the final "1" signal with the pulse width equal to $N \times T$ at the transmultiplexer output, see Figure 3.29. This feature was realized by proper choice of the RZ pulse width and correct alignment of the adjacent signals in the time domain. To achieve transmultiplexing to the RZ format the input RZ pulse width has to be very short. The limitation here is a slow falling edge of the converted signal. It can be concluded from Figure 3.28 that to achieve the RZ signal at the transmultiplexer output the adjacent signals have to be spaced in the time domain at least 200 ps.

The 1550 nm OTDM signal was fed into an OTDM receiver. The OTDM receiver consisted of an OTDM demultiplexer, a variable ATT, a data receiver, and a BER tester. An IM driven by a 2.5 GHz "1000" periodic electrical signal realized demultiplexing of the 10 Gbit/s data stream to the 2.5 Gbit/s data stream. The demultiplexer was synchronized using an electrical clock signal.

Figure 3.30 visualizes the BER curves for the transmultiplexed signals and a reference signal as a function of measured optical power before the data receiver. As a reference we used the aggregate 10 Gbit/s signal at the output of the second AWG, i.e. four time interleaved 2.5 Gbit/s WDM signals in 1310 nm wavelength

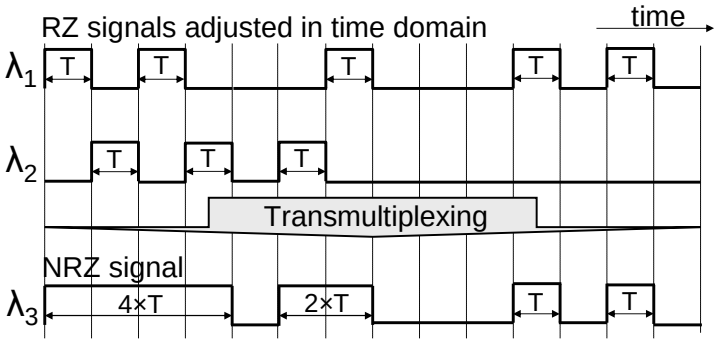

Figure 3.29: RZ-to-NRZ transmultiplexing, T-pulse width

domain. Both reference and transmultiplexed signals were evaluated in the same OTDM receiver. No BER error-floor was observed. All four demultiplexed reference signals showed almost identical performance as well as all four transmultiplexed signals. The transmultiplexing power penalty at BER=10^{-9} was 3 dB.

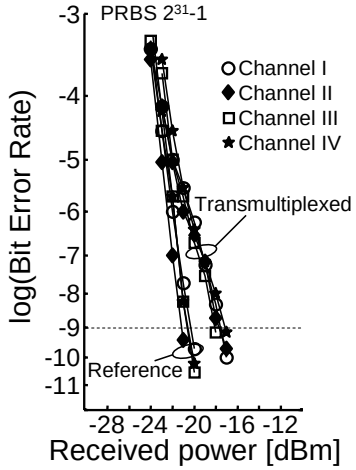

Figure 3.30: BER measurements of 4×2.5 Gbit/s to 10 Gbit/s transmultiplexing

In Section 3.3.3, 1310-to-1550 nm wavelength conversion with simultaneous NRZ-to-RZ data format conversion was demonstrated. In the last experiment, the 1550 nm CW source was replaced by a 10 GHz optical clock at 1550 nm generated by a mode-locked laser. The input power of the 1310 nm signals remained unchanged and the average power of the 1550 nm clock signal was set to 7 dBm. The pulse FWHM was measured using an autocorrelator at the transmultiplexer output to be 2.2 ps. The eye diagrams for the transmultiplexed 1550 nm signal show a clear eye opening, see Figure 3.31. However, signal distortions due to the limited extinction ratio of the transmultiplexed signal are visible in the "0" level as well as variations in the "1" level.

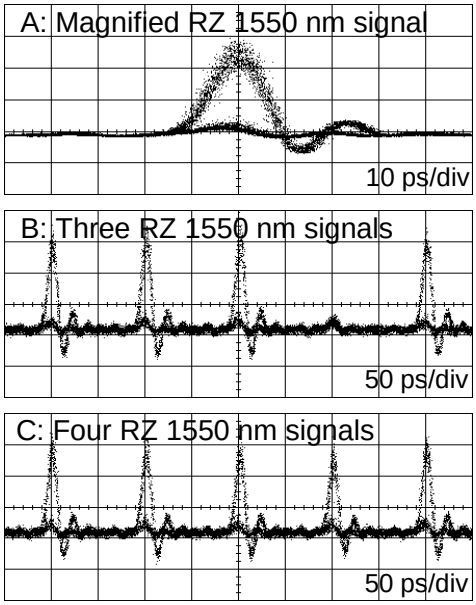

Figure 3.31: Transmultiplexed RZ 1550 nm signals

Results of the BER measurements are presented in Figure 3.32. As a reference a 2.5 Gbit/s 2 ps FWHM signal at 1550 nm was used. Again, no error-floor was observed, all channels showed almost identical performance and the transmultiplexing power penalty at BER=10^{-9} was 2.8 dB. These results demonstrate that the transmultiplexed 1550 nm signal can be used as a tributary channel in an OTDM data stream up to 160 Gbit/s.

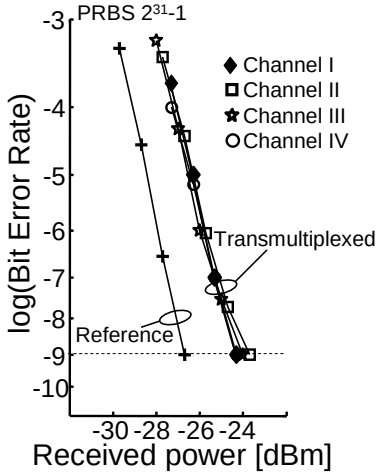

Figure 3.32: BER measurements of 4×2.5 Gbit/s to 10 Gbit/s transmultiplexing with simultaneous NRZ-to-RZ data format conversion

3.5 Synchronization of the 1310-to-1550 nm interconnect

The presented wavelength conversion concept operates asynchronously without any re-timing and buffering capabilities but it may provide some signal regeneration capabilities. Basically, the 1310 nm data is copied into the 1550 nm signal preserving timing of the input signal. In the case of 1310-to-1550 nm wavelength conversion without data format conversion the situation is simple. A single data stream at 1310 nm is copied into one data stream at 1550 nm. Then the 1550 nm data stream is transported further through the core network. Therefore synchronization is not required. However, when 1310-to-1550 nm wavelength conversion with simultaneous NRZ-to-RZ data format conversion or transmultiplexing is required, to achieve uniform network operation synchronization of access and core network is necessary.

The important assumption is that the access network acts as a slave with respect to the core network and therefore the clock signal of the access network has to be synchronized to the core network. The access network node receives the data from the core network. Therefore the clock signal of the core network is distributed to the access nodes. The clock signal of the access node synchronizes to the received signal from the core network. As a result, the access node is roughly synchronized to the core network. To perform final synchronization the optical delay lines compensating for changes in the phase of the incoming signal and adjustment of the clock signal generator in the access node can be applied. Both cases require an active control loop.

In the first case, the control loop is realized in the interface node and is formed by a clock signal comparator, a delay line control and a delay line. The difference between core and access network clock signals is detected and applied to control the optical delay line. By adjusting the optical delay line, changes in the phase of the incoming data signal from the access node are compensated. This solution allows for compensation of slowly varying phase changes. The advantage is that the compensation takes place in the interface node and therefore simplifying architecture of the access node.

In the second case, the difference between clock signals is detected and sent to the access node, e.g. by an additional control channel realized as a logical channel or at a separate wavelength. In the access node, the clock frequency is adjusted to compensate the clock signal difference. The advantage of this scheme is that it allows precise compensation for the clock signal variations. However, it requires an additional control channel. Moreover, the control loop reacts with the delay caused by processing electronics and it complicates design/architecture of the access node. Figure 3.33 visualizes both cases. In practical applications to achieve maximum flexibility both solutions have to be applied.

An interesting case is when a reflective SOA (R-SOA) is utilized in the access nodes. In the access systems utilizing the R-SOA, the remote optical source, placed in the central office or the core-to-access interface node, sends the CW optical signal to the access node, where the CW signal is modulated with the user data. Next, the modulated signal is sent back from the access node to, e.g. the core-to-access

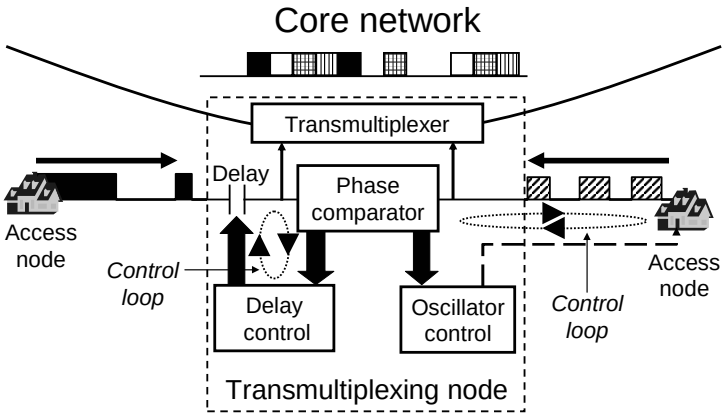

Figure 3.33: Schematic diagram of access and core network synchronization

interface node [96, 97]. The advantage of this access network system is that the optical sources are removed from the access nodes simplifying system design and management.

However, when instead of the CW signal the RZ signal is sent to the access node, a simple synchronization method of incoming from the user data signals can be realized, see Figure 3.34. An RZ signal generator in the interface node generates a RZ signal at the certain clock frequency. The RZ signal is transported through the fibre link to the access node. In the access node, the RZ signal is modulated with the user data. To perform modulation, the clock signal retrieved from the RZ signal is used to synchronize driving electronics. To retrieve the clock signal from the RZ signal an electrical low-pass filter can be used.

Then the modulated RZ signal is coming back to the converter node. In the converter node the RZ signal is converted with simultaneous data format conversion into an (OTDM) data stream at the desired wavelength. The converted data stream is transmitted further through the core network.

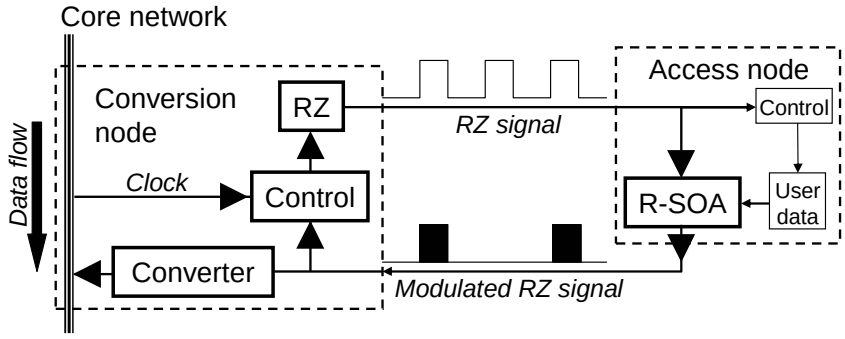

Figure 3.34: Schematic diagram of access and core network synchronization utilizing R-SOA

To control the RZ signal generator two clock signals are used: the clock signal of the core network and the clock signal of the modulated RZ signal. In the case of a difference between the core network clock signal and the RZ clock signal, the RZ generator frequency is adjusted to eliminate difference. As a result, the incoming modulated RZ signal is synchronized to the core network. The presented solution has the advantage of simplifying architecture of the access node, while achieving high flexibility in synchronization of incoming data signals. Moreover, the control scheme is very simple to realize and delays are reduced to minimum.

When exclusively wavelength and data format conversion is required the RZ signal can have, e.g. 80-90% duty cycle. The slow recovery time of the SOA eliminates virtually the RZ data format at the converter output. However, in the transmultiplexing applications the RZ signals may have already the desired duty cycle, i.e. 20-25% in the case of 4-to-1 transmultiplexing. As a result, NRZ-to-RZ conversion is omitted simplifying the transmultiplexing node architecture.

3.6 Conclusions

In this chapter transparent optical connectivity between the 1310 nm and the 1550 nm wavelength domain has been investigated. First, potential applications of ultra-wide band wavelength conversion were identified. Transmission in the 1310 nm wavelength domain is standardized for the up-stream communication, from the user, in the access networks. To realize transparent optical connectivity between access and core network, all-optical 1310-to-1550 nm wavelength up-conversion is necessary. To achieve this a novel 1310-to-1550 nm wavelength conversion technique is proposed.

The proposed wavelength conversion technique is based on nonlinear polarization rotation in a single SOA. Through variations in the SOA birefringence, changes in the signal polarization state are enforced, which are further explored by the polarization filter. This effect was applied to the signals in the transparency region of the SOA. As a result, 1310-to-1550 nm wavelength conversion was realized using a single 1310 nm SOA.

The static and dynamic operation of the wavelength converter based on the proposed technique was successfully evaluated in various experiments. It was demonstrated that the proposed technique has in general 2R regeneration capabilities, and non-inverting or inverting operation can be achieved. Error-free non-inverting and inverting conversion at 10 Gbit/s was achieved. The limiting factor was slow recovery time of the SOA. By replacing a CW source with an optical clock source, 1310-to-1550 nm wavelength conversion with simultaneous NRZ-to-RZ data format conversion was achieved. This simultaneous wavelength and data format conversion is particularly important when the core network utilizes 160 Gbit/s or higher OTDM transmission. Operation of the proposed wavelength converter was verified in the transmission experiments as well. Error-free 1310-to-1550 nm wavelength conversion in between two SSMF transmission links was realized.

To realize efficient conversion of the multiple data streams from the access net-

work into the core network a novel transmultiplexing technique was proposed and realized. Transmultiplexing allows multiplexing of multiple low bit rate data streams into one data stream. The proposed 1310-to-1550 nm transmultiplexing technique utilized nonlinear polarization rotation in an SOA. Error-free 2×5 Gbit/s to 10 Gbit/s and 4×2.5 Gbit/s to 10 Gbit/s transmultiplexing has been demonstrated.

The proposed 1310-to-1550 nm wavelength conversion/transmultiplexing technique has several key advantages: it enables transparent all-optical networking, a single SOA is used, it operates at high bit rates (demonstrated 20 Gbit/s), it offers in general 2R regeneration, NRZ-to-RZ data format conversion and the converted RZ signal can be used as a tributary channel in an OTDM data stream. In principle, the proposed technique may be used for any up-conversion from the SOA gain region with simultaneous NRZ-to-RZ data format conversion. The other semiconductor based 1310-to-1550 nm wavelength converters had a limited speed to below 500 Mbit/s [68,69] and in general lack of regeneration capabilities, or they required complicated control mechanism (demonstrated operation below 1.5 Gbit/s) [70]. The periodically polled $LiNbO_3$ waveguide has an advantage of high speed operation. However, it lacks regeneration capabilities, it is polarization sensitive, and it is extremely expensive.

In the practical realizations couple of constrains have to be addressed. For the proper operation of the proposed wavelength converter, precise polarization adjustment of the 1550 nm signal is necessary. However, since this signal will be generated locally in the wavelength conversion node the polarization state of the 1550 nm signal can be easily controlled by application of polarization maintaining components. It was shown in the presented experiments that the proposed wavelength converter is less sensitive to the polarization state of the 1310 nm signal. Nevertheless, to achieve optimal and stable performance a tuneable polarization controller can be applied at the 1310 nm input of the 1310-to-1550 nm wavelength converter. The other constrain are high losses in the 1310 nm SOA experienced by the 1550 signal which affects indirectly quality of the 1550 nm signal. This can be alleviated twofold: by application of a high output power 1550 nm CW laser or post-amplification. The combination of both solutions will give the best OSNR value of the post-amplified 1550 nm signal.

The advantages and disadvantages of the proposed wavelength conversion technique apply to the transmultiplexing operation as well. The presented by others techniques, based on a nonlinear-optical loop mirror [94] or an EAM [95] allowed transmultiplexing up to an aggregate OTDM data stream of 60 Gbit/s and 80 Gbit/s respectively. However, the other techniques transmultiplex signals exclusively within one wavelength band with a remote prospect to realize 1310-to-1550 nm transmultiplexing.

The demonstrated results prove that the proposed concept is a strong candidate to realize transparent optical connectivity between access-metro and core networks in all-optical communication networks.

Chapter 4

GT-UNI based add-drop multiplexing

This chapter discusses application of the 1310 nm SOA in an all-optical add-drop multiplexer. Using the 1310 nm SOA in a gain-transparent ultrafast nonlinear interferometer (GT-UNI) configuration, all-optical OTDM add-drop multiplexing of 1550 nm signals was realized. The add-drop multiplexer was tested in the laboratory as well as in field trial experiments showing excellent performance up to 160 Gbit/s.[1]

4.1 OTDM technology

Future optical communication networks will operate with much higher transfer capacities per fibre than the present ones. It is an open issue whether this will be accomplished by a higher number of wavelengths per fibre (wavelength division multiplexing) or by higher bit rates per wavelength, or most likely a combination of both. Present optical transmission systems offer a transmission capacity up to 40 Gbit/s per wavelength channel. The bit rate of the transmitted signals is presently limited by electronics. Only very recently, electronics operating at 100 Gbit/s was demonstrated [52]. The solution that overcomes this limitation is optical time division multiplexing (OTDM) [103].

In an OTDM system, data streams at a base bit rate are interleaved in the time domain to form a data stream at a higher bit rate. To achieve this, the data streams have to be encoded into pulses with duration much smaller than a base repetition rate. Figure 4.1 shows an example of the OTDM data stream. A data stream at the base bit rate B is encoded onto return-to-zero (RZ) pulses with repetition rate $T = 1/B$. N of such base rate data streams form after multiplexing in the time domain a final data stream at an aggregate bit rate $N \times B$. One RZ pulse occupies a fraction of a time slot $t_S = 1/(N \times B)$.

[1] Parts of this chapter are published in [98–102]

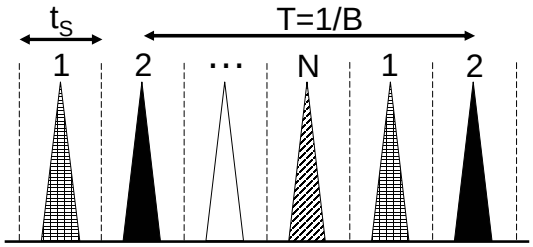

Figure 4.1: Sketch of an OTDM data stream

The OTDM transmission system consists of an OTDM transmitter, a transmission link, and an OTDM receiver, see Figure 4.2. In the transmitter an OTDM data stream is generated. First, short RZ pulses are generated. As a source of RZ pulses passive or active mode locked lasers are used. An alternative is the application of an electro-absorption modulator (EAM) driven by the electrical clock signal carving pulses from a CW input signal. Then the data stream is encoded onto RZ pulses and finally multiplexed in the time domain.

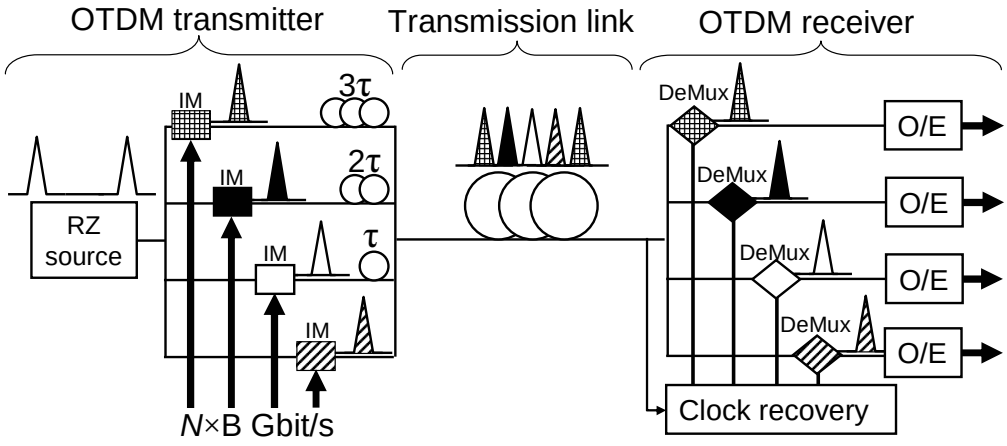

Figure 4.2: OTDM transmission system

Subsequently, the OTDM data stream is transmitted through the fibre link. The fibre link consists of the transmission fibre, optical amplifiers, as well as dispersion and PMD compensation. After the transmission link, the OTDM data stream enters the OTDM receiver. In the OTDM receiver, the OTDM data stream is demultiplexed to the base rate data streams. After optical-to-electrical conversion the base rate data streams are processed further in the electrical domain. To realize demultiplexing nonlinear effects in a fibre or an SOA can be utilized. Again, an alternative is demultiplexing utilizing an electrically driven EAM. To achieve proper operation of the demultiplexer a clock recovery sub-system is necessary. The clock recovery sub-system synchronizes operation of the demultiplexer with the incoming ODTM data stream.

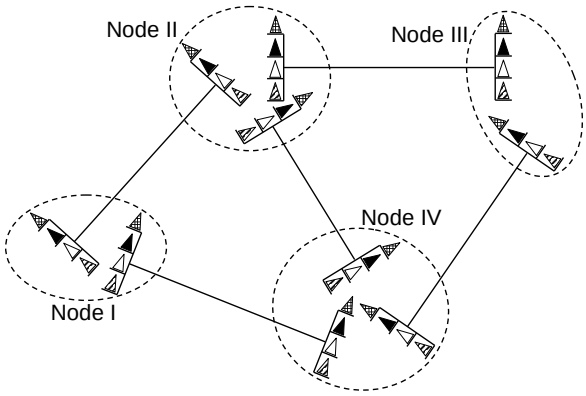

Figure 4.3: OTDM transmission network

Using the presented OTDM transmission system any transmission network can be realized, e.g. the one presented in Figure 4.3. The presented network is based on point-to-point connections. However, such a solution suffers a lack of efficient switching capabilities. To remove one data channel from the incoming data stream (drop operation) and to insert simultaneously a new data stream (add operation) all channels have to be first demultiplexed and only then a new OTDM data stream can be formed. This approach requires a significant number of OTDM demultiplexers in each switching node, which complicates system architecture and significantly increases the system cost.

To achieve network flexibility a new network component is required. An all-optical add-drop multiplexer will perform add and drop operations without unnecessary demultiplexing of all channels. In an intermediate step (through operation) one empty time slot is created in the incoming OTDM data stream. The through operation is also called in the literature the continue operation. To keep consistent with the previous publications the through term will be used. Drop, through, and add operations in the add-drop multiplexer are schematically visualized in Figure 4.4. Obviously, the add-drop multiplexer has to be synchronized and therefore a clock recovery sub-system is required.

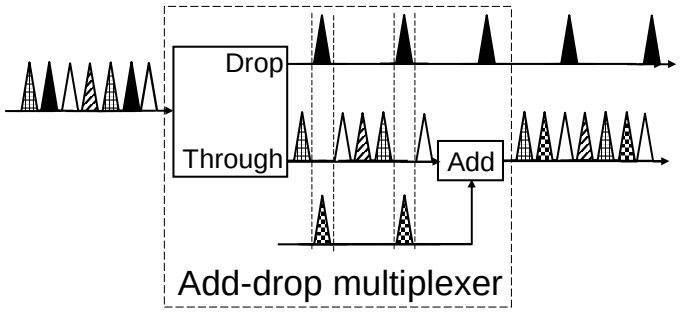

Figure 4.4: Add-drop multiplexer

The add-drop multiplexer can be applied in networks based on the ring structure as well as on the mesh structure. In both cases, flexible all-optical switching is achieved allowing all-optical OTDM networking. A schematic example of both network types is presented in Figure 4.5. In each network node, add-drop operation is performed.

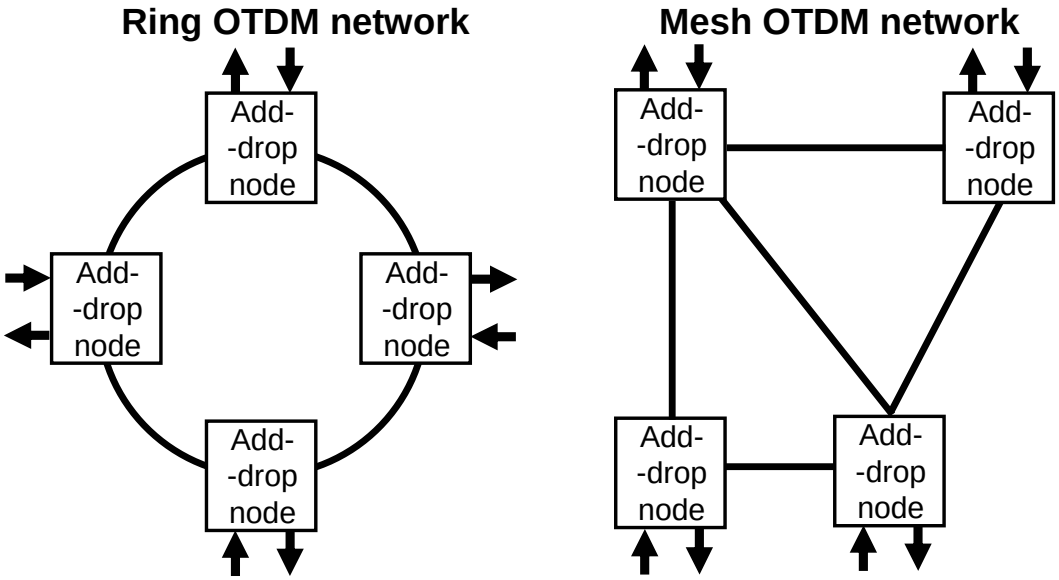

Figure 4.5: Ring and mesh add-drop network

Several all-optical add-drop multiplexers operating at 40 Gbit/s based on an electro-absorption modulator [104], cross phase modulation in the fibre [105], and a monolithic Mach-Zehnder Interferometer [106] have been demonstrated. Switches based on semiconductor components are promising candidates to realize add-drop multiplexing because of the high potential for photonic integration.

In the case of the SOA based interferometric switches there are two factors that limit the switch performance. First, component imperfections limit performance of interferometric setups like a Mach-Zehnder Interferometer. Secondly, the slow SOA recovery time and therefore gain variations cause an amplitude modulation of the data signals passing through the SOA. The first problem can be overcome by applying the switch where the operations: drop, through, and add can be optimized separately. The second problem can be solved by utilizing a switch configuration where the data signal is not affected by the gain recovery of the SOA. Here, an add-drop multiplexer will be presented where both limitations are alleviated. It is achieved by utilizing the gain-transparent (GT) operation of the ultra-fast nonlinear interferometer (UNI).

Research presented in this chapter was conducted in the framework of the European Commission 5^{th} Framework Programme FASHION (ultraFAst Switching in HIgh-speed OTDM Networks) project.

4.2 Gain-transparent ultrafast nonlinear interferometer

4.2.1 Gain-transparent switching

In a conventional interferometric switch configuration the data and control signals are co-located in the gain region of the SOA. The optical control pulse depletes the carriers in the SOA causing a change of gain (amplitude) and refractive index (phase). The phase change experienced by the data signal is used for interferometric switching. However, the gain change causes an amplitude modulation of the transmitted data. This unwanted effect degrades the quality of the further transmitted signal. Moreover, ASE noise is added to the transmitted data signal. Figure 4.6a shows schematically the conventional mode of the SOA operation. Both the data and the control signals are co-located in the gain region of the switching SOA.

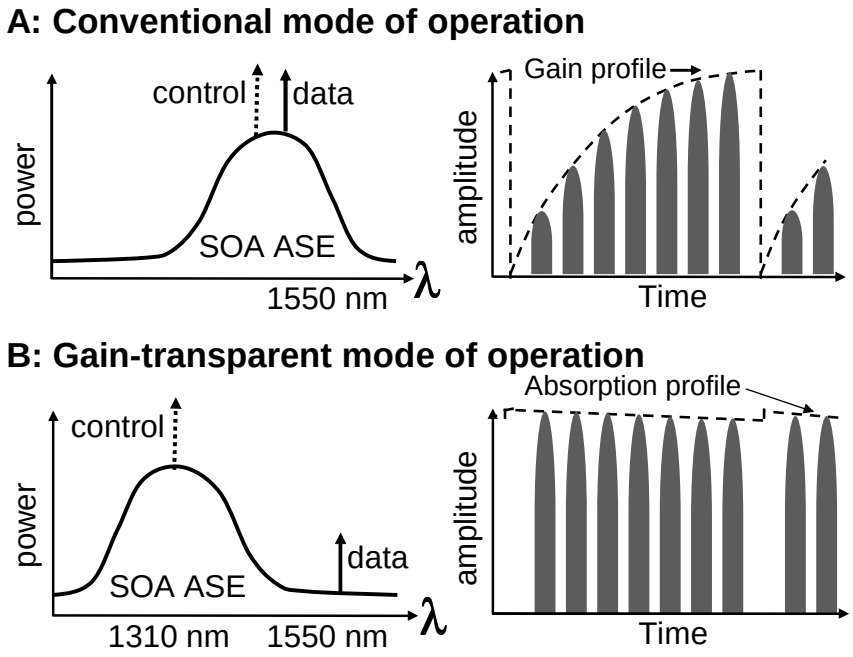

Figure 4.6: Conventional and gain-transparent operation of the SOA

In a gain-transparent mode of operation, only the control signal is located in the gain region of the SOA. The gain-transparent operation of the SOA is shown in the Figure 4.6b. The control signal is located at 1310 nm. The data signal is located at 1550 nm. However, the control signal changes the refractive index at 1310 nm as well as 1550 nm with an associated phase shift for the data channel enabling the interferometric switching. However, the amplitude change of the data signal is insignificant and no ASE noise is added. The optical spectra captured in a gain-transparent configuration are shown in Figure 3.7. It has been demonstrated that a gain-transparent operating SOA shows three times smaller phase shift, but also eight times smaller gain variations in comparison to a conventionally operated SOA [107].

The gain-transparent operation of the SOA was first applied to realize wavelength conversion from 1300-to-1550 nm in a Mach-Zehnder Interferometer (MZI) [70]. Later applications to the demultiplexing experiments in a SLALOM and a MZI configuration have been shown [108–111]. In this thesis applications of nonlinear polarization rotation in the transparency region of the SOA have been already demonstrated in Chapter 3.

4.2.2 Principe of ultrafast nonlinear interferometer

Polarization switching in an ultra-fast nonlinear interferometer (UNI) was first reported in [112] and furthermore with the improved setup in [113]. The principle of UNI switching can be described as follows. First, two orthogonal polarization modes of the incoming data stream are delayed against each other in the time domain, see Figure 4.7a. Then, the data stream together with a control pulse is injected into a switching SOA, see Figure 4.7b. The control pulse induces gain and phase changes. However, those changes are not experienced in the same way by the orthogonal polarization modes of the input data stream. The leading pulse "2" does not experience the phase change, but the trailing pulse "2'" and the following pulses "3" and "3'" experience the phase change. To achieve the maximum switching performance the control pulse has to be located just after the leading "2" pulse and the trailing "2'" pulse just after the control pulse. Limitation here is the pulsewidth of the control and data pulses.

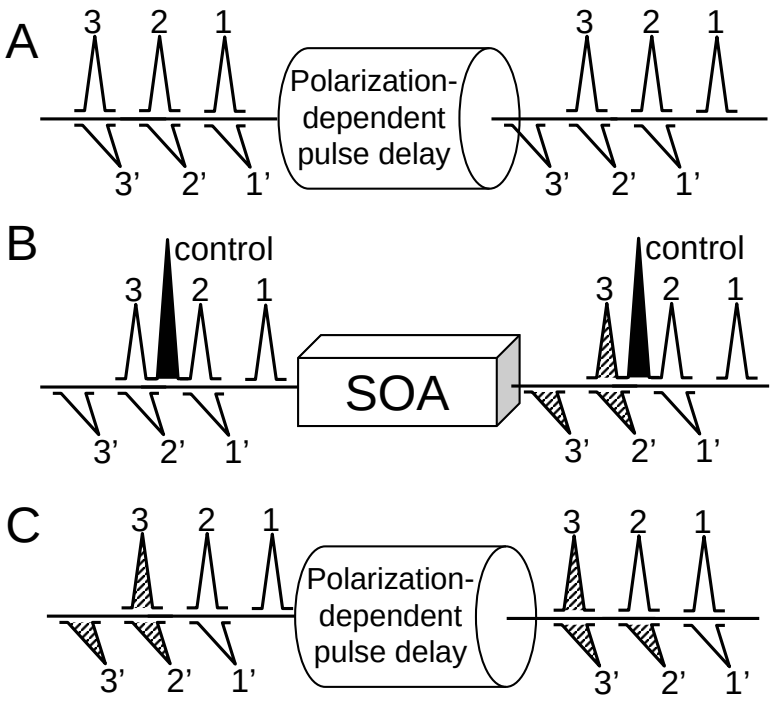

Figure 4.7: Scheme of ultrafast nonlinear interferometer

After the SOA, the control pulse is separated from the data stream and the pulse delay between the orthogonal polarization modes is cancelled, see Figure 4.7c. As a result, the orthogonal sub-pulses pair "1-1'" does not have the phase difference and the pair "3-3'" has the negligible phase difference caused by the slow recovery time of the SOA. However, pair "2-2'" has the significant phase difference. In Chapter 3, it was shown that the phase difference between the orthogonal pulses can be utilized to realize polarization switching. Therefore the recombined pulse "two" has a different polarization state with respect to the pulses "one" and "three".

Polarization switching described and utilized in the previous chapter was based on birefringence of the SOA, i.e. asymmetry of the SOA gain. Here, polarization switching is achieved by introducing a phase shift between the time delayed orthogonal polarization modes. In both cases the phase variations lead to the polarization state changes that are further explored to achieve switching of the data signals. However, the GT-UNI switch was not based on nonlinear polarization rotation.

The demultiplexing experiment at 40 Gbit/s utilizing the UNI switch was described in [114] and later at 80 Gbit/s in [115]. The 160-to-10 Gbit/s and 160-to-40 Gbit/s demultiplexing experiments in the GT-UNI switch were presented in [116, 117]. The polarization independent GT-UNI switch was described in [118]. However, add-drop multiplexing was not investigated in the GT-UNI switch.

4.2.3 GT-UNI switch

Figure 4.8 shows the experimental set-up of the GT-UNI switch. Figure 4.9 presents one of the GT-UNI switch realizations. The operation principle of the GT-UNI switch can be explained as follows. An OTDM data signal at 1550 nm enters the GT-UNI switch by an optical circulator (Circ1). Subsequently, the data is launched into a highly birefringent polarization maintaining fibre (PMF). The polarization state at the PMF input, controlled by a polarization controller (PC1), is set such that the data pulses have equal components in the main axes of the PMF. Thus, after leaving the PMF, each data pulse is split into an orthogonally polarized fast and slow pulse with approximately equal intensities, and both sub-pulses are separated in time relative to each other by a delay τ_{sw} equal in the proposed scheme to 5 ps.

An alternative method to achieve pulse delay in the time domain of the orthogonal polarization modes is presented in Figure 4.10. The polarization state of the incoming data signal is adjusted in such a way that after the PBS both orthogonal polarization modes have equal amplitudes. In one of the arms an optical delay line is inserted. The delay line adjusts the relative delay between pulses. Finally, both pulses are recombined after the following PBS. The presented method has the advantage of more flexible adjustment of the τ_{sw} delay. However, to achieve reliable operation thermal stabilization is required. Therefore in the proposed GT-UNI setup a solution based on the PMF was applied, which is more resilient to temperature changes. Since the GT-UNI switch is based on delay between two orthogonal polarization modes, it is polarization sensitive. Hence, at the 1550 nm OTDM input of the GT-UNI switch an (automatic) polarization control has to be applied.

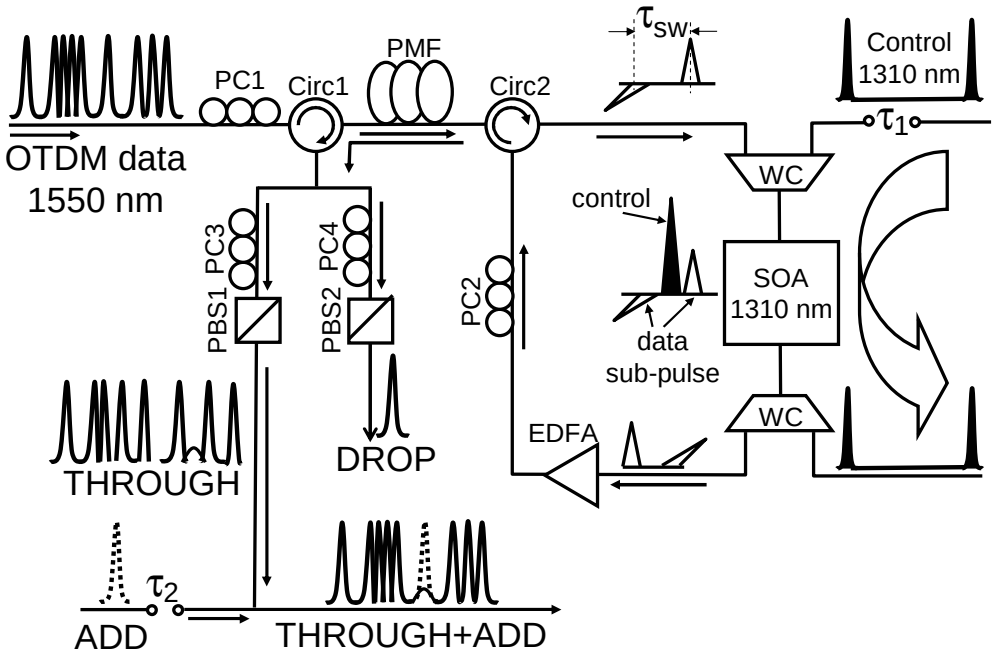

Figure 4.8: GT-UNI switch

Next, the two sub-pulses are coupled via Circ2 into a fold-back loop containing a 1310 nm SOA. The 1310 nm SOA is a 800 μm MQW amplifier and the gain peak is at 1290 nm (29 dB gain with 300 mA drive current). The data pulses in the SOA experience an attenuation of more than 20 dB. This loss is attributed to fibre-SOA coupling, waveguide scattering, and free-carrier absorption in the SOA active layer. After passing the SOA, the sub-pulses are amplified in an erbium-doped fibre amplifier (EDFA). In the 1310 nm SOA no ASE noise is added to the data signal. However, due to high attenuation the data signal experiences OSNR reduction in the following EDFA.

After amplification, the sub-pulses are re-launched into the same birefringent PMF by Circ2. Here, the polarization state of the data sub-pulses is adjusted by the PC2 in such a way, that the sub-pulse fast component is projected into the slow axis of the PMF, and vice versa. By this, the delay between the two sub-pulses is reversed and a recombined pulse will appear at the PMF end.

At the output of the Circ1, the recombined OTDM data signal is split into two arms: drop and through. Each arm contains a polarization filter formed by a polarization controller (PC3 and PC4) in combination with a polarization beam splitter (PBS1 and PBS2). In the absence of a control pulse, both data sub-pulses experience the same conditions in the loop, and therefore the polarization state of the recombined pulse is unchanged. As a result, the recombined pulse with the unchanged phase conditions and therefore the polarization state will leave the GT-UNI switch via the through port (PC3 and PBS1).

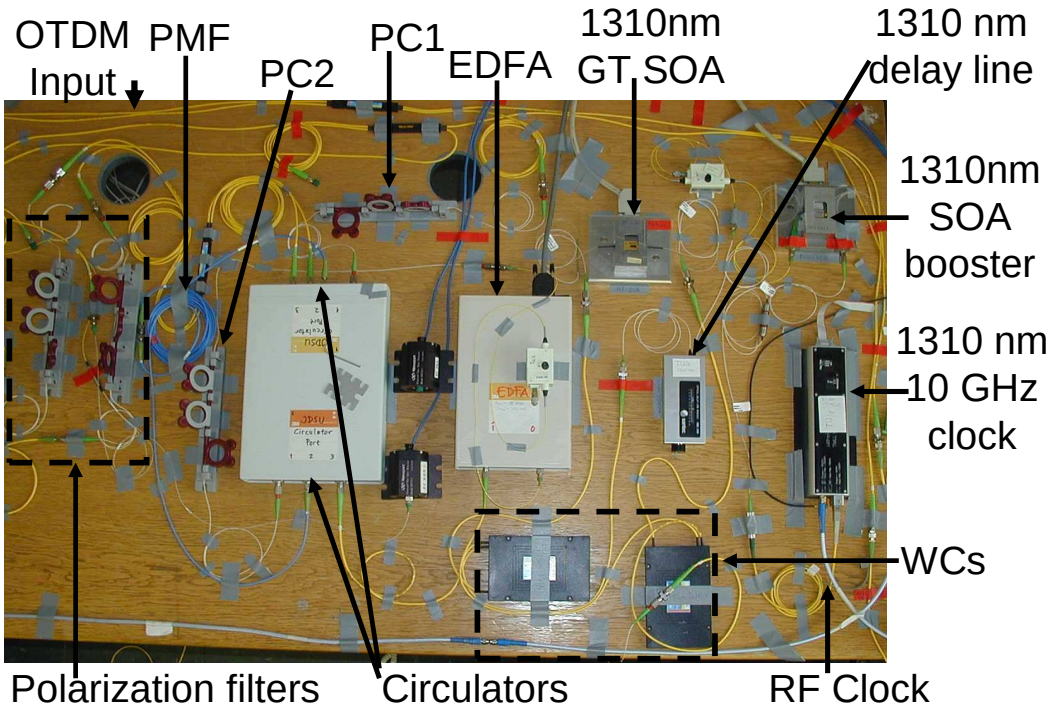

Figure 4.9: Photography of the GT-UNI switch

For switching, a high-intensity control pulse is launched into the SOA. A 1310 nm mode-locked semiconductor laser generates the periodic control pulses. A variable delay τ_1 is used to adjust the temporal position of the control pulses with respect to the data pulses. For optimum switching performance, a high-intensity control pulse should be inserted between the two data sub-pulses. The insertion is realized through a coarse wideband wavelength coupler (WC).

After saturating the SOA, the control pulses are removed from the loop by a second WC. By doing so, the control signals can be reused for other applications. One of the applications is monitoring of the control signal. In such a way, the control signal is monitored without losses in signal power before the switching SOA. Another application is the reuse of the control signal in the following GT-UNI switch, placed in the same add-drop node. Hence, one control signal source can provide the control signal to several switches allowing multiple add-drop multiplexing in the same add-drop node. This reduces the add-drop switch cost and complexity while increasing switching capabilities.

When a single control pulse is present between the data sub-pulses, the leading sub-pulse preserves its original phase and the trailing sub-pulse experiences a phase shift. The polarization state of the recombined data pulse is rotated with respect to the polarization state of unswitched one. Hence, the data pulse leaves the switch via the drop port (PC4 and PBS2).

In the ideal case, the nonlinear phase shift is π rad and orthogonal polarization

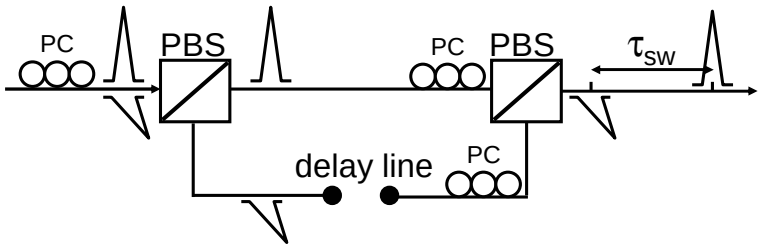

Figure 4.10: Delay of the orthogonal polarization components using the PBS and the delay line

rotation takes place. Hence, a single PBS can be used to achieve drop and through operations. If the phase shift is less than π rad, as in most practical cases, a fraction of drop pulses appears in the through port, causing reduction of a contrast ratio between remaining through channels and the emptied time slot and detrimental optical crosstalk for a possible add channel. In the proposed setup, drop and through channels are optimized separately in parallel. Therefore the cross-talk caused by the limited polarization rotation is minimized.

After one channel is dropped, a new base rate data channel is inserted into the empty time slot in the through data stream. The add operation is realized in a passive fibre combiner, where the through and the add data streams merge together. To achieve proper alignment in the time domain of the newly added channel an additional delay line is used τ_2. As a result, a new OTDM data stream is formed at the through and the add output.

The proposed setup differs from the setup presented in [116]. In the GT-UNI loop an optical amplifier (EDFA) is included. Because of this, the reduction of signal quality due to the OSNR degradation is minimized. However, the most important improvement is the application of the first circulator (Circ1). In the initial setup [116], only one circulator was applied. By adding a second circulator more flexibility in the system optimization is achieved. First, cancellation of the pulse delay by means of PC2 adjustment does not influence directly any of the outputs, as in the previously reported setup [116]. Therefore the properly recombined OTDM signal is realized at the output of the Circ1. Moreover, by application of a 3 dB power splitter the drop and through operations are optimized separately compensating for the limited phase change.

4.3 GT-UNI based add-drop multiplexer

4.3.1 Switching window characteristics

In the previous section, a gain-transparent ultrafast nonlinear interferometer was described. The proposed interferometer supports simultaneous add-drop multiplexing. Next, the add-drop multiplexer was evaluated in the laboratory experiments. First, the switching window was measured.

The switching window characteristics were measured by injecting the 1550 nm repetitive pulses into the add-drop switch. Figure 4.11 shows the experimental setup. The GT-UNI switch presented in Figure 4.8 was extended by addition of a 1310 nm mode-locked laser operating with the repetition frequency of 10 GHz and a 1310 nm SOA to amplify the control signal. The control pulse had the pulse width of 3 ps and the avarage power of about +8 dBm. These two components are not shown in Figure 4.11. As a source of a 1550 nm signal a fibre mode-locked laser with the repetition frequency of 10 GHz was used (2 ps pulse width). To the drop and through outputs of the GT-UNI switch power meters were connected. The output power was measured as a function of the control signal time delay. Before measurements the GT-UNI switch was adjusted to give optimal switching performance.

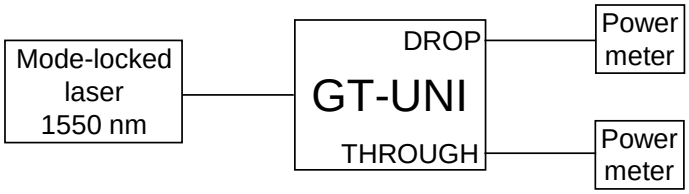

Figure 4.11: Evaluation setup of the GT-UNI switching window

Results of the switching window measurements are visualized in Figure 4.12. A high drop and through contrast of more than 20 dB was measured. The estimated switching window width at half maximum was 4.7 ps for the drop operation and 6.2 ps for the through operation. Taking into account that the 160 Gbit/s OTDM signal has a time interval between adjacent pulses of 6.25 ps, these values indicate that the presented switch allows add-drop multiplexing at a bit rate up to 160 Gbit/s. In [113] the UNI switch was presented with a switching window width of 200 fs. However, only the drop operation was reported. In the next experiments dynamic operation of the GT-UNI based add-drop multiplexer was evaluated.

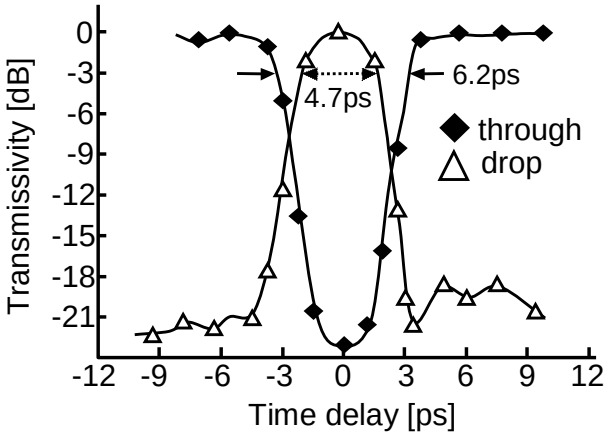

Figure 4.12: GT-UNI switching window measurements

4.3.2 80 Gbit/s add-drop multiplexing

Figure 4.13 shows the experimental setup of 80 Gbit/s add-drop multiplexing. Optical clock pulses of 2 ps FWHM at 1550 nm with repetition rate 9.95328 GHz were generated in a fibre mode locked laser (FMLL). The optical clock signal was modulated in an external intensity modulator at bit rate 9.95328 Gbit/s with PRBS length of $2^7 - 1$. To compensate for losses in the modulator, the modulated signal was amplified in an EDFA. Then the 10 Gbit/s RZ signal was interleaved in the time domain to form an OTDM data stream at 80 Gbit/s.

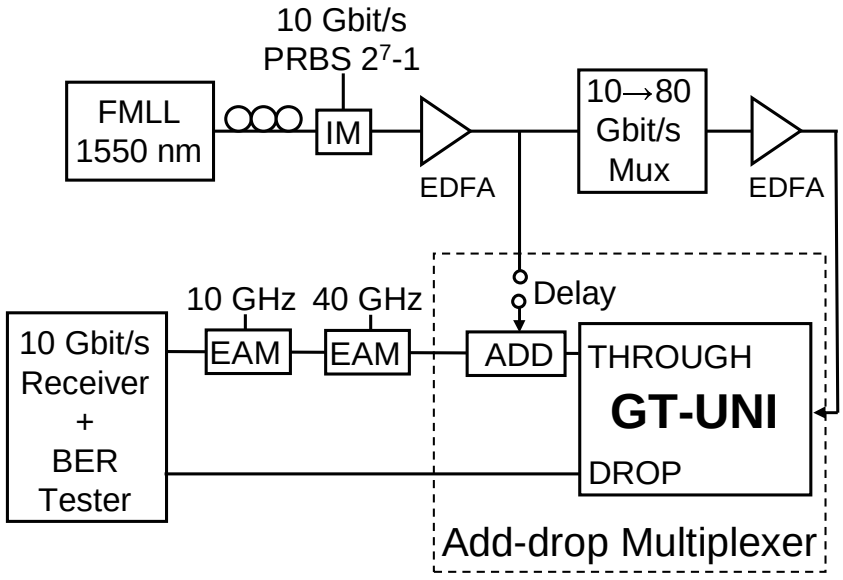

Figure 4.13: 80 Gbit/s add-drop multiplexing experimental setup

Interleaving was realized with polarization maintaining fibre based delay and add stages. The stage delay was chosen in such a way that PRBS characteristics of the output OTDM signal were preserved. To realize that the input PRBS data stream is delayed and added by $(2^7 - 1)/n$ bit periods with $n = 2, 4, 8, ...$ It was achieved by adjustment of the delay line as well as amplitude of the delayed signals to maximize suppression of the base rate clock component. The 80 Gbit/s time interleaved data stream was interleaved in further experiments to form a 160 Gbit/s PRBS data stream, as depicted in Figure 4.14.

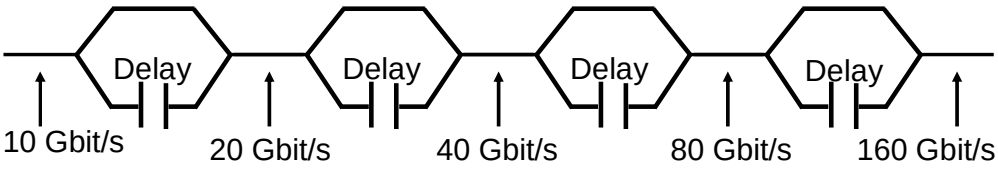

Figure 4.14: 10-to-160 Gbit/s multiplexing based on delay and add stages

After amplification, the 80 Gbit/s OTDM data stream was injected into an add-drop multiplexer. In the add-drop multiplexer, the GT-UNI performed the add and through operations. The drop channel was directly evaluated in a 10 Gbit/s receiver by means of a BER tester. In the empty time slot of the through channel an add channel was inserted. It was realized in a passive fibre coupler. The position of the add channel was adjusted in the time domain by an optical delay line. The resulting add+through data stream was then gated in a tandem configuration of EAMs.

The first EAM was driven by an RF signal at frequency 40 GHz (4×9.95328 GHz). The second EAM was driven by the 9.95328 GHz RF signal. The DC-bias of the EAMs and amplitude of the RF signals were adjusted to achieve sufficiently narrow switching window, i.e. 10 ps. Such a narrow gating window was necessary to demultiplex the 80 Gbit/s OTDM data stream to the 10 Gbit/s base rate tributaries. The demultiplexed add+through channels were finally evaluated in the 10 Gbit/s receiver and the BER tester.

Figure 4.15 presents eye diagrams of the outputs of the GT-UNI switch. Figure 4.15a shows a 80 Gbit/s input data stream, Figure 4.15b a 10 Gbit/s drop channel, and Figure 4.15c seven remaining 10 Gbit/s channels in the through port. The perfect clearing of the drop time slot is visible. After dropping one channel a 10 Gbit/s data channel at the same wavelength was inserted in the empty time slot to form again the 80 Gbit/s data stream, see Figure 4.15d. All eye diagrams in Figure 4.15 show a clear open eye and indicate proper operation of the GT-UNI switch at 80 Gbit/s.

Next, the BER measurements were performed. As a reference, an optimized 10 Gbit/s signal in a back-to-back configuration was measured. Figure 4.16a shows the BER measurements for eight drop channels and for seven 10 Gbit/s through channels. The average power penalty at BER=10^{-9} for the drop channels was 3.7 dB and for the through channels 2.7 dB. The difference between the worst and the best channel in both cases was about 1.4 dB, proving proper operation of the GT-UNI switch. The BER performance spreading was mainly caused by the environmental instabilities influencing the 10-to-80 Gbit/s multiplication stage. Figure 4.16b presents the BER performance of one of the drop channels and the inserted, in the empty time slot, add channel, demonstrating OTDM networking. The sensitivity penalty at BER=10^{-9} for the drop channel was 4.0 dB and for the inserted add channel 3.0 dB. The sensitivity penalty was caused by a combination of the reduction of OSNR, polarization misalignment, and in the case of the inserted add channel the interferometric crosstalk with the residual optical signal of the dropped channel. However, these interferometric effects were so small, that they are barely observed in Figure 4.15 and in the BER measurements.

In the conducted experiment excellent performance of a GT-UNI add-drop switch was demonstrated. Error-free operation of drop, through and add functionalities was achieved. Insignificant penalties for all operations were observed. These results indicate the great potential of the GT-UNI switch for OTDM networking. In the next experiments, the GT-UNI switch will be evaluated in the 160 Gbit/s add-drop networking experiments.

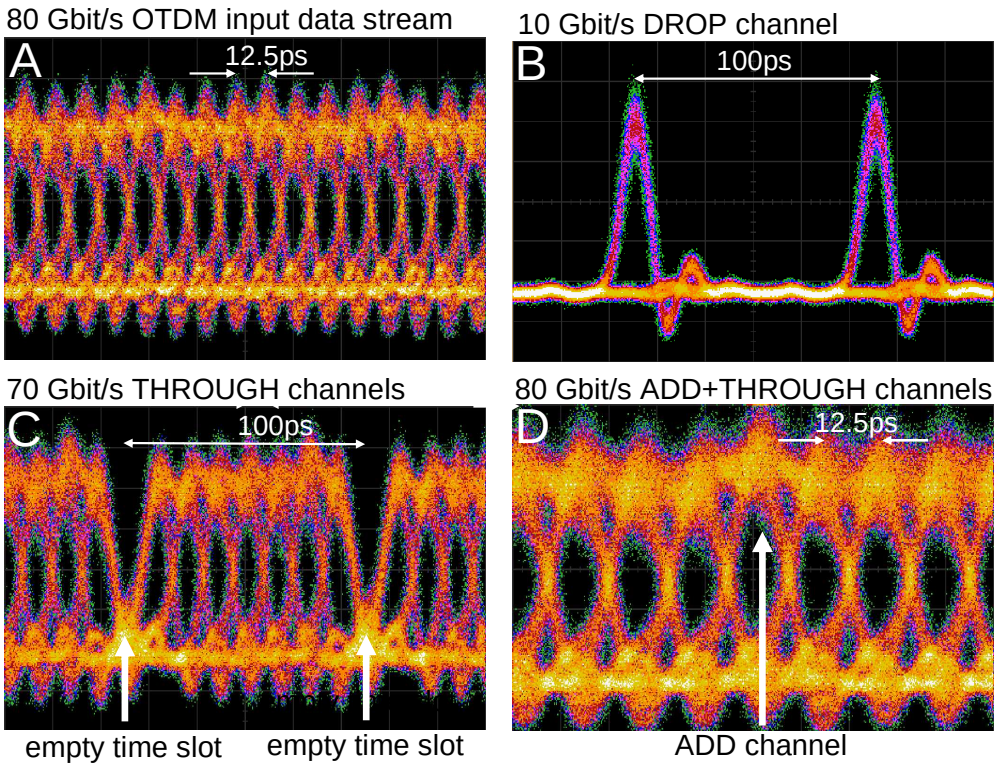

Figure 4.15: Measured 80 Gbit/s eye diagrams

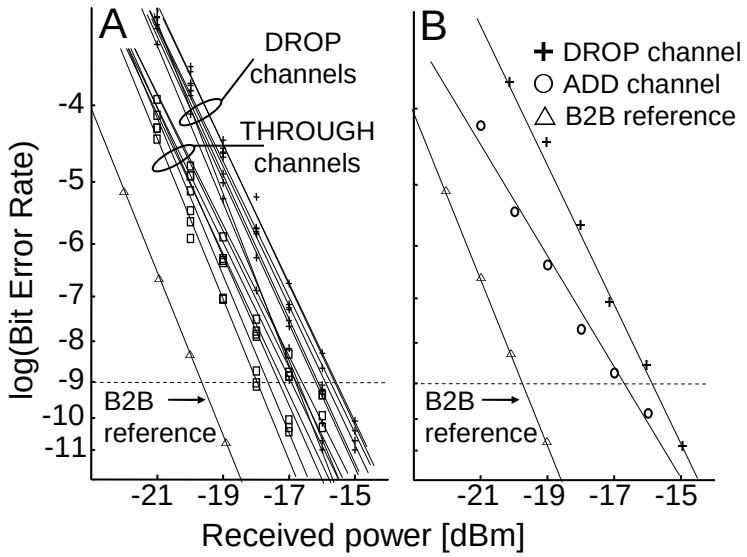

Figure 4.16: BER measurements of 80 Gbit/s add-drop multiplexing

4.4 160 Gbit/s GT-UNI based add-drop node

The experiments presented in the previous section were performed in a back-to-back configuration. No transmission was included and the experimental system was synchronized using an electrical master clock signal. In this section, add-drop multiplexing experiments including transmission through fibre links will be described. The sketch of the investigated OTDM add-drop network is shown in Figure 4.17.

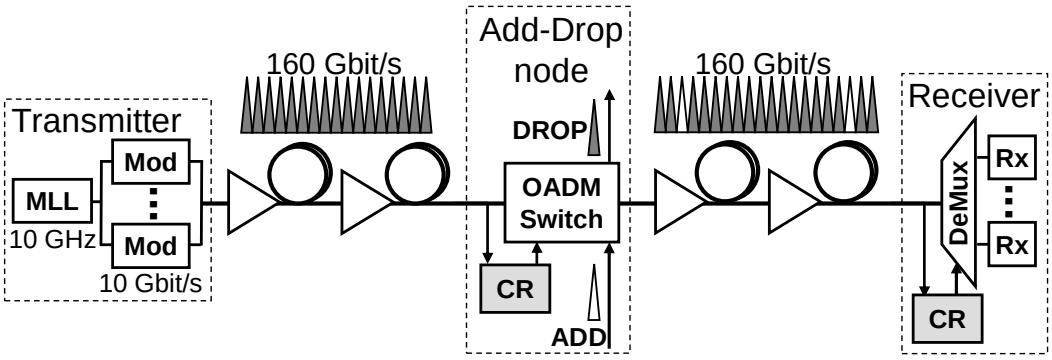

Figure 4.17: Add-drop multiplexing in between two transmission links; CR clock recovery

4.4.1 Clock recovery

Clock recovery (CR) is an essential part of any transmission system. The transmitted data signal experiences random time position variations during propagation through the transmission fibre. These fluctuations lead to a signal phase uncertainty at the network node. An appropriate clock recovery is especially crucial in ultra high-speed OTDM systems, where the data channels are multiplexed in the time domain. In the OTDM data processing node a part of the input data signal is used to drive a clock recovery sub-system, see Figure 4.17. The clock recovery sub-system locks to the incoming data signal and generates a base rate clock signal. This type of clock recovery where the recovered clock is at a base rate is called a pre-scaled subharmonic clock recovery.

The influence on demultiplexing performance of crosstalk and timing jitter is investigated in [119]. It is shown that large timing jitter between the signal and control pulses causes an error floor in the BER performance. The relative root-mean square (rms) timing jitter value is estimated as the sum of squared rms jitter values of the data signal and the clock signal.

$$\sigma_{relative} = \sqrt{\sigma_{signal}^2 + \sigma_{clock}^2} \tag{4.1}$$

It was found that the minimum BER is obtained when the switching window width equals the data signal time slot width and the rms value of the relative timing jitter

has to be less than 1/12.2 times the data signal time slot width to ensure BER$< 10^{-9}$ and 1/14.1 times the data signal time slot width to ensure BER$< 10^{-12}$ [119]. For the 160 Gbit/s data signal T_{slot} is equal to 6.25 ps, which leads to $\sigma_{relative}<$512 fs at BER$< 10^{-9}$ and $\sigma_{relative}<$ 443 fs at BER$< 10^{-12}$.

Many CR methods have been reported. Among them phase-locked loop (PLL) based systems are the most established ones [120]. A PLL based CR utilizing EAMs has advantages in terms of stability and compactness. An EAM based CR scheme was demonstrated in [121, 122]. A CR setup based on a differential scheme in a bidirectionally operated EAM (200 kHz holding range) was presented in [123]. Here, a novel CR scheme employing a single EAM will be described and evaluated.

Figure 4.18 presents the setup of the proposed CR, which consists entirely of commercially available components. An input 160 Gbit/s (16×10 Gbit/s) OTDM signal enters an electro-optical PLL oscillator through a 40 GHz EAM. The EAM output is detected by a photodetector (PD), amplified by a limiting amplifier (LA), and bandpass filtered by a combination of a high-Q filter (Q∼1000) and a bandpass amplifier (BPA). A radio frequency (RF) mixer combines the filtered data signal with a locally generated 10 GHz clock of a voltage-controlled oscillator (VCO) for phase detection. The resulting phase error is processed in an active lowpass filter (LPF) and is subsequently used to drive the VCO. The gating signal is derived from the VCO output, which is then quadrupled (×4) to 40 GHz.

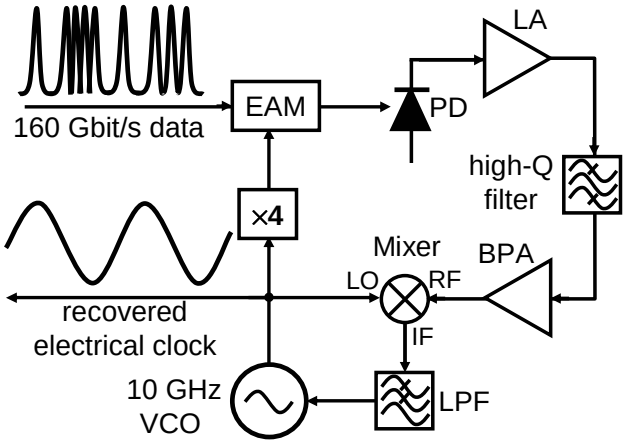

Figure 4.18: Schematic of the proposed clock recovery circuit

The quadrupler consists of two doublers in cascade, each sandwiched by high-gain amplifiers. For normal operation (∼5−8 dBm input power), the amplifiers produce sufficient power to saturate the doublers, resulting in a frequency multiplied output signal (40 GHz sine) with a constant amplitude. However, if the input power is below threshold (<3 dBm), the power to the first doubler is too low to switch on the amplifier, which in turn provides too little power for the second doubler. As a consequence, the output 40 GHz signal has a strong amplitude component with 100 ps interval, see Figure 4.20a. This effect is further pronounced by the nonlinear

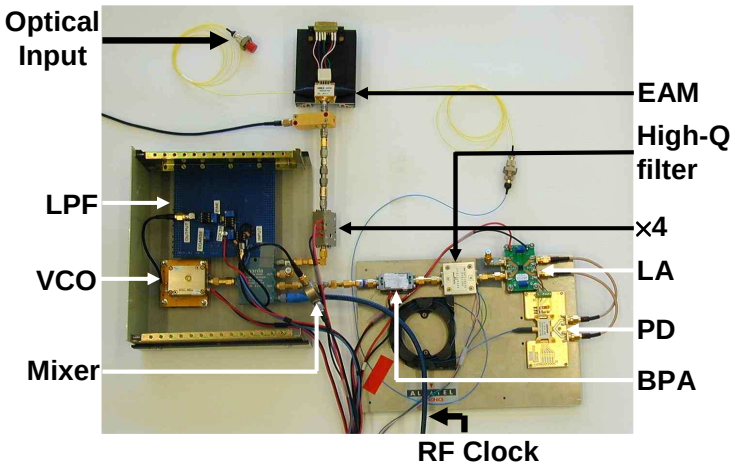

Figure 4.19: Photography of the clock recovery setup

characteristic of the EAM. Figure 4.20b shows a 160-to-40 Gbit/s demultiplexed by the EAM signal, which has a strong 10 Gbit/s component.

The performance of the clock recovery was evaluated in two steps. First, the recovered signal trace, the RF spectrum and the rms timing jitter of the recovered clock signal were measured. Secondly, the clock recovery setup was applied in back-to-back 160-to-10 Gbit/s demultiplexing experiments.

Figure 4.21 shows the signal trace, the RF spectrum and the single sideband (SSB) phase noise of the recovered clock. The carrier-to-noise ratio at 10 kHz offset was measured to be 92 dBc/Hz. Integrating the single sideband phase noise over an interval 10 kHz−10 MHz resulted in the rms timing jitter of around 205 fs. The rms timing jitter measured by a digital communication analyzer with a precision time base module confirmed this value.

Figure 4.22 shows the measured rms timing jitter as a function of the EAM input optical power. The rms timing jitter decreases as the input optical power to the EAM increases. This is largely caused by the increase of the signal-to-noise ratio of the photodiode output for higher input powers. For input powers between

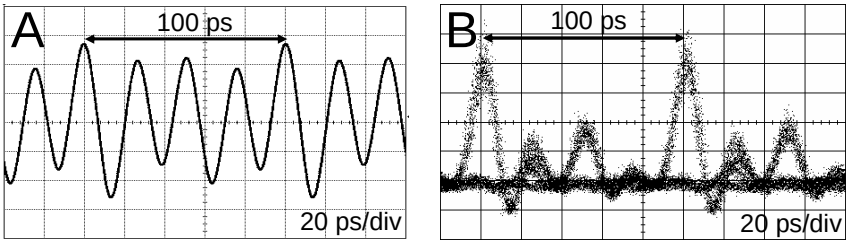

Figure 4.20: Response of the quadrupler (A) and of the EAM (B) for a 160 Gbit/s OTDM input signal

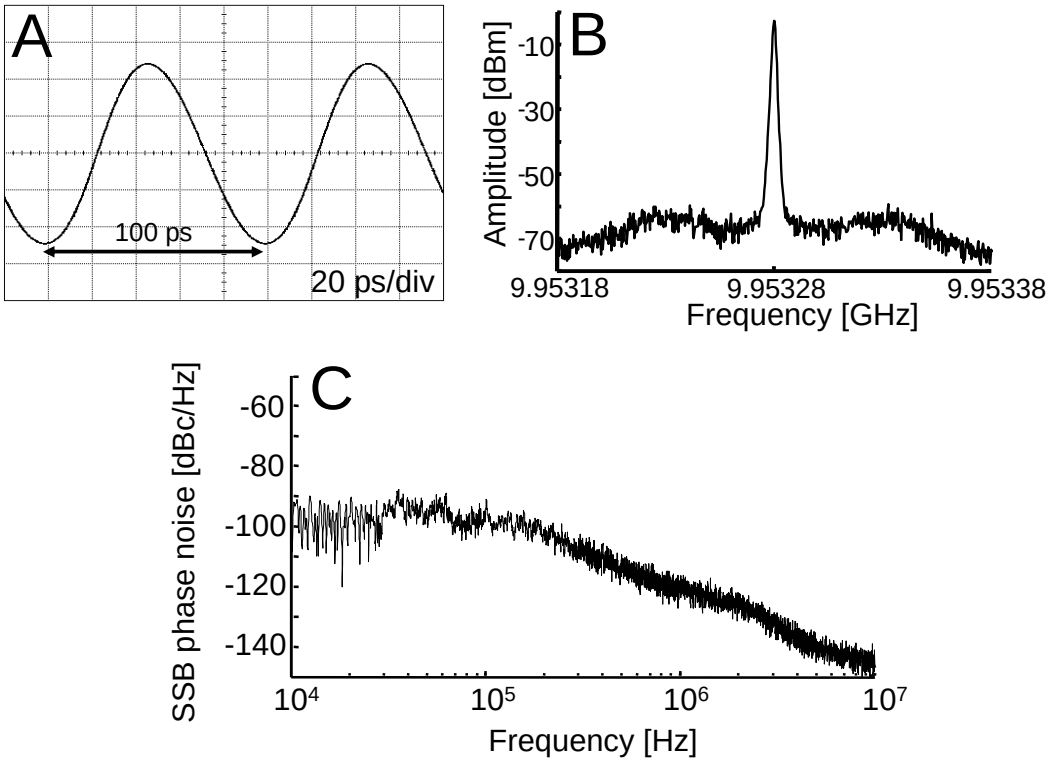

Figure 4.21: Measured trace (A), RF spectrum (B), and the single sideband noise (C) of the recovered clock signal

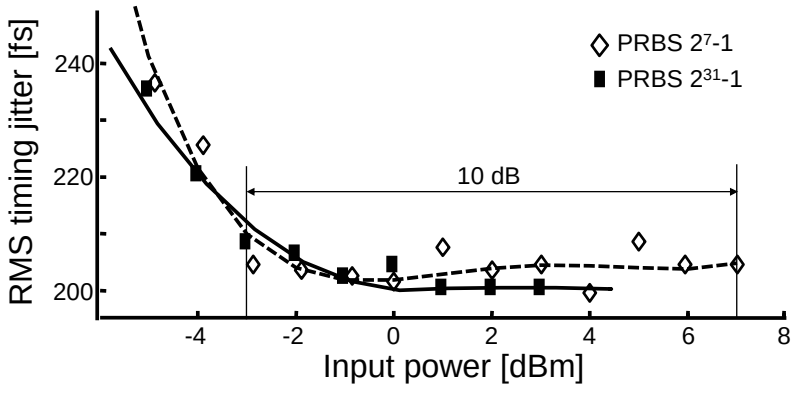

Figure 4.22: The rms timing jitter versus the input optical power

-4 and +6 dBm the rms timing jitter was 200-210 fs, which correspond to the VCO jitter performance. Switching the PRBS length to $2^{31}-1$ produced almost identical results. However, in this case the PRBS character of the 160 Gbit/s signal was not preserved and the data channels were somewhat correlated. A true 160 Gbit/s PRBS signal based on a $2^{31}-1$ PRBS will require extremely long delays in the passive 10-to-160 Gbit/s multiplexer.

The rms timing jitter of less than 250 fs was measured over the wavelength range 1545-1560 nm. The holding range of the clock recovery setup was examined by adjusting the base rate once locking was achieved. The holding range was verified to be approximately 10 MHz, which is limited by the bandwidth of the operational amplifiers in the LPF. The presented measurements show excellent quality of the recovered clock signal. According to the calculations presented above, the proposed clock recovery should allow error-free 160-to-10 Gbit/s demultiplexing.

Finally, the performance of the recovered clock signal was investigated in 160-to-10 Gbit/s back-to-back demultiplexing experiments. The experimental setup is given schematically in Figure 4.23.

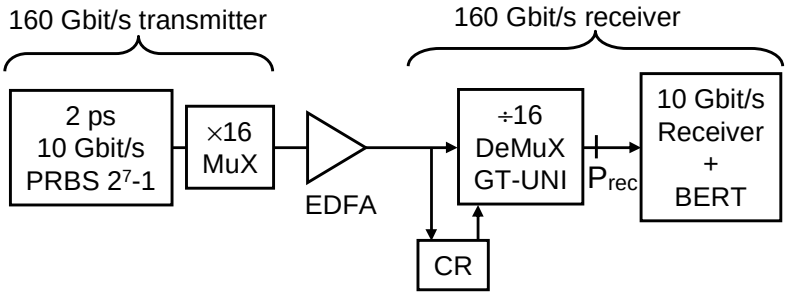

Figure 4.23: 160-to-10 Gbit/s back-to-back demultiplexing setup

The receiver consisted of an optical amplifier, a 160-to-10 Gbit/s demultiplexer, a 10 GHz clock recovery setup, and a 10 Gbit/s optical receiver. The BER was evaluated in a BER tester (BERT). The sensitivity performance was related to input power to the optical receiver at BER=10^{-9}. For 160-to-10 Gbit/s demultiplexing the drop output of the GT-UNI switch was used. The power of the input signal was +10 dBm for the GT-UNI switch and +3 dBm for the CR setup. The results of measurements using the master and the recovered clock signals are depicted in Figure 4.24.

The sensitivity values for the master clock were observed in general to be ≈1 dB worse than those for the recovered clock because the master clock was not always phase-matched to the data coming from the transmitter, as the transmitter contained relatively long fibres. Moreover, the RF amplifiers used to deliver the RF signal degraded performance of the electrical master clock signal. This difference is insignificant if the complexity and the large variations of the ambient conditions of the experimental setup during laborious and time-consuming BER measurements are taken into account.

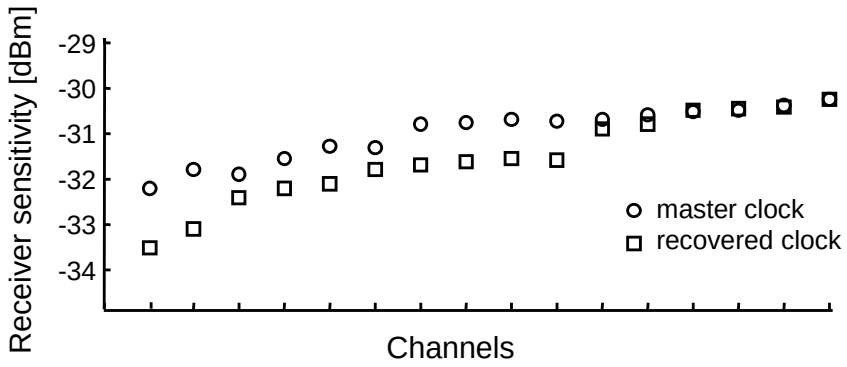

Figure 4.24: CR evaluation: receiver sensitivity values at BER=10^{-9}

4.4.2 Transmission experiments

The demultiplexing performance of the GT-UNI based add-drop switch was further evaluated in the transmission experiments. Laboratory and field trial experiments were performed. To provide synchronization to the incoming data stream a clock recovery sub-system was applied.

Laboratory transmission

Figure 4.25 presents the laboratory transmission setup. The 160 Gbit/s data stream, obtained by bit-interleaving 16×10 Gbit/s channels (1.6 ps pulse-width, 2^7-1 PRBS, and 1551 nm wavelength), was launched into a transmission line consisting of two SSMF spans of about 80 km each, the DCF modules, and the EDFAs. EDFAs were used to compensate for the losses in SSMF and DCFs.

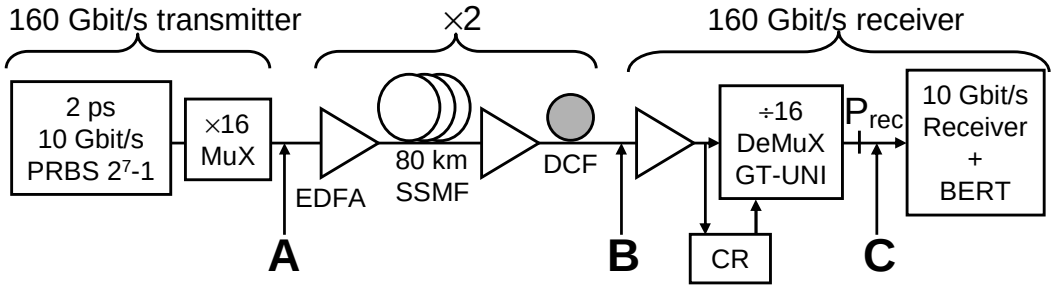

Figure 4.25: 160 Gbit/s laboratory transmission setup

Figure 4.26 shows the eye diagrams captured using an optical sampling oscilloscope (OSO) before (A) and after (B) 160 km transmission. The eye shape is preserved and the eye diagram is clearly open after 160 km transmission. The pulse-width was measured to be 1.9 ps after the transmission link. The system penalty due to polarization mode dispersion was alleviated by coupling the optical data signal to the principal states of polarization of the transmission link.

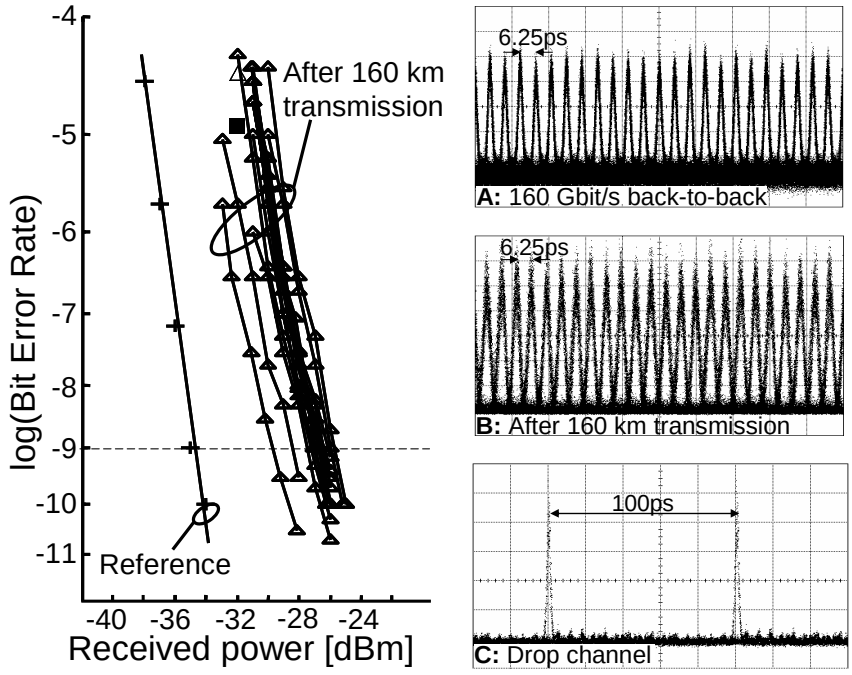

Figure 4.26: Results of 160 Gbit/s laboratory transmission experiments

After the transmission link, the GT-UNI based demultipexing node was placed. In the demultiplexing node, first the clock recovery was performed. Average optical power was about +10 dBm at the GT-UNI input and about +3 dBm at the clock recovery input. The recovered electrical clock was used to synchronize the GT-UNI demultiplexer (the rms timing jitter of about 210 ps). The demultiplexed drop signals were evaluated in a 10 Gbit/s receiver in combination with a BER tester.

Figure 4.26 presents the BER values of the demultiplexed channels as a function of input power to the 10 Gbit/s receiver. Figure 4.26c shows the 10 Gbit/s drop signal captured using the OSO. A proper operation of the demultiplexer is visible and the neighbouring channels are adequately suppressed. For reference, a BER measurement of a 10 Gbit/s back-to-back signal in an identical optical pre-amplified receiver is shown. The drop channels of the GT-UNI show a sensitivity penalty of about 5-9 dB in comparison to the 10 Gbit/s reference signal. Spreading over all channels was present due to imperfections and instabilities in the multiplication and compensation stage.

Field trial transmission

Next, field trial transmission experiments were conducted. Figure 4.27 shows the experimental setup. The 160 Gbit/s transmitter and receiver were sited in Ipswich. The EDFAs and DCFs were co-located in Ipswich and Newmarket, United Kingdom.

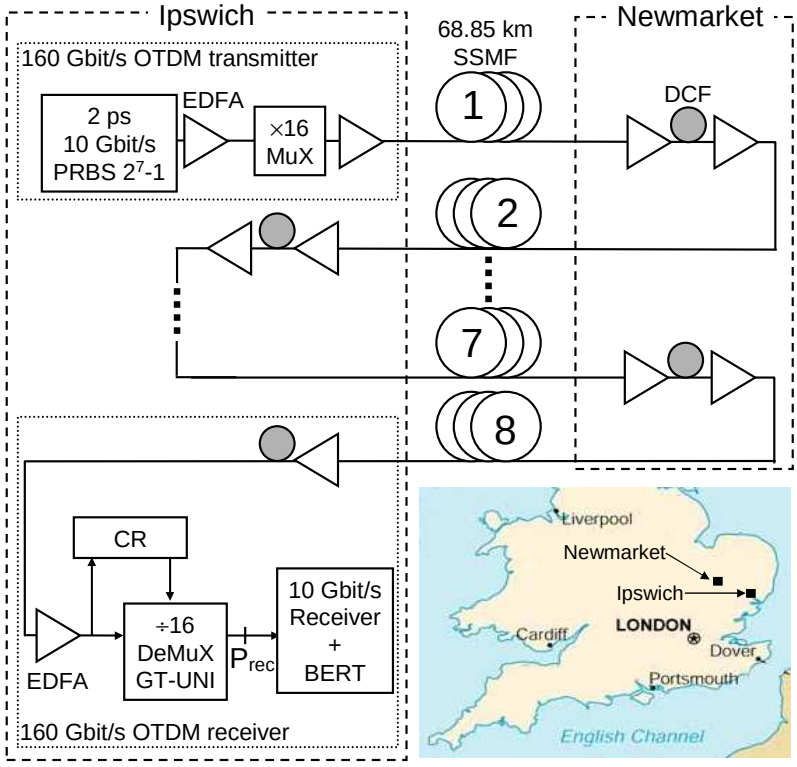

Figure 4.27: 160 Gbit/s field-trial transmission setup

In the transmitter, a 160 Gbit/s data stream was generated by interleaving copies of a 10 Gbit/s return-to-zero (RZ) signal, which was generated in an erbium-glass oscillator pulse generating laser (ERGO-PGL). The ERGO-PGL generated the clock pulses with a pulse width of 2 ps FWHM at a wavelength of 1551.7 nm and at a repetition rate of 9.95328 GHz. The signal was modulated with PRBS of length 2^7-1 in an external intensity modulator. 10-to-160 Gbit/s multiplication of the data stream was achieved with four PMF based delay and add stages. To get a realistic 160 Gbit/s data stream the delay was adjusted such that an input 2^7-1 PRBS at 10 Gbit/s resulted in an output 2^7-1 PRBS at 160 Gbit/s (PRBS-maintaining multiplication). Due to the long fibres in the transmitter and no thermal stabilization, this subsystem was a source of instabilities in the further experiments.

The transmission line consisted of up to eight 68.85 km spans of SSMF, DCFs, and EDFAs to compensate for the losses in SSMF and DCMs. The fibres have been buried in the ground for more than five years and are connecting Ipswich and Newmarket. The fibre parameters are shown in Table 4.1. Launch powers into the transmission fibers and the DCM were 8 dBm and 6 dBm, respectively. Degradation due to PMD was minimized by coupling the data signal to the principal states of polarization of the fibre link. Chromatic dispersion of the link was compensated with granularity down to 10 m and dispersion slope was 100% compensated. This

Table 4.1: Fibre parameters for the total length of 68.85 km per fiber

Span no.	Loss dB	CD ps/nm	PMD ps
1	15.3	1156	0.74
2	16.8	1159	0.51
3	16.7	1162	0.66
4	16.5	1159	0.52
5	16.2	1165	1.00
6	16.6	1159	0.71
7	15.6	1160	1.20
8	16.9	1149	2.60

dispersion management resulted in an optical pulse train with a pulsewidth of 2.2 ps before a 160 Gbit/s demultiplexer. Eye diagrams captured using an OSO at the various points of the experimental setup are shown in Figure 4.28. The eye opening is clear and the signal shape is preserved indicating proper compensation of chromatic dispersion and minimization of the PMD influence.

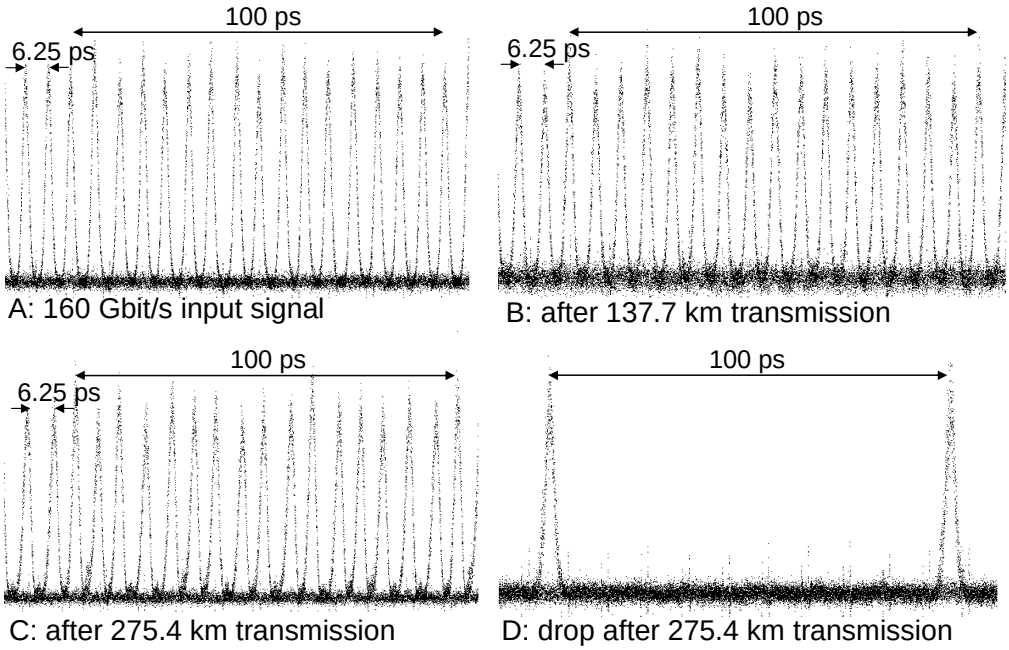

Figure 4.28: 160 Gbit/s eye diagrams captured in various points of the field transmission setup

In the receiver node, the GT-UNI switch acted as a demultiplexer. The demultiplexed signals were evaluated in the 10 Gbit/s optical receiver in combination with the BER tester. A fraction of the incoming data signal was coupled to a clock re-

covery circuit. The input signal was +10 dBm for the GT-UNI switch and +3 dBm for the CR setup. The resulting BER curves are shown in Figure 4.29. As a reference the back-to-back demultiplexing results were used. The average back-to-back sensitivity at BER=10^{-9} was -32.0 dBm, see Figure 4.29a. The spread in the sensitivity for the different channels for the back-to-back measurements was found to be 3.3 dB. This spread was caused mainly by fluctuations in the multiplexer alignment due to temperature changes (up to 15°C). For the transmission experiments additional spreading can be explained by changes of the residual chromatic dispersion and PMD. Since a reconfiguring of the fine-tuning fibre would have been necessary, an adaptation of the chromatic dispersion during the measurement was not possible.

After 137.7 km of transmission the average sensitivity at BER=10^{-9} was -31.0 dBm. This gave the power penalty of 1 dB introduced by 137.7 km transmission. The corresponding BER curves are depicted in Figure 4.29b. After 275.4 km of transmission the average sensitivity at BER=10^{-9} was -30.0 dBm. This gives a power penalty of 2 dB introduced by 275.4 km of transmission. When compared to 137.7 km transmission one can see that the penalty increased approximately by the same amount as when changing from a back-to-back to two spans. The BER curves for four spans of transmission are depicted in Figure 4.29c.

Experimental results of transmission over eight spans show significant spreading, see Figure 4.29d. During the first measurement a BER value less than 10^{-9} was reached for the three adjacent channels. In the next measurements, the transmission system showed worse performance. BERs in the order of 10^{-9} could be measured again, but only for some tens of seconds, not long enough to execute reliable measurements.

These spreadings in the performance were mainly due to the statistical impact of PMD, for which no compensation was possible during the course of the project, and due to variations of chromatic dispersion. Due to the long measurement time necessary to take the sensitivity curves of all channels and the rather fast fluctuations of the transmission performance, a reliable readjustment of dispersion compensation modules was impossible. Moreover, the system tolerances for the dispersion variations after such a long transmission span are very tight requiring almost perfect compensation [124].

To examine the evolution in time of the residual chromatic dispersion after the transmission link, RZ pulses from the ERGO laser pulse source were coupled into a 275 km transmission link (as described earlier) and the pulse width of the received pulses after transmission was measured with the OSO. The results are shown in Figure 4.30. During the measurement the pulse width was recorded every 2.5 minutes. The pulsewidth varied from 2.5 ps to more than 5 ps FWHM. The latter number is much too high for 160 Gb/s transmission, where each bit slot has a duration of only 6.25 ps. After applying the tuneable dispersion compensator the pulsewidth stayed nearly constant at the initial value of about 3 ps [125]. The residual variations in the pulsewidth are attributed primarily to higher-order PMD. As a consequence, tuneable dispersion compensation is mandatory in 160 Gbit/s transmission systems.

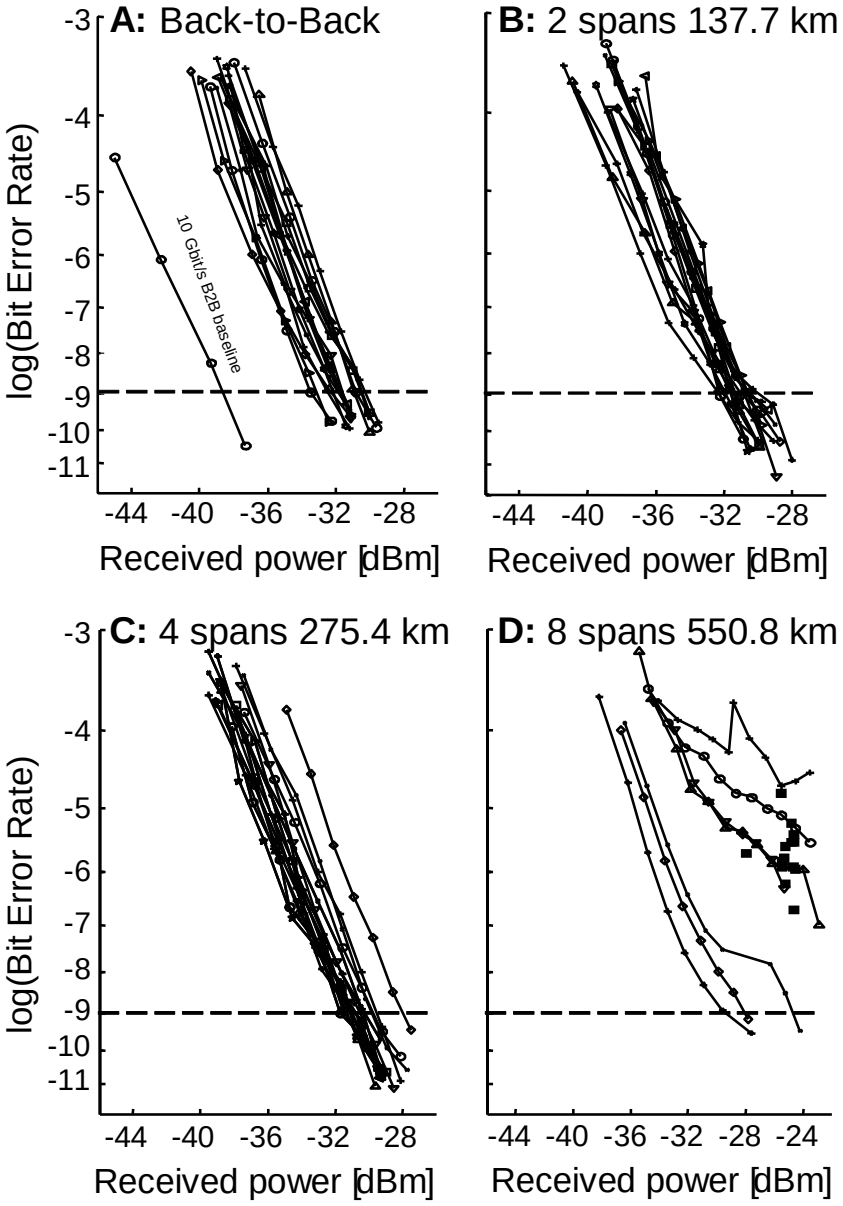

Figure 4.29: Results of BER measurements of 160 Gbit/s OTDM field transmission experiments

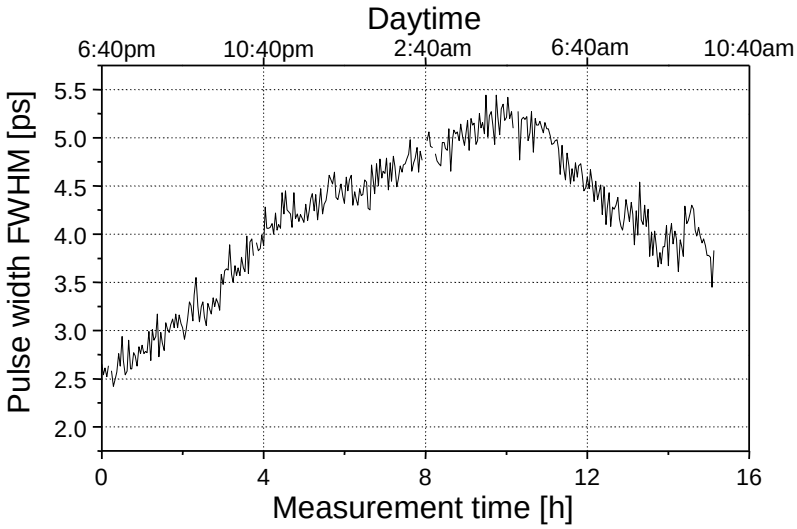

Figure 4.30: Measured evolution of the pulsewidth after transmission over 275 km

4.4.3 OTDM add-drop networking experiments

In the previous experiments demultiplexing capabilities of the GT-UNI switch were tested and evaluated in the laboratory and the field trial transmission experiments. In the next step, complete OTDM switching functionalities were tested in the field trial environment. The experimental setup of the OTDM network is presented in Figure 4.31. The OTDM network consisted of an OTDM transmitter, an add-drop node and an OTDM receiver. The transmitter, the add-drop node and the receiver were co-llocated in Ipswich, while the transmission took place between Ipswich and Newmarket. For OTDM add-drop experiments fibre spans #1 to #4 were chosen, see Table 4.1.

In the transmitter, described in detail in Section 4.4.2, a 160 Gbit/s OTDM signal was generated, see Figure 4.32a. The 160 Gbit/s signal was injected into the first transmission link (spans #1 and #2). To achieve optimal signal quality at the add-drop node and at the receiver node, fine dispersion compensation and PMD alleviation had to be performed twice. First, before the add-drop node and secondly before the receiver node. This is in contrast to the previous transmission experiments, where fine dispersion compensation and PMD alleviation was performed only at the end of the transmission link. Therefore in the OTDM add-drop networks fine dispersion compensation and PMD alleviation have to be realized before each OTDM node.

After the first transmission link, the 160 Gbit/s signal entered the GT-UNI based add-drop node. In the add-drop node part of the signal was tapped off to drive the CR circuit. The power to the GT-UNI switch (+10 dBm) and to the CR circuit (+3 dBm) was the same as in the transmission experiments. The CR circuit synchronized the GT-UNI switch as well as an add channel. The add channel was generated with

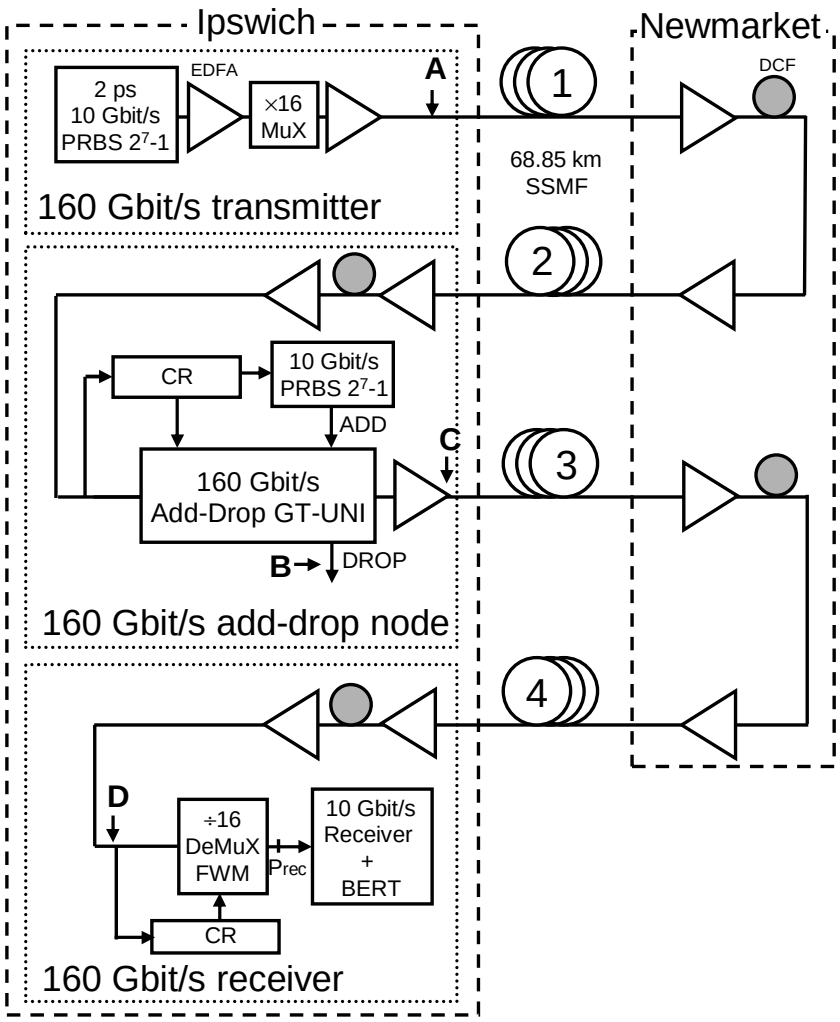

Figure 4.31: 160 Gbit/s OTDM networking experimental setup

a fibre ring laser (9.95328 GHz 2.2 ps FWHM) modulated with a $2^7 - 1$ PRBS in an external intensity modulator. Wavelength, amplitude, phase, and polarization of the added channel were adjusted to meet the transmitted signal in the through port. The final combination of the through and add data streams was realized by a passive coupler. The eye diagrams of drop and through signals are presented in Figure 4.32b-c.

After the second transmission link (spans #3 and #4) the 160 Gbit/s signal was fed into a 160 Gbit/s OTDM receiver, see Figure 4.32d. In the OTDM receiver, a CR circuit similar to the one in the add-drop node, however showing a slightly worse performance was applied. FWM in an SOA was used as demultiplexing technique [126]. A second erbium glass solid state laser (control pulse laser) which generated pulses of 2 ps FWHM at a wavelength of 1543 nm was synchronized via the CR circuit to

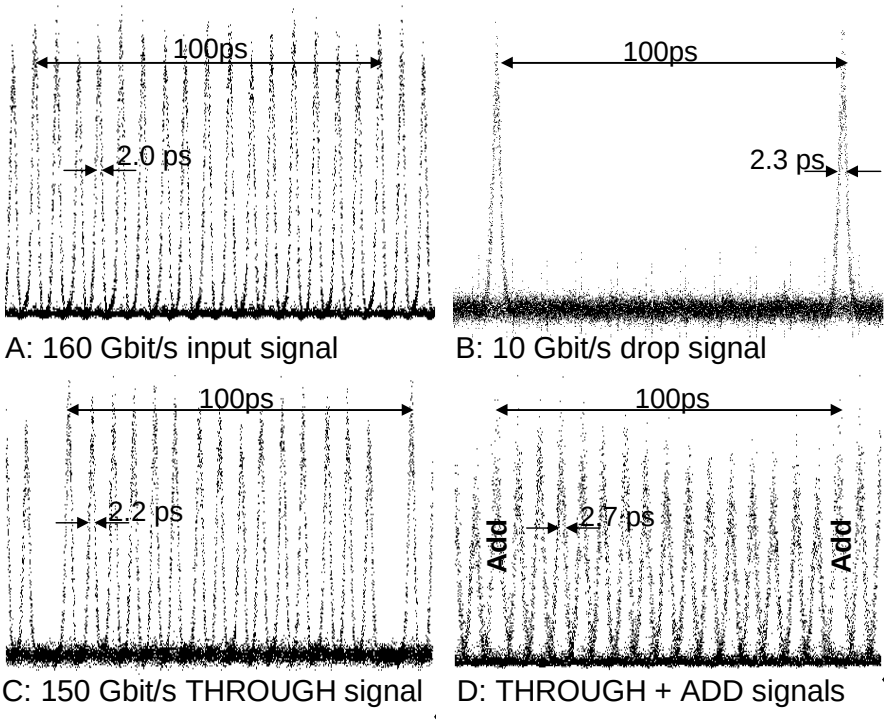

Figure 4.32: Eye diagrams of 160 Gbit/s OTDM networking experiments

the 16^{th} subharmonic of the 160 Gbit/s data signal. The pulses of the control laser were superposed with the data signal. The wavelength configuration relative to the gain maximum of the SOA has been optimized as described in [127]. The FWM product was filtered with a narrow band filter and fed into a standard pre-amplified 10 Gbit/s receiver. The BER curves were measured by attenuating the input signal into the 10 Gbit/s receiver.

In the presented eye diagrams, recorded with an optical sampling oscilloscope (OSO), see Figure 4.32, it can be observed that the pulse width evolved from 2.0 ps at the transmitter output, to 2.2 ps in the through port, and 2.7 ps before the OTDM receiver. The pulse width evolution was caused by the residual dispersion. The eye pattern is clearly open for all channels and good drop and through operation is visible. From all eye diagrams it can be seen that the pulse shape and quality were well preserved during transmission and switching. Minor amplitude variations of the through channels due to the residual absorption changes in the GT-SOA and the phase difference between sub-pulses can be observed.

Figure 4.33 shows BER curves of transmission and switching functions measured using the OTDM receiver node. The back-to-back BER curve in Figure 4.33a was the reference for the networking measurements. The sensitivities of about -24.0 dBm with FWM in SOA were measured in the back-to-back configuration. The difference

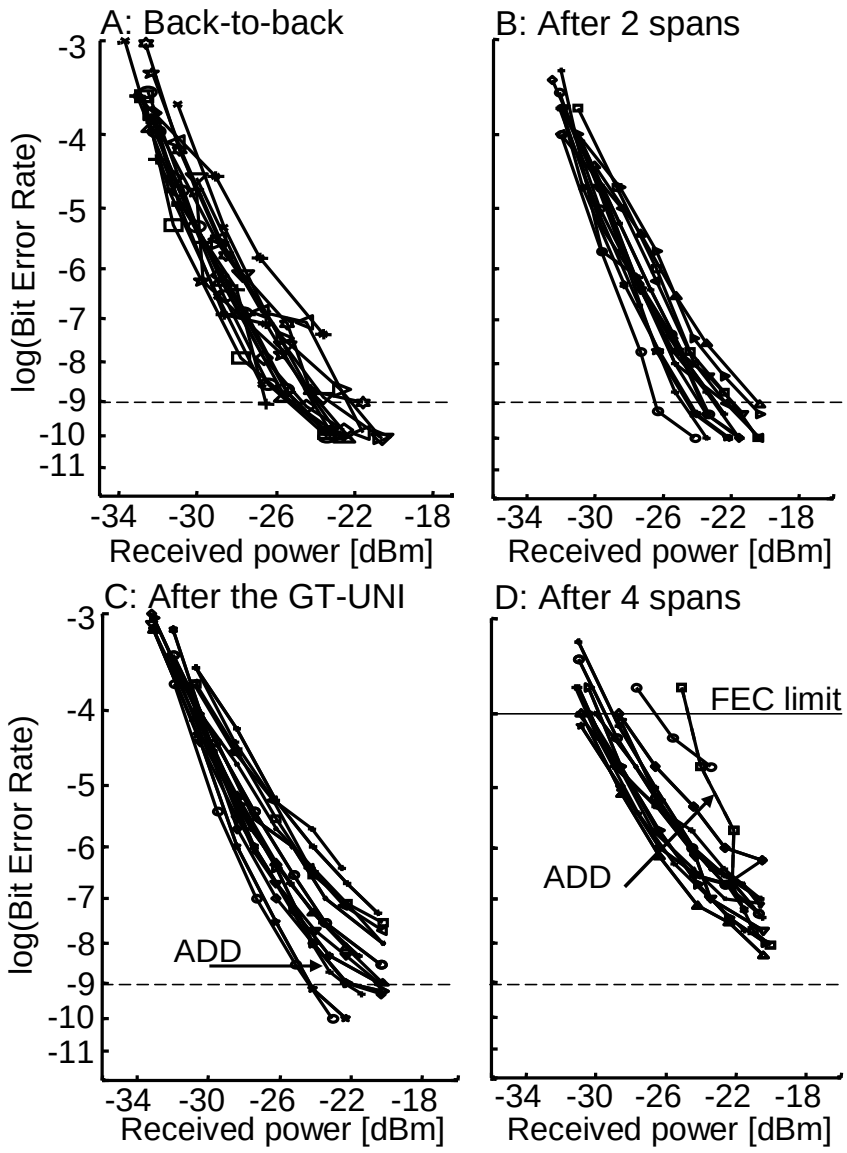

Figure 4.33: BER performance of 160 Gbit/sOTDM networking

of 8 dB with respect to the measurements with the GT-UNI based demultiplexer (see Figure 4.29) can be explained by the fact that a FWM product is inherently of low power (<-20 dBm) and a substantial amount of OSNR is lost in the demultiplexing process. In the GT-UNI, the power levels of the signal never drop to such small values. Therefore the degradation of the OSNR was less pronounced in the GT-UNI switch.

Figure 4.33b shows the BER results of FWM demultiplexing before the add-drop node. The average sensitivity was observed to be -23.3 dBm, resulting in a 137.7 km

transmission power penalty ≈1 dB. This result agrees in general with the transmission power penalty measured with the GT-UNI based demultiplexer, see Figure 4.29. Directly after the add-drop node the average sensitivity for the through and add channels was −20.7 dBm (see Figure 4.33c). This sensitivity value leads to a power penalty of approximately 2.6 dB in the 160 Gbit/s add-drop node. This penalty is largely caused by OSNR degradation in the GT-UNI switch. After additional two spans transmission (see Figure 4.33d) the quality of the signal degraded, however it was significantly above the forward error-correction threshold for BER$<10^{-12}$. This degradation was caused by the fact that the operational margins are very narrow for this transmission range. The time varying effects like dispersion or PMD started to become detrimental to the signal quality. Unfortunately as is the transmission experiments continuous re-adjustment of dispersion compensation was impossible.

4.5 Conclusions

In this chapter, applications of the 1310 nm SOA to OTDM switching were evaluated. To achieve a competitive advantage over existing technologies the OTDM technology has to enable flexible all-optical switching, i.e. add-drop multiplexing. The all-optical OTDM switches presented by the others were operating up to bit rate of 40 Gbit/s, basically speed of the commercially available electronics. To increase the allowable bit rate a new add-drop switching technique was necessary.

The proposed add-drop technique is based on a gain-transparent operation of an ultrafast nonlinear interferometer using a 1310 nm SOA. In this way the data signal was significantly less affected by the control signal via carrier recovery of the SOA and simultaneous optimization of the drop and through channels was possible. The proposed GT-UNI switch was extensively tested in laboratory experiments. Satisfying operation of all add-drop functionalities was achieved and error-free operation at 80 Gbit/s was demonstrated with insignificant penalty.

To provide synchronization of the GT-UNI switch to the incoming data signal a novel clock recovery method was developed. A simple and compact subharmonic 10 GHz clock recovery setup using a single unidirectional EAM was demonstrated. The recovered clock signal exhibited a low rms timing jitter of around 205 fs over a wide range of optical input powers and wavelengths. The clock recovery setup was tested successfully in the transmission experiments allowing 160-to-10 Gbit/s error-free demultiplexing.

Finally, the developed GT-UNI switch was tested in the field trial experiments. First, transmission experiments were performed. The GT-UNI switch in combination with the developed clock recovery scheme allowed error-free transmission at 160 Gbit/s over a distances of up to 550 km of field-installed legacy fibre. In the following experiments, a fully functional 160 Gbit/s OTDM add-drop network constructed with the field deployed fibre has been demonstrated. All network functionalities, i.e. transmission, clock recovery, and switching showed satisfying performance. Variations of PMD and dispersion limited the performance of 160 Gbit/s transmis-

sion. Therefore to cope with the time varying effects a tuneable dispersion compensator is mandatory. The presented results proved that OTDM add-drop networks are feasible.

During the course of the OTDM networking project, it turned out that another group was also working on a 160 Gbit/s add-drop switch using the GT-UNI concept. The presented add-drop switch [128] had a similar performance to the one developed at Eindhoven University of Technology. The main differences between setups developed at TU/e and Heinrich-Hertz-Institut, Berlin, Germany are that there no EDFA was placed in the GT-UNI loop, the polarization dependent pulse delay based on the optical delay line was applied (see Figure 4.10), and the PBSs were applied instead of the circulators. Moreover, several other 160 Gbit/s and above OTDM add-drop multiplexing experiments were demonstrated afterwards. The alternative add-drop switches utilized a nonlinear optical loop mirror [129, 130], a Kerr-gate [131] or two standing wave enhanced electro-absorption modulators [132].

The developed GT-UNI switch allowed 160 Gbit/s add-drop multiplexing with the tributary 10 Gbit/s. Operation with the tributary 40 Gbit/s can be significantly affected by the SOA recovery time as demonstrated in [117]. The add-drop switches based on nonlinear effects in an optical fibre are free from this limitation. 320 Gbit/s add-drop multiplexing with the tributary 10 Gbit/s [130] and 40 Gbit/s [131] has been demonstrated. However, similarly to the GT-UNI switch they required polarization control of the OTDM and control signals. Moreover, the fibre based switches have little prospect for photonic integration. Therefore stability issues have to be definitely address here.

The EAM based switch [132] allowed 160 Gbit/s add-drop multiplexing with the tributary 40 Gbit/s. The presented EAM based switch utilized two, in general polarization insensitive, standing wave enhanced electro-absorption modulators, one to achieve drop functionality and a second one to realize through functionality. Therefore the advantages of this switch are compactness, polarization insensitivity, and stability. However, with the currently available devices only operation with the tributary 40 Gbit/s is possible.

Chapter 5

Conclusions

This thesis reports on applications of the 1310 nm semiconductor optical amplifiers (SOAs) in fibre optic communication networks. SOAs are versatile components that can be used for optical signal amplification and all-optical signal processing.

The 1310 nm SOA can support cost-effective high-speed multi-wavelength transmission in the 1310 nm wavelength domain. From the presented analysis it has been concluded that the 1310 nm wavelength domain is particularly interesting to realize high speed (>10 Gbit/s) multi-wavelength transmission in the metro transmission range due to the virtual absence of dispersion related penalties for standard single-mode fibre. As an optimal operation wavelength band the wavelength range 1306-1319 nm was pinpointed.

The amplification performance of the SOA is limited by the ASE noise and saturation effects. Accumulation of the ASE noise limited the transmission reach in the conducted experiments to 200 km. Saturation effects limit the maximum SOA output power to a few dBm per channel. In the multi-channel transmission scheme the power of all signals has to be taken into account when choosing the operating point of the SOA. Due to the low dispersion value, transmission systems operating in the 1310 nm wavelength domain may suffer from the nonlinear four-wave mixing effect. This effect can be minimized by reducing the input power or by applying a special channel allocation grid. The FWM countermeasures may decrease bandwidth utilization efficiency. The presented results of experiments, e.g. 4×40 Gbit/s transmission over 50 km of SSMF showed undoubtedly that cost-effective transmission in the metro area can be realized utilizing the 1310 nm SOAs.

The 1310 nm SOA can be utilized to realize transparent optical connectivity between the 1310 nm and 1550 nm wavelength domains. 1310-to-1550 nm transparent optical connectivity simplifies network architecture by omitting optical-electrical-optical conversions between access and core networks. Nonlinear polarization rotation in the transparency region of the 1310 SOA allowed 1310-to-1550 nm wavelength conversion as well as the aggregation (transmultiplexing) of multiple data streams in the 1310 nm wavelength domain into one data stream in the

1550 nm wavelength domain. The performance limiting factor was the SOA recovery time. Hence, to achieve operation at high bit rates, SOAs with a short recovery time (a few dozen of ps at 10 Gbit/s) have to be applied. Error-free 1310-to-1550 nm wavelength conversion and transmultiplexing have been successfully demonstrated.

To achieve optimal operation of the proposed wavelength converter, the polarization state of optical signals has to be carefully adjusted and controlled. To allow efficient transmultiplexing the use of arrayed-waveguide gratings is necessary. However, this requires standardization of the wavelength grid in the 1310 nm wavelength domain. The current standardization covers only channels with a spacing of 20 nm. The future standardization can be based on the 100 GHz or even 50 GHz grid.

To realize 1310-to-1550 nm wavelength conversion with simultaneous NRZ-to-RZ data format conversion or 1310-to-1550 nm transmultiplexing, synchronization of the access and core networks is necessary. The most promising candidate to realize synchronization of the access and core networks is application of RZ signals in combination with the reflective-SOA in the user terminal node.

The 1310 nm SOA can be applied as a switching element to realize all-optical switching of 1550 nm optical signals. By applying the 1310 nm SOA in a gain transparent (GT) configuration for use in an ultrafast nonlinear interferometer (UNI), all-optical add-drop multiplexing of the 1550 nm data signal was realized. In the proposed configuration the 1550 nm data signal was not affected by the gain dynamics of the 1310 nm SOA. Moreover, simultaneous adjustement of drop and through channels was possible. A drawback of the GT-UNI switch is polarization sensitivity. This can be alleviated by application of the automatic polarization control at the input of the GT-UNI switch.

The GT-UNI switch has been extensively tested in the laboratory. Field-trial experiments showed error-free transmission at 160 Gbit/s over up to 550 km of SSMF and also realization of a fully functional 160 Gbit/s OTDM add-drop network. The performance of the transmission experiments was limited by time varying effects like polarization mode dispersion and changes in the dispersion value caused by environmental instabilities. Hence, to realize ultra high-speed networks tuneable compensation of time varying effects is obligatory.

The presented results underline that the 1310 nm semiconductor optical amplifier is a versatile component of optical networks and allows realization of cost-effective transmission, transparent optical connectivity, and all-optical gain-transparent switching. Therefore it can support several indispensable functionalities in optical communication networks.

References

[1] K.C. Kao and G.A. Hockham. Dielectric-fibre surface waveguides for optical frequencies. *IEE Proceedings*, 113(7):1151–1158, July 1966.

[2] F.P. Kapron, D.B. Keck, and R.D. Maurer. Radiation losses in glass optical waveguides. *Applied Physics Letters*, 17:423–425, November 1970.

[3] H.G. Weber, S. Ferber, M. Kroh, C. Schmidt-Langhorst, R. Ludwig, V. Marembert, C. Boerner, F. Futami, S. Watanabe, and C. Schubert. Single channel 1.28 Tbit/s and 2.56 Tbit/s DQPSK transmission. In *ECOC '2005*, volume 6, pages 3–4, Glasgow, Scotland, September 2005.

[4] `www.lucent.com`.

[5] Y. Liu, E. Tangdiongga, Z. Li, H. de Waardt, A.M.J. Koonen, G.D. Khoe, and H.J.S. Dorren. Error-free 320 Gb/s SOA-based wavelength conversion using optical filtering. In *OFC '2006*, volume 2, page PDP28, Anaheim, CA, March 2006.

[6] M.T. Hill, A. Srivatsa, N. Calabretta, Y. Liu, H. de Waardt, G.D. Khoe, and H.J.S. Dorren. 1×2 optical packet switch using all-optical header processing. *Electronics Letters*, 37(12):774–775, June 2001.

[7] C.G.P. Herben, C.G.M. Vreeburg, D.H.P. Maat, X.J.M. Leijtens, Y.S. Oei, F.H. Groen, J.W. Pedersen, P. Demeester, and M.K. Smit. A compact integrated InP-based single-phasar optical crossconnect. *IEEE Photonics Technology Letters*, 10(5):678–680, May 1998.

[8] M.T. Hill, H.J.S. Dorren, T. de Vries, X.J.M. Leijtens, J.H. den Besten, B. Smalbrugge, Y.S. Oei, H. Binsma, G.D. Khoe, and M.K. Smit. A fast low-power optical memory based on coupled micro-ring lasers. *Nature*, 432(7014):206–209, November 2004.

[9] R.S. Jacobsen, K.N. Andersen, P.I. Borel, J. Fage-Pedersen, L.H. Frandsen, O. Hansen, M. Kristensen, A.V. Lavrinenko, G. Moulin, H. Ou, Ch. Peucheret,

B. Zsigri, and A. Bjarklev. Strained silicon as a new electro-optic material. *Nature*, 441(7090):199–202, May 2006.

[10] M. Abrams, P.C. Becker, Y. Fujimoto, V. O'Byrne, and D. Piehler. FTTP deployments in the United States and Japan-equipment choices and service providers imperatives. *IEEE J. Lightwave Technology*, 23(1):236–246, January 2005.

[11] `www.onsnetnuenen.nl`.

[12] A.M.J. Koonen, H.P.A. van den Boom, A. Ng'oma, M. Garcia Larrode, J. Zeng, and G.D. Khoe. POF application in home systems and local systems. In *Conference on Polymer Optical Fibre 2005*, volume 1, pages 165–168, Hong Kong, China, September 2005.

[13] J.P. Turkiewicz, M.T. Hill, G.D. Khoe, and H. de Waardt. Cost-effective transmission concept for LAN/MAN/SAN applications. In *ECOC '2005*, volume 4, page Th1.4.2, Glasgow, Scotland, September 2005.

[14] J.P. Turkiewicz, A.M.J. Koonen, G.D. Khoe, and H. de Waardt. Do we need 1310 nm transmission in modern networks? In *ECOC '2006*, volume 3, page We.3.P.153, Nice, France, September 2006.

[15] `www.corning.com`.

[16] M.J. O'Mahony. Non-linear optical transmission systems. *European Transactions on Telecommunications and Related Technologies*, 4(6):629–640, December 1993.

[17] D. Derickson. *Fibre Optic Test and Measurement*. Prentice Hall PTR, 1998.

[18] P.-K. Lau and T. Makino. Effects of laser diode parameters on power penalty in 10 Gb/s optical fiber transmission systems. *IEEE J. Lightwave Technology*, 15(9):1663–1668, September 1997.

[19] A. Mecozzi, E. Iannone, and F. Matera. *Nonlinear Optical Communication Networks*. John Wiley & Sons, INC., 1998.

[20] M. Fullery. Three approaches to solving dispersion compensation at 10G. *LIGHTWAVE*, (11):15, November 2005.

[21] International Telecommunication Union. Recommendation G.652 characteristics of a single-mode optical fibre and cable, 03/2003.

[22] F. Heismann. Polarization mode dispersion: fundamentals and impact on optial communication systems. In *ECOC '1998*, volume 2, pages 51–79, Nice, France, September 1998.

[23] A.R. Chraplyvy. Limitations on lightwave communications imposed by optical-fibre nonlinearities. *IEEE J. Lightwave Technology*, 8(10):1548–1557, October 1990.

[24] G. Keiser. *Optical Fibre Communications*. McGraw-Hill, 2000.

[25] K.O. Hill, D.C. Johnson, B.S. Kawasaki, and R.I. MacDonald. CW three-wave mixing in single-mode optical fibres. *Journal of Applied Physics*, pages 5098–5106, 1978.

[26] N. Shibata, R. Braun, and R. Waarts. Phase-mismatch dependence of efficiency of wave generation through four-wave mixing in a single-mode optical fiber. *IEEE J. Quantum Electronics*, QE-23(7):1205–1210, July 1987.

[27] K. Inoue. Four-Wave Mixing in an optical fibre in the zero-dispersion wavelength region. *IEEE J. Lightwave Technology*, 10(11):1553–1561, November 1992.

[28] F. Forghieri, R.W. Tkach, and A.R. Chraplyvy. WDM system with unequally spaced channels. *IEEE J. Lightwave Technology*, 13(5):889–897, May 1995.

[29] W.C. Babcock. Intermodulation interference in radio systems. *Bell System Technical Journal*, 31:63–73, January 1953.

[30] J.-S. Lee, D.H. Lee, and Ch.-S. Park. Periodic allocation of a set of unequally spaced channels for WDM systems adopting dispersion-shifted fibres. *IEEE Photonics Technology Letters*, 10(6):825–827, June 1998.

[31] S. Kojima and T. Numai. Theoretical analysis of modified repeated unequally spaced frequency allocations in FDM lightwave transmission systems. *IEEE J. Lightwave Technology*, 24(7):2786–2796, July 2006.

[32] J. Vojtech, M. Karasek, and J. Radil. Extending the reach of 10GE at 1310 nm. In *ICTON '2005*, volume 2, pages 39–42, Barcelona, Spain, July 2005.

[33] Y. Fujimoto and M. Nakatsuka. Optical amplification in bismuth-doped silica glass. *Applied Physisc Letters*, 82(19):3325–3326, May 2003.

[34] Y.-S. Seo, Y. Fujimoto, and M. Nakatsuka. Optical amplification in the 1300 nm telecommunications window in a Bi-doped silica fiber. In *CLEO '2006*, volume 1, page CTuI6, Long Beach, California, May 2006.

[35] M.J. Adams, J.V. Collins, and I.D. Henning. Analysis of semiconductor laser optical amplifiers. *IEE Proceedings*, 132(1):58–63, February 1985.

[36] M.T. Hill, H. de Waardt, G.D. Khoe, and H.J.S. Dorren. Short-pulse generation in interferometers employing semiconductor optical amplifier. *IEEE J. Quantum Electronics*, 39(7):886–895, July 2003.

[37] F. Girardin, G. Guekos, and A. Houbavlis. Gain reocery of bulk semiconductor optical amplifiers. *IEEE Photonics Technology Letters*, 10(6):784–786, June 1998.

[38] R.J. Manning and D.A.O. Davis. Three-wavelength device for all-optical signal processing. *Optics Letters*, 19(12):889–891, June 1994.

[39] Y. Liu, E. Tangdiongga, Z. Li, S. Zhang, H. de Waardt, G.D. Khoe, and H.J.S. Dorren. Error-free all-optical wavelength conversion at 160 Gb/s using a semiconductor optical amplifier and an optical bandpass filter. *IEEE J. Lightwave Technology*, 24(1):230–236, January 2006.

[40] T. Akiyama, N. Hatori, Y. Nakata, H. Ebe, and M. Sugawara. Pattern-effect-free semiconductor optical amplifier achieved using quantum dots. *IEE Electronics Letters*, 38(19):1139–1140, September 2002.

[41] M. J. Connelly. *Semiconductor Optical Amplifiers*. Kluwer Academic Publishers, 2002.

[42] I. Kaminov and L. Li. *Optical fibre telecommunications IVB*. Academic Press, 2002.

[43] T. Durhuus, B. Mikkelsen, C. Joergensen, S.L. Danielsen, and K.E. Stubkjaer. All-optical wavelength conversion by semiconductor optical amplifiers. *IEEE J. Lightwave Technology*, 14(6):942–954, June 1996.

[44] A. Gladisch, S. Szuppa, and R.-P. Braun. 10 Gb/s Ethernet in the metro area. In *ECOC '2004*, volume 3, page We 2.6.1, Stockholm, Sweden, September 2004.

[45] A.M.J. Koonen, H. de Waardt, J.G.L. Jennen, J.P.C. Verhoosel, D. Kant, M. de Vos, A. de Ardenne, and E.J. Veldhuizen. A very high capacity optical fibre network for large-scale antenna constellations: the RETINA project. In *NOC '2002*, volume 1, pages 165–172, Ipswich, UK, June 2002.

[46] H. de Waardt, L.F. Tiemeijer, and B.H. Verbeek. 2×10 Gbit/s WDM 1310-nm optical transmission over 63.5-km Standard Single-Mode Fibre using optical preamplifiers. *IEEE Photonics Technology Letters*, 7(1):104–107, January 1995.

[47] T.N. Nielsen, P.B. Hansen, A.J. Stentz, V.M. Aquari, J.R. Pedrazzani, A.A. Abramov, and R.P. Espindola. 8×10 Gb/s 1.3-μm unrepeatered transmission over a distance of 141 km with Raman post- and pre-amplifiers. *IEEE Photonics Technology Letters*, 10(10):1492–1494, October 1998.

[48] J.G.L. Jennen, R.C.J. Smets, H. de Waardt, G.H. van den Hoven, and A.J. Boot. 4×10 Gbit/s NRZ transmission in the 1310 nm window over 80 km of Standard Single Mode Fibre using Semiconductor Optical Amplifiers. In *ECOC '98*, volume 1, pages 235–236, Madrid, Spain, September 1998.

[49] J.P. Turkiewicz, E. Tangdiongga, G.D. Khoe, and H. de Waardt. All-semiconductor 1310-nm 90-Gbit/s WDM transmission for LAN/MAN applications. In *ECOC '2002*, volume 4, page 11.5.2, Copenhagen, Denmark, September 2002.

[50] J.G.L. Jennen, H. de Waardt, and G. Acket. Modelling and performance analysis of WDM transmission links employing semiconductor optical amplifiers. *IEEE J. Lightwave Technology*, 19(8):1116–1124, August 2001.

[51] M. Duelk. Next-Generation 100G Ethernet. In *ECOC '2005*, volume 2, page Tu3.1.2, Glasgow, Scotland, September 2005.

[52] P.J. Winzer, G. Raybon, and M. Duelk. 107-Gb/s optical ETDM transmitter for 100G Ethernet. In *ECOC '2005*, volume 2, page Th4.1.1, Glasgow, Scotland, September 2005.

[53] G. Raybon, P.J. Winzer, and C.R. Doerr. 10×107-Gbit/s electronically multiplexed and optically equalized NRZ transmission over 400 km. In *OFC '2006*, volume 1, page PDP32, Anaheim, California, March 2006.

[54] M. Daikoku, I. Morita, H. Taga, H. Tanaka, T. Kawanishi, T. Sakamoto, T. Miyazaki, and T. Fujita. 100Gbit/s DQPSK transmission experiment without OTDM for 100G Ethernet transport. In *OFC '2006*, volume 1, page PDP36, Anaheim, California, March 2006.

[55] R.H. Derksen, G. Lehmann, C.-J. Weiske, C. Schubert, R. Ludwig, S. Ferber, C. Schmidt-Langhorst, M. Möller, and J. Lutz. Integrated 100 Gbit/s ETDM receiver in a transmission experiment over 480 km DMF. In *OFC '2006*, volume 1, page PDP37, Anaheim, California, March 2006.

[56] R. Nagarajan, C.H. Joyner, R.P. Schneider, J.S. Bostak, T. Butrie, A.G. Dentai, V.G. Dominic, P.W. Evans, M. Kato, M. Kauffman, D.J.H. Lambert, S.K. Mathis, A. Mathur, R.H. Miles, M.L. Mitchell, M.J. Missey, S. Murthy, A.C. Nilsson, F.H. Peters, S.C. Pennypacker, J.L. Pleumeekers, R.A. Salvatore, R.K. Schlenker, R.B. Taylor, H.S. Tsai, M.F. Van Leeuwen, J. Webjorn, M. Ziari, D. Perkins, J. Singh, S.G. Grubb, M.S. Reffle, D.G. Mehuys, F.A. Kish, and D.F. Welch. Large-scale photonic integrated circuits. *IEEE J. Selected Topics Quantum Electronics*, 11(1):50–65, January 2005.

[57] A. Wonfor, R.V. Penty, I.H. White, J. Kenton White, A.E. Kelly, and C. Tombling. Uncooled 40 Gb/s transmission over 40 km single mode fiber using multi-level modulation of a highly linear laser,. In *OFC 2004*, volume 1, Anaheim, USA, February 2004.

[58] J.P. Turkiewicz, G.D. Khoe, and H. de Waardt. All-optical 1310 nm to 1550 nm wavelength conversion by utilizing nonlinear polarisation in a semiconductor optical amplifier. *IEE Electronics Letters*, 41(1):29–30, January 2005.

[59] J.P. Turkiewicz, G.D. Khoe, and H. de Waardt. All-optical 1310 nm WDM to 1550 nm OTDM transmultiplexing. *IEE Electronics Letters*, 41(10):605–607, May 2005.

[60] J.P. Turkiewicz, J.J. Vegas Olmos, G.D. Khoe, and H. de Waardt. 1310-nm to 1550-nm wavelength conversion by utilizing nonlinear polarization rotation in a semiconductor optical amplifier. In *OFC '2005*, volume 1, page OME48, Anaheim, California, March 2005.

[61] J.P. Turkiewicz, J.J. Vegas Olmos, G.D. Khoe, and H. de Waardt. Performance assessment of 1310 to 1550 nm wavelength conversion. In *ECOC '2005*, volume 3, page We1.5.3, Glasgow, Scotland, September 2005.

[62] J.P. Turkiewicz, J.J. Vegas Olmos, A.M.J. Koonen, G.D. Khoe, and H. de Waardt. All-optical 1310-to-1550 nm wavelength conversion including transmission over two fibre links. In *LEOS Benelux '2005*, volume 1, pages 189–192, Mons, Belgium, December 2005.

[63] J.P. Turkiewicz, M.T. Hill, J.J. Vegas Olmos, A.M.J. Koonen, G.D. Khoe, and H. de Waardt. All-optical 4×2.5 Gbit/s 1310 nm WDM to 10 Gbit/s 1550 nm OTDM transmultiplexing. In *ECOC '2006*, volume 2, page Tu3.4.7, Nice, France, September 2006.

[64] M. Nakamura, H. Ueda, S. Makino, T. Yokotani, and K. Oshima. Proposal of networking by PON technologies for full and Ethernet services in FTTx. *IEEE J. Lightwave Technology*, 22(11):2631–2640, November 2004.

[65] A.M.J. Koonen. Fiber to the home/fiber to the premises: what, where, and when? *Proceedings of the IEEE*, 94(5):911–934, May 2006.

[66] H.J. Thiele, P.J. Winzer, J.H. Sinsky, L.W. Stulz, L.E. Nelson, and F. Fidler. 160-Gb/s CWDM capacity upgrade using 2.5-Gb/s rated uncooled directly modulated lasers. *IEEE Photonics Technology Letters*, 16(10):2389–2391, October 2004.

[67] C.Q. Xu, H. Okayama, and M. Kawahara. Wavelength conversion between the two silica windows at 1.31 and 1.55 μm using difference frequency generation. *IEE Electronics Letters*, 30(25):2168–2169, December 1994.

[68] P.E. Barnsley and P.J. Fiddyment. Wavelength conversion from 1.3 to 1.55 μm using split contact amplifiers. *IEEE Photonics Technology Letters*, 3(3):256–258, March 1995.

[69] D.N. Maywar, Y. Nakano, and G.P. Agrawal. 1.31-to-1.55 μm wavelength conversion by optically pumpig a distributed feedback amplifier. *IEEE Photonics Technology Letters*, 12(7):858–860, July 2000.

[70] J.P.R. Lacey, G.J. Pendock, and R.S. Tucker. All-optical 1300-nm to 1550-nm wavelength conversion using cross-phase modulation in a semiconductor optical amplifier. *IEEE Photonics Technology Letters*, 8(7):885–887, July 1996.

[71] E. Collett. *Polarized light: fundamentals and applications.* Marcel Dekker, Inc., 1993.

[72] R.J. Manning, A. Antonopulos, R. Le Roux, and A.E. Kelly. Experimental measurement of nonlinear polarization rotation in semiconductor optical amplifiers. *IEE Electronics Letters*, 37(4):229–231, February 2001.

[73] H.J.S. Dorren, D. Lenstra, Y. Liu, M.T. Hill, and G.D. Khoe. Nonlinear polarization rotation in semiconductor optical amplifiers: theory and application to all-optical flip-flop memories. *IEEE J. Quantum Electronics*, 39(1):141–147, January 2003.

[74] B.F. Kennedy, S. Philippe, P. Landais, A.L. Bradley, and H. Soto. Experimental investigation of polarisation rotation in semiconductor optical amplifiers. *IEE Proceedings-Optoelectronics*, 151(2):114–118, April 2004.

[75] Y. Liu, J.P. Turkiewicz, E.J.M. Verdurmen, H. de Waardt, G.D. Khoe, and H.J.S. Dorren. All-optical wavelength conversion by utilizing cross-polarization modulation in an electro-absorption modulator. In *ECOC '2003*, volume 4, page We4.P.78, Rimini, Italy, September 2003.

[76] G. Contestabile, N. Calabretta, M. Presi, and E. Ciaramella. Single and multicast wavelength conversion at 40 Gb/s by means of fast nonlinear polarization switching in an SOA. *IEEE Photonics Technology Letters*, 17(12):2652–2654, December 2002.

[77] D.M. Patrick, A.D. Ellis, D.A.O. Davis, M.C. Tathan, and G. Sherlock. Demultiplexing using polarization rotation in a semiconductor laser amplifier. *IEE Electronics Letters*, 30(4):341–342, February 1994.

[78] M.F.C. Stephens, M. Asghari, R.V. Penty, and I.H. White. Demonstration of ultrafast all-optical wavelength conversion utilizing birefringence in semiconductor optical amplifiers. *IEEE Photonics Technology Letters*, 9(4):449–451, April 1997.

[79] Y. Liu, M.T. Hill, E. Tangdiongga, H. de Waardt, N. Calabretta, G.D. Khoe, and H.J.S. Dorren. Wavelength conversion using nonlinear polarization rotation in a s single semiconductor optical amplifier. *IEEE Photonics Technology Letters*, 15(1):90–92, January 2003.

[80] C.S. Wong and H.K. Tsang. Polarization-independent wavelength conversion at 10 Gb/s using birefringence switching in a semiconductor optical amplifier. *IEEE Photonics Technology Letters*, 15(1):87–89, January 2003.

[81] H. Soto, D. Erasme, and G. Guekos. 5-Gb/s XOR optical gate based on cross-polarization modulation in a semiconductor optical amplifier. *IEEE Photonics Technology Letters*, 13(4):335–337, April 2001.

[82] H. Soto, C.A. Diaz, J. Topomondzo, D. Erasme, L. Schares, and G. Guekos. All-optical AND gate implementation using cross-polarization modulation in a semiconductor optical amplifier. *IEEE Photonics Technology Letters*, 14(4):498–500, April 2002.

[83] G. Gavioli and P. Bayvel. Novel 3R regenerator based on polarization switching in a semiconductor optical amplifier-assisted fiber Sagnac interferometer. *IEEE Photonics Technology Letters*, 15(9):1261–1263, September 2003.

[84] Y. Liu, M.T. Hill, H. de Waardt, G.D. Khoe, D. Lenstra, and H.J.S. Dorren. All-optical flip-flop memory based on two coupled polarization switches. *IEE Electronics Letters*, 38(16):904–906, August 2002.

[85] N. Storkfelt, B. Mikkelsen, D.S. Olesen, M. Yamaguchi, and K.E. Stubkjaer. Measurements of carrier lifetime and linewidth enhancement factor for 1.5 mm ridge-waveguide laser amplifier. *IEEE Photonics Technology Letters*, 3(7):632–634, July 1991.

[86] C. Joergensen, T. Durhuus, C. Braagaard, B. Mikkelsen, and K.E. Stubkjaer. 4 Gb/s optical wavelength conversion using semiconductor optical amplifiers. *IEEE Photonics Technology Letters*, 5(6):657–660, June 1993.

[87] M.T. Hill, E. Tangdiongga, H. de Waardt, G.D. Khoe, and H.J.S. Dorren. Carrier recovery time in semiconductor optical amplfier that employ holding beams. *Optics letters*, 27(18):1625–1627, September 2002.

[88] H.G. Weber, R. Ludwig, C. Schmidt, C. Schubert, J. Berger, E. Hilliger, M. Kroh, V. Marembert, C. Boerner, S. Ferber, and H.J. Ehrke. 160 Gbit/s transmission technology. In *ECOC '2002*, volume 2, page 2.1.1, Copenhagen, Denmark, September 2002.

[89] J.P.R. Lacey, M.V. Chan, R.S. Tucker, A.J. Lowery, and M.A. Summefield. All-optical WDM to TDM transmultiplexer. *IEE Electronics Letters*, 30(19):1612–1613, February 1994.

[90] D. Norte and A.E. Willner. Demonstration of an all-optical data format transparent WDM-to-TDM network node with extinction ratio enhancement for reconfigurable WDM networks. *IEEE Photonics Technology Letters*, 8(5):715–717, May 1996.

[91] K.A. Williams, M.F.C. Stephens, D. Nesset, A.E. Kelly, R.V. Penty, and M.J. Fice. WDM-TDM transmultiplexing at 40 Gbit/s using an integrated DFB laser amplifier. In *ECOC '1999*, volume 2, pages 168–169, Nice, France, September 1999.

[92] M.R.H. Daza, H.F. Liu, M. Tsuchiya, Y. Ogawa, and T. Kamiya. All-optical WDM-to-TDM conversion with total capacity of 33 Gb/s for WDM network links. *IEEE J. Selected Topics Quantum Electronics*, 3(5):1287–1294, October 1997.

[93] B.-E. Olsson, L. Rau, and D.J. Blumenthal. WDM to OTDM multiplexing using an ultrafast all-optical wavelength converter. *IEEE Photonics Technology Letters*, 13(9):1005–1007, September 2001.

[94] J. Yu, K. Kojima, and N. Chand. WDM-OTDM transmultiplexing using a nonlinear optical loop mirror. In *OFC '2002*, volume 1, pages 756–757, Anaheim, USA, March 2002.

[95] M. Hayashi, H. Tanaka, K. Ohara, T. Otani, and M. Suzuki. OTDM transmitter using WDM-TDM conversion with an electroabsorption wavelength converter. *IEEE J. Lightwave Technology*, 20(2):236–242, February 2002.

[96] P. Healey, P. Townsend, C. Ford, L. Johnston, P. Townley, I. Lealman, L. Rivers, S. Perrin, and R. Moore. Spectral slicing WDM-PON using wavelength-seeded reflective SOAs. *IEE Electronics Letters*, 37(19):1181–1182, September 2001.

[97] J. Prat, C. Arellano, V. Polo, and C. Bock. Optical network unit based on a bidirectional reflective semiconductor optical amplifier for fiber-to-the-home networks. *IEEE Photonics Technology Letters*, 17(1):205–207, January 2005.

[98] J.P. Turkiewicz, E. Tangdiongga, G. Lehmann, H. Rohde, W. Schairer, G.D. Khoe, and H. de Waardt. Simultaneous high speed OTDM add-drop multiplexing using GT-UNI switch. *IEE Electronics Letters*, 39(10):795–796, May 2003.

[99] J.P. Turkiewicz, E. Tangdiongga, G. Lehmann, H. Rohde, W. Schairer, Y.R. Zhou, E.S.R. Sikora, A. Lord, D.B. Payne, G.D. Khoe, and H. de Waardt. 160 Gb/s OTDM networking using deployed fiber. *IEEE J. Lightwave Technology*, 23(1):225–235, January 2005.

[100] J.P. Turkiewicz, E. Tangdiongga, G.D. Khoe, and H. de Waardt. Clock recovery and demultiplexing performance of 160-Gb/s OTDM field experiments. *IEEE Photonics Technology Letters*, 16(6):1555–1557, June 2004.

[101] J.P. Turkiewicz, H. Rohde, W. Schairer, G. Lehmann, E. Tangdiongga, G.D. Khoe, and H. de Waardt. All-optical OTDM add-drop node at 16x10 Gbit/s in between two fibre links of 150 km. In *ECOC '2003*, volume 5, page Th4.4.5, Rimini, Italy, September 2003.

[102] J.P. Turkiewicz, A. Lord, D. Payne, W. Schairer, H. Rohde, G. Lehmann, E.S.R. Sikora, Y.R. Zhou, E. Tangdiongga, G.D. Khoe, and H. de Waardt.

Field trial of 160Gbit/s OTDM add/drop node in a link of 275 km deployed fiber. In *OFC '2004*, volume 1, page PDP1, Anaheim, California, March 2004.

[103] S. Spälter, M. Heid, S.L. Jansen, G. Lehmann, E. Meissner, and B. Lanki. Ultra fast switching in OTDM networks. In *ECOC '2002*, volume 4, page 11.4.1, Copenhagen, Denmark, September 2002.

[104] I.D. Philips, A. Gloag, D.G. Moondie, N.J. Doran, I. Bennion, and A.D. Ellis. Drop and insert multiplexing with simultaneous clock recovey using an electroabsorption modulator. *IEEE Photonics Technology Letters*, 10(2):291–293, February 1998.

[105] L. Rau, S. Rangarajan, W. Wang, and D.J. Blumenthal. All-optical add-drop of OTDM channel using an ultra-fast fiber based wavelength converter. In *OFC '2002*, volume 1, pages 259–261, Anaheim, USA, March 2002.

[106] S. Fischer, M. Dülk, E. Gamper, W. Vogt, W. Hunziker, E. Gini, H. Melchior, A. Buxens, H.N. Poulsen, and A.T. Clausen. All-optical regenerative OTDM add-drop multiplexing at 40 Gbit/s using monolithic InP Mach-Zehnder interferometer. *IEEE Photonics Technology Letters*, 12(3):335–337, March 2000.

[107] C. Schubert, L. Schares, C. Schmidt, G. Guekos, and H. G. Weber. Phase dynamics in gain-transparent semiconductor optical amplifiers. In *ECOC '2003*, volume 4, pages 1062–1063, Rimini, Italy, September 2003.

[108] S. Diez, R. Ludwig, and H.G. Weber. Gain-transparent SOA switch for high-bitrate OTDM add/drop multiplexing. *IEEE Photonics Technology Letters*, 11(1):60–62, January 1999.

[109] S. Diez, C. Schubert, H.-J. Ehrke R. Ludwig, U. Feiste, C. Schmidt, and H.G. Weber. 160 Gbit/s all-optical demultiplexing using hybrid gain-transparent SOA Mach-Zehnder interferometer. *IEE Electronics Letters*, 36(17):1484–1486, August 2000.

[110] G. Toptchiyski, S. Randel, K. Petermann, S. Diez, E. Hiliger, C. Schmidt, C. Schubert, R. Ludwig, and H.G. Weber. Analysis of switching windows in a gain-transparent-SLALOM configuration. *IEEE J. Lightwave Technology*, 18(12):2188–2195, October 2000.

[111] C. Schubert, J. Berger, S. Diez, H.-J. Ehrke, R. Ludwig, U. Feiste, C. Schmidt, H.G. Weber, G. Toptchiyski, S. Randel, and K. Petermann. Comparison of interferometric all-optical switches for demultipexing applications in high-speed OTDM systems. *IEEE J. Lightwave Technology*, 20(4):618–624, October 2002.

[112] K. Tajima, S. Nakamura, and Y. Sugimoto. Ultrafast polarization-discriminating Mach-Zehnder all-optical switch. *Applied Physics Letters*, 67(25):3709–3711, December 1995.

[113] S. Nakamura, Y. Ueno, and K. Tajima. Ultrafast (200-fs switching, 1.5-Tb/s demultiplexing) and high-repetition (10 GHz) operations of a polarization-discriminating symmetric Mach-Zehnder all-optical switch. *IEEE Photonics Technology Letters*, 10(11):1575–1577, November 1998.

[114] N.S. Patel, K.A. Rauschenbach, and K.L. Hall. 40-Gb/s demultiplexing using an ultrafast nonlinear interferometer (UNI). *IEEE Photonics Technology Letters*, 8(12):1695–1697, December 1996.

[115] B.S. Robinson, S.A. Hamilton, and E.P. Ippen. Demultiplexing of 80-Gb/s pulse-position modulated data with an ultrafast nonlinear interferometer. *IEEE Photonics Technology Letters*, 14(2):206–208, February 2002.

[116] C. Schubert, S. Diez, J. Berger, R. Ludwig, U. Feiste, H.G. Weber, G. Toptchiyski, K. Petermann, and V. Krajinovic. 160-Gb/s all-optical demultiplexing using gain-transparent ultrafast-nonlinear interferometer (GT-UNI). *IEEE Photonics Technology Letters*, 13(5):475–477, May 2001.

[117] G. Toptchiyski, S. Randel, K. Petermann, C. Schubert, J. Berger, and H.G. Weber. Characterization of switching windows of an 160-Gb/s all-optical demultiplexer with data base rates of 10 and 40 Gb/s. *IEEE Photonics Technology Letters*, 14(4):534–536, April 2002.

[118] C. Schubert, J. Berger, U. Feiste, R. Ludwig, C. Schmidt, and H.G. Weber. 160-Gb/s polarization insensitive all-optical demultiplexing using a gain-transparent ultrafast nonlinear interferometer (GT-UNI). *IEEE Photonics Technology Letters*, 12(11):1200–1201, November 2001.

[119] M. Jinno. Effect of crosstalk and timing jitter on all-optical time-division demultiplexing using a nonlinear fibre Sagnac interferometer switch. *IEEE J. Quantum Electronics*, 30(12):2842–2853, December 1994.

[120] O. Kamatani, S. Kawanishi, and M. Saruwatari. Prescaled 6.3 GHz clock recovery from 50-Gb/s TDM optical signal with 50 GHz PLL using four-wave mixing in a travelling-wave laser diode optical amplifier. *IEE Electronics Letters*, 30(10):807–809, May 1994.

[121] D.T.K. Tong, B. Mikkelsen, G. Raybon, T.N. Nielsen, K.F. Dreyer, and J.E. Johnson. Optoelectronic phase-locked loop with balanced photodetection for clock recovery in high-speed optical time-division-multiplexed systems. *IEEE Photonics Technology Letters*, 12(8):1064–1066, August 2000.

[122] D.T.K. Tong, K.L. Deng, B. Mikkelsen, G. Raybon, K.F. Dreyer, and J.E. Johnson. 160 Gbit/s clock recovery using electroabsorption modulator-based phase-locked loop. *IEE Electronics Letters*, 36(23):1951–1952, November 2000.

[123] C. Boerner, C. Schubert, C. Schmidt, E. Hiliger, V. Marembert, J. Berger, S. Ferber, E. Dietrich, R. Ludwig, B. Schmauss, and H.G. Weber. 160-Gb/s

clock recovery with electro-optical PLL using a bidirectionally operated electroabsorption modulator as a phase comparator. *IEE Electronics Letters*, 39(14):1071–1073, August 2003.

[124] G. Lehmann, E. Meissner, S. Spälter, Y.R. Zhou, E.S.R. Sikora, and A. Lord. Dispersion tolerances at 160 Gb/s. In *NOC '2002*, volume 1, pages 95–100, Darmstadt, Germany, June 2002.

[125] S. Wielandy, P.S. Westbrook, M. Fishteyn, P. Reyes, W. Schairer, H. Rohde, and G. Lehmann. Demonstration of automatic dispersion control for 160 Gbit/s transmission over 275 km of deployed fibre. *IEE Electronics Letters*, 40(11):690–691, May 2004.

[126] H. Rohde, W. Schairer, and G. Lehmann. All-optical add/drop multiplexer for high speed optical networks based on four-wave mixing in SOA. In *ECOC '2003*, volume 3, pages 810–811, Rimini, Italy, September 2003.

[127] S. Jansen, G.D. Khoe, H. de Waardt, M. Heid, S. Spälter, E. Meissner, C. Weiske, and A. Schoepflin. Optimizing the wavelength configuration for FWM-based demultiplexing in a SOA. In *OFC '2003*, volume 2, pages 539 – 541, Atlanta, GA, March 2003.

[128] C. Schubert, C. Schmidt, S. Ferber, R. Ludwig, and H.G. Weber. Error-free all-optical add-drop multiplexing at 160 Gbit/s. *IEE Electronics Letters*, 39(14):1074–1076, August 2003.

[129] E.J.M. Verdurmen, Y. Zhao, E. Tangdiongga, J.P. Turkiewicz, G.D. Khoe, and H. de Waardt. Error-free all-optical add-drop multiplexing using HNLF in a NOLM at 160 Gbit/s. *IEE Electronics Letters*, 41(6):349–350, March 2005.

[130] E.J.M. Verdurmen, J.P. Turkiewicz, E. Tangdiongga, G.D. Khoe, and H. de Waardt. Towards all-optical 320 Gb/s add-drop multiplexing using a nonlinear optical loop mirror. In *ECOC '2005*, volume 4, pages 925–926, Glasgow, Scotland, September 2005.

[131] C. Schubert, C. Schmidt-Langhorst, K. Schulze, V. Marembert, and H.G. Weber. Time division add-drop multiplexing up to 320 Gbit/s. In *OFC '2005*, volume 4, page OThN2, Anaheim, CA, March 2005.

[132] C. Hsu-Feng, J.E. Bowers, and D.J. Blumenthal. Compact 160-Gb/s add-drop multiplexer with a 40-Gb/s base rate using electroabsorption modulators. *IEEE Photonics Technology Letters*, 16(6):1564–1566, June 2004.

List of abbreviations

ASE	Amplified Spontaneous Emission
ATT	Attenuator
AWG	Arrayed Wave-guide Grating
BER	Bit Error Ratio
CR	Clock Recovery
CW	Continuous Wave
CWDM	Coarse Wavelength Division Multiplexing
DFB	Distributed Feedback Lasers
DGD	Differential Group Delay
DSF	Dispersion-Shifted Fibre
DWDM	Dense Wavelength Division Multiplexing
EAM	Electro-Absorption Modulator
EDFA	Erbium-Doped Fibre Amplifier
ER	Extinction Ratio
FEC	Forward-Error Correction
FWHM	Full-Width at Half Maximum
FWM	Four-Wave Mixing
GT-UNI	Gain Transparent Ultrafast Nonlinear Interferometer
GVD	Group Velocity Dispersion
IM	Intensity Modulator
LAN	Local Area Network
LD	Laser Diode
MAN	Metropolitan Area Network
MZI	Mach-Zehnder Interferometer
NF	Noise Figure
NRZ	Nonreturn-to-Zero
OBP	Optical Band-Pass Filter
OSA	Optical Spectrum Analyzer

OSNR	Optical Signal-to-Noise Ratio
OSO	Optical Sampling Oscilloscope
OTDM	Optical Time Division Multiplexing
PBS	Polarization Beam Splitter
PMF	Polarization Maintaining Fibre
PC	Polarization Controller
PMD	Polarization Mode Dispersion
PON	Passive Optical Network
PRBS	Pseudo-Random Bit Sequence
RF	Radio Frequency
RZ	Return-to-Zero
SAN	Storage Area Network
SDH	Synchronous Digital Hierarchy
SMF	Single-Mode Fibre
SOA	Semiconductor Optical Amplifier
SSMF	Standard Single-Mode Fibre
TE	Transverse Electric
TM	Transverse Magnetic
WDM	Wavelength Division Multiplexing
XGM	Cross-Gain Modulation

List of publications

Journal Papers

1. **Invited paper** J.P. Turkiewicz, E. Tangdiongga, G. Lehmann, H. Rohde, W. Schairer, Y. R. Zhou, E.S.R. Sikora, A. Lord, D.B. Payne, G.D. Khoe and H. de Waardt: "160 Gb/s OTDM networking using deployed fiber", *IEEE Journal of Lightwave Technology*, vol. 23, no. 1, pp. 225–235, January 2005.

2. J.P. Turkiewicz, G.D. Khoe and H. de Waardt: "All-optical 1310 nm WDM to 1550 nm OTDM transmultiplexing", *IEE Electronics Letters*, vol. 41, no. 10, pp. 605–607, May 2005.

3. J.P. Turkiewicz, G.D. Khoe, H. de Waardt: "All-optical 1310 nm to 1550 nm wavelength conversion by utilizing nonlinear polarisation in a semiconductor optical amplifier", *IEE Electronics Letters*, vol. 41, no. 1, pp. 29–30, January 2005.

4. J.P. Turkiewicz, E. Tangdiongga, G.D. Khoe and H. de Waardt: "Clock recovery and demultiplexing performance of 160-Gb/s OTDM field experiments", *IEEE Photonics Technology Letters*, vol. 16, no. 6, pp. 1555–1557, June 2004.

5. J.P. Turkiewicz, E. Tangdiongga, H. Rohde, W. Schairer, G. Lehmann, G.D. Khoe and H. de Waardt: "Simultaneous high speed OTDM add-drop multiplexing using GT-UNI switch, *IEE Electronics Letters*, vol. 39, no. 10, pp. 795–796, May 2003.

6. M. Garcia Larrode, A.M.J. Koonen, J.J. Vegas Olmos, E.J.M. Verdurmen, and J.P. Turkiewicz: "Dispersion tolerant radio-over-fibre transmission of 16QAM and 64QAM radio signals at 40GHz", *Accepted for publication IEE Electronics Letters.*

7. J.J. Vegas Olmos, I. Tafur Monroy, J.P. Turkiewicz, Y. Liu and A.M.J. Koonen: "Self-controlled all-optical label and payload separator for variable length bursts in a Time-Serial IM/DPSK Scheme", *IEEE Photonics Technology Letters*, vol. 17, no. 8, pp. 1692–1694, August 2005.

8. E.J.M. Verdurmen, Y. Zhao, E. Tangdiongga, J.P. Turkiewicz, G.D. Khoe and H. de Waardt: "Error-free all-optical add-drop multiplexing using HNLF in a NOLM at 160 Gbit/s", *IEE Electronics Letters*, vol. 41, no. 6, pp. 349–350, March 2003.

9. J.J. Vegas Olmos, I. Tafur Monroy, J.P. Turkiewicz, N. Calabretta, H.J.S. Dorren and A.M.J. Koonen: "Asynchronous all-optical label extraction in a time-serial IM/DPSK scheme supporting variable packet length operation", *Microwave and Optical Technology Letters*, vol. 46, no. 5, pp. 453–454, September 2005.

10. E. Tangdiongga, J.P. Turkiewicz, G.D. Khoe, H. de Waardt: "Clock recovery by a fibre ring laser employing a linear optical amplifier", *IEEE Photonics Technology Letters*, vol. 16, no. 2, pp. 611–613, February 2004.

11. E. Tangdiongga, J.P. Turkiewicz, W. Schairer, H. Rohde, G. Lehmann, A. Lord, D.B. Payne, E.S.R. Sikora, Y.R. Zhou, G.D. Khoe and H. de Waardt: "160 Gbit/s OTDM add-drop networking using 275 km installed fibres" *IEE Electronics Letters*, vol. 40, no. 9, pp. 552–554, April 2004.

12. J.J. Vegas Olmos, I. Tafur Monroy, Y. Liu, M. Garcia Larrode, J.P. Turkiewicz, H.J.S. Dorren and A.M.J. Koonen: "Asynchronous, self-controlled, all-optical label and payload separator using nonlinear polarization rotation in a semiconductor optical amplifier" *Optics Express*, vol. 12, no. 18, pp. 4214-4219, September 2004.

International Conferences

13. **Invited paper** H. de Waardt, E. Tangdiongga, J.P. Turkiewicz and G.D. Khoe: "Optical networking beyond 40 Gbit/s", *in Proceedings of Optical Fiber Communications (OFC 2005)*, pp. OWK7, Anaheim, California, March 2005.

14. **Invited paper** H. Rohde, A. Lord, D.B. Payne, G. Lehmann, W. Schairer, E. Tangdiongga, J.P. Turkiewicz, H. de Waardt, G.D. Khoe, E.S.R. Sikora and Y.R. Zhou: "Towards high-speed optical networks of the future: an overview of 160 Gbit/s transmission and networks", *in Proceedings of Asia-Pacific Optical Communications Conference (APOC 2004)*, Beijing, China, November 2004.

15. **Invited paper** H. Rohde, A. Lord, D.B. Payne, G. Lehmann, W. Schairer, E. Tangdiongga, J.P. Turkiewicz, H. de Waardt, G.D. Khoe, E.S.R. Sikora and

Y.R. Zhou: "Optimized design methodologies of hierarchical optical networks", *in Proceedings of Asia-Pacific Optical Communications Conference (APOC 2004)*, Beijing, China, November 2004.

16. **Post-deadline paper** J.P. Turkiewicz, A. Lord, D. Payne, E. Tangdiongga, G.D. Khoe, H. de Waardt, W. Schairer, H. Rohde, G. Lehmann, E.S.R. Sikora, and Y.R. Zhou: "Field trial of 160Gbit/s OTDM add/drop node in a link of 275 km deployed fiber", *in Proceedings of Optical Fiber Communications (OFC 2004)*, pp. PDP1, Anaheim, California, March 2004.

17. **Post-deadline paper** J.P. Turkiewicz, H. Rohde, W. Schairer, G. Lehmann, E. Tangdiongga, G.D. Khoe and H. de Waardt: "All-optical OTDM add-drop node at 16x10 Gbit/s in between two fibre links of 150 km", *in Proceedings of European Conference on Optical Communication (ECOC 2003)*, pp. TH4.4.5., Rimini, Italy, September 2003.

18. J.P. Turkiewicz, M.T. Hill, J.J. Vegas Olmos, A.M.J. Koonen, G.D. Khoe and H. de Waardt: "All-optical 4×2.5 Gbit/s 1310 nm WDM to 10 Gbit/s 1550 nm OTDM transmultiplexing", *in Proceedings of European Conference on Optical Communication (ECOC 2006)*, Tu3.4.7, Nice, France, September 2006.

19. J.P. Turkiewicz, A.M.J. Koonen, G.D. Khoe and H. de Waardt: "Do we need 1310 nm transmission in modern networks?", *in Proceedings of European Conference on Optical Communication (ECOC 2006)*, We.3.P.153, Nice, France, September 2006.

20. J.P. Turkiewicz, M.T. Hill, G.D. Khoe and H. de Waardt: "Cost-effective transmission concept for LAN/MAN/SAN applications", *in Proceedings of European Conference on Optical Communication (ECOC 2005)*, pp. Th1.4.2., Glasgow, Scotland, September 2005.

21. J.P. Turkiewicz, J.J. Vegas Olmos, G.D. Khoe and H. de Waardt: "Performance assessment of 1310 to 1550 nm wavelength conversion. proc. ECOC 05 conference", *in Proceedings of European Conference on Optical Communication (ECOC 2005)*, pp. We1.5.3., Glasgow, Scotland, September 2005.

22. J.P. Turkiewicz, J.J. Vegas Olmos, G.D. Khoe and H. de Waardt: "1310-nm to 1550-nm wavelength conversion by utilizing nonlinear polarization rotation in a semiconductor optical amplifier", *in Proceedings of Optical Fiber Communications (OFC 2005)*, pp. OME48, Anaheim, California, March 2005.

23. J.P. Turkiewicz, E. Tangdiongga, G.D. Khoe and H. de Waardt: "All-semiconductor 1310-nm 90-Gbit/s WDM transmission for LAN/MAN applications", *in Proceedings of European Conference on Optical Communication (ECOC 2002)*, pp. 11.5.2., Copenhagen, Denmark, September 2002.

24. J.J. Vegas Olmos, J.P. Turkiewicz, M. Garcia Larrode, I. Tafur Monroy, A.M.J. Koonen, V. Polo, A. Ausiro, J. Prat: "FSK-WDM to IM-OTDM conversion for Fiber-to-the-Premises access networks", *in Proceedings of Optical Fiber Communications (OFC 2006)*, pp. OFE6, Anaheim, California, March 2006.

25. E.J.M. Verdurmen, J.P. Turkiewicz, E. Tangdiongga, G.D. Khoe and H. de Waardt: "Towards all-optical 320 Gb/s add-drop multiplexing using a nonlinear optical loop mirror", *in Proceedings of European Conference on Optical Communication (ECOC 2005)*, pp. Th3.1.7., Glasgow, Scotland, September 2005.

26. J.J. Vegas Olmos, I. Tafur Monroy, J.P. Turkiewicz, M. Garcia Larrode, R. Geldenhuys, A.M.J. Koonen: "An all-optical time-serial label and payload separator generating a synchronization pulse", *in Proceedings of European Conference on Optical Communication (ECOC 2005)*, pp. Mo4.4.2., Glasgow, Scotland, September 2005.

27. G. Lehmann, G.D. Khoe, H. de Waardt, W. Schairer, H. Rohde, E.S.R. Sikora, Y.R. Zhou, A. Lord, D. Payne, J.P. Turkiewicz, E. Tangdiongga: "160 Gbit/s OTDM transmission field trial over 550 km of legacy SSMF", *in Proceedings of European Conference on Optical Communication (ECOC 2004)*, pp. WE1.5.2., Stockholm, Sweden, September 2004.

28. E. Tangdiongga, J.P. Turkiewicz, A. Lord, D. Payne, G.D. Khoe, H. de Waardt, H. Rohde, W. Schairer, G. Lehmann, Y.R. Zhou, E.S.R. Sikora: "Ultrafast switching in high-speed OTDM networks", *in Proceedings of European Conference on Optical Communication (ECOC 2004)*, pp. TU1.1.4., Stockholm, Sweden, September 2004.

29. G. Lehmann, A. Lord, D. Payne, H. Rohde, W. Schairer, J.P. Turkiewicz, E. Tangdiongga, G.D. Khoe, H. de Waardt, E.S.R. Sikora and Y.R. Zhou: "The architecture of optical time domain multiplexed add-drop nodes in a meshed network", *in Proceedings of European Conference on Networks & Optical Communications (NOC 2004)*, pp. 367-373., Eindhoven, The Netherlands, June 2004.

30. Y. Liu, J.P. Turkiewicz, E.J.M. Verdurmen, H. de Waardt, G.D. Khoe, H.J.S. Dorren: "All-optical wavelength conversion by utilizing cross-polarization modulation in an electro-absorption modulator" *in Proceedings of European Conference on Optical Communication (ECOC 2003)*, pp. We4.P.78., Rimini, Italy, September 2003.

31. M.I. Macias, J.P. Turkiewicz, J.J. Vegas Olmos, A.M.J.Koonen and I. Tafur Monroy: "A novel data vortex switch for photonic slot routing", in *in Proceedings of European Conference on Optical Communication (ECOC2003)*, Tu1.4.2., Rimini, Italy, 2003.

32. M.I. Macias, J.P.Turkiewicz, J.J. Vegas Olmos, A.M.J.Koonen and I. Tafur Monroy: "High-throughput, self-routing, optical switch for photonic slot routing", in *in Proceedings of London Communications Symposium 2003*, pp. 249–253, London, UK, September 2003.

Regional Conferences

33. J.P. Turkiewicz, J.J. Vegas Olmos, A.M.J. Koonen, G.D. Khoe and H. de Waardt: "All-optical 1310-to-1550 nm wavelength conversion including transmission over two fibre links", in *Proceedings of IEEE/LEOS 10th Annual Symposium Benelux Chapter*, pp. 189–192, Mons, Belgium, December 2005.

34. J.P. Turkiewicz, G.D. Khoe and H. de Waardt: "A novel 1310 nm to 1550 nm wavelength converter", in *Proceedings of IEEE/LEOS 9th Annual Symposium Benelux Chapter*, pp. 21–24, Gent, Belgium, December 2004.

35. J.P. Turkiewicz, E. Tangdiongga, G.D. Khoe and H. de Waardt: "All-optical 10-GHz clock recovery from 160 Gbit/s OTDM signals using a mode-locked fibre ring laser", in *Proceedings of IEEE/LEOS 7th Annual Symposium Benelux Chapter*, pp. 47–50, Amsterdam, The Netherlands, December 2002.

36. J.P. Turkiewicz, E. Tangdiongga and H. de Waardt: "High capacity WDM transmission in the 1310 nm wavelength domain for the RETINA network purposes", in *Proceedings of IEEE/LEOS 7th Annual Symposium Benelux Chapter*, pp. 270–273, Amsterdam, The Netherlands, December 2002.

37. J.P. Turkiewicz and H. de Waardt: "Transmission impairments due to four-wave mixing in the 1310 nm window", in *Proceedings of IEEE/LEOS 6th Annual Symposium Benelux Chapter*, pp. 161–164, Brussels, Belgium, December 2001.

38. J.J. Vegas Olmos, E.J.M. Verdurmen, I. Tafur Monroy, J.P. Turkiewicz, N. Yan, H. de Waardt and A.M.J. Koonen: "Wavelength conversion with multicasting capabilities deploying highly nonlinear fiber for time-serial labelled networks", in *Proceedings of IEEE/LEOS 10th Annual Symposium Benelux Chapter*, pp. 181–184, Mons, Belgium, December 2005.

39. Y. Liu, J.P. Turkiewicz, S. Zhang, E. Tangdiongga, E.J.M. Verdurmen, H. de Waardt, D. Lenstra, G.D. Khoe and H.J.S. Dorren: "40 Gbit/s SOA-based wavelength conversion assisted by a narrow optical bandpass filter", in *Proceedings of IEEE/LEOS 9th Annual Symposium Benelux Chapter*, pp. 251–254, Gent, Belgium, December 2004.

Referable work

40. J.P. Turkiewicz: "WDM technology in the 1310 nm wavelength domain", Stan Ackermans Institute, Centre for Technological Design, April 2002, ISBN 90-444-0187-4.

Curriculum vitæ

Jarosław Piotr Turkiewicz was born in Koszalin, Poland in 1974. He received his M.Sc. degree with distinction in telecommunications engineering from the Faculty of Electronics and Information Technology of Warsaw University of Technology, Poland in 1998. From 1997 to 1999 he was working at the Polish Telecom Research and Development Centre.

In 2000 he started the post-master studies at the Stan Ackermans Institute, Eindhoven University of Technology, The Netherlands. The design project concerned the WDM transmission system for the LOFAR (LOw Frequency ARray) antenna system. In 2002 he joined the COBRA Research Institute, Eindhoven University of Technology. From 2002 to 2003 he participated in the European project FASHION (ultraFAst Switching in HIgh-speed Optical time-division multiplexed Networks). Recently, he concentrated on ultra-wideband wavelength conversion and transmission in the 1310 nm wavelength domain.

He authored and co-authored more than 35 journal and conference papers. He acts as a reviewer for IEEE Photonics Technology Letters, IEE Proceedings of Optoelectronics, and IEE Electronics Letters. In 2005 he was awarded the IEEE Laser&Electro-Optics Society Graduate Student Fellowship.

Acknowledgements

At this point, I want to express my gratitude to all people who helped me with realization of my Ph.D. thesis.

First of all, I would like to acknowledge prof.ir. Giok-Djan Khoe for giving me the opportunity to perform the presented research in such an inspiring environment. Moreover, I wish to thank prof.ir. Ton Koonen. His fresh view on fibre-optic communication inspired me many times.

I am very grateful to my direct supervisor dr.ir. Huug de Waardt. During my work Huug provided me guidance, has been always open for discussion, and helpful with the encountered problems. Huug took care not only for scientific matters but also the administrative ones. What is most important, Huug provided the right degree of scientific freedom and was always open for new ideas.

Further, I would like to thank my all present and former colleges from the Electro-optical communications TU/e group for inspiring collaboration and many wonderful moments. In particular, I acknowledge Eduward Tangdiongga for cooperation especially during a FASHION project, Harm Dorren for fruitful discussions, Henri van den Boom for de algemeen gezelligheid, Juan-Jose Vegas Olmos for making essential opto-electronic components permanently available, Martin Hill for the inspiring trips, Hyun-Do Jung for his enthusiastic attitude, Liu Young, Zhonggui Li, and Shaoxian Zhang for discussions about SOA-related matters and "Ni Hao", Dirk van den Borne and Sander Jansen for inspiring chats about fibre-optic business, Erwin Verdurmen for translation services and some ground breaking and unforgettable achievements, Georgi Petkow and Javier Molina Vazquez for peacefully sharing the office and help with computer and non-computer related problems, Christos "Heretic" Tsekrekos for making me aware of differences and similarities, Bas Huiszoon for help with simulations, Maria Garcia Larrode for cheering up, and finally Kevin Williams for thesis corrections.

Our technicians Peter van Bennekom, Frans Huijskens, and Johan "de Brabander" van Zantvoort have had always time to help me with important issues like splicing a fibre or finding a proper RF adapter. Moreover, despite his heavy work load Johan managed to find time to relax providing additional lessons: Houdoe–Brabants voor beginners. In contrast, Frans is trying to pronounce properly some

Polish words, just to mention one: barszcz. Jak się masz Frans? Dobrze, dziękuję bardzo!

The ECO group is working closely with the Radiocommunications and Optoelectronic devices TU/e groups. Here, I wish to thank Tim Schenk, Xaveer Lijtens, Luc Augustin, Yohan Barbarin, Francisco Soares, Martijn Heck, Tjibbe de Vries, and Jan Hendrik den Besten for scientific and non-scientific discussion especially during the COBRA colloquium and LEOS-Benelux events.

Work in modern organizations is impossible without massive support from secretaries. Here, I would like to express my gratitude to always helpful SAI-ICT and ECO secretaries: Rian van Gaalen, Els Gerritsen, and Susan de Leeuw. Rian helped me voluntary with my Dutch course which ended with the NT2 certificate. Rian bedankt, zonder jou het zou nooit gebeuren!

During work in a FASHION project I had a unique opportunity to collaborate with inspiring people from British Telecom and Siemens. Dave Payne, Yu-Rong Zhou, Ed Sikora, Andrew Lord, Harald Rohde, Wolfgang Schairer, Gottfried Lehmann, Mario Heid, and Stefan Spälter many thanks for wonderful cooperation during and after the FASHION project.

Prof.dr.ir. Anders Bjarklev, prof.ir. Ton Koonen, and prof.dr.hab.inż. Jerzy Siuzdak are gratefully acknowledged for their valuable input to this thesis.

Moreover, I am thankful to Noe, Dani, Alex, Ari, Nicole, Jaap, Marco, Robert, and "brother" Jonathan for relaxing after-work moments.

I am indebted to my family and friends in Poland for their permanent support. Especially, I would like to express my gratitude to my uncles Jerzego, Marka, and Wiesława as well as their families. Thank you for your unswerving faith in my! Moreover, I wish Monika good luck with having me as a “szwagier”. My mates Andrzej, Grzegorz, Marce, Marcin B., Marcin K., Majewscy, and Tomasz are always supporting me in one or another form, many thanks! I am grateful to Krzysztof Perlicki for introducing to me fibre-optic telecommunications and long-term fruitful collaboration.